

Cover Page



Universiteit Leiden



The handle <http://hdl.handle.net/1887/22212> holds various files of this Leiden University dissertation.

Author: Wilde, Adriaan Hugo de

Title: Host factors in nidovirus replication

Issue Date: 2013-11-13

Host factors in nidovirus replication

ADRIAAN HUGO DE WILDE

Host factors in nidovirus replication

Adriaan H. de Wilde

PhD Thesis, Leiden University, 2013

The work presented in this dissertation was performed in the Department of Medical Microbiology of Leiden University Medical Center. This research was financially supported in part by TOP grant 700.57.301 from the Council for Chemical Sciences of the Netherlands Organization for Scientific Research (NWO-CW) and by the European Union Seventh Framework Programme (FP7/2007-2013) under SILVER grant agreement n° 260644.

Cover: "MHV draakje"; Syncytium formation of MHV-infected cells. Courtesy of Dr. Yvonne van der Meer

ISBN: 978-94-6169-432-4

Lay-out and printing: Optima Grafische Communicatie, Rotterdam, The Netherlands

All rights reserved. No part of this thesis may be reproduced or transmitted in any form or by any means without prior written permission of the author.

Host factors in nidovirus replication

Proefschrift

ter verkrijging van
de graad van Doctor aan de Universiteit Leiden,
op gezag van Rector Magnificus prof. mr. C.J.J.M. Stolker,
volgens besluit van het College voor Promoties
te verdedigen op woensdag 13 november 2013
klokke 15.00 uur

door
Adriaan Hugo de Wilde
geboren te Hazerswoude-Dorp
in 1984

PROMOTIECOMMISSIE:

Promotor:

Prof. dr. E.J. Snijder

Co-promotor:

Dr. M.J. van Hemert

Overige leden:

Dr. V. Thiel (Kantonal Hospital, St Gallen en Vetsuisse Faculty, University of Zürich, Zwitserland)

Prof. dr. P. ten Dijke

Prof. dr. A.E. Gorbalenya

Prof. dr. C. van Kooten

“Wat er ook gebeurt, altijd blijven lachen...”

TABLE OF CONTENTS**PAGE**

	List of abbreviations	8
Chapter 1	General introduction	13
Chapter 2	The <i>in vitro</i> RNA synthesizing activity of the isolated arterivirus replication/transcription complex is dependent on a host factor	33
Chapter 3	Cyclophilin inhibitors block arterivirus replication by interfering with viral RNA synthesis	57
Chapter 4	Cyclosporin A inhibits the replication of diverse coronaviruses	77
Chapter 5	A kinome-wide siRNA screen identifies proviral and antiviral host factors in SARS-coronavirus replication, including PKR and early secretory pathway proteins	87
Chapter 6	MERS-coronavirus replication induces severe <i>in vitro</i> cytopathology and is strongly inhibited by cyclosporin A or interferon-alpha treatment	109
Chapter 7	General discussion	129
	References	143
	Nederlandse samenvatting	171
	Curriculum Vitae	177
	List of publications	181

LIST OF ABBREVIATIONS

-RNA	negative-stranded RNA
+RNA	positive-stranded RNA
aa	amino acid
ACE2	Angiotensin-converting enzyme 2
ActD	Actinomycin D
ARDS	Acute Respiratory Distress Syndrome
Arf	ADP-ribosylation factor
ATP	adenosine triphosphate
avg	average
BCoV	Bovine coronavirus
BHK	Baby hamster kidney
BFA	Brefeldin A
CDK	cyclin-dependent protein kinase
CM	convoluted membrane
COP	coatomer protein complex
CsA	cyclosporin A
CoV	coronavirus
CPE	cytopathic effect
CTP	cytidine triphosphate
Cy3	indocarbocyanine 3
Cyp	cyclophilin
DAA	direct-acting antiviral
DDX	DEAD-box protein
DENV	dengue virus
DMEM	Dulbecco's Modified Eagle Medium
DMSO	dimethyl sulfoxide
DMV	double-membrane vesicle
DNA	deoxyribonucleic acid
DPP4	dipeptidyl peptidase-4
ds	double-stranded
DTT	dithiothreitol
DUB	deubiquitinating enzyme
E protein	envelope protein
EAV	Equine arteritis virus
EDEM	ER degradation-enhancing alpha-mannosidase-like protein
eIF	eukaryotic translation initiation factor
EM	electron microscopy

EMEM	Eagle's Minimal Essential Medium
ER	endoplasmic reticulum
ERGIC	ER-Golgi intermediate compartment
ExoN	exonuclease N
FA	formaldehyde
FDA	Food and Drug Administration
g	genomic
GAPDH	glyceraldehyde 3-phosphate dehydrogenase
GBF1	guanine nucleotide exchange factor 1
GFP	green fluorescent protein
GMEM	Glasgow Minimum Essential Medium
HCoV	human coronavirus
HCV	hepatitis C virus
HDA	host-directed antiviral
HeLa	Henrietta Lacks
HEPES	4-(2-hydroxyethyl)-1-piperazineethanesulfonic acid
HIV	human immunodeficiency virus
hnRNP	heterogeneous nuclear ribonucleoprotein
HPF	high-pressure freezing
HR	heptad repeat
HRI	heme-regulated inhibitor
Huh	human hepatoma
IBV	infectious bronchitis virus
IC ₅₀	half maximal inhibitory concentration
IF	immunofluorescence
IFN	interferon
IRF	IFN-regulatory factor
IgG	immunoglobulin G
IL	interleukin
ISG	interferon-stimulated gene
IVRA	<i>in vitro</i> RNA synthesis assay
kb	kilobase
kDa	kilo Dalton
Lys	lysine
M protein	membrane protein
MADP1	zinc finger CCHC-type and RNA-binding motif 1
MDA-5	melanoma differentiation-associated protein 5
MERS	Middle East Respiratory Syndrome
MERS-CoV	MERS-coronavirus

MHV	mouse hepatitis virus
MOI	multiplicity of infection
MP	main protease
mRNA	messenger RNA
MT	methyl transferase
N	nucleus
N protein	nucleocapsid protein
nsp	non-structural protein
ORF	open reading frame
PABP	poly(A)-binding protein
PBS	phosphate-buffered saline
PCBP	poly(C)-binding protein
PEG-IFN	pegylated IFN- α
PERK	PKR-like endoplasmic reticulum kinase
PFA	paraformaldehyde
p.i.	post infection
p.t.	post transfection
PKR	double-stranded RNA-activated protein kinase
PLP	papain-like protease
PNS	post-nuclear supernatant
pp	polyprotein
PPlase	peptidyl-prolyl isomerases
P-PMO	peptide-conjugated antisense phosphorodiamidate morpholino oligomer
PRRSV	Porcine Reproductive and Respiratory Syndrome Virus
PTB	polypyrimidine tract-binding protein
PV	poliovirus
RBD	receptor-binding domain
RC	replication complex
RdRp	RNA-dependent RNA polymerase
RF	replicative form
RFS	ribosomal frameshift
RI	replicative intermediate
RIG-I	retinoic acid-inducible gene 1
RLR	Rig-I-like receptor
RNA	ribonucleic acid
RNase	ribonuclease
RNAi	RNA interference
RTC	replication and transcription complex
RVN	reticulovesicular network

S protein	Spike protein
SARS	Severe Acute Respiratory Syndrome
SARS-CoV	SARS-coronavirus
SD	standard deviation
SDS-PAGE	sodium-dodecyl sulfate polyacrylamide gel electrophoresis
sg	subgenomic
shRNA	short-hairpin RNA
siRNA	small interfering RNA
ss	single-stranded
TBK1	TANK-binding kinase 1
TfR	transferrin receptor
TGEV	transmissible gastroenteritis virus
TRAF3	TNF receptor-associated factor 3
TRS	transcription regulatory sequences
UTR	untranslated region
WNV	West Nile virus
wt	wild-type

Chapter 1

General introduction

NIDOVIRUSES AS EMERGING PATHOGENS: IMPACT AND CHALLENGES

Emerging infections are a major cause of morbidity and mortality world-wide, and many pandemics and outbreaks have had an enormous medical, societal and economic impact [1]. Emerging infectious diseases are defined by their appearance in a population for the first time, or by an existing disease that rapidly increases in incidence or geographic range [2]. One of the best-known human pathogens is influenza A virus, which is responsible for the seasonal flu epidemics causing approximately 250,000 to 500,000 deaths annually [3]. In addition, highly pathogenic strains do emerge regularly. Examples were the viruses causing the 1918 Spanish Flu, the 1957 Asian flu, the 1968 Hong Kong flu and the 2009 swine flu pandemics, which highlighted the severity and global effects that virus outbreaks can have on society. Human immunodeficiency virus (HIV) is a well-known example of a virus that had a disastrous impact on society and still is a major health problem in developing countries, causing an estimated 1.7 billion deaths in 2011 [4]. In addition, hepatitis C virus (HCV) infection has been called the silent epidemic since about 130 million individuals worldwide are estimated to be chronically infected, and more than 350,000 people die each year from HCV-related liver disease. About 27% of all cases of liver cirrhosis and hepatocellular carcinomas are attributed to HCV infection [5].

Between November 2002 and July 2003, an outbreak of a previously unknown severe acute respiratory syndrome (SARS) occurred in Southern China and Hong Kong. Accelerated by air travel, the disease rapidly spread to several parts of the world and nearly became a pandemic. SARS-coronavirus (SARS-CoV) was identified as the causative agent of this zoonotic infection [6-8], for which >8,000 cases and 774 deaths were reported worldwide [9]. Although in death toll not comparable to influenza, HIV or HCV, the 2003 SARS-CoV outbreak caused worldwide unrest and had a serious impact on global economy (estimated losses \$ 30-100 billion; [10]). SARS-CoV initially causes lower respiratory tract disease, which can lead to a progressive and potentially lethal atypical pneumonia with clinical symptoms that include fever, malaise, lymphopenia, and in some cases also diarrhoea. Two years after the outbreak, horse-shoe bats were identified as the likely source of the SARS virus, which is believed to have been transferred to humans via the civet cat as intermediate host [11, 12]. Apparently, adaptation to the human host predominantly required a small number of mutations in the receptor-binding domain of the SARS-CoV spike (S) protein, which mediates cell binding and entry [13]. Therefore, the re-emergence of SARS-CoV or zoonotic transfer of other animal coronaviruses to humans remains a serious public health concern.

Almost a decade after the SARS-CoV outbreak the fear for the emergence of the next highly pathogenic coronavirus has become a painful reality. In June 2012 a novel coronavirus, now termed Middle East Respiratory Syndrome coronavirus (MERS-CoV)

[14], was isolated from a 60 year-old Saudi Arabian male who died from acute respiratory distress syndrome (ARDS) and multiple organ failure, including renal failure [15, 16]. MERS-CoV can cause a lower respiratory tract infection with symptoms that include coughing and high fever. Up to August 2013, 94 confirmed MERS-CoV cases have been recorded, of which 46 were fatal [17], and new cases continue to be reported regularly. The majority of fatalities involved patients with underlying diseases, and the reported case fatality rate of about 50% might be an overestimation (due to underreporting of milder or asymptomatic cases). Initially, most MERS-CoV cases were attributed to isolated zoonotic transmissions, although the evidence for human-to-human transmission is increasing as several (secondary) MERS-CoV infections have now been documented, involving patients that had not travelled to the Arabian Peninsula. A number of small clusters of MERS have been reported in the UK, Jordan, Italy, Tunisia, Saudi-Arabia and France. However, transmission seems inefficient and does not appear to have extended beyond these small clusters that, thus far, have all occurred in health care settings or among close family contacts. Although the hunt for the natural reservoir of the virus is still ongoing, the close relatedness to multiple bat coronaviruses and the ability of the virus to efficiently replicate in bat cell lines make bats the most likely natural animal res-

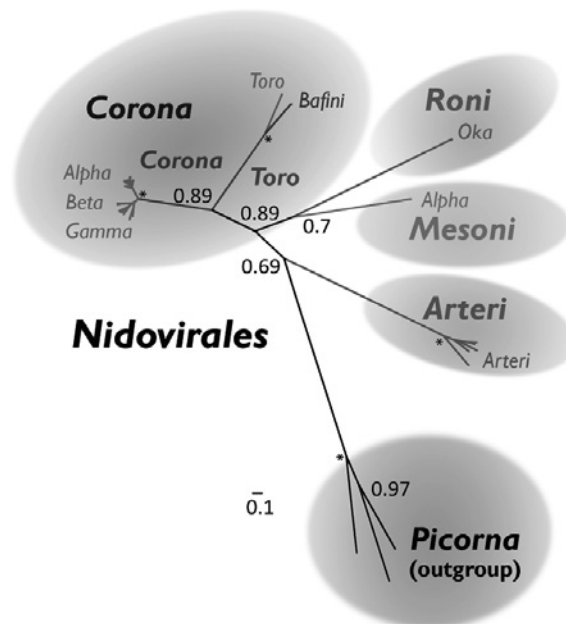


Fig. 1 – RNA polymerase-based nidovirus phylogenetic tree. To infer phylogenetic relationships between nidoviruses, partially constrained trees were calculated using the nidovirus-wide conserved RNA-dependent RNA polymerase (RdRp) domain. Picornaviruses were used as a domain-specific out group. Courtesy of Dr. Chris Lauber and Prof. Alexander E. Gorbalenya, Leiden University Medical Center, The Netherlands. Reprinted with permission from [26].

ervoir [16, 18]. However, other animals, like camels, have been mentioned as potential (intermediate) host or reservoir as well.

Besides the highly pathogenic SARS-CoV and MERS-CoV, which received considerable scientific and media attention over the past decade, two established human coronaviruses - HCoVs OC43 and 229E - have been known since the 1960s. These viruses cause mild respiratory disease and, after rhinoviruses, are a leading cause of common colds (10-30% of the cases) [19-21]. More recently, two additional coronaviruses have been discovered in humans, HCoV-NL63 [22] and HCoV-HKU1 [23]. Interestingly, recent findings suggest that all established human coronaviruses originate from zoonotic transfer from bats [24].

Coronaviruses are not only known as important human pathogens, also a number of severe veterinary diseases have been linked to coronavirus infection. This is illustrated by the recent emergence of a novel variant of porcine epidemic diarrhoea virus, which is closely-related to a strain that caused a large outbreak killing almost one million piglets in China in 2010. Mortality among pigs younger than four weeks has commonly been over 50% and more than 100 cases have been reported since May 2013 in the USA alone [25].

The coronaviruses, together with arteri-, mesoni- and roniviruses, are grouped in the order Nidovirales (Fig. 1). Besides coronaviruses, this order includes the distantly related arterivirus family, which includes some serious veterinary pathogens. Porcine reproductive and respiratory syndrome virus (PRRSV), for example, has emerged as the most prevalent swine disease in the world, causing an estimated annual loss of \$664 million in the USA alone [27]. The arterivirus EAV, besides being an equine pathogen, has been extensively used as a model virus to study nidovirus molecular biology and virus-host interactions.

The economic impact of nidovirus infections, the recent emergence of highly pathogenic zoonotic coronaviruses, the concerns that new coronaviruses will emerge in the future and the lack of effective antiviral strategies make it painfully clear that our preparedness and options to treat or prevent diseases caused by these viruses are very limited. This highlights the urgency of advancing our knowledge on (the replication of) these viruses, which should ultimately contribute to the development of (broad spectrum) antiviral strategies to combat infections by known nidoviruses and those that might emerge in the future.

THE NIDOVIRUS REPLICATIVE CYCLE

Nidoviruses belong to the positive-stranded RNA (+RNA) viruses and their genome acts as a messenger RNA (mRNA) that is directly translated into viral proteins by the host

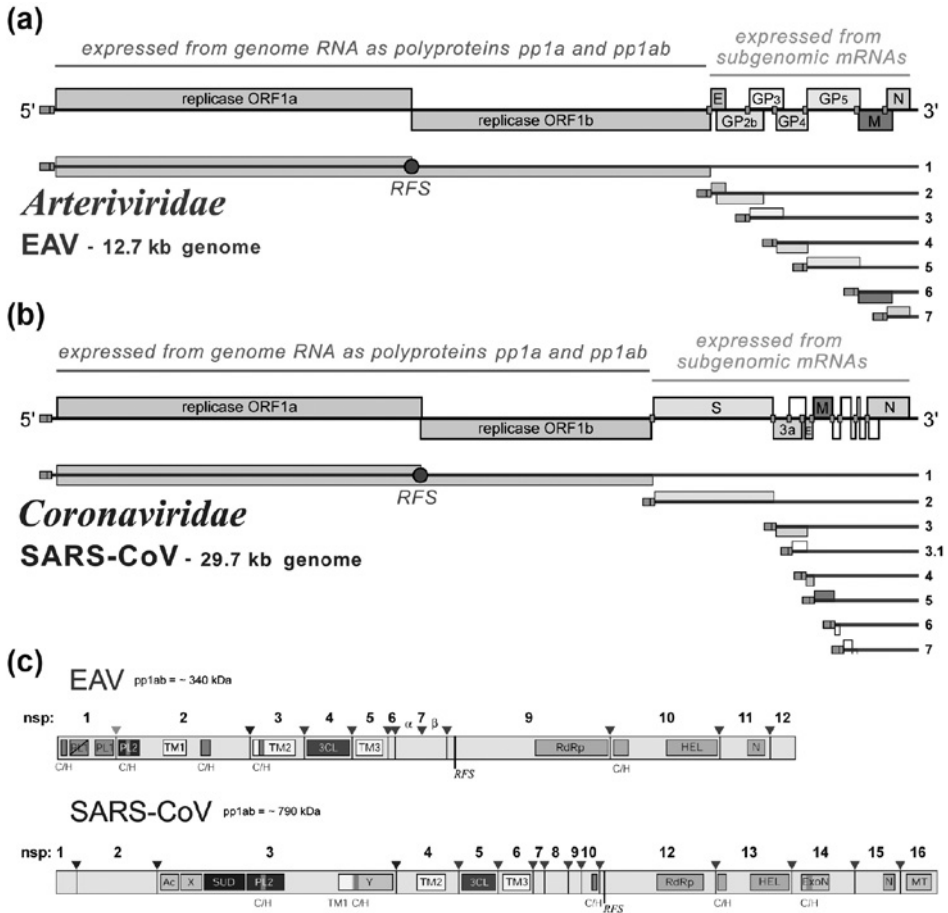


Fig. 2 – EAV and SARS-CoV genome organisation. (A, B) Nidovirus genome structure and expression strategy, illustrated using EAV (A) and SARS-CoV (B). The open reading frames in the viral genome are indicated at the top of each schematic. Note that the arterivirus and coronavirus genomes are drawn to different scales. The names of the replicase gene and structural protein genes are given (see also [41]). Below the genome organisation, the structural relationships of the genome and sg mRNAs are depicted. The leader sequence and Transcription Regulatory Sequences (TRSs) are indicated as blue and orange boxes, respectively. The ribosomal frameshifting (RFS) element found in the genome-length mRNA1 is indicated and green lines mark the translated region of each mRNA, whereas translationally silent regions are indicated by red lines. Only the translated ORFs are shown for each mRNA. Reprinted with permission from [40]. (C) Domain organisation of the EAV and SARS-CoV replicase pp1ab. Arrows represent sites in pp1ab that are cleaved by papain-like proteases (orange and blue) or chymotrypsin-like protease (main protease; MP). The cleavage products, the location and names of domains that have been identified are highlighted. They include diverse domains with conserved Cys and His residues (C/H), putative transmembrane domains (TM), domains with conserved features (AC, X and Y), and domains that have been associated with proteolysis (PL1, PL2, and MP), RNA-dependent RNA synthesis (RdRp), helicase, exonuclease (ExoN), uridylate-specific endoribonuclease, methyl transferase (MT) and cyclic phosphodiesterase activities. Please note that SARS-CoV and EAV polyproteins are drawn to different scales. Reprinted with permission from [37].

cell's translational machinery. A typical feature of nidoviruses, and all other +RNA viruses (reviewed in [28]), is that their replication takes place in the cytoplasm of the infected cell, in association with modified intracellular membranes that presumably form a platform for the assembly of the +RNA viral replication complexes (RCs) that engage in RNA synthesis [29-36].

Compared to other +RNA viruses, most nidoviruses have exceptionally large genomes (from 20 to over 30 kilobases (kb)), but arteriviruses form a special lineage (Fig. 1) with genomes of about 13-16 kb in length [37, 38]. Nidoviruses have a characteristic polycistronic genome organisation and employ a unique mechanism of discontinuous RNA synthesis to express the ORFs located downstream of the replicase ORF1ab (see Fig. 2). They generate a nested set ('nidus' is Latin for nest) of subgenomic (sg) mRNAs encoding these structural and accessory proteins. The sg mRNAs are 3' co-terminal but they also contain a common 5' leader sequence. The leader and "body" segments of the sg RNAs are joined during discontinuous negative strand RNA synthesis, which produces a sg-length template for each of the sg mRNAs [39, 40].

The nidovirus replicative cycle (see Fig. 3) starts with the translation of the viral genome by host ribosomes, which results in the expression of two large replicase polyproteins (pp1a and pp1ab). Translation of the larger pp1ab from open reading frame 1ab (ORF1ab) involves a -1 ribosomal frameshift (RFS) near the 3' end of ORF1a, a regulatory mechanism that probably evolved to ensure lower expression levels of ORF1b-encoded proteins compared to ORF1a-encoded nsps [42-44]. To derive the mature replicase proteins, the two polyproteins are subsequently processed by virally-encoded papain-like accessory proteases (PLP1 and/or PLP2) and a chymotrypsin-like main protease (MP; also referred to as 3C-like protease) into 13 to 16 non-structural proteins (nsps; or collectively referred to as 'the replicase') [45-47]. A schematic overview of the EAV and SARS-CoV replicase is given in Fig. 2. These replicase subunits contain a variety of (enzymatic) activities and functions required for viral RNA synthesis and capping [45, 46], like helicase and RNA-dependent RNA polymerase (RdRp) functions. The presence of an endoribonuclease, located in arterivirus nsp11 and coronavirus nsp15, is a conserved feature of vertebrate nidoviruses [48], while an exoribonuclease domain was identified in most nidoviruses, with the exception of arteriviruses [49]. The latter was postulated to promote the fidelity of RdRp-mediated RNA synthesis, since in the case of coronaviruses inactivation of ExoN activity resulted in a ~15-fold increase of the error rate during viral genome replication. Consequently, this activity was postulated to contribute to a primitive form of RNA proofreading [50, 51], although the mechanistic details of ExoN function remain to be elucidated.

Nidoviruses encode their own RdRp which is crucial for viral RNA synthesis, as the host cell only contains DNA-dependent RNA polymerases that are responsible for the transcription of cellular mRNAs, tRNAs and ribosomal RNAs. The viral RdRp, the helicase,

and other replicase proteins, together with recruited host cell proteins, form membrane-associated replication/transcription complexes (RTCs; [52, 53]), which localise to virus-induced replication structures in the perinuclear region of the infected cell [29-36].

Nidovirus infection causes the extensive remodelling of intracellular membranes into a structure that has been described as a reticulovesicular network (RVN) of modified endoplasmic reticulum (ER), which is continuous with its membrane donor and includes double-membrane vesicles (DMVs). EAV DMVs are ~100 nm in size, while for coronaviruses much larger DMVs have been reported with a diameter of up to 300 nm.

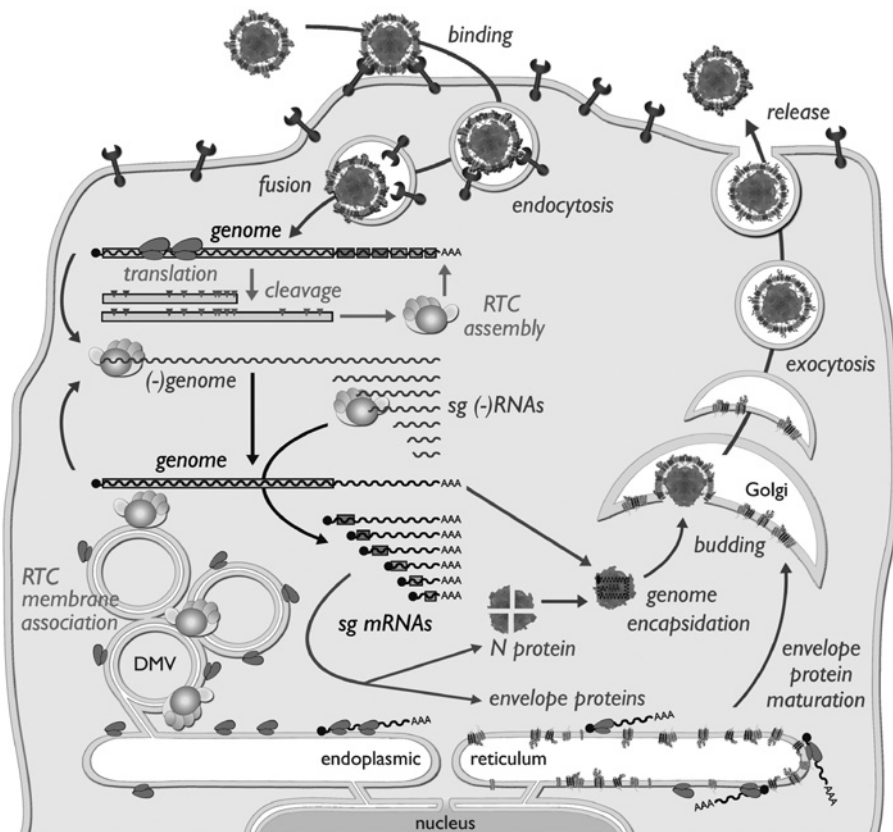


Fig. 3 - Schematic overview of the nidovirus replicative cycle. Following entry by receptor-mediated endocytosis and release of the genome into the cytosol, genome translation yields the pp1a and pp1ab replicase polyproteins. Following polyprotein cleavage by multiple internal proteases, the viral nsps assemble into a replication/transcription complex (RTC) that engages in minus-strand RNA synthesis. Both full-length and subgenomic (sg)-length minus strands are produced, with the latter templating the synthesis of sg mRNAs required to express the structural protein genes in the 3'-proximal quarter of the genome. Ultimately, novel genomes are packaged into nucleocapsids that become enveloped by budding from smooth intracellular membranes, after which the new virions leave the cell by following the exocytic pathway. See text for more details. Reprinted with permission from [41].

In the case of coronaviruses, also convoluted membranes (CM) and vesicle packets, apparently arising from the merger of DMVs, were described. On the basis of ultrastructural studies, including electron tomography, all these membrane structures were concluded to be derived from and continuous with the ER [29, 30]. Nevertheless, other studies have suggested late endosomes and autophagosomes [32, 54], or EDEMosomes [55] to be the source of these membranes. The membrane association of nidovirus RTCs likely provides a scaffold for their assembly, might constitute a suitable environment for RNA synthesis, or could play a role in evading the innate immune response [29, 30, 52, 53]. Although the role(s) of cellular membranes in nidovirus replication remain(s) far from understood, they may shield the viral RNA, in particular double-stranded RNA (dsRNA) that is formed as an intermediate of viral replication, from detection by innate immune sensors [30]. The modified membrane structures might also play a role in increasing the local concentration of (membrane-associated) proteins and other components required for efficient replication [56]. The membrane-associated RTCs synthesise a full-length negative-stranded RNA that serves as template for genome synthesis. In addition, discontinuous RNA synthesis generates a set of negative-stranded sg-length templates [39], which serve as templates for sg mRNA synthesis (Fig. 2). Encapsidation of the newly synthesised genome by the nucleocapsid (N) protein and assembly by budding of nucleocapsids into the lumen of pre-Golgi (ERGIC) compartments is followed by the release of infectious virus into the extracellular space via the exocytic pathway [57-59].

NIDOVIRUS-HOST INTERACTIONS

+RNA viruses interact with the infected host cell at many levels during their replicative cycle. Thus far, a handful of host cell proteins with a role in virus replication have been identified [60-65]. Host factors play a role in virtually all steps of the nidovirus life cycle, including viral entry, gene expression, RNA synthesis and virus release. Moreover, host factors are targeted or hijacked to modulate host gene expression and antiviral defences, to create a more suitable environment for viral replication. The interaction with the infected host also plays a decisive role in pathogenesis and the outcome of infection. This paragraph presents a brief overview of some of the host factors and processes that are involved in or affected by nidovirus infection.

The effect of nidovirus infection on the host cell's translation machinery

Several +RNA viruses were reported to interfere with host protein synthesis to limit the translation of cellular mRNAs and favour the synthesis of viral proteins, resulting in the most favourable conditions for viral replication and the production of infectious progeny (as reviewed in [66]). Protein synthesis is a process that is critical for the viral replicative

cycle, as well as for the host cell to be able to respond to infection by mounting an antiviral (innate) immune response. In eukaryotic cells, translation is initiated by formation of the heterotrimeric eIF2 complex, which is composed of the regulatory α -subunit, the tRNA-binding β -subunit, and a GTP-binding γ -subunit. The eIF2 complex is responsible for loading of the 40S subunit with Met-tRNA_i, followed by the recruitment of the cap-binding complex eukaryotic translation initiation factor 4F (eIF4F) to this pre-initiation complex. The 43S complex then serves as a scaffold for the binding of several additional proteins, including eIF3, to the capped 5' end of the mRNA. Upon this activation step, the 43S pre-initiation complex attaches to the mRNA and scans in the 5' to 3' direction for a translation initiation codon. At this point, the 60S subunit joins and protein synthesis starts (reviewed in [67]). Poly(A)-binding protein (PABP), which binds to the poly(A)-tail of mRNAs, is also involved in stimulating protein synthesis.

The eIF2 complex is inactivated by phosphorylation of its alpha subunit (eIF2 α). This step can be carried out by four mammalian kinases in response to various (external) triggers. These are the PKR-like endoplasmic reticulum kinase (PERK), eukaryotic translation initiation factor 2- α kinase 4 (also known as GCN2), heme-regulated inhibitor (HRI), and double-stranded RNA-activated protein kinase (PKR). The latter is a serine/threonine protein kinase that is activated by dsRNA, a hallmark of viral infection. PKR is a key player in the innate immune response to virus infection by inducing upregulation of antiviral gene expression, including the production of interferons (IFNs).

Viruses have evolved various strategies to counteract PKR-mediated antiviral immune signalling [68]. Coronaviruses appear to modulate the cellular translation machinery to their own benefit, as for example infectious bronchitis virus (IBV) appears to (weakly) antagonise the antiviral activity of PKR through two independent mechanisms: a block of PKR activation was observed and the expression of growth arrest and DNA-damage-inducible 34 protein (GADD34) was induced in infected cells [69]. Both processes reduce phosphorylation of eIF2 α in IBV-infected cells [69]. Also transmissible gastroenteritis virus (TGEV) has been reported to modulate the host cell's translation machinery through its protein 7, which regulates the dephosphorylation of eIF2 α through an interaction with protein phosphatase 1 (PP1). PP1 is a key regulator of the host antiviral response and its inhibition by TGEV protein 7 leads to a reduction in cytopathicity [70]. The S proteins of both SARS-CoV and IBV were found to physically interact with eIF3F, to modulate host translation, and the expression of pro-inflammatory cytokines interleukin 6 (IL-6) and IL-8 at a later stage of infection [71]. Therefore, this interaction may play an important regulatory role in coronavirus pathogenesis.

The SARS-CoV N protein was shown to associate with eIF1 α to block protein translation and cell proliferation, and SARS-CoV nsp1 was identified as a eukaryotic translation inhibitor that represses multiple steps of translation initiation. SARS-CoV nsp1 does so by inhibiting 48S initiation complex formation and interfering with the conversion of

the 48S complex into the 80S initiation complex [72]. In addition, the multifunctional SARS-CoV nsp1 is also able to directly bind the 40S subunit to inhibit its function in translation [73]. This nsp1-40S subunit complex is furthermore able to induce cleavage of cellular mRNA to reduce cellular translation to an even larger extent [74].

Taken together, modulation of host protein synthesis through different and often multiple mechanisms has a profound effect on the cell and 'viral translation modulators' likely contribute to coronavirus pathogenicity.

Nidovirus-induced rearrangement of host cell membranes

As outlined above, a common characteristic of +RNA viruses is the fact that their replication takes place in the cytoplasm of the infected cell and is intimately associated with virus-induced membrane structures (reviewed in [28, 56, 75]). In general, virus-induced membrane alterations can be divided into two different types of structures: single-membrane invaginations with negative membrane curvature and positively curved convoluted tubular-vesicular membrane networks. For a recent review, see [28]. In the case of membrane invaginations, the replication machinery is located on the inside of the invagination and the replication compartment is connected to the cytoplasm by an opening wide enough to allow the in-flow of nucleotides and export of synthesised RNA. Examples are the structures induced by Dengue virus (DENV), West Nile virus, Flock House virus and Semliki Forest virus, for which RNA synthesis appears to take place within membrane invaginations originating from either the ER [76, 77], the outer mitochondrial membrane [78], or the plasma membrane [79].

In tubular-vesicular replication structures, the viral replicase is (for most viruses) assumed to be localised to the external membranous surface facing the cytoplasm. Viruses like poliovirus and HCV induce complex networks of modified membranes, such as protrusions originating from cis-Golgi membranes or the ER that transform from single-membrane tubular compartments into double-membrane structures [80, 81]. Also nidoviruses belong to the group that induces the formation of tubular-vesicular replication structures [29-31]. For nidoviruses, however, convincing evidence about the exact localisation of viral RTCs is still lacking. Within the RVN of SARS-CoV-infected cells, dsRNA was particularly found inside DMVs while the majority of the viral replicase subunits colocalised with the CMs [30]. Furthermore, DMVs in SARS-CoV-infected cells appear to be sealed, which poses the question how export of newly synthesised RNA from the interior of DMVs is organised [30].

This division according to membrane alterations induced may reflect an evolutionary divergence between +RNA virus groups and suggests that the mechanisms of membrane remodelling may be significantly different among +RNA viruses [28].

Nidovirus-induced cell cycle deregulation

The cell cycle is a series of highly regulated events that lead to cell division, and the process can be divided into four distinct phases: G1, S, G2, and M. The first three phases are collectively referred to as the interphase, and the M phase stands for mitosis, the actual cell division [82]. The regulation of the cell cycle involves processes that are crucial to the survival of a cell, as well as the prevention of uncontrolled cell division. The molecular events that control the cell cycle are ordered, directional and highly regulated by cyclin-dependent protein kinases (CDKs). Passage through the cell cycle requires activation of the different CDKs by e.g. cyclin regulatory subunits. To promote cell cycle progression towards the replication of DNA, CDK/cyclin complexes phosphorylate proteins which triggers and activates DNA replication [83].

Like many other viruses (reviewed in [84]), nidoviruses have been shown to extensively manipulate and arrest cell cycle progression to benefit from the physiological state of the cell when it is arrested in that specific phase. For example, IBV-infected cells were shown to go into cell cycle arrest in the S phase, by activating the cellular DNA damage response [85]. This is beneficial to virus replication since factors that are normally needed for DNA replication and are upregulated in the S phase, are now recruited to the cytoplasm by the virus. For example, DDX1, a cellular RNA helicase of the DExD/H family, interacts with coronavirus nsp14 [86] and was reported to be hijacked to enhance efficient coronavirus replication. Bhardwaj *et al.* have shown that coronavirus nsp15 interacts with retinoblastoma protein (pRb) and thereby inhibits the function of this protein, resulting in the enhanced expression of genes that are normally repressed by pRb and in an increased proportion of cells in the S phase of the cell cycle [87]. Similar effects have been observed in MHV-infected cells, which showed decreased hyper-phosphorylation of pRb, an event that is necessary for the progression from the G1 towards the S phase [88, 89].

Nidoviruses modulate host innate immune responses

During infection, there is a continuous interplay between the virus and the infected host. Cells respond to infection by mounting an antiviral response, which in the case of +RNA viruses is often triggered by the dsRNA molecules that are formed as intermediates during viral RNA replication. These dsRNA molecules are foreign to the cell and can be recognised by the intracellular sensors of the Rig-I-like receptor (RLR) family, like retinoic acid-inducible gene 1 (RIG-I) and melanoma differentiation-associated protein 5 (MDA-5) (reviewed in [90]). Activation of these sensors eventually leads to the activation of transcription factor IFN-regulatory factor 3 (IRF3). This transcription factor upregulates the expression of IFN- β , which in turn activates the JAK-STAT signalling cascade that induces the expression of antiviral interferon-stimulated genes (ISGs). This ultimately

Table 1. Examples of RNA-binding proteins described for nidoviruses. (Abbreviations: PABP: poly(A)-binding protein; PCBP: poly(C)-binding protein; hnRNP: heterogeneous nuclear ribonucleoprotein; PTB: polypyrimidine tract-binding protein; MADP1: zinc finger CCHC-type and RNA-binding motif 1; DDx: DEAD-box protein; BCov: bovine coronavirus)

Protein	Nidovirus	Cellular function	(Proposed) Function in viral RNA synthesis	Reference
PABPs	BCov, TGEV, PRRSV	RNA-binding protein that binds to the poly(A) tail of cellular mRNA. Involved in mRNA translation	Binds to the 3'end of the viral genome. Signal for genome replication.	[115-117]
PCBP1, PCBP2	PRRSV	RNA/DNA binding proteins involved in RNA metabolism	Binds to PRRSV nsp1 β . Regulatory role in viral RNA replication.	[118]
hnRNP A0	TGEV	Involved in RNA splicing	Binds the 3'end of the viral genome.	[116]
hnRNP A1	MHV, SARS-CoV, TGEV	Involved in RNA transport, processing, and splicing.	Binds the 3'end of the viral genome.	[116, 119-122]
hnRNP A2B1	TGEV	Involved in RNA transport and splicing.	Binds the 3'end of the viral genome.	[116, 123]
hnRNP Q	TGEV	Involved in RNA processing and splicing.	Binds the 3'end of the viral genome.	[116]
hnRNP U	TGEV	Involved in RNA processing and splicing.	Binds the 3'end of the viral genome.	[116]
p100 kDa coactivator	EAV, TGEV	Involved in transcription and RNA interference.	Binds the 3'end of the TGEV genome, and binds to EAV nsp1.	[116, 124]
Annexin A2	IBV	Cellular RNA-binding protein.	Modulates IBV frameshifting efficiency.	[125]
Mitochondrial Aconitase	MHV	Component of the citric acid cycle, converts citrate into isocitrate.	Binds the 3'end of the viral genome.	[126]
MADP1	SARS-CoV, IBV	Involved in RNA splicing.	Binds the 5'end of the viral genome. Exact function in RNA synthesis currently unknown.	[127]
PTB	TGEV, SHEV, MHV	Involved in RNA splicing.	Binds the 3'end of the viral genome. Regulates viral transcription.	[116, 128, 129]

results in an antiviral state of the infected cell and neighbouring cells. ISGs were shown to target virtually all steps in the viral cycle in order to restrict viral replication [91].

Innate immune signalling pathways are extensively regulated by ubiquitination. A number of proteins involved in signal transduction – e.g. RIG-I, TANK-binding kinase 1 (TBK1), and TNF receptor-associated factor 3 (TRAF3) – were recently shown to be activated by Lys63-linked ubiquitination [92]. Notably, ubiquitin-mediated regulation offers excellent possibilities for negative feedback and viral immune evasion, since ubiquitination can be reversed by deubiquitinating enzymes (DUBs). Viruses have evolved a multitude of mechanisms to evade or counteract the innate immune response (reviewed in [93]). Like many other +RNA viruses, nidoviruses express several proteins that have been implicated in immune evasion. First of all, the coronavirus papain-like protease 2 domain (PL2^{pro}) [94–97] and the TGEV PL1^{pro} domain [98] within nsp3 were shown to harbour deubiquitination (DUB) activity. This DUB activity may remove ubiquitin from innate immune signalling factors to suppress the induction of an antiviral state, and indeed was shown to reduce IFN signalling [96, 99]. A similar DUB activity has been described for the arteriviruses EAV and PRRSV. The PLP2 domain in nsp2 has potent *in vitro* DUB activity [100, 101], and compared to wt EAV, infection with an EAV mutant that lacks this DUB activity resulted in an increased innate immune response [102].

A multitude of SARS-CoV nsps, structural and accessory proteins [103] and also many other nidovirus proteins have been implicated in blocking IFN-mediated signalling through a variety of mechanisms. Besides inhibition of cellular mRNA translation (see above), SARS-CoV nsp1 was shown to block IFN signalling by reducing the amount of phosphorylated STAT1 (p-STAT1) in infected cells [104]. In addition, the SARS-CoV ORF6 protein [105, 106] and PRRSV nsp1 β [107, 108] were shown to block p-STAT1 import into the nucleus, and this block was suggested to reduce the expression of genes that affect virus-induced pathogenesis. Similar observations regarding the blocking of IFN signalling were made for the ORF3b protein of SARS-CoV [106] and SARS-like CoVs [109], SARS-CoV nsp7, nsp15, and N protein [110], albeit that the mechanism by which these proteins block IFN signalling is not fully understood.

TBK1 was shown to be a target of both MHV PLP2 [95, 111] and the SARS-CoV membrane (M) protein [112]. MHV PLP2 deubiquitinates and binds TBK1, as well as IRF3, and SARS-CoV M protein binds TRAF1 to prevent binding of TRAF1 to TBK1 and eventually to prevent nuclear translocation of this complex to block IRF3-mediated signalling. SARS-CoV PL^{pro} was shown to interact with IRF-3, to inhibit phosphorylation and nuclear translocation of IRF-3, thereby disrupting the activation of type I IFN responses [113].

Host factors directly involved in viral RNA synthesis

Another class of host factors involved in viral replication are the RNA-binding proteins. The 3' and 5' end of viral RNA genomes contain key regulatory elements for their replica-

tion [114], and albeit that the precise role of host factors interacting with these signals is in general poorly understood, RNA-binding proteins have been identified as frequently used enhancers of viral RNA synthesis. A summary of proteins that are known to bind nidovirus RNAs is listed below (Table 1).

DIRECT-ACTING AND HOST-DIRECTED ANTIVIRALS FOR INHIBITING NIDOVIRUS INFECTION

Antiviral research efforts have resulted in prophylactic or therapeutic possibilities, including vaccines and antiviral drugs, to combat the diseases caused by a small number of human pathogens. Despite these efforts, HCV is the only +RNA virus for which specific antiviral drugs have currently been approved. Antiviral drugs can be divided into direct-acting antivirals (DAA) and host-directed antivirals (HDA). Most antivirals are DAAs and inhibit essential processes in the viral replicative cycle. However, when using DAAs antiviral drug resistance is a serious problem, in particular when combating RNA viruses, due to their high mutation rate and potential for rapid adaptation. Thus, the possibility to target host factors rather than viral proteins is receiving increasing attention as an alternative approach (reviewed in [130, 131]). In contrast to DAA-based therapy, the use of drugs targeting host factors should not lead to drug resistance.

The previous paragraphs summarised how nidoviruses have evolved multiple mechanisms to hijack or manipulate cellular components and pathways to promote their efficient replication. Insight into these virus-host interactions does not only yield valuable information on the molecular details of the nidovirus replicative cycle, but can also be a starting point for the development of antiviral strategies. However, one should keep in mind that targeting host factors can have cytotoxic or other undesirable side-effects. Below, first the application of some of the more classical antiviral approaches to the inhibition of nidoviruses will be discussed, and subsequently the possibilities, advantages and disadvantages of targeting host factors will be evaluated.

Neutralising antibodies and viral entry or fusion inhibitors

The early stages of nidovirus infection can be blocked by virus neutralisation or by interfering with viral entry into host cells. Coronavirus entry is mediated by an interaction of the S protein with its entry receptor, which is the angiotensin converting enzyme 2 (ACE2) for SARS-CoV. During the early phase of the SARS-CoV outbreak, convalescent plasma, obtained from recovered SARS patients, was transferred to newly infected SARS patients, which resulted in a significant drop in viral load and a higher discharge rate from the hospital. This demonstrates that neutralising antibodies can protect against SARS-CoV [132, 133]. However, the amount of convalescent plasma is limited since

blood from persons that have recovered from SARS is needed. To circumvent this, recombinant human antibodies against the SARS-CoV S protein – using human antibodies might reduce the side effects in patients – have been made, and were shown to block the S-ACE2 interaction (reviewed in [134]). For example, Ter Meulen *et al.* and Van den Brink *et al.* have shown that anti-SARS-CoV S antibodies neutralise SARS-CoV in cell culture and in a ferret animal model. Prophylactic administration of (a combination of) these human monoclonal antibodies reduced replication of SARS-CoV in the lungs of ferrets, completely prevented the development of SARS-CoV-induced lung pathology and abolished virus shedding [135-137].

Another class of compounds that block viral entry are inhibitors of vacuolar (or endosomal) acidification, like ammonium chloride and the FDA-approved anti-malaria drug chloroquine. These compounds, in cell culture and in animal models, has been shown to block the entry of nidoviruses [138-143], including SARS-CoV [144].

Since SARS-CoV is an enveloped virus, fusion of the viral envelope with cellular membranes is needed for entry into host cells. Virus binding is mediated by the interaction of the receptor binding domain in the S1 region of the S protein with the ACE2 receptor. The S2 region contains heptad repeat 1 (HR1) and HR2 domains, which play an important part in SARS-CoV fusion with target cells. Binding of the receptor-binding domain (RBD) of S1 to the receptor ACE2 triggers a conformational change of the S2 region from a pre-fusion form to a fusogenic form, resulting in insertion of the putative fusion peptide into the target cell membrane and association of HR1 and HR2 domains to form a six-helix bundle fusion core structure. This brings the viral envelope and target cell membrane into close proximity for fusion [145].

Many laboratories have tried to develop strategies that block this fusion step. These include inhibitors, e.g. peptides that block the interaction between HR1 and HR2 to prevent the formation of a fusogenic complex or by blocking S protein oligomerisation (reviewed in [145]).

Viral protease inhibitors

Viral proteases play a crucial role in the processing of polyproteins into active viral replicase subunits, a strategy that is employed by many viruses. Therefore, proteases are classical targets for the development of antiviral therapies, e.g. against human pathogens like HCV and HIV-1 (for recent reviews, see [146, 147]).

Nidovirus proteases, like the main protease that mediates many steps in polyprotein processing, have crucial roles in the viral replication cycle. For this reason, these proteases are interesting drug targets and many research groups have attempted to identify or develop protease inhibitors that are either SARS-CoV nsp5-specific or broadly active against coronavirus main proteases. Several small-molecule inhibitors or peptide-like protease inhibitors have been reported to effectively block protease activity *in vitro* and

infection in cell culture at concentrations in the low-micromolar range [148-152]. The SARS-CoV papain-like protease (PL^{pro}) was shown to also harbour immune evasion properties (see above) by inhibiting IRF3-mediated signalling [113]. The compound GRL0617 yielded promising results regarding its inhibitory effect on SARS-CoV replication, presumably by targeting this function of PL^{pro} [153]. These developments make it clear that targeting nidovirus proteases may be an interesting strategy to block viral replication.

Inhibitors of the viral polymerase and other viral proteins

A unique feature of +RNA viruses, including nidoviruses, is the synthesis of new viral RNA from an RNA template, which is performed by a virus-encoded RdRp. Thus, targeting the viral polymerase is a straightforward approach for antiviral therapy. A first class of RdRp inhibitors are the nucleoside analogues, which are incorporated into the newly synthesised viral RNA and abrogate RNA synthesis or lead to the accumulation of a lethal number of mutations. In view of the lack of known inhibitors of coronavirus replication, Ribavirin, a well-known nucleoside analogue, was used during the 2003 SARS outbreak, since this purine analogue showed potent, broad antiviral activity against several other +RNA viruses like HCV [154]. However, there is conflicting data on the effectiveness of Ribavirin against SARS-CoV infection in cell culture [155-157] and *in vivo* [157, 158]. Furthermore, treatment of infected cells with a combination of Zn²⁺ and the zinc-ionophore pyrithione was shown to block replication of SARS-CoV and EAV, possibly by impairing RdRp activity [159]. Recently, Liu *et al.* showed that peptides that target the PRRSV polymerase can block replication, which suggests that peptides that target nidovirus nsps could form the basis for antiviral strategies [160].

The viral helicase has been shown to play an important role in the nidovirus replicative cycle, and therefore is another interesting target for antiviral therapy. Several studies identified antivirals that are directed to the SARS-CoV helicase and inhibited SARS-CoV replication in cell culture. A screen by Kao *et al.* identified HE602 as a potent SARS-CoV helicase inhibitor, and this compound reduced SARS-CoV plaque formation with an IC₅₀ of 6 µM. Tanner *et al.* identified bananins as SARS-CoV helicase inhibitors [161]. These compounds block SARS-CoV replication with an IC₅₀ of less than 10 µM without any cytotoxicity at high concentrations. Yang *et al.* showed that bismuth complexes effectively block SARS-CoV replication by inhibiting both the unwinding and ATPase activities of the SARS-CoV helicase [162, 163]. Later on, several other helicase inhibitors, like Myricetin and Scutellarein (IC₅₀s of 2.71 and 0.86 µM, respectively), were identified [164]. These inhibitors specifically block the ATPase function of the helicase. SSYA10-001 and aryl diketo acids block the helicase unwinding activity [165], however these compound were not tested in cell culture, so their effect on virus replication remains to be analysed. Furthermore, Liu *et al.* showed that several helicase-directed peptides could be used as PRRSV antiviral agents, although this was not further explored.

A few small molecules were reported to inhibit the MT activity of SARS-CoV nsp16, such as S-adenosyl-L-homocysteine, Sinefungin [166] and aurintricarboxylic acid [167]. Furthermore, two peptides were identified that inhibit the methyltransferase activity of SARS-CoV nsp16 [168].

The only coronavirus structural protein of which the function can thus far be blocked by small-molecule inhibitors is the envelope (E) protein, which mediates viral assembly and morphogenesis. Hexamethylene amiloride was recently shown to inhibit HCoV-229E and MHV replication by blocking E protein function, suggesting that the nidovirus E protein could be used as drug target as well [169].

Antisense morpholino oligomers and RNAi approaches to block nidovirus replication

A different class of molecules that can block virus replication are peptide-conjugated antisense phosphorodiamidate morpholino oligomers (P-PMOs). These molecules, which are resistant to cellular nucleases, are designed to target viral genome sequences and inhibit viral gene expression by a steric blockade. Two P-PMOs targeting the SARS-CoV leader TRS region in the 5' untranslated region appeared most effective, however after several passages escape mutants were observed [170]. Nevertheless, the use of these P-PMOs in an animal model for MHV showed the potency of these molecules *in vivo* [171]. Another study by Ahn *et al.* showed that an antisense nucleic acid oligomer that prevented the -1 RFS suppressed SARS-CoV replication in cell culture [172]. These P-PMOs have also been shown to block arterivirus replication. P-PMOs that are directed to the 5'UTR of the EAV genome showed a significant block in virus amplification in the low micromolar range [173]. PRRSV replication in cell culture appeared also sensitive to treatment with P-PMOs that are directed towards the 5'UTR of the viral genome [174-176]. PRRSV-infected piglets showed reduced viremia, and elevated levels of antiviral genes in P-PMO-treated piglets, suggesting that using these P-PMOs could be considered as PRRSV control strategy [177].

Through a mechanism known as RNA interference (RNAi), small interfering RNA (siRNA) molecules can target complementary (viral) mRNA strands for degradation, and can thus specifically target viral mRNAs in infected cells. The ability of siRNAs to inhibit viral gene expression offers a mechanism that can be exploited for novel therapeutics. *In vitro* experiments have shown for multiple nidoviruses that blocking infection using RNAi might also be a viable approach [178-182]. Although currently not applicable in humans, the use of RNAi in animal models has shown some potential to combat +RNA viruses that cause respiratory disease (reviewed in [183, 184]), including SARS-CoV [185, 186]. However, several hurdles have to be taken, since targeting of specific tissues and reaching effective levels of siRNAs are still challenges that have to be addressed.

Currently, most assays using antisense oligonucleotides (P-PMOs or siRNAs) have been applied to directly target nidovirus replication, however these molecules can also be used to target host factors that are involved in virus replication. As mentioned before, targeting host factors might cause a higher barrier for the development of viral resistance, although the chance of developing side effects might also increase upon depletion of host factors.

Corticosteroids and IFN as immunomodulatory antiviral agents

The use of the immunomodulatory corticosteroids to treat SARS patients is controversial and remains debated. Administration of high doses of corticosteroids to SARS patients, mostly in combination with Ribavirin, hardly showed any effect and serious side-effects, including progressive viral infection, have been observed (reviewed in [187]).

In this respect, the antiviral effect of the immunomodulatory agent IFN is more promising. IFN was shown to trigger the innate immune response by the transcription of ISGs that have a role in combating virus infection. ISG expression results in an antiviral state of infected and neighbouring non-infected cells, to limit virus replication and spread [91]. IFN is a registered drug for the treatment of HCV, and is also explored as antiviral agent for nidoviruses (in particular for SARS-CoV and MERS-CoV). Treatment with type I IFNs inhibits coronavirus replication in cell culture [188-192] and, for example, protected type I pneumocytes against SARS-CoV infection in macaques [190]. This inhibition was observed despite the immune evasive properties of the SARS-CoV ORF6 protein that inhibits IFN signalling by blocking the nuclear translocation of p-STAT1, which is essential for transcriptional activation of downstream antiviral genes. Despite the potency of IFN as antiviral agent, HCV treatment with IFN triggered the development of side effects like fatigue, malaise, apathy, and cognitive changes in several patients [193].

Concluding remarks

This paragraph summarises (potential) antiviral strategies for the treatment of infections with nidoviruses, in particular SARS-CoV. Most strategies are aimed towards targeting the virus directly, and in many cases, replication was effectively blocked in cell culture. Currently, intervention strategies for nidoviruses in humans have not been approved yet, and some of the abovementioned approaches might form a basis for the development of such strategies. As mentioned before, there is a high risk of development of resistance when the viral structural proteins or replicase subunits are targeted, as exemplified by the development of escape mutants by only a few mutations upon using e.g. neutralising antibodies [194]. Multiple studies have identified host factors that are involved in nidovirus replication (reviewed in [65]), and these might be suitable targets for the development of HDAs. The observation of the development of resistance against

single-DAA treatments would argue for the development of HDAs and combination therapies using both DAAs and HDAs as an effective intervention strategy.

OUTLINE OF THIS THESIS

In this thesis, the interplay between nidoviruses and the infected host cell was investigated, to better understand virus replication and hopefully provide additional starting points for the development of antiviral strategies. **Chapter 2** describes the partial purification of active EAV RTCs from infected cells and the development of an *in vitro* assay for EAV RNA synthesis. Arterivirus RNA-synthesising activity was shown to depend on intact membranes, and isolation of RTCs by using differential centrifugation showed that viral RNA synthesis is dependent on a cytosolic host protein with a mass between 59 and 70 kDa, which does not cosediment with the RTC.

In **chapter 3**, the *in vitro* assay described in chapter 2 was used to identify the immunosuppressant drug cyclosporin A (CsA) as an inhibitor of EAV RNA synthesis. This chapter also shows that CsA blocks replication of EAV and the swine arterivirus PRRSV in cell culture. Cyclophilin A (CypA) appears to be an important host factor for EAV replication since its depletion reduced the production of EAV progeny.

CsA may be a nidovirus-wide inhibitor of replication since this compound also blocked coronavirus replication. **Chapter 4** describes that SARS-CoV, HCoV-229E, and mouse hepatitis virus (MHV) replication in cell culture is effectively blocked by CsA treatment. However, knockdown of either CypA or CypB did not reduce SARS-CoV replication, leaving the possibility that CsA blocks replication of different nidoviruses via different mechanisms.

Chapter 5 describes an siRNA library screen that aimed to identify cellular kinases and signalling pathways involved in the SARS-CoV replicative cycle. In total, ninety antiviral and forty proviral hits were found. Two factors that were identified as hits in the primary screen – PKR as antiviral and COPB2 as proviral factor – were validated in follow-up experiments. Depletion of PKR resulted in enhanced SARS-CoV replication and increased release of SARS-CoV progeny. COPB2 knockdown severely reduced SARS-CoV replication and release of virus progeny, and implicated COP-I coated vesicles in virus replication. The identification of proviral and antiviral factors in the siRNA screen enhances our understanding of the replication of SARS-CoV and coronaviruses in general, and may define novel targets for coronavirus antiviral therapy.

We also investigated (**chapter 6**) the replication characteristics of the recently identified MERS-CoV, including the kinetics of viral RNA synthesis and viral progeny release, and demonstrated that viral RNA synthesis is associated with the virus-induced membrane structures.

Furthermore, we describe an assay to measure MERS-CoV-induced cytopathology and its application to the screening for compounds that block MERS-CoV infection. CsA was identified as a potential anti-MERS-CoV compound in this assay. In addition, treatment with pegylated IFN- α (PEG-IFN) significantly inhibited infection, and MERS-CoV was shown to be much more sensitive to PEG-IFN treatment than SARS-CoV, an observation that may have implications for the treatment of MERS-CoV infection. Finally, **chapter 7** summarises the findings that are described in this thesis.

Chapter 2

The *in vitro* RNA synthesizing activity of the isolated arterivirus replication/transcription complex is dependent on a host factor

Martijn J. van Hemert, Adriaan H. de Wilde,
Alexander E. Gorbalenya, and Eric J. Snijder

J. Biol. Chem. (2008) vol. 283, no. 24, pp. 16525–16536

Reprinted with permission

ABSTRACT

The cytoplasmic replication of positive-stranded RNA viruses is associated with characteristic, virus-induced membrane structures that are derived from host cell organelles. We used the prototype arterivirus, equine arteritis virus (EAV), to gain insight into the structure and function of the replication/transcription complex (RTC) of nidoviruses. RTCs were isolated from EAV-infected cells and their activity was studied using a newly developed *in vitro* assay for viral RNA synthesis, which reproduced the synthesis of both viral genome and subgenomic mRNAs. A detailed characterization of this system and its reaction products is described. RTCs isolated from cytoplasmic extracts by differential centrifugation were inactive unless supplemented with a cytosolic host protein factor, which - according to subsequent size fractionation analysis - has a molecular mass in the range of 59-70 kDa. This host factor was found to be present in a wide variety of eukaryotes. Several EAV replicase subunits cosedimented with newly made viral RNA in a heavy membrane fraction that contained all RNA-dependent RNA polymerase activity. This fraction contained the characteristic double membrane vesicles (DMVs) that were previously implicated in EAV RNA synthesis and could be immunolabeled for EAV nonstructural proteins (nsps). Replicase subunits directly involved in viral RNA synthesis (nsp9 and nsp10) or DMV formation (nsp2 and nsp3) exclusively cosedimented with the active RTC. Subgenomic mRNAs appeared to be released from the complex, while newly made genomic RNA remained more tightly associated. Taken together, our data strongly support a link between DMVs and the RNA-synthesizing machinery of arteriviruses.

INTRODUCTION

Positive-strand RNA viruses form the largest group of animal viruses and include many important human pathogens, like poliovirus, hepatitis A and C virus, dengue virus, yellow fever virus, West Nile virus and various human coronaviruses. Although these viruses differ in many aspects of their biology, including genome size, organization, and expression strategy, they are united by the fact that their RNA genome is replicated by cytoplasmic enzyme complexes. These complexes are associated with virus-induced membrane structures that are derived from host cell organelles (for reviews see [75, 195, 196]). Such membrane structures might function as scaffold for the replication machinery, provide a suitable microenvironment for viral RNA synthesis, serve to recruit membrane-bound host proteins, and/or provide protection against the host cell's antiviral responses (e.g. RNA degradation or responses triggered by the double-stranded (ds) RNA intermediates of viral RNA synthesis).

Nidoviruses (corona-, roni-, and arteriviruses) have exceptionally large polycistronic RNA genomes and employ a unique transcription mechanism to produce a nested set of subgenomic (sg) mRNAs. Therefore, among positive-strand RNA viruses, nidovirus RNA synthesis is considered to be of unparalleled complexity [37, 196]. In nidovirus-infected cells, newly synthesized viral RNA and many replicase subunits were found to colocalize in discrete foci in the perinuclear region [32, 33, 35, 197-208]. Electron microscopy of this area revealed the presence of large numbers of typical paired membranes and double membrane vesicles (DMVs) [31, 32, 35, 201, 208-212]. For the coronaviruses mouse hepatitis virus (MHV) and SARS-coronavirus (SARS-CoV) and the arterivirus equine arteritis virus (EAV), immunoelectron microscopy revealed that both viral nonstructural proteins (nsps) presumed to be part of the replication/transcription complex (RTC) and de novo made viral RNA are associated with these membranes [31, 32, 35, 201]. Based on these results, DMVs have been postulated to carry the enzyme complex that is responsible for nidovirus replication and sg mRNA synthesis.

One of the best studied nidovirus models is the arterivirus prototype EAV, which has been used extensively to study both replicase functions and the mechanism of nidovirus RNA synthesis. Of the 12.7 kb EAV genome (RNA1) 75% is occupied by the large replicase gene that consists of the open reading frames (ORFs) 1a and 1b. The EAV replication cycle starts with the translation of RNA1 to synthesize two large replicase polyproteins: the 1727-aa ORF1a-encoded pp1a and the 3175-aa pp1ab, which is synthesized after a -1 ribosomal frameshift that occurs immediately upstream of the ORF1a termination codon and results in the extension of pp1a with the ORF1b-encoded part of the replicase (reviewed in [213]). Subsequently, pp1a and pp1ab undergo extensive autoproteolytic processing by three ORF1a-encoded proteases, which leads to the generation of 13 end products (nsps), named nsp1 to nsp12 (a recently described cleavage within nsp7 yields

nsp7 α and nsp7 β [214]). Most of these replicase subunits appear to become associated with intracellular membranes in the perinuclear region of the infected cell [33, 201, 202], where they are thought to assemble into RTCs. The ORF1b-encoded subunits contain the core enzymatic activities that are involved in viral RNA synthesis, like the RNA-dependent RNA polymerase (RdRp) and RNA helicase [215, 216], while ORF1a encodes, in addition to the three protease domains, several putative trans-membrane subunits. The latter appear to play a more 'structural' role by inducing DMV formation [217] and presumably anchoring the RTC to intracellular membranes [32].

In EAV-infected cells, the RTC mediates the synthesis of genomic RNA (RNA1) and a nested set of six sg mRNAs (RNA2 - RNA7). These transcripts are 3' co-terminal and also contain a common 211-nt 5'-leader sequence that is identical to the 5' end of RNA1. Each sg mRNA is thought to be produced from its own subgenome-length minus strand template. The latter are produced via a mechanism of discontinuous minus strand RNA synthesis during which sequences encoding sg RNA "leader" and "body" are joined (for recent reviews, see [40, 196]). The production of a set of sg transcripts is a characteristic feature of nidoviruses and serves to regulate the expression of the viral structural protein genes from the 3'-proximal part of the genome. Therefore, their synthesis is referred to as 'transcription', to distinguish it from the process of replication. Viral RNA synthesis involves partially and fully double-stranded intermediates, known as replicative intermediates (RI) and replicative forms (RF), which are thought to be associated with plus- and minus-strand RNA synthesis, respectively [218, 219].

The isolation of replication complexes and the development of *in vitro* RNA synthesis assays (IVRAs) have proven to be valuable tools for studying the mechanistic details of the replication of several viruses. However, robust *in vitro* systems supporting the synthesis of the full spectrum of viral RNAs produced in nidovirus-infected cells have not been described and therefore we set out to develop such a system for EAV. The purification of active, membrane-associated RTCs should enhance our insight into their structure and function, including the molecular details of nidovirus replication and transcription. We now describe the development, optimization, and characterization of such an *in vitro* system for EAV, in which both genome-sized and sg RNAs, mainly of positive polarity, were synthesized. The characterization of partially purified and enzymatically active RTCs revealed that several EAV nsps, including the nsp9-RdRp, cosedimented with endogenous and newly synthesized viral RNA in fractions that contained double membrane structures. Subgenomic mRNAs appeared to be released from the RTC-containing fraction, while a large proportion of newly synthesized genomic RNA remained associated with it. Remarkably, the isolated RTC was not active unless it was supplemented with a preparation containing a cytosolic host protein factor. This host factor was found to be present in a wide variety of eukaryotes, and its preliminary characterization indicated that it has a molecular mass in the range between 59 and 70 kDa.

MATERIALS AND METHODS

Cells, virus and antisera

BHK-21 cells were cultured and infected with EAV (Bucyrus strain) at a multiplicity of infection of 5, essentially as described [220], except that cells were grown in GMEM (Gibco) supplemented with 5% or 2% fetal calf serum before and after infection, respectively. HeLa cells and Vero E6 cells were grown in DMEM supplemented with 10% fetal calf serum. C6/36 cells were grown as described [221]. One-day old de yolked zebrafish embryos were obtained from Christoph Bagowski (Department of Integrative Zoology, Institute of Biology, Leiden University). *Saccharomyces cerevisiae* strain FY1679 was grown in YPD. A new nsp9 rabbit antiserum was raised against bacterially expressed recombinant nsp9 [215]. The other antisera used in this study have been described previously [201, 222, 223].

Isolation of enzymatically active RTCs from EAV-infected cells

Approximately 1×10^8 EAV-infected BHK-21 cells were harvested by trypsinization at 6 h post infection (p.i.), when infection was carried out at the commonly used temperature of 39.5°C, or 10 h p.i. when infection was done at 37°C. Cells were resuspended in 2 ml hypotonic buffer (20 mM HEPES, 10 mM KCl, 1.5 mM MgOAc, 1 mM DTT, 133 U/ml RNaseOUT (Invitrogen) and 2 µg/ml actinomycin D (ActD), pH 7.4). During harvesting and lysis 2 µg/ml ActD was present in all solutions used. The number of harvested cells was determined using a counting chamber and the percentage of infected cells was checked by immunofluorescence microscopy as described [33]. After incubation on ice in hypotonic buffer for 15 min, cells were disrupted in an ice-cold ball-bearing homogenizer (Isobiotek) with 16 µm clearance. HEPES, sucrose and DTT were added to yield a lysate containing 35 mM HEPES, pH 7.4, 250 mM sucrose, 8 mM KCl, 2.5 mM DTT, 1 mM MgOAc, 2 µg/ml ActD and 130 U/ml RNaseOUT. Nuclei, large debris and any remaining intact cells were then removed by two subsequent centrifugation steps at 1,000 x g and 4°C for 5 min and the post-nuclear supernatant (PNS) was either assayed immediately for RdRp activity or stored at -80°C, at which activity could be retained for at least 1 year. Protein concentrations were determined using the Bio-Rad protein assay reagent.

In vitro RNA synthesis assay (IVRA)

Following optimization of reaction conditions (as described under "Results"), standard 28-µl IVRA mixtures contained 25 µl of EAV-infected cell lysate (either PNS, S10, P10 or combinations), 30 mM HEPES pH 7.4, 220 mM sucrose, 7 mM KCl, 2.5 mM DTT, 2.5 mM MgOAc, 2 µg/ml ActD, 25 U RNaseOUT, 20 mM creatine phosphate (Sigma), 10 U/ml creatine phosphokinase (Sigma), 1 mM ATP, 0.25 mM GTP, 0.25 mM UTP, 0.6 µM CTP and 0.12 µM, 10 µCi [α - 32 P]CTP (GE Healthcare). Unless otherwise indicated, standard reactions

were performed for 100 min at 30°C. Reactions were terminated by the addition of 60 µl 5% lithium dodecyl sulfate, 0.1 M Tris-HCl, 0.5 M LiCl, 10 mM EDTA, 5 mM DTT, 0.1 mg/ml Proteinase K, pH 8.0. After an incubation of 15 min at 42°C, unincorporated label was removed using RNase-free Micro Bio-spin 30 columns (Bio-Rad) and RNA was isolated, dissolved in 20 µl of 1 mM sodium citrate, pH 6.5, and analyzed as described below.

Isolation, gel electrophoresis and detection of RNA

RNA was isolated by acid phenol extraction and isopropanol precipitation with Glyco-Blue (Ambion) as coprecipitant, essentially as described [224]. Denaturing formaldehyde agarose gel electrophoresis was performed as described [225]. Semi-denaturing 7 M urea-3% polyacrylamide gel electrophoresis was performed essentially as described [226]. Before loading, samples were either incubated at 42°C for 15 min or heat-denatured for 3 min at 96°C, followed by rapid cooling on ice. For detection of IVRA products, PhosphorImager screens were directly exposed to dried gels, after which screens were scanned with a Personal Molecular Imager FX (Bio-Rad) and incorporation of label was quantified using Quantity One v4.5.1 software. Incorporation of [α - 32 P]CTP was quantified by correlating the measurements to those from membrane strips containing known quantities of [α - 32 P]CTP. For the detection of unlabeled EAV RNA, direct hybridization of agarose gels was performed [225] using a 32 P-labeled oligonucleotide probe (5'-TTG-GTTCCTGGGTGGCTAATAACTACTT-3') that is complementary to the 3'-end of all EAV mRNAs. For quantitative analysis, known quantities of *in vitro* transcripts were run on the same gel.

Hybridization of IVRA products

In vitro transcribed RNAs (1 µg) corresponding to the ORF7 region (nt 12313-12660) of the EAV genome (RNA7+) or its complementary sequence (RNA7-) were immobilized to Hybond N+ membrane (GE Healthcare). Equal amounts of total cellular RNA isolated from mouse L cells and full-length Sindbis virus RNA transcripts were included as negative controls. The membrane with the immobilized probes was hybridized (0.8 ml volume; 16 h at 60°C) with half of the 32 P-labeled RNA recovered from a 28-µl IVRA. Membranes were washed twice for 20 min at 60°C with 4 ml of 15 mM NaCl, 1 mM NaH₂PO₄, 0.1 mM EDTA, 0.05% SDS, pH 7.0. To confirm the specificity of the immobilized probes, membranes were also hybridized with either 32 P-labeled RNA7+ or 32 P-labeled RNA7- transcript. Hybridization was quantified by PhosphorImager analysis as described above.

LiCl fractionation and RNase treatment of IVRA products

IVRA reactions were terminated with lithium dodecyl sulfate and proteinase K as described above. After removal of unincorporated label, the LiCl concentration was raised to 2 M and samples were incubated at -20°C for 16 hours (40). RI and single-stranded

(ss) RNA were pelleted by centrifugation for 1 hour at 16,000 x g and 4°C. Pellets were washed with 70% ethanol, dried and dissolved in 1 mM sodium citrate. The 2 M LiCl supernatant was desalted using Micro Bio-spin 30 columns (Bio-Rad). Samples were treated with a mix of RNase A (2.5 U/ml) and RNase T1 (100 U/ml) under low salt conditions (15 mM NaCl, 2 mM sodium citrate pH 7.2) or high salt conditions (750 mM NaCl, 75 mM sodium citrate pH 7.2) for 15 min at 37°C. Double-stranded RNA was specifically degraded by incubation with RNase III (Ambion; 50 U/ml) for 15 min at 37°C in 650 mM NaCl, 60 mM sodium citrate, 10 mM MgOAc, 1 mM DTT, 10 mM Tris-HCl, pH 7.2. After RNase treatment, RNA was isolated as described above, except that the phenol extraction step was omitted.

Subcellular fractionation by differential centrifugation, ultrafiltration, and size exclusion chromatography

PNS fractions of BHK-21, HeLa, Vero E6, and C6/36 cells were prepared by mechanical disruption as described above for EAV-infected BHK-21 cells. A yeast PNS and a zebrafish PNS were prepared in a similar way except that yeast cells from a 50-ml culture were disrupted by vortexing in the presence of 500 µm diameter glass beads in 0.5 ml hypotonic buffer, and zebrafish cells from 200 one-day old zebrafish embryos were disrupted in 200 µl hypotonic buffer by passing them through a 27-gauge needle. The total protein concentration in all lysates was between 1 and 5 mg/ml. PNS fractions were centrifuged for 10 min at 4°C at 5,000 x g, 10,000 x g and 16,000 x g yielding supernatants S5, S10, S16 and pellets P5, P10, and P16 respectively. Pellets were resuspended in dilution buffer (35 mM HEPES, 250 mM sucrose, 8 mM KCl, 2.5 mM DTT, 1 mM MgOAc pH 7.4) by carefully pipetting (20x) in 1/5 to 1/10 of the volume of the PNS from which the pellet was prepared. For IVRAs, 5 µl of a pellet fraction was mixed with either 20 µl dilution buffer or 20 µl of a 'supernatant fraction', after which reactions were performed as described above. The S16 fraction was centrifuged for 1 h at 200,000 x g to yield a S200 supernatant fraction. Low molecular weight compounds (<6 kDa) were removed from S16 by size exclusion chromatography using Micro Bio-spin 6 columns (Bio-Rad), yielding fraction F>6. Ultrafiltration of S16 through filters with cut-off sizes of 10 kDa (Millipore Biomax 10K NMWL), 100 kDa (Millipore Biomax 100K NMWL) and 1000 kDa (Vivascience Vivaspin 1,000,000 MWCO) yielded filtrates F<10, F<100 and F<1000, respectively.

Gel filtration chromatography

A HeLa S200 fraction (240 µg protein in 200 µl) was fractionated by gel filtration chromatography using an ÄKTA FPLC (GE Healthcare) and a Superdex 200 HR10/30 column (GE Healthcare) at 4°C. The column was equilibrated with 20 mM HEPES, pH 7.4, 150 mM KCl, 2 mM DTT, 1 mM MgOAc. Elution was done in the same buffer, at a flow rate of 0.5 ml/min, and 0.5-ml fractions were collected after the first 7 ml (which represented the

void volume of the column). For each fraction, the buffer was exchanged to dilution buffer using Micro Bio-spin 6 desalting columns (Bio-Rad). The Superdex column was calibrated with the HMW calibration kit (GE Healthcare) to obtain size estimates for the protein fractions obtained.

Protease and nuclease treatment

Fraction S16 was treated for 15 min at 30°C with 2 mg/ml, 0.4 mg/ml, 0.08 mg/ml and 0 mg/ml of proteinase K, after which the protease was inactivated by adding 2 mM PMSF and samples were cleaned up with Micro Bio-spin 6 columns (Bio-Rad). Inactivation of proteinase K by this procedure was confirmed by testing the stability of ³⁵S-labeled control proteins during a 100-min incubation. S16 was treated with 75 U/ml of micrococcal nuclease (Fermentas) in the presence of 2 mM CaCl₂ for 30 min at 30°C, after which the nuclease was inactivated by the addition of 5 mM EGTA. The extent of RNA degradation was monitored using a ³H-uridine-labeled *in vitro* transcript.

SDS-PAGE and Western blot analysis

After SDS-PAGE, proteins were transferred to Hybond-P PVDF membrane (GE Healthcare) by semi-dry blotting. Membranes were blocked with 1% casein in PBS containing 0.1% Tween-20 (PBST) and were incubated with mono-specific anti-EAV replicase rabbit antisera: anti-nsp1 (1:2000), anti-nsp2 (1:2000), anti-nsp3 (1:2000), anti-nsp4 (1:2000), anti-nsp7-8 (1:2000), anti-nsp9 (1:5000) or anti-nsp10 (1:2000) antisera, all diluted in PBST containing 0.5% casein and 0.1% BSA. Peroxidase-conjugated swine anti rabbit IgG antibody (DAKO) and the ECL-plus kit (GE Healthcare) were used for detection. The SilverQuest kit (Invitrogen) was used for silver staining of SDS-PAGE gels.

Electron microscopy

Formvar-coated grids were placed on top of 25- μ l drops of P10 fractions and incubated at room temperature for 1 minute. After blocking with 1% BSA in PBS, grids were incubated with a rabbit anti-nsp3 or preimmune serum (1:200) in PBS containing 1% BSA for 30 min and bound rabbit IgG was detected with 15 nm protein A-gold. After fixation with 1.5% glutaraldehyde and negative staining with 3% uranyl acetate, grids were viewed with a Philips CM-10 transmission electron microscope at 100 kV. For ultrastructural analysis of native DMVs, EAV-infected BHK-21 cells grown on coverslips (Thermanox) were cryofixed by high-speed plunge freezing in liquid ethane, freeze substitution, and embedding in LX-112 epoxy resin [30]. Ultrathin sections were contrasted with uranyl acetate and lead hydroxide and viewed with a Philips CM-10 transmission electron microscope at 100 kV.

RESULTS

EAV RTC activity in cytoplasmic extracts.

To study the EAV RTC, we sought to isolate the virus-specific RNA-synthesizing activity from infected BHK-21 cells by mechanical disruption and cell fractionation. Metabolic labeling of EAV RNA synthesis with [³H]uridine revealed that it was maximal by 6 h p.i. (data not shown) and therefore RTCs were routinely isolated at this time point. In general, approximately 10⁸ infected cells were used to prepare a cytoplasmic extract (PNS) with a total protein concentration of 2 to 5 mg/ml.

The PNS described above was used in IVRAs (see Materials & Methods), in which the incorporation of [α -³²P]CTP into viral RNA was analyzed in a reaction mixture containing nucleoside triphosphates (NTPs), Mg²⁺, an energy regenerating system (creatine phosphate and creatine phosphokinase), and an inhibitor of cellular transcription (ActD). We used labeled CTP in our assays to minimize background incorporation that could result from the presence of cellular terminal transferases, which preferentially use ATP and UTP [227].

In a time course experiment (Fig. 1A), we observed the accumulation of several *in vitro*-synthesized, ³²P-labeled RNA species with sizes corresponding to those of the EAV genome (RNA1) and all six sg mRNAs (RNAs 2 to 7). Upon incubations longer than 100 min, the amount of labeled RNA decreased, probably due to the combination of the (continuous) activity of endogenous RNases and a decreasing synthesis rate. The half-life of viral RNA in PNS at 30°C was estimated to be approximately 20 or 40 min, depending on whether we analyzed the integrity of 3'-terminal sequences (hybridization) or the degradation of [³H]uridine labeled RNA molecules to fragments smaller than 20 nt (data not shown). Concurrently, it was found that after a 100-min incubation only 2-10% remained of the endogenous EAV RNA or of an *in vitro*-made transcript when it was added to the assay (data not shown). The addition of fresh reaction components (NTPs and energy regenerating system) at 80 or 100 min into the assay did not boost product formation (data not shown), suggesting that the decrease in incorporation was not due to depletion of reaction components or cellular phosphatases [228], but rather to the absence of (re)initiation of RNA synthesis (in our system) or to loss of RTC activity. We favor the latter explanation, since a >75% reduction in activity was observed when the PNS was preincubated, prior to the IVRA, for 1 h at 4°C or 20°C (with or without reaction components), suggesting that the RTC activity is not very stable at these temperatures (data not shown).

IVRAs performed using varying Mg²⁺ concentrations revealed that RTC activity is strongly dependent on Mg²⁺ with a relatively narrow optimum (Fig. 1B). Further optimization in the 2-4 mM range (data not shown) indicated 2.5 mM Mg²⁺ to be optimal, yielding maximal amounts of EAV-specific RNA products and minimal amounts of host

cell-derived background incorporation. Mg^{2+} could not be replaced by Mn^{2+} , which strongly inhibited the RNA-synthesizing activity (Fig. 1B), even in the presence of Mg^{2+} (data not shown). Addition of Mn^{2+} led to the accumulation of many small, labeled products, suggestive of abortive RNA synthesis, possibly due to compromised RdRp processivity.

IVRAs performed at 25°C, 30°C, and 37°C were compared, with maximum yields obtained at 30°C (data not shown). The optimal pH for the RNA-synthesizing activity was 7.5 (Fig. 1C), since at lower pH hardly any incorporation was observed while at higher pH a decrease in EAV-specific incorporation was accompanied by a strong increase in the synthesis of background products (Fig. 1C). Both the energy regenerating system and exogenous NTPs were essential for activity (Fig. 1D).

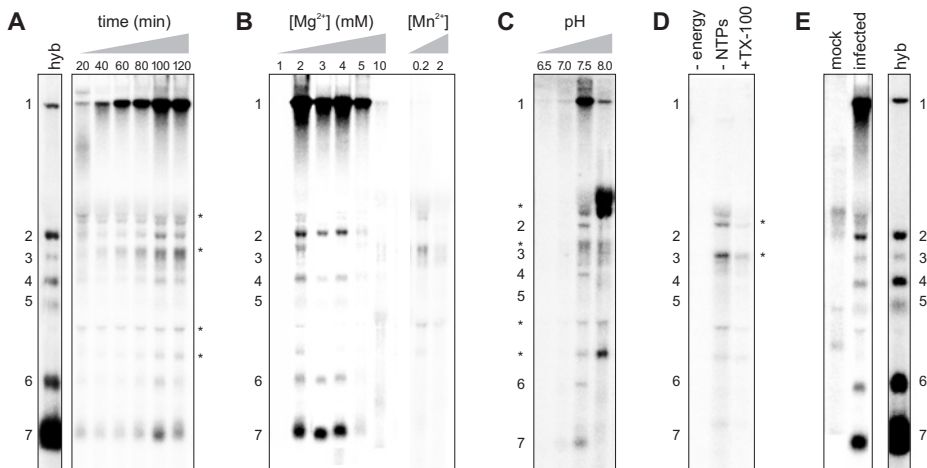


Fig. 1. Reaction products from *in vitro* RNA synthesis assays on cytoplasmic extracts from EAV- and mock-infected cells. Incorporation of $[\alpha\text{-}^{32}\text{P}]\text{CTP}$ in IVRA products was analysed on denaturing formaldehyde-agarose gels followed by PhosphorImager analysis. Marker lanes (hyb) depict the positions of EAV RNA1-7 and contain RNA isolated from infected cells, hybridised with a probe complementary to the 3'-end of all EAV RNAs. The positions of genomic RNA (1) and sg RNA (2-7) are indicated next to the gels. Optimization of reaction conditions. (A) Time course analysis of the RNA synthesis assay. After initiation of an assay, samples were taken at the times indicated above each lane and RNA was isolated and analyzed as described under "Experimental Procedures". (B) IVRAs carried out with varying Mg^{2+} concentrations or in the presence of Mn^{2+} , as indicated above the lanes. (C) Reactions performed at the pH indicated above each lane. (D) Effect of the absence of the energy regenerating system (-energy) or nucleoside triphosphates (-NTP) or the presence of 0.1% Triton X-100 (+TX-100). (E) IVRA performed under fully optimised conditions with cytoplasmic extracts from mock-infected (mock) or EAV-infected cells (infected). * indicates bands that are not EAV-specific and are also detected in assays performed on lysates of mock-infected cells.

Effect of low molecular weight compounds on EAV RTC activity *in vitro*.

Addition of KCl, which stimulated the *in vitro* activity of another RdRp [229], did not increase EAV RTC activity. As reported for other viruses [227, 229], Ca^{2+} strongly inhibited *in vitro* RTC activity, but addition of EGTA had no (stimulating) effect in the case of EAV (data not shown). Ionic and non-ionic detergents like SDS, DOC, NP-40, CHAPS (data not shown) and Triton-X-100 (Fig. 1D) all completely abolished the accumulation of radiolabeled viral RNA when added to IVRAs at 0.5x or 5x their critical micelle concentration, suggesting a crucial role for membranes. Addition of 0.4 mM cap analogue (m7GpppG) had no effect (data not shown), whereas raising the DTT concentration to 10 mM or adding 2 mM spermidine resulted in a 60% and 40% reduction, respectively. Therefore, none of the aforementioned compounds, which have been used to stimulate the *in vitro* activity of replication complexes of other RNA viruses, were included in the assay that was used for further studies.

The translation inhibitor cycloheximide had no significant effect on the *in vitro* RTC activity (data not shown). In conjunction with the observed lack of ^{35}S -methionine incorporation during IVRAs (data not shown), this suggests that (continued) protein synthesis is not required for RdRp activity of the EAV RTC *in vitro*.

Kinetics of EAV RTC activity *in vitro*.

The K_m for NTPs reported for *in vitro* assays with the replication complexes of other RNA viruses is in the range of 3-15 μM [229, 230]. Consequently, we presumed that the low CTP concentration (0.12 μM) would strongly limit RdRp activity when only radiolabeled CTP would be present in EAV IVRAs. To study the kinetics of RNA synthesis by the EAV RTC *in vitro*, reactions were performed with varying amounts of unlabeled CTP (up to 200 μM), using a fixed concentration of 0.12 μM [α - ^{32}P]CTP as a tracer. The incorporation

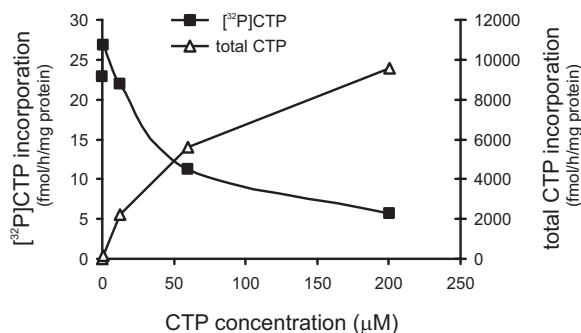


Fig. 2. Kinetics of *in vitro* CTP incorporation into viral RNA by the EAV RTC. The incorporation of [α - ^{32}P]CTP into total viral RNA at various CTP concentrations was quantified as described under "Experimental Procedures" and is expressed as fmol [α - ^{32}P]CTP incorporated per mg of protein per hour reaction time (squares). The total CTP incorporation (triangles) was calculated based on the specific activity of the isotope.

of [α - 32 P]CTP into viral RNA was quantified and the total CTP incorporation was calculated based on the known specific activity (Fig. 2A). At high specific activity, when the [α - 32 P]CTP was not supplemented with cold CTP, ~ 22.4 fmol of [α - 32 P]CTP per mg protein per hour was incorporated into viral RNA (Fig. 2A). At low specific activity, when radiolabeled CTP was supplemented with 200 μ M of unlabeled CTP, the CTP incorporation rate increased over 400-fold to 9,566 fmol/h/mg protein, while the incorporation rate of [α - 32 P]CTP decreased only 4-fold to 5.8 fmol/h/mg protein. For Sindbis virus and West Nile virus similar results have been reported: product detection was better using high specific activity radiolabel, while total CTP incorporation was higher when low specific activities of radiolabel were used [227, 228]. Using a double reciprocal plot of $1/S$ versus $1/V$, the K_m of the RTC for CTP was estimated to be 48 μ M and a V_{max} of 11,000 fmol CTP/h/mg protein was calculated. Using 0.12 μ M [α - 32 P]CTP as a tracer, maximum incorporation of radiolabel was detected when the labeled CTP was supplemented with 0.6 μ M of cold CTP (Fig. 2A). Despite the reaction rate of only 160 fmol CTP/h/mg protein, these conditions were used in subsequent experiments to ensure optimal detection of RNA products.

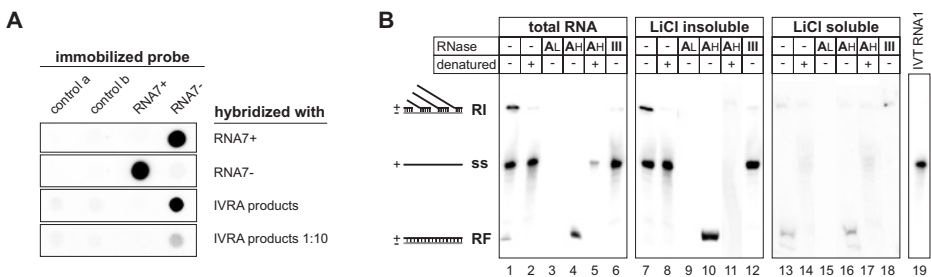


Fig. 3. Analysis of IVRA reaction products. (A) Determination of the polarity of *in vitro* synthesized EAV RNA. Control RNA from L-cells (control a) and Sindbis virus (control b) and RNA probes with either the sense sequence of the 3'-end of the EAV genome (RNA7+) or its complementary sequence (RNA7-) were immobilized on membranes. These membranes were hybridized with 32 P-labeled RNA7+ or RNA7- to determine the specificity of the method and with IVRA reaction products to determine the polarity of *in vitro* synthesized EAV RNA (IVRA products). Hybridization of a membrane with a 1:10 dilution of IVRA products was done to assess the sensitivity of the method. (B) Incorporation of [α - 32 P]CTP into the RI, RF and ss RNA forms of *in vitro* synthesized EAV genomic RNA. After a standard IVRA, isolated total RNA (lanes 1-6) underwent various treatments and was analyzed in a semi-denaturing 7 M urea-3% polyacrylamide gel. Completely double-stranded, LiCl-soluble RF RNA (lanes 13-18) was separated from LiCl-insoluble ss and partially ss RI RNAs (lanes 7-12) by fractionation in 2 M LiCl. Samples were treated with RNaseA/T1 either using high salt conditions (AH), under which ss RNA is specifically degraded, or under low salt conditions (AL), causing degradation of all RNA. Double-stranded RNA was specifically degraded by RNase III treatment, as indicated above the lanes (III). Some samples were heat-denatured prior to running the gel. The position of ss RNA1 in this gel system was determined using 32 P-labeled *in vitro* transcribed RNA1 (IVT RNA1). Only RNA1 is visible in this figure, as the sg RNAs migrated off the gel under the electrophoresis conditions applied. The positions of RI, RF and ss RNA are indicated next to the gel.

EAV RTC activity *in vitro* under optimized conditions.

Fig. 1E depicts the results of a fully optimized IVRA performed using PNS from mock- and EAV-infected cells. Besides EAV-specific products, several minor labeled RNA species with sizes not corresponding to those of the known EAV RNAs were observed. Probably these are cellular RNAs since they were also, often more prominently, detected in assays performed with PNS from mock-infected cells (Fig. 1E). Since host cell nuclei had been removed and ActD was present, it is unlikely that these aberrant products resulted from (residual) host cell transcription. Hence, cellular activities, such as terminal transferases, were likely responsible for the labeling of host RNAs [227]. A severe reduction in the synthesis of EAV-specific radiolabeled RNA products was observed when using CTP as the only NTP in the reaction (Fig. 1D), indicating that a bona fide RdRp activity rather than a template- and NTP-independent terminal transferase activity was monitored in our assay. The intensity of the background bands could be minimized by carefully optimizing the reaction conditions (especially with respect to pH and Mg^{2+} concentration), resulting in the majority of label being incorporated into EAV-specific products.

Characterization of EAV-specific RNAs synthesized *in vitro* by the RTC.

To determine the polarity of the EAV RNAs that are produced by the EAV RTC *in vitro*, ^{32}P -labeled IVRA products were hybridized to membranes containing immobilized sense (RNA7+) or antisense (RNA7-) probes representing a part (ORF7) of the 3'-proximal region of the EAV genome (Fig. 3A). The specificity of this method was confirmed by hybridizing these membranes with ^{32}P -labeled, *in vitro* produced RNA7+ and RNA7- control transcripts (Fig. 3A). The ^{32}P -labeled IVRA products strongly hybridized to the RNA7- probe (Fig. 3A), indicating that the EAV RNAs synthesized were mainly of positive polarity. The quantity of radiolabeled material that hybridized to immobilized RNA7+ or control RNA was at least 60-fold less than that captured by the RNA7- probe. The fact that negative sense products were hardly detected was not due to low sensitivity of the assay, as the positive sense RNA was still readily detectable when 10x less IVRA products were used in the hybridization assay (Fig. 3A).

To study the incorporation of $[\alpha\text{-}^{32}P]\text{CTP}$ into RI, RF and ss RNAs, reaction products were analyzed by LiCl fractionation and by treatment with RNases that specifically degrade either ds or ss RNA. Subsequently, products were analyzed in a semi-denaturing 7 M urea-3% polyacrylamide gel (Fig. 3B), allowing the separation of the RI, RF and ss RNA forms [226]. In view of the anticipated complexity of the data for the various sg RNAs (which would yield a complex pattern of up to 18 additional bands), the present analysis is limited to genomic RNA and the analysis of the RI, RF and ss forms of the sg RNAs will be described elsewhere.

Approximately 68% of the radiolabel was detected in a product that migrated at the position of ss RNA1, 30% was in a slower migrating RI and 2% of the label was found

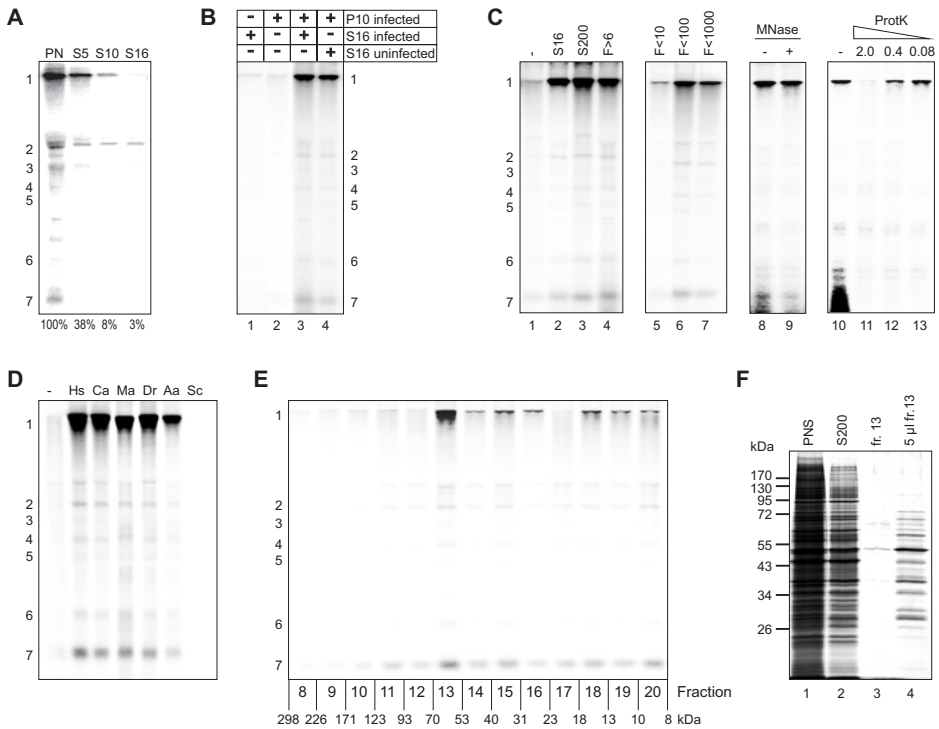


Fig. 4. Characterization of a host factor required for EAV RTC activity. IVRAs were performed and products were analyzed as described in the legend to Fig. 1. (A) RTC activity in cellular fractions obtained by differential centrifugation of the PNS. IVRAs were performed on the lysate before centrifugation (PNS) and the supernatant after centrifugation for 10 minutes at 5,000 x g (S5), 10,000 x g (S10) and 16,000 x g (S16). (B) IVRAs containing either S16 or P10 alone or P10 supplemented with either S16 from infected cells or mock-infected cells as indicated above the lanes. (C) Ability of fractions to stimulate activity of sedimented RTCs. IVRAs were performed with 5 μ l P10 supplemented with 20 μ l of dilution buffer (lane 1) or various fractions (lanes 2-13). S16 & S200, 16,000 x g and 200,000 x g supernatant fractions prepared from the PNS of EAV-infected cells. F>6 was prepared from S16 by removal of molecules with a molecular mass <6 kDa by size exclusion chromatography. F<10, F<100 and F<1000 were prepared from S16 by ultrafiltration over filters with 10, 100 and 1000 kDa cut-offs, respectively. S16 was treated (+) or mock-treated (-) with micrococcal nuclease (MNase) or 0, 2.0, 0.4 or 0.08 mg/ml proteinase K as indicated above lanes 10-13. (D) IVRAs performed with RTCs isolated from infected BHK-21 cells (5 μ l of P10) and supplemented with 20 μ l of dilution buffer (-) or 20 μ l of S200 fractions from HeLa cells (*Homo sapiens*; Hs), Vero E6 cells (*Cercopithecus aethiops*; Ca), BHK-21 cells (*Mesocricetus auratus*; Ma), 1-day old zebrafish embryos (*Danio rerio*; Dr), C6/36 cells (*Aedes albopictus*; Aa) or yeast cells (*Saccharomyces cerevisiae*; Sc), all diluted to result in the addition of 30 μ g of total protein per IVRA reaction. (E) Purification of the host factor from a HeLa cell S200 fraction by gel filtration. IVRAs were performed with isolated RTCs (P10) supplemented with various fractions from the gel filtration column, as indicated at the bottom of the gel. The molecular mass range of each fraction was extrapolated from a calibration curve and is indicated under the fraction numbers. (F) Analysis of 0.5 μ l of PNS, S200, and column fraction 13 by SDS-PAGE and silver staining (lane 1-3). Lane 4 contains 5 μ l of column fraction 13.

in the faster migrating RF form of RNA1 (Fig. 3B, lane 1). When the IVRA products were heat-denatured prior to electrophoresis, a product migrating at the position of ss RNA was visible (Fig. 3B, lane 2). After degradation of ss RNA by RNase A/T1 treatment under high salt conditions, only a band at the position of the nuclease resistant RF form was observed (Fig. 3B, lane 4). The increased intensity of the RF band in lane 4 (compared to lane 1) was likely due to the redistribution of label from the RI form, which was converted into RF through degradation of nascent strands. Likewise, the denaturation of RNase A/T1-treated RNA converted the RF into ssRNA (lane 5). All RNAs were completely degraded upon RNase A/T1 treatment under low salt conditions (lane 3). After treatment with the ds RNA-specific RNase III, labeled products were observed almost exclusively at the position of ss RNA1 (lane 6).

The LiCl-insoluble fraction contained the (partially ss) RI and ss RNA1 and no RF RNA, the latter being LiCl-soluble (Fig. 3B, lane 7 and 13). After RNase A/T1 treatment of the LiCl pellet fraction, the ss RNA was no longer detectable and the RI was converted into the RF (Fig. 3B, lane 10). Upon denaturation of this sample, the band migrating at the RF position disappeared and a smear appeared at the position between the ssRNA and RF bands in the gel, which probably represented abrogated and partially degraded labeled molecules that had originally been part of the ds regions of the RI (lane 11).

The RF form was soluble in 2 M LiCl (Fig. 3B, lane 13), which indicates that it was completely double-stranded. This was further substantiated by the observation that it was fully degraded by RNase III and completely resistant to RNase A/T1-treatment (lanes 16 and 18). After denaturation of LiCl-soluble RNA that was either untreated or RNase A/T1-treated, a discrete band migrating at the expected position of ssRNA was observed. This indicates that, unlike the RI (lane 11), the RF was completely double-stranded and consisted of two full-length molecules of opposite polarity (lanes 14 and 17).

Taken together, these data indicate that the EAV RTC catalyzed the incorporation of nucleotides into the RI and RF forms of RNA1 *in vitro* and that ss genomic RNA was released from (one or both of) these forms.

EAV RTC activity depends on a cytosolic host factor.

To determine whether isolation of active EAV RTCs can be achieved by differential centrifugation, we first determined the g-force required to remove RdRp activity from the PNS. Supernatants prepared by centrifugation at 5,000 x g, 10,000 x g, or 16,000 x g retained 38%, 8%, and 3% of the activity, respectively (Fig. 4A). For subsequent experiments pelleting at 10,000 x g was used, as we were able to routinely remove about 95% of activity from the PNS, while the pellet could still be readily resuspended (this was more difficult for a 15,000 x g pellet, increasing the risk of mechanical damage to the RTC by sheering forces). The activity producing the background product migrating directly above RNA2 in all lanes of the gel in Fig. 4A remained in the cytosolic fractions,

suggesting that it is soluble, and could thus be separated from the RTC by this method. Surprisingly, the resuspended P10 pellet only exhibited very weak RTC activity (Fig 4B, lane 2). However, this activity could be stimulated considerably with an aliquot of a supernatant fraction (S16; lane 3). Importantly, S16 prepared from mock-infected cells was equally capable of restoring the RTC activity of P10, demonstrating that the factor involved must be of host origin (lane 4).

To determine the nature of the host factor required for RTC activity, the S16 fraction was fractionated by centrifugation, ultrafiltration, and size exclusion chromatography, and was also treated with either a nuclease or a protease (Fig. 4C). The host factor did not pellet at 200,000 x g (Fig. 4C, lane 3), suggesting it is a soluble cytosolic component, not

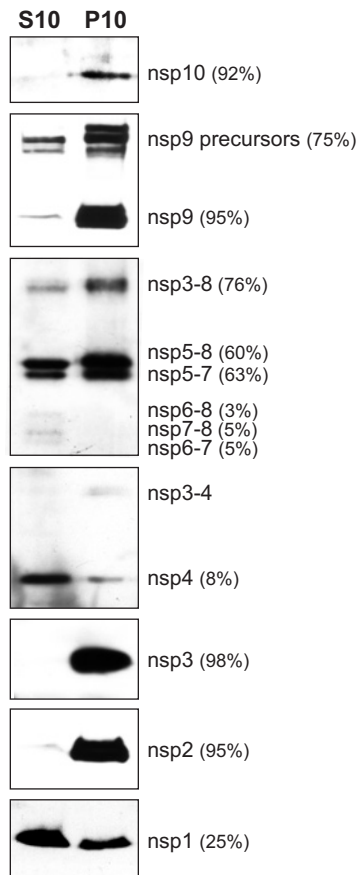


Fig 5. Distribution of nsps after fractionation of the PNS from EAV-infected cells into a 10,000 x g supernatant (S10) and RTC-containing pellet (P10). Equivalent amounts of S10 and P10 derived from the same number of cells were analyzed by Western blotting with anti-nsp10, anti-nsp9, anti-nsp7-8, anti-nsp4, anti-nsp3, anti-nsp2, and anti-nsp1 antibodies. Numbers in brackets indicate the percentage of the protein that is present in the P10 fraction.

associated with cellular organelles. A fraction from which molecules smaller than 6 kDa had been removed by size exclusion chromatography retained the ability to activate the isolated RTC (Fig. 4C, lane 4), indicating that the factor(s) is not a low molecular weight compound, like an NTP or metal ion. The host factor was removed by ultrafiltration using a filter with a 10 kDa cut-off value, but passed through filters with 100 kDa or 1000 kDa cut-offs (Fig. 4C, lanes 5-7). Nuclease treatment had no effect, while protease treatment destroyed the ability of an S16 fraction to activate pelleted RTCs (Fig. 4C, lanes 8-13). Taken together these data indicate that the host factor that is required for the activity of isolated RTCs is a soluble cytosolic protein with a native molecular mass in the range of 10-100 kDa.

To determine whether the host factor is also present in other cell types than BHK-21 cells, S200 fractions from various (uninfected) mammalian, fish, insect and yeast cells were tested for their ability to activate RTCs isolated from EAV-infected BHK-21 cells (Fig. 4D). With the exception of yeast, S200 fractions from all organisms tested were able to reconstitute RTC activity of the P10 fraction, indicating that the host factor is likely to be conserved in animal cells.

The host factor was further purified from a HeLa cell S200 fraction by gel filtration chromatography, since we anticipated that the available data on the human genome and proteome would facilitate future identification of the factor by e.g. mass spectrometry. Each gel filtration fraction was analyzed for the presence of the host factor by adding it to an IVRA with pelleted RTCs (P10 fraction) isolated from EAV-infected BHK-21 cells (Fig. 4E). Fraction 13, which contains proteins with a mass of 53-70 kDa, exhibited the maximum stimulatory effect on RTC activity (Fig. 4E). In an independent experiment, in which slightly different column fractions were collected, the host factor was retrieved in the fraction containing 59-78 kDa proteins (data not shown). Taken together these studies suggest that the (native) mass of the host factor is between 59 and 70 kDa.

Compared to PNS or an S200 fraction, the protein concentration of column fraction 13 was greatly reduced and its composition was clearly less complex (Fig. 4F, lane 1-3), without affecting its ability to stimulate the RTC, indicating that we have achieved a significant purification of the host factor. However, fraction 13 still contained over 30 proteins, as could be observed when a 10-fold larger sample was analyzed (Fig. 4F, lane 4), and therefore additional purification steps will be required for the unequivocal identification of the host factor. A potential complicating factor for this follow-up might be that the host factor is (part of) one of the homo- or hetero-multimeric complexes that are apparently present in fraction 13, which would explain the presence of several polypeptides with a mass smaller than 53 kDa in this fraction (Fig. 4F, lane 4).

Quantitative analysis revealed that the sedimentation procedure used to prepare P10 fractions led also to a substantial non-recoverable loss of RTC activity with a significant variation between individual experiments. Typically, 10-50% of the activity that was

originally present in the PNS could be recovered in P10 fractions when assayed in the presence of the trans-activating host factor. The considerable loss of activity was apparently not due to the resuspension procedure of the RTC pellets, since resuspending less vigorously or not at all further reduced the recovery of activity (data not shown). The P10 fractions typically contained 3-7% of the protein that was present in the PNS. Therefore, despite the low yield, a 2- to 13-fold increase in specific RTC activity was achieved when comparing P10- to PNS-based samples.

Distribution of EAV nsps between S10 and P10 fractions.

To start defining the composition of the RTC and the potential roles of the various EAV nsps in viral RNA synthesis, the distribution of these proteins between the P10 and S10 fractions was investigated by western blotting (Fig. 5). As anticipated, nsp2 and nsp3 were almost exclusively present in the P10 fraction. These subunits contain hydrophobic domains [33, 202], have been implicated in virus-induced membrane modifications, and likely are a structural component of the DMVs [217]. The nsp9-RdRp and nsp10-helicase subunits were also predominantly found in P10. Significant amounts of larger nsp9 precursors were recovered from the cytosolic S10 fraction, likely representing replicase polyproteins and cleavage intermediates, whose processing is relatively slow [223]. Mature nsp4-main protease largely remained in S10, separated from the nsp9-RdRp and nsp10-helicase, suggesting its presence is not (or no longer) required for RTC activity. On the other hand the long-lived nsp3-4 processing intermediate [231] was present in the P10 fraction, probably through membrane association of its hydrophobic nsp3 part [33]. Also a large proportion of the nsp3-8, nsp5-8 and nsp5-7 intermediates cosedimented with the RTC, probably as a result of the membrane-association of the hydrophobic nsp5 part of these proteins. Polypeptides lacking this hydrophobic domain, like the nsp6-8,

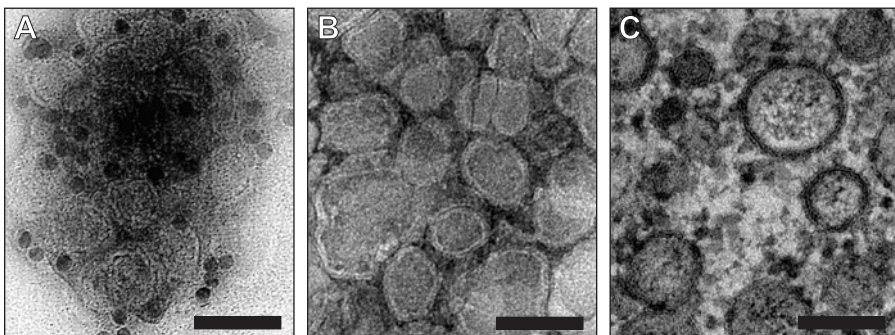


Fig 6. Electron micrographs of the RTC-containing P10 fraction and EAV-infected cells. (A) Immunoelectron microscopy with anti-nsp3 rabbit serum on the chemically fixed P10 fraction. (B) Control labeling of the P10 fraction with preimmune serum from the same animal. (C) Electron micrograph of a thin section of cryofixed EAV- infected BHK-21 cells. Scale bar: 100 nm.

nsp7-8 and nsp6-7 products of the minor proteolytic processing pathway [232], were mainly recovered from the cytosolic fraction (Fig. 5). In the case of nsp1, a multifunctional autoprotease whose zinc finger domain has been directly implicated in EAV transcription [233-235], approximately 75% of the protein was found in the cytosolic S10 fraction, but ~25% of the protein was recovered from the RTC-containing P10 fraction, which is in line with its essential role in sg RNA synthesis. A comparable nsp1 distribution was observed *in vivo* by immunofluorescence microscopy of infected cells (D.D. Nedialkova, E.J. Snijder, *et al.*, unpublished observations).

DMVs are present in the RTC-containing P10 fraction.

The RTC-containing P10 fraction was analyzed by electron microscopy (negative staining) in combination with an immunogold labeling for nsp3 (Fig. 6A). The fraction contained abundant vesicles with a diameter of 60-80 nm that clearly appeared to have a double membrane and labeled strongly when using an anti-nsp3 rabbit serum. Immunogold labeling was not observed when the preimmune serum of the same rabbit

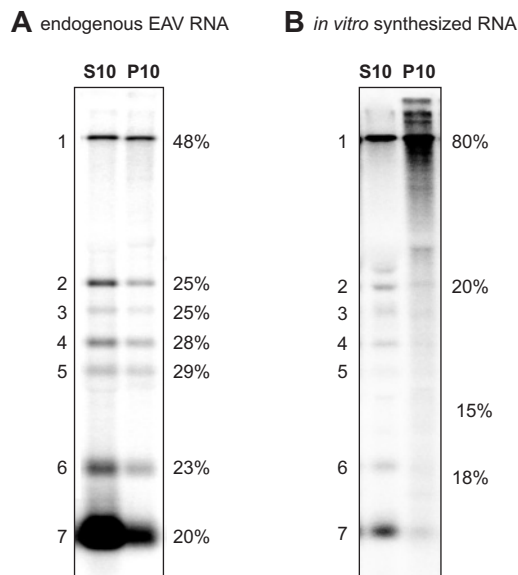


Fig 7. Distribution of endogenous and newly *in vitro* synthesized EAV RNA. (A) Distribution of endogenous EAV RNA. Viral RNA recovered from the 10,000 x g supernatant (S10) and pellet (P10) obtained after centrifugation of the PNS of EAV-infected cells was analyzed by denaturing formaldehyde-agarose electrophoresis and hybridization with a ³²P-labeled probe complementary to the 3'-end of all EAV RNAs. (B) Distribution of *in vitro* synthesized EAV RNA. After an IVRA, the PNS was fractionated into a 10,000 x g supernatant (S10) and pellet (P10). ³²P-labeled *in vitro* synthesized RNA was visualized by denaturing formaldehyde-agarose electrophoresis and direct PhosphorImager analysis. The percentage of each RNA species that is present in the P10 fraction is indicated to the right of each gel. Numbers for RNA 3, 4, 5 are absent in panel B because the signal obtained with the P10 fraction was too low to be reliably quantified.

was used (Fig. 6B). These structures were slightly smaller than the DMVs observed in infected cells (Fig. 6C; [201]), which might be due to differences in fixation methods. The overall morphology, presence of a double membrane, and abundant presence of nsp3 were all consistent with the notion that the P10 fraction is enriched for the virus-induced DMVs that are observed in EAV-infected cells. Such structures were not observed in P10 fractions prepared from mock-infected cells (data not shown).

Distribution of EAV RNA between S10 and P10 fractions.

The distribution of endogenous EAV RNA between the P10 and S10 fractions was analyzed by quantitative hybridization of RNA isolated from these fractions using a probe complementary to the 3'-end of all EAV mRNAs. Endogenous genomic RNA was approximately evenly distributed between the cytosolic S10 fraction and the RTC-containing P10 (Fig. 7A). Conversely, sg mRNAs were mainly recovered from the cytosolic S10 fraction (Fig. 7A). This differential distribution of genome versus sg mRNA was even more striking for newly synthesized RNA that was labeled *in vitro* using PNS, after which a fractionation into P10 and S10 was performed (Fig. 7B). The bulk of newly made genomic RNA remained associated with the RTC in P10, while only a small fraction, presumably single-stranded RNA released from the RTC, was present in S10. In contrast, newly made sg mRNAs were mainly recovered from the cytoplasmic S10 fraction suggesting their rapid release from the complex in which they had been synthesized.

DISCUSSION

Characterization of EAV RTC activity *in vitro*.

In this study, we describe the first procedure for the isolation of an active arterivirus RTC from infected cells and the initial biochemical characterization of its composition and RNA synthesizing activity. Using EAV, one of the best studied nidovirus models, we succeeded in obtaining an RTC preparation capable of the *in vitro* synthesis of both viral genomic RNA and all sg RNAs. The isolated RTC incorporated radiolabel into EAV-specific products in a reaction mixture containing [α - 32 P]CTP, Mg $^{2+}$ and an energy regenerating system. The absence of such products in IVRAs performed with lysates from mock-infected cells, and their dependence on the presence of all four NTPs, demonstrated that they resulted from genuine viral RdRp activity. To our knowledge, this is the first robust *in vitro* system for nidovirus replication and transcription. RdRp activity in cell lysates has been reported previously for the (very distantly) related coronaviruses MHV and TGEV [236-240], but these activities were in some cases barely detectable and appeared to be rather unstable. Furthermore, reaction products were not characterized [236, 238], there were discrepancies between the sizes of *in vitro* and *in vivo* synthesized viral RNA

[237, 240], only genome-sized RNA was detected [239] or conflicting observations were reported [237-239, 241]. The EAV *in vitro* assay described here should facilitate studies into the role of membranes, host factors and viral proteins involved in replication and transcription and allow for the more detailed characterization of the nidovirus RTC at the molecular level.

Up to 100 min into the reaction, radiolabeled products accumulated, after which a decrease was observed, probably due to a decreasing RNA synthesis rate in combination with a steady rate of degradation by cellular nuclease activity. Consistent with our results, nucleases in BHK-21 cell extracts were previously reported to be responsible for the cessation of *in vitro* RdRp activity of other viruses [228, 242, 243]. The K_m for CTP of the EAV RTC was estimated to be 48 μM , slightly higher than values (3-15 μM) reported for other viruses [229, 230] and the V_{max} of CTP incorporation was calculated to be approximately 11,000 fmol/h/mg protein. This is approximately 5-fold higher than the *in vitro* RdRp activity reported for several flaviviruses (1000-2700 fmol/h/mg; [229, 244, 245]), more than 20-fold higher than activities previously reported for brome mosaic virus (59) and the coronaviruses TGEV [240] and MHV [236], and 5- to 20-fold lower than values reported for several alpha- and picornaviruses [228, 246-248]. For EAV an up to 13-fold increase in specific activity could be achieved when the RTC was partially purified by sedimentation at 10,000 x g. Incorporation of radiolabel into the RI, RF and ss forms of EAV RNA1 was observed, mainly into RNA of positive polarity, which is in line with the asymmetric synthesis of a large excess of plus strands over minus strands that is commonly observed *in vivo*.

The *in vitro* activity of the EAV RTC was strongly dependent on Mg^{2+} , as also reported for other positive-stranded RNA viruses [227, 229, 230, 236, 239, 244, 246-258]. For EAV, Mn^{2+} could not replace Mg^{2+} , and had a strong inhibitory effect, even at low concentrations and despite the presence of Mg^{2+} . This suggested that it competes for Mg^{2+} binding, while interfering with enzymatic activity. EAV RTC activity was also inhibited by other divalent cations, like Zn^{2+} and Ca^{2+} (manuscript in preparation), as has also been found for West Nile virus and Japanese encephalitis virus RdRp activity [227, 229]. A strong inhibitory effect of Mn^{2+} on *in vitro* RdRp activity was reported for various other viruses [240, 246, 247, 250, 252, 259], although for several flaviviruses Mn^{2+} could substitute for Mg^{2+} to a limited extent [227, 229, 253-255, 257, 260]. Addition of Mn^{2+} to the EAV IVRA promoted the accumulation of small products, suggesting elongation/processivity was affected, as was observed for Japanese encephalitis virus, hepatitis C virus and brome mosaic virus [229, 255, 261]. The inhibition of the EAV RTC activity by Mn^{2+} contrasts with the Mn^{2+} -dependence of the purified EAV nsp9-RdRp that was recently reported [215]. However, this nsp9-RdRp activity was only observed on artificial templates rather than natural templates.

An energy regenerating system was essential for EAV RTC activity, which might for example be due to the ATP-dependence of the nsp10-helicase that presumably plays a key role in RNA synthesis and/or release of ss RNA. Supporting this idea, in a pestivirus *in vitro* RdRp assay, radiolabel was only detected in ds RNA and no longer in ss RNA in the absence of an energy regenerating system [245].

Thus far, it remains unclear whether the isolated RTC is capable of initiation of viral RNA synthesis *in vitro* or is only elongating nascent RNA molecules (plus strands in RIs) initiated *in vivo*. Continuous incorporation of label in short sg RNAs, like RNA7, up to 100 min after the start of the assay might indicate initiation of RNA synthesis *in vitro*, since in the absence of initiation, accumulation of short RNAs would be expected to peak before that of longer molecules. On the other hand, the isolated RTC did not evidently utilize an exogenous replication-competent plus strand RNA (replicon EDI [262]) as template for RNA synthesis (data not shown). However, it should be noted that such a positive sense RNA may be a poor template in our assay for a variety of reasons related to the properties of the RTC, like the predominant synthesis of plus strands, exogenous macromolecules being unable to enter (preformed) membrane-associated RTCs, or RTC formation occurring in *cis*, e.g. in conjunction with translation of the RNA, which is not likely to occur in this *in vitro* assay (see below). In support of this latter notion, it was found that preformed poliovirus replication vesicles, resulting from the expression of viral proteins, did not participate in the formation of active replication complexes after poliovirus superinfection [263].

No measurable protein synthesis was observed in our PNS and the addition of the translation inhibitor cycloheximide had little effect on viral RNA synthesis *in vitro*, suggesting that continued protein synthesis is not required for *in vitro* RTC activity, as was also reported for poliovirus, hepatitis C virus and Kunjin virus [264-266]. However, for the coronavirus MHV, translation inhibition blocked viral RNA synthesis (particularly minus strand synthesis) both *in vivo* [241] and *in vitro* [236, 239]. These conflicting observations, might reflect fundamental differences in the mechanism of replication of arteri- and coronaviruses or might be due to technical differences between the systems used.

The activity of isolated RTCs depends on a cytosolic host factor.

EAV RTC activity was associated with heavy membrane structures that could be sedimented from PNS at 10,000 x g (P10). The addition of non-ionic detergents destroyed all RTC activity, consistent with an important role of membranes in RTC structure and/or function, a common feature of many positive-stranded RNA viruses. Hardly any RTC activity was detected in the resuspended P10 fraction when it was assayed in a standard IVRA. The activity was however considerably stimulated when the reaction was supplemented with the S16 fraction from either infected or mock-infected BHK-21 cells, and

further experiments suggested that a cytosolic host protein is required for RTC activity. This host factor was also present in the cytosol of the various mammalian, fish and insect cells that were tested, but not in yeast cells, suggesting it is highly conserved in animal cells (Fig. 4D). The host factor was partially purified from the cytosol of HeLa cells by gel filtration chromatography, revealing a native mass of between 59 and 70 kDa. The future, unambiguous identification of the host protein factor required for EAV RTC activity will depend on the successful development of a protocol allowing its further purification without loss of activity. Follow-up studies to explore this issue are currently in progress.

Besides EAV, the fact that the activity of isolated membrane-associated viral replication complexes depends on a host factor has only been reported for poliovirus [264] and not for the isolated membrane-associated replication complexes of various other viruses [229, 255, 267-270]. Whether this is due to fundamental differences between replication complexes of different viruses or due to variations in isolation and assay procedures remains to be seen. For instance, host factors might be involved in the RNA synthesis of all viruses, but their copurification with the active complex might depend on the mode of their association with the replication complex.

Structural characterization of the isolated EAV RTC.

Ultrastructural analysis of the RTC-containing heavy membrane pellet fraction by immunoelectron microscopy revealed the presence of nsp3-containing DMVs, resembling those observed in EAV-infected cells [201]. Analysis of the distribution of replicase subunits between the cytoplasmic S10 fraction and the RTC-containing P10 fraction, revealed that proteins previously implicated in viral RNA synthesis (nsp9-RdRp and nsp10-helicase; [215, 216]) and DMV formation (nsp2 and nsp3; [217]) exclusively cosedimented with the active RTC. In contrast, the main protease nsp4 was found predominantly in the cytosolic S10 fraction and not cosedimenting with RTC activity, suggesting its presence is not (or, rather, no longer) required for RTC activity. The P10 fraction also contained substantial amounts of the nsp3-8, nsp5-8, nsp5-7 processing intermediates and the multifunctional nsp1 [233-235], which is in line with its essential role in sg RNA synthesis. In general, these data are in agreement with previously reported immunofluorescence and electron microscopy data [33, 201, 202].

The bulk of newly synthesized EAV genomic RNA remained associated with the RTC, while sg mRNAs were mainly found in the cytoplasmic fraction, suggesting their rapid release from the complex by which they had been synthesized. It is unlikely that the relative enrichment in genomic RNA is merely due to the slow release of labelled ss RNA from the RI, as 68% of radiolabel was present in the ss form and only 30% in the RI form of RNA1. These results might reflect the existence of separate pools of RNAs with distinct roles in the viral life cycle. The molecules that were released from the RTC might be destined for translation, leading to the synthesis of structural proteins (mRNA2-7)

and additional replicase subunits (mRNA1). The RNA1 molecules that remained associated with the RTC might serve as new templates for replication and transcription and/or become incorporated into new virions, assuming packaging occurs in coordination with replication. In this context, the reported partial colocalization of the N protein with the RTC of EAV [270] and other nidoviruses [32] is an interesting observation. Intracellular virions that were already present upon cell lysis probably contributed to the amount of (mainly unlabeled) endogenous genomic RNA recovered from the cytosolic fraction.

In conclusion, DMV-like double membrane structures, newly *in vitro* synthesized viral RNA, and several key replicase subunits cosedimented with EAV RTC activity, which was also found to be dependent on a cytosolic host factor. Taken together, these data confirm and extend the link between these modified membranes and nidovirus replication and transcription. Our analysis indicates that membranes are essential for RTC function, e.g. to protect the RTC against the observed cellular nuclease activity. In addition, sequestering the RTC in specific membrane-bounded compartments might be important for separating and/or coordinating different processes in the viral life-cycle (e.g. replicase processing, replication, translation, and packaging), which might be reflected by the differential distribution of genomic and sg RNA and the various viral proteins.

ACKNOWLEDGMENTS

We thank Kèvin Knoops and Mieke Mommaas from the Section Electron Microscopy, Department of Molecular Cell Biology, Leiden University Medical Center for electron microscopy, Peter Bredenbeek for C6/36 cells, and Danny Nedialkova for sharing materials and interesting discussions. Zebrafish embryos were a generous gift of Christoph Bagowski of the Department of Integrative Zoology, Institute of Biology, Leiden University. This research was supported by a grant from the Council for Chemical Sciences of the Netherlands Organization for Scientific Research (NWO-CW grant 700.52.306).

Chapter 3

Cyclophilin inhibitors block arterivirus replication by interfering with viral RNA synthesis

Adriaan H. de Wilde, Yanhua Li, Yvonne van der Meer, Grégoire Vuagniaux, Robert Lysek, Ying Fang, Eric J. Snijder, and Martijn J. van Hemert

J. Virol. 2013, 87(3):1454-1464

Reprinted with permission

ABSTRACT

Virus replication strongly depends on cellular factors, in particular on host proteins. Here we report that the replication of the arteriviruses equine arteritis virus (EAV) and porcine reproductive and respiratory syndrome virus (PRRSV) is strongly affected by low-micromolar concentrations of cyclosporin A (CsA), an inhibitor of members of the cyclophilin (Cyp) family. In infected cells, the expression of a green fluorescent protein (GFP) reporter gene inserted into the PRRSV genome was inhibited with an IC_{50} of 5.2 μ M, whereas the GFP expression of an EAV-GFP reporter virus was inhibited with an IC_{50} of 0.95 μ M. Debio-064, a CsA analog that lacks its undesirable immunosuppressive properties, inhibited EAV replication with an IC_{50} that was three-fold lower than that of CsA, whereas PRRSV-GFP replication was inhibited with an IC_{50} similar to that of CsA. The addition of 4 μ M CsA after infection prevented viral RNA and protein synthesis in EAV-infected cells, and CsA treatment resulted in a 2.5 to 4-log reduction of PRRSV or EAV infectious progeny. A complete block of EAV RNA synthesis was also observed in an *in vitro* assay using isolated viral replication structures. The siRNA-mediated knockdown of Cyp family members revealed that EAV replication strongly depends on the expression of CypA, but not CypB. Furthermore, upon fractionation of intracellular membranes in density gradients, CypA was found to cosediment with membranous EAV replication structures, which could be prevented by CsA treatment. This suggests that CypA is an essential component of the viral RNA-synthesizing machinery.

INTRODUCTION

The replication of RNA viruses strongly depends on their successful interplay with the host cell at multiple levels. By now, a wide variety of host cell proteins have been implicated in RNA virus replication and some of these might in fact constitute interesting targets for antiviral therapy [60]. Thus, the possibility to target host factors rather than viral proteins is receiving increasing attention as an alternative and promising antiviral approach (reviewed in [130, 131]). In contrast to antiviral therapy that aims to inhibit viral protein functions, the use of drugs targeting host factors should not lead to drug resistance, which is a common problem when combating RNA viruses due to their high mutation rate and potential for rapid adaptation.

The drug cyclosporin A (CsA) was previously found to inhibit the replication of a number of RNA viruses [271-275]. Recently, multiple laboratories, including our own, reported that also the replication of various (human) coronaviruses, including SARS-coronavirus (SARS-CoV), can be inhibited by CsA treatment [276-278]. This drug affects the function of several members of the cellular cyclophilin (Cyp) protein family, which consists of peptidyl-prolyl isomerases (PPIase) that act as chaperones to facilitate protein folding, and are involved in protein trafficking and immune cell activation [279, 280]. Although Cyps share many similarities in terms of structure and activity, important differences in specific functions and subcellular localization have been documented [280]. In line with the inhibition of virus replication by CsA, Cyp family members were identified as essential host factors in the replicative cycle of several virus groups (reviewed in [281]).

The drug CsA has been widely used as an immunosuppressant, e.g. in organ transplant patients [282], as its binding to various Cyps impairs calcineurin activity and abrogates the T cell response. As Cyps appeared to be relevant targets for antiviral therapy, several Cyp inhibitors have been developed that lack the immunosuppressive properties of CsA, which would be an undesirable side-effect during antiviral therapy. The efficacy of several of such compounds, e.g. Debio-025 and NIM811, is currently being explored in clinical trials for the treatment of hepatitis C virus (HCV) infection [283-285].

Since the replication of coronaviruses like SARS-CoV is inhibited by CsA [276, 277], we investigated whether this drug also inhibits the distantly related arteriviruses, which together with the coronavirus and ronivirus families constitute the order Nidovirales [286]. The arterivirus porcine reproductive and respiratory syndrome virus (PRRSV) is one of the leading veterinary pathogens, causing an estimated annual loss of 664 million dollars in the swine industry in the USA alone [27]. Equine arteritis virus (EAV), in addition to being a relevant horse pathogen, has been used for decades as a model to dissect the molecular details of arterivirus and nidovirus replication [287].

Arteriviruses are positive-stranded RNA viruses with a genome size of about 13-16 kb [37]. Their complex genome expression strategy involves genome translation to

produce the polyprotein precursors for the viral nonstructural proteins (nsps) as well as the synthesis of a nested set of subgenomic (sg) mRNAs to express the structural proteins [40]. The viral nsps, presumably together with various host factors, are thought to assemble into membrane-associated replication and transcription complexes (RTCs) that drive viral RNA synthesis (for recent reviews, see [37, 47]). Arterivirus RNA synthesis was reported to be associated with a virus-induced network of endoplasmic reticulum (ER)-derived membrane structures, including large numbers of double-membrane vesicles [29]. Many arteriviral proteins were found to be associated with these membrane structures, on which viral RNA synthesis was found to depend [33, 52]. However, thus far, the identity and role of proviral host factors involved in the replicative cycle of arteriviruses has remained largely unexplored.

Using EAV and PRRSV, our studies on the inhibition of nidovirus replication by CsA have now been extended to arteriviruses and explored the mechanism of action of the compound in more detail. We show that low micromolar concentrations of CsA can fully block arterivirus RNA synthesis and that the non-immunosuppressive cyclophilin inhibitor Debio-064 is an even more potent inhibitor. These compounds probably exert their effect through their inhibition of CypA, as RNAi-mediated knockdown of CypA strongly affected EAV RNA synthesis and CypA was found to cosediment with EAV replication structures.

MATERIALS AND METHODS

Cell culture, infection, and virus titration

BHK-21 [288], Vero E6 [220], and MARC-145 cells [289] were cultured as described previously. 293/ACE2 cells [74] were cultured in Dulbecco's modified Eagle's medium (DMEM; Lonza) supplemented with 8% FCS, 100 U/ml of penicillin and 100 µg/ml of streptomycin, 2 mM L-Glutamine, and 12 µg/ml Blastidicin (PAA). A cell culture-adapted derivative of the EAV Bucyrus isolate [290] and GFP-expressing recombinant EAV [291] were used to infect monolayers of BHK-21, Vero E6, and 293/ACE2 cells at an MOI of 5 as described previously [220, 288]. MARC-145 cells were infected with a GFP-expressing recombinant PRRSV (SD01-08-GFP) at an MOI of 0.1 as previously described [292]. EAV titers in cell culture supernatants were determined by plaque assay on BHK-21 cells [288], whereas PRRSV titers were determined by fluorescent focus assay (FFA) on MARC-145 cells, as described previously [293]. For IC_{50} determinations, cells were grown in black 96-well plates (Greiner), infected with EAV-GFP or PRRSV-GFP and treated with compounds in octuplet. GFP reporter expression was quantified by measuring fluorescence in a 96-well plate reader, using an excitation wavelength of 485 nm and emission wavelength of 535 nm.

Antibodies and drugs

Rabbit polyclonal antibodies against CypA (Abcam), CypB (Abcam), and Calnexin (BD), a goat polyclonal antiserum against GAPDH (Santa Cruz), and a mouse monoclonal antibody (mAb) against β -actin (Sigma) were used. Rabbit antisera recognizing the EAV replicase subunits nsp3 [201] and nsp9 [52], and the EAV membrane (M) protein [220], and a mAb against the EAV nucleocapsid (N) protein [294] have been described previously. The cyclophilin inhibitors CsA (Sigma) and Debio-064 (Debiopharm, Switzerland) were dissolved in DMSO. CsA was stored as 50 mg/ml stock at -20°C and Debio-064 was stored as a 10 mM stock at 4°C in aliquots for single use. The IC_{50} of inhibitors was calculated with Graphpad Prism 5 using the nonlinear regression model.

Immunofluorescence microscopy

EAV-infected or mock-infected BHK-21 cells, grown on coverslips at 39.5°C , were fixed with 3% paraformaldehyde in PBS, permeabilized with 0.1% Triton X-100, and processed for immunofluorescence microscopy as described previously [33]. Specimens were examined with a Zeiss Axioskop 2 fluorescence microscope with an Axiocam HRc camera and Zeiss Axiovision 4.4 software.

Western blot analysis

After SDS-PAGE, proteins were transferred to Hybond-LFP membranes (GE Healthcare) by semi-dry blotting. Membranes were blocked with 1% casein in PBS containing 0.1% Tween-20 (PBST), and were incubated with anti-nsp3 (1:2000), anti-nsp9 (1:2000), anti-M (1:2000), anti-N (1:10,000), anti-CypA (1:1000), anti-CypB (1:2000), or anti- β -actin (1:50,000) antisera, diluted in PBST with 0.5% casein. Biotin-conjugated swine-anti-rabbit IgG (1:2000) or goat-anti-mouse IgG (1:1000) antibodies (DAKO) and Cy3-conjugated mouse-anti-biotin (1:2500) were used for detection. Blots were scanned with a Typhoon 9410 imager (GE Healthcare) and analyzed with ImageQuant TL software.

Isolation of EAV RTC-containing replication structures and *in vitro* RNA synthesis assays

EAV replication structures were isolated from BHK-21 or Vero E6 cells, and *in vitro* RNA synthesis assays were performed essentially as described previously [52]. In short, approximately 1×10^8 EAV-infected BHK-21 or Vero E6 cells were harvested at 6 or 7 h p.i., and cells were lysed to obtain a post nuclear supernatant (PNS) [52]. A standard *in vitro* RNA synthesis assay contained 20 μl of PNS (the equivalent of 6×10^4 cells) from EAV-infected BHK-21 cells, 5 μl of an inhibitor solution or 5 μl of RTC dilution buffer (control). Following gel electrophoresis, ^{32}P -labeled reaction products were analyzed by denaturing agarose gel electrophoresis and by exposing a PhosphorImager screen directly

to the dried gel, after which screens were scanned with a Typhoon 9410 imager (GE Healthcare), and incorporation of label was quantified using ImageQuant TL software.

Density gradient fractionation

Subcellular fractionation of PNS was performed in continuous 0-30% OptiPrep density gradients in RTC dilution buffer. The gradients were prepared in 13.2 ml Ultra Clear centrifugation tubes (Beckman Coulter) using a Gradient Master (Biocomp). One ml of PNS from Vero E6 cells was carefully loaded on top of the preformed gradient. After centrifu-

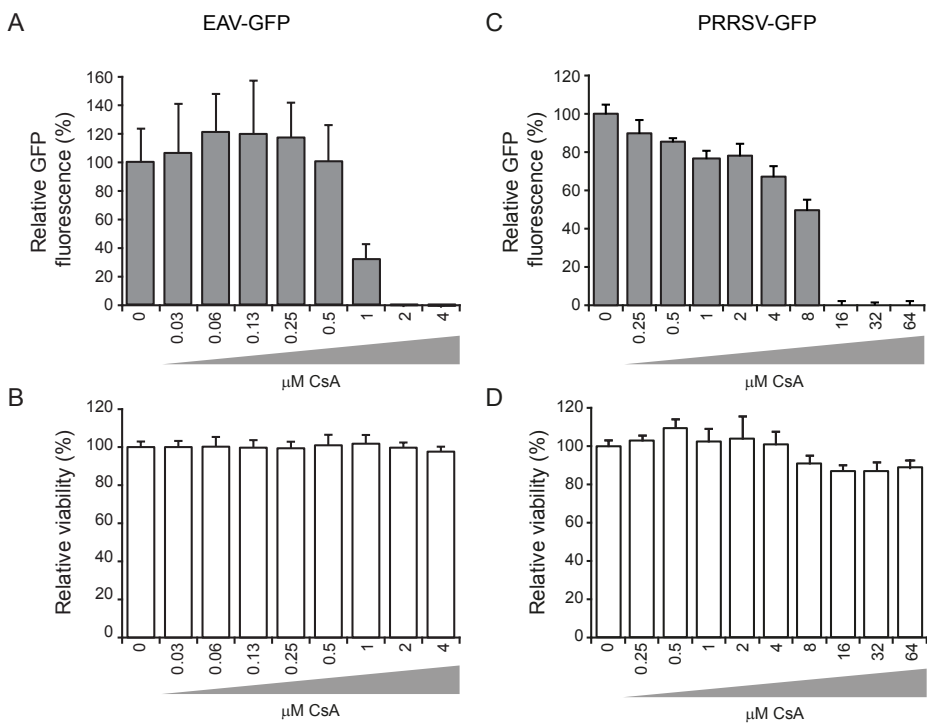


Fig. 1. Cyclosporin A treatment blocks EAV-GFP and PRRSV-GFP replication. (A) BHK-21 cells were infected with EAV-GFP at a MOI of 5 and at 1 h p.i. the inoculum was replaced by medium containing different concentrations of CsA, as indicated on the x-axis. Cells were fixed at 18 h p.i. and GFP reporter expression was quantified and normalized to the GFP signal of control cells (100%) treated with DMSO (solvent concentration equal to that of the cultures that received 4 μM CsA). (B) The effect of CsA on cell viability, compared to untreated control cells (100%), was determined using the CellTiter 96[®] AQ_{UEOUS} Non-Radioactive Cell Proliferation Assay (Promega). Graphs show the results (avg and SD) of a representative experiment in quadruplo. (C) MARC-145 cells were infected with PRRSV-GFP at a MOI of 0.1 and at 1 h p.i. the inoculum was replaced by medium with CsA. Cells were fixed at 24 h p.i. and GFP reporter expression was quantified and normalized to the signal in solvent-treated control cells (100%). (D) The effect of CsA on the viability of the MARC-145 cells, compared to untreated control cells (100%). Graphs show the results (avg and SD) of a representative experiment (n=8). All experiments were repeated at least twice.

gation for 17 h at 48,000 x g in a SW41 rotor at 4°C, the gradient was fractionated into 0.5 ml fractions. The density of each fraction was determined with a refractometer (GETI).

Metabolic labeling of viral RNA synthesis

Labeling of viral RNA with [³H]uridine was performed essentially as described previously [295]. Briefly, at 4.5 h p.i. 4×10^5 EAV-infected BHK-21 cells in 4-cm² dishes were given medium containing 10 µg/ml actinomycin D (ActD; Sigma-Aldrich), and either 4 µM CsA or 0.01% DMSO as solvent control. After 1 h, viral RNA synthesis was labeled by adding 100 µCi of [³H]uridine to the medium. The ³H-labeled RNAs were isolated, separated in denaturing agarose gels, and visualized by fluorography. To verify that equal amounts of total RNA were loaded, the gel was hybridized with a ³²P-labeled oligonucleotide probe (5'-TTCACGCCCTCTTGA ACTCTCTCTTC -3') recognizing 28S ribosomal RNA, as described previously [52].

RNA interference

ON-TARGETplus smartpool siRNA duplexes (Dharmacon) against CypA (PPIA; cat. nr. L-004979-04) and CypB (PPIB; cat. nr. L-004606-00) were used to silence CypA and CypB expression in 293/ACE2 cells. A non-targeting siRNA (D-001810-10) was used as a control and a GAPDH-targeting siRNA (D-001830-10) was used to monitor transfection and knockdown efficiency. Stock solutions of 2 µM were prepared by dissolving siRNAs in 1x siRNA buffer (Dharmacon). For transfection of cells in 96-well clusters, 1×10^4 293/ACE2 cells per well were transfected with a 100-µl mixture containing 100 nM siRNA, 0.2 µg DharmaFECT1 (Dharmacon), OptiMEM (Invitrogen), and antibiotic-free culture medium, according to the manufacturer's instructions. For cells in 12-well clusters, 600 µl transfection mixtures were used. Medium was replaced at 24 h post transfection (p.t.) by antibiotic-free culture medium, and at 48 h p.t. cells were infected with EAV-GFP or wt EAV. Duplicate cultures were used to either prepare lysates to analyze protein expression levels or to monitor cell viability using the CellTiter 96® AQ_{ueous} Non-Radioactive Cell Proliferation Assay (Promega), according to the manufacturer's instructions.

RESULTS

EAV-GFP and PRRSV-GFP replication is inhibited by CsA.

The effect of CsA on arterivirus replication was investigated in cell culture using two representatives of the arterivirus family, EAV and PRRSV (European genotype). For the initial experiments, we employed GFP-expressing recombinant viruses, since quantification of GFP expression provides a rapid and reliable method to detect inhibition of virus replication. BHK-21 cells were grown in 96-well plates and infected at an MOI of

5 with GFP-expressing recombinant EAV [291]. Upon removal of the inoculum (1 h p.i.), medium containing 0.03 to 4 μM of CsA was given, and at 18 h p.i. cells were fixed and GFP expression was quantified. We observed a strong dose-dependent inhibition of EAV-GFP replication (Fig. 1A) in the absence of significant cytotoxic effects at the CsA concentrations used (Fig. 1B). The half maximal inhibitory concentration (IC_{50}) of CsA for EAV-GFP replication in BHK-21 cells was determined to be 0.95 μM .

A similar experiment was performed with PRRSV-GFP in MARC-145 cells (Fig. 1C). Although less sensitive to CsA treatment than EAV-GFP, the replication of PRRSV-GFP was completely blocked at 16 μM of CsA and an IC_{50} of 5.22 μM was determined. Cell viability was only slightly affected by CsA concentrations above 4 μM (Fig. 1D).

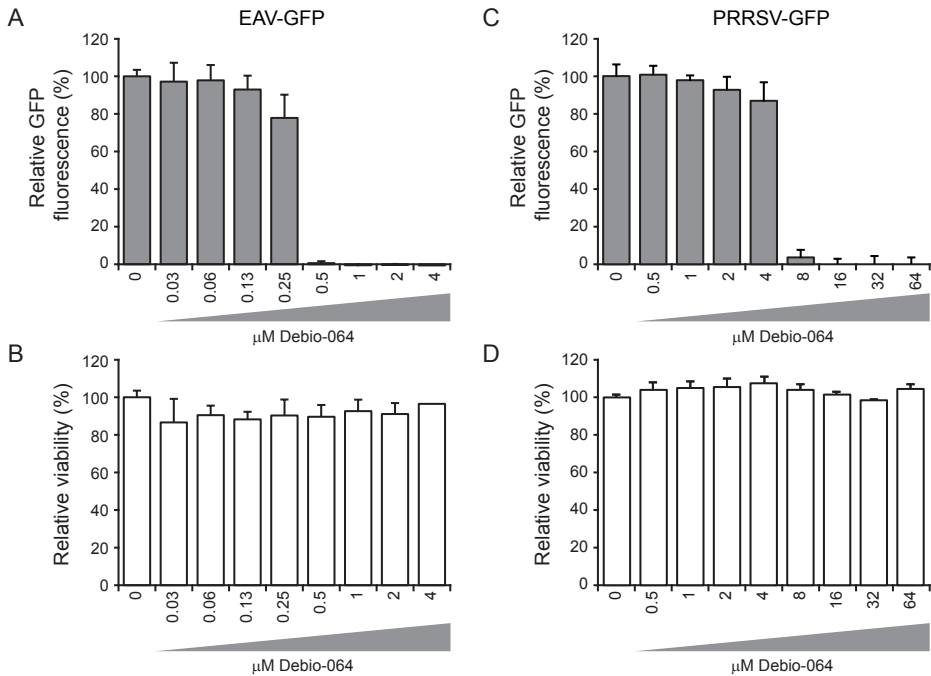


Fig. 2. The CsA analog Debio-064 blocks EAV-GFP and PRRSV-GFP replication. (A) EAV-GFP-infected BHK-21 cells (MOI of 5) were incubated with various concentrations of Debio-064 from 1 h p.i. onwards. Cells were fixed at 18 h p.i. and GFP reporter expression was quantified and normalized to the GFP signal of control cells (100%) that were treated with DMSO (solvent concentration equal to medium containing 4 μM Debio-064). (B) The effect of Debio-064 on BHK-21 cell viability, compared to untreated control cells (100%). (C) PRRSV-GFP-infected MARC-145 cells (MOI of 0.1) were incubated with various concentrations of Debio-064 from 1 h p.i. onwards. Cells were fixed at 24 h p.i. and GFP reporter expression was quantified and normalized to the GFP signal of control cells (100%) that were treated with DMSO. (D) The effect of Debio-064 on MARC-145 cell viability, compared to control cells (100%). Results (avg and SD) of a representative quadruplicate experiment are shown and all experiments were repeated at least twice.

The cyclophilin inhibitor Debio-064 blocks EAV-GFP and PRRSV-GFP replication.

Although CsA has been found to effectively block the replication of various RNA viruses in cell culture [281], its use in antiviral therapy would be complicated by the immune suppression [296] that is a major side effect. Therefore, several alternative Cyp inhibitors have been developed that lack the immune suppressive properties of CsA, like SCY-635, NIM811, and Debio-025, which all block HCV replication [284, 285, 297].

In this study we tested whether the non-immunosuppressive Cyp inhibitor Debio-064 is able to block EAV-GFP and PRRSV-GFP replication (Fig. 2A). Debio-064 is a structurally modified cyclosporin exhibiting an approximately 5-fold higher affinity for CypA in comparison to CsA. Debio-064 is 300-fold less active than CsA at inhibiting mouse T-cell proliferation induced by concanavalin A, suggesting that the compound does not inhibit calcineurin [298]. EAV-GFP-infected BHK-21 cells (Fig. 2B) or PRRSV-GFP-infected MARC-145 cells (Fig. 2D) were treated with various non-cytotoxic concentrations of Debio-064 and viral replication was quantified as described for CsA treatment. Compared to CsA, Debio-064 had a stronger inhibitory effect on EAV-GFP replication. At a concentration of 0.5 μM Debio-064, the EAV-GFP signal was hardly detectable (Fig. 2A), and an IC_{50} of 0.29 μM was determined, which is about 3-fold lower than that of CsA. For PRRSV-GFP, an almost complete block in GFP expression was observed at 8 μM and an IC_{50} of 5.14 μM was determined (Fig. 2C), which is comparable to the inhibitory effect of CsA on PRRSV-GFP replication.

CsA and Debio-064 prevent arterivirus protein expression.

In our initial experiments, we tested the effect of CsA on the replication of a GFP-expressing recombinant EAV. To verify that also wild-type (wt) EAV replication could be inhibited by the drug, we analyzed wt EAV-infected BHK-21 cells that were treated with 0.25 to 8 μM of CsA. At 6 h p.i., cells were lysed and lysates were subjected to Western blot analysis. The expression of viral nonstructural proteins (the nsp5-8 precursor and nsp9) and the structural M and N proteins was hardly detectable after 4- μM CsA treatment, while a clear reduction in protein expression could already be observed at 2 μM of CsA (Fig. 3A). As observed for EAV-GFP, Debio-064 had a stronger inhibitory effect than CsA on the replication of wt EAV. Viral protein expression was clearly reduced in the presence of 0.5 μM of the drug, and became almost undetectable at 1 μM of Debio-064 (Fig. 3B).

The effect of CsA and Debio-064 was further characterized by immunofluorescence microscopy of infected cells. For wt EAV, dsRNA (data not shown) and viral proteins were undetectable after a dose of 4 μM CsA (Fig. 3C) or 1 μM Debio-064 (Fig. 3D). In the case of PRRSV-GFP-infected MARC-145 cells (data not shown) maximal inhibition was observed at a 16 μM CsA dose. However, as previously observed for coronavirus-infected Vero E6, 17C11, or Huh7 cells [276], a small fraction of the MARC-145 cells remained capable of

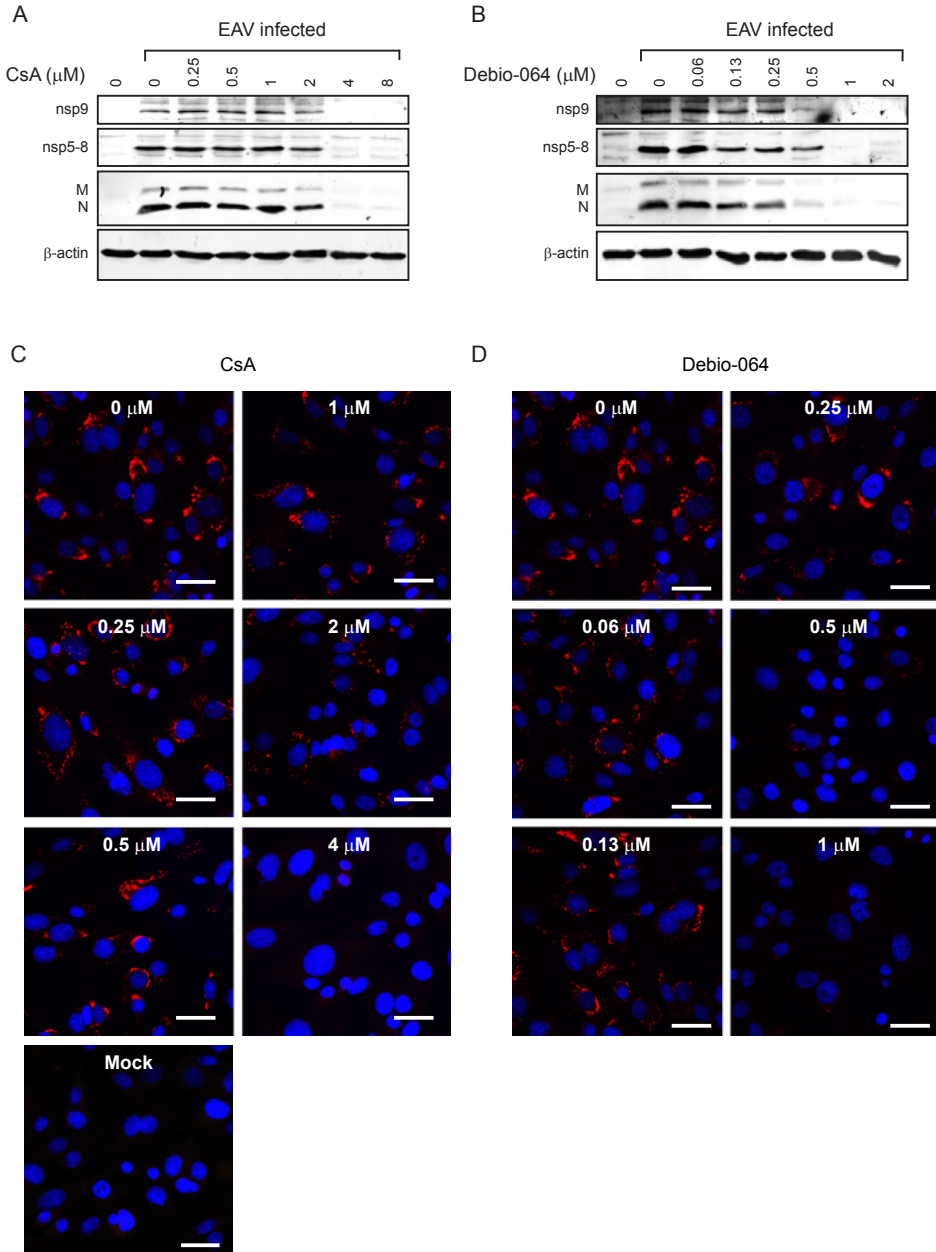


Fig. 3. CsA and Debio-064 treatment block viral protein expression in cells infected with wild-type EAV. BHK-21 cells were infected with EAV (MOI 5) and treated from 1 h p.i. on with CsA (A) or Debio-064 (B) at the concentration indicated above each lane. Cells were lysed at 6 h p.i. and viral protein expression was analyzed by SDS-PAGE and Western blotting with antibodies against nsp9 and nsp5-8, the M protein and the N protein. β -actin was used as loading control. For immunofluorescence microscopy, mock-infected or EAV-infected and CsA- (C) or Debio-064-treated (D) cells were fixed at 6 h p.i. and stained with an anti-nsp3 antiserum. The drug concentrations used are indicated in each panel. Scale bar, 50 μ m.

supporting PRRSV-GFP virus replication, even at high CsA doses of up to 64 μM (data not shown). We did not observe such a small, residual population of apparently drug-insensitive cells in EAV-infected BHK-21 cultures treated with either CsA or Debio-064 (Fig. 3C-D).

CsA and Debio-064 block the production of arterivirus infectious progeny.

To assess to which extent CsA and Debio-064 treatment affected infectious progeny titers, we performed plaque assays to measure EAV titers at 12 h p.i. using supernatants from infected (MOI 5) BHK-21 cells that had been treated with CsA or Debio-064 (Fig. 4A). CsA strongly reduced EAV progeny titers, with an almost 4-log reduction at 4 μM CsA. Treatment probably completely abolished virus production as the titers observed after treatment with 4 μM CsA were similar to those measured at 1 h p.i., which likely reflected the remainder of the high MOI inoculum used (data not shown). These data correlated well with the barely detectable expression of nsp5-8, nsp9, M, and N protein and the lack of dsRNA after treatment with 4 μM CsA (Fig. 3A and C). Treatment with Debio-064 also resulted in a \sim 4-log reduction of infectious progeny at 2 μM , while a 2- to 3-log reduction was already achieved by treatment with 1 μM of the compound.

Using a fluorescent focus assay, we also analyzed the production of PRRSV-GFP infectious progeny in 24 h p.i.-culture supernatants of CsA-treated MARC-145 cells. As observed for EAV, the production of PRRSV-GFP infectious progeny was affected by CsA treatment, although significantly higher concentrations were required. At 16 μM of CsA, a \sim 1.5-log reduction in the yield of infectious progeny was observed, while an apparently complete block (2.5-log reduction) required a dose of 32 μM (Fig. 4B; grey

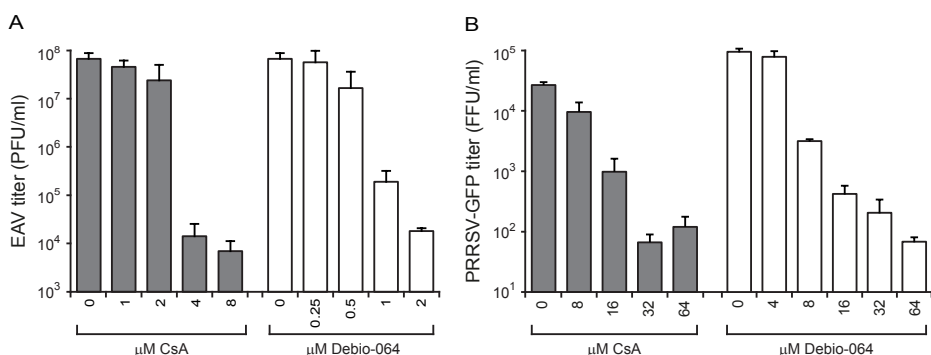


Fig. 4. Treatment of infected cells with cyclophilin inhibitors strongly reduces arterivirus yields. (A) EAV-infected BHK-21 cells (MOI of 5) were treated with various concentrations of CsA (grey bars) or Debio-064 (white bars) from 1 h p.i. onwards, and virus titers in the culture medium at 12 h p.i. were determined by plaque assay. (B) MARC-145 cells infected with PRRSV-GFP (MOI 0.1) were treated from 1 h p.i. onwards with the CsA (grey bars) or Debio-064 (white bars) concentrations indicated below the x-axis and virus titers in the medium at 24 h p.i. were determined by fluorescent focus assay.

bars). Treatment with Debio-064 resulted in a ~1.5-log reduction at 16 μM and a ~2.5-log reduction of infectious progeny at 32 μM (Fig. 4B; white bars), which is comparable to the reduction in PRRSV progeny observed upon CsA treatment.

Cyclophilin inhibitors affect EAV RNA synthesis both *in vivo* and *in vitro*.

The above experiments showed that CsA can effectively block both EAV and PRRSV replication in cell culture. To establish that this lack of viral protein synthesis was due to a block of viral RNA synthesis, we measured the effect of CsA treatment on EAV RNA

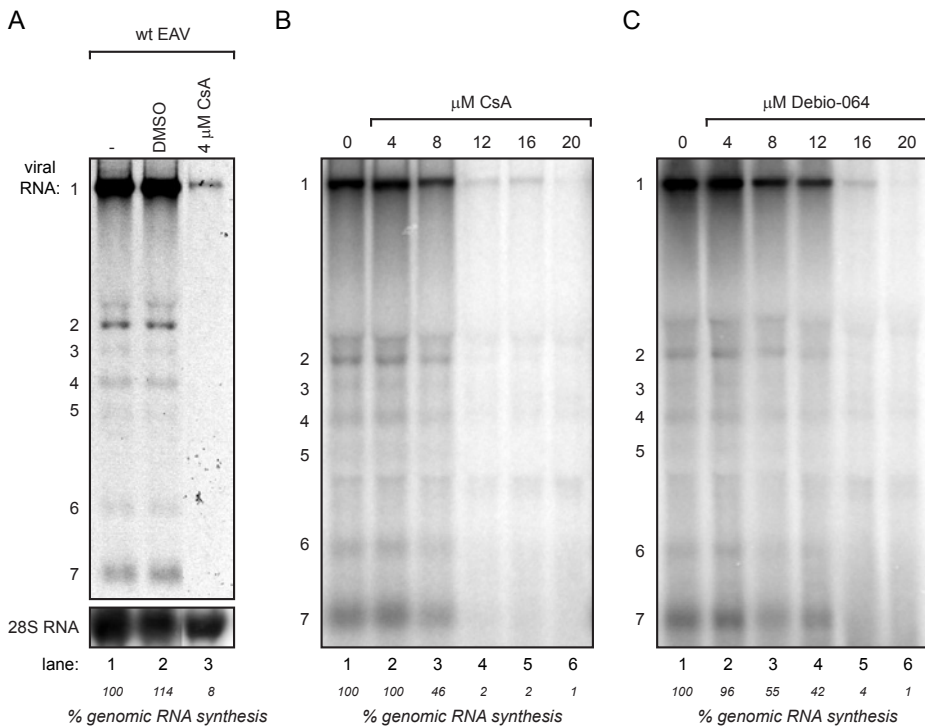


Fig. 5. The *in vitro* and *in vivo* RNA-synthesizing activity of EAV RTCs can be blocked by CsA or Debio-064 treatment. (A) Metabolic labeling of EAV-infected cells with [^3H]uridine between 5.5 and 6.5 h p.i. in the presence or absence of 4 μM CsA. Total RNA was isolated, analyzed in denaturing agarose gels, and detected by fluorography. The amount of [^3H]uridine that was incorporated into viral genomic RNA was quantified and normalized to that in EAV-infected, untreated control cells (100%). 28S RNA detected by hybridization with a ^{32}P -labeled probe (lower panel) was used as a control to correct for variations in loading during viral RNA quantification. (B and C) Semi-purified RTCs isolated from EAV-infected BHK-21 cells at 6 h p.i. were used in an *in vitro* RNA synthesis assay in which [^{32}P]CTP is incorporated into viral RNA. Reactions, performed in the presence of various concentrations of CsA (B) or Debio-064 (C) as indicated above the lanes, were terminated after 100 minutes. RNA was isolated and reaction products were analyzed in denaturing formaldehyde agarose gels. The positions of the genomic RNA (1) and sub-genomic RNAs (2-7) are indicated next to the gels.

synthesis in infected Vero E6 cells *in vivo*, by metabolic labeling with [³H]uridine (in the presence of actinomycin D). When 4 μM of CsA was given at 4.5 h p.i., ³H incorporation into viral RNA during a pulse labeling from 5.5 to 6.5 h p.i. was reduced to 8% of the incorporation measured for non-treated control cells (Fig. 5A). To obtain more insight into the mechanism by which CsA inhibits arterivirus replication, we tested its effect in a previously developed *in vitro* assay to study the RNA-synthesizing activity of semi-purified EAV RTCs [52]. These assays were performed with PNS from EAV-infected BHK-21 cells and the reactions, during which ³²P-labeled CTP is incorporated into viral RNA, were conducted in the presence of various concentrations of CsA. In the absence of the drug, *in vitro* synthesis of EAV genomic and sg RNAs was observed (Fig. 5B, lane 1), as documented previously [52]. RNA synthesizing activity was completely abolished when the reaction was performed in the presence of 12 μM of CsA (lane 4), while a >50% reduction of viral RNA synthesis was observed in the presence of 8 μM CsA (lane 3). Comparable results were obtained with Debio-064, which also caused a >50% reduction of EAV RTC activity around 8 μM and a complete inhibition at 16 μM Debio-064 (Fig. 5C; lane 3 and 5). These data strongly suggest that Cyp inhibitors can directly affect the RNA-synthesizing capacity of the membrane-associated EAV RTCs in PNS samples. We recognize that the concentrations needed to fully block EAV RTC activity *in vitro* are ~3-fold higher than those required to block virus replication in cell culture. This might be due to differences in the experimental set-up, as the PNS used for the *in vitro* reaction constituted a concentrated preparation of RTCs (and host factors), and reaction conditions might influence the interaction between Cyps and their inhibitor.

EAV replication depends on cyclophilin A.

CsA is known to inhibit the PPIase activity of several members of the cyclophilin family. In particular CypA and CypB have been implicated in the replication of several viruses (reviewed in [281]). We therefore analyzed the effect of siRNA-mediated knock-down of CypA and CypB expression levels on the replication of EAV-GFP. We made use of the same human 293/ACE2 cells that we previously used to study the role of Cyps in SARS-CoV replication [276]. This cell line was also susceptible to EAV infection, although only ~40% of the cells became GFP-positive after a high MOI infection with EAV-GFP, as judged by immunofluorescence microscopy of infected cells fixed at 8 h p.i. (data not shown).

Knockdown of CypA and CypB expression was monitored by Western blot analysis and a ~80% reduction of expression was typically observed compared to the level in control cells transfected with a non-targeting control siRNA (Fig. 6A). Depletion of CypA or CypB did not have a significant effect on cell viability during the 48 h of the knock-down experiment (Fig. 6B). Compared to control cells, knockdown of CypB expression did not influence GFP reporter expression when these cells were infected with EAV-GFP, in which GFP fluorescence was measured at 24 h p.i. (Fig. 6C). In contrast, knockdown

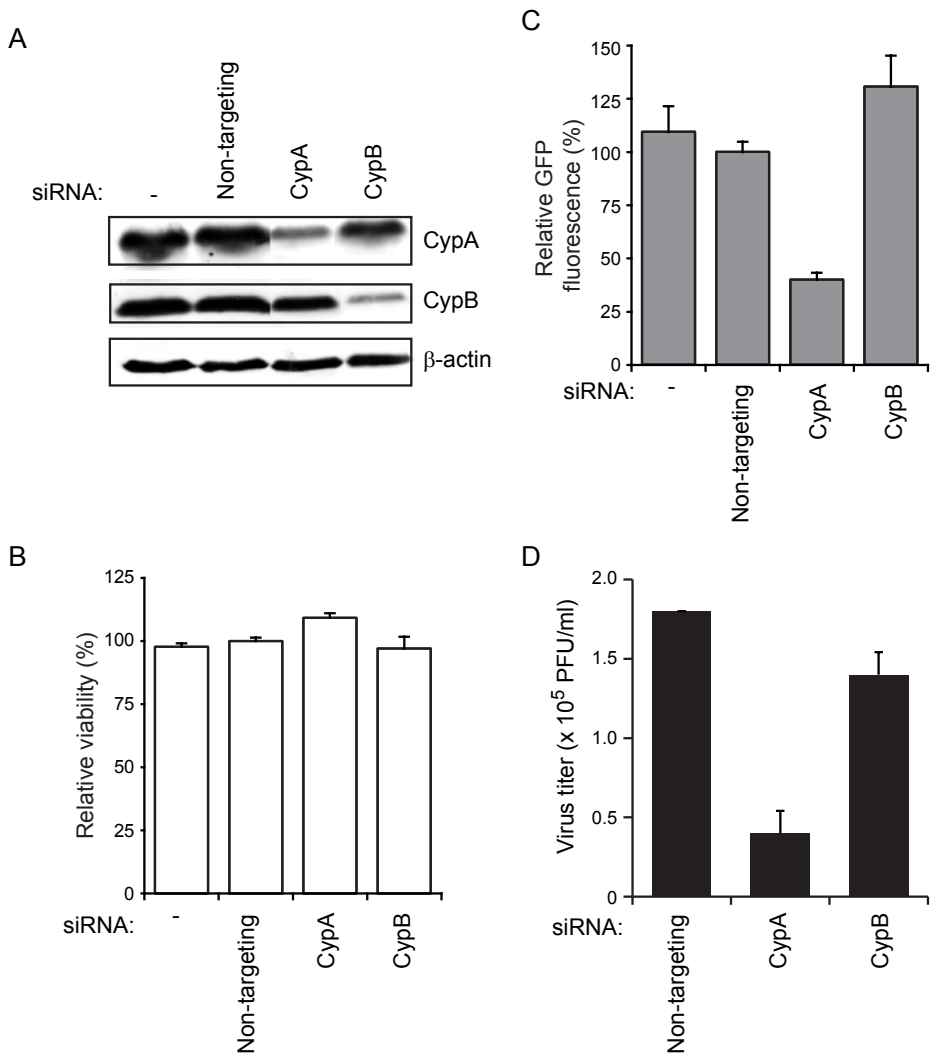


Fig. 6. RNAi-mediated knock-down of CypA, but not CypB, strongly affects EAV replication. 293/ACE2 cells were transfected with a non-targeting control siRNA or siRNAs targeting CypA or CypB. Knockdown of CypA (A, upper panel) and CypB (A, middle panel) levels was monitored by Western blotting with CypA- and CypB-specific antisera. β -actin was used as loading control. (B) Viability of cells 48 h post transfection with the various siRNAs normalized to the MTS signal of cells transfected with the non-targeting control siRNA (100%). (C) GFP reporter expression of cells transfected with the siRNAs indicated below the graph, and infected 48 h post-transfection with EAV-GFP at an MOI of 5. Cells were fixed at 24 h p.i. and GFP fluorescence was quantified and normalized to that in infected cells transfected with non-targeting siRNA. (D) Virus titers at 32 h p.i. in the culture medium of cells transfected with the siRNAs indicated below the graph, and infected 48 h post transfection with wt EAV at an MOI of 0.01.

of CypA resulted in a ~60% reduction of the GFP signal in EAV-GFP-infected cells, compared to that of the control cells (Fig. 6C). Furthermore, wt EAV titers at 32 h p.i. in the culture medium of infected 293/ACE2 cells (MOI 0.01) that had been depleted for CypA showed a ~4-fold decrease in virus progeny compared to control cells (Fig. 6D). These data strongly suggest that EAV replication and the production of virus progeny depend on the availability of the host factor CypA.

Cyclophilin A cosediments with EAV RTCs.

Since our RNAi experiments suggested that EAV RNA synthesis depends on the availability of CypA, we investigated whether CypA cosediments with EAV RTC-containing membranes. We therefore fractionated post-nuclear supernatants (PNS) from EAV-infected and mock-infected Vero E6 cells in a 0-30% OptiPrep density gradient. Gradient fractions were analyzed by Western blot using antisera against CypA, CypB, several EAV nsps, and various organelle marker proteins (Fig. 7). Densities in the gradient ranged from 1.04 g/ml to 1.18 g/ml (Fig. 7A) and the low-density fractions of both EAV-infected and mock-infected PNS contained the cytosolic marker glyceraldehyde 3-phosphate dehydrogenase (GAPDH), while several organelle markers, like the ER protein calnexin and the mitochondrial marker CoxIV (data not shown) were found in higher-density fractions (Fig. 7B-C). This confirmed the separation of membrane-containing fractions from the cytosol. The membrane-associated EAV RTCs, detected with an antiserum directed against nsp9 (RdRp), sedimented at densities around 1.15 g/ml (Fig. 7C). The nsp9-containing fraction also contained significant amounts of the normally cytosolic CypA (Fig. 7C). Upon density gradient fractionation of PNS from uninfected cells CypA was only found in the low-density cytosolic fractions (Fig. 7B), but in PNS from EAV-infected cells a fraction of CypA was found to cosediment with the RTC-containing membranes (compare fraction 3 in Fig. 7B and C). CypB, being an ER-associated protein, was observed in the high-density gradient fractions of both mock- and EAV-infected cell lysates (Fig. 7B). Therefore the protein was present in the fractions containing the EAV RTCs, in particular in the nsp9-containing fraction (Fig. 7C, fraction 3-4), but was clearly more dispersed in the gradient with mock-infected PNS.

To analyze whether CsA can prevent the cosedimentation of CypA with EAV RTCs, we pretreated the PNS from EAV-infected cells with 12 μ M of CsA - the concentration that completely inhibited EAV RTC activity *in vitro* - for 30 minutes on ice before separating the material in an OptiPrep density gradient. Subsequently, the high-density nsp9-containing membrane fractions were analyzed for the presence of CypA by Western blotting (Fig. 7D). In the absence of CsA a clear cosedimentation of CypA and nsp9 was observed, while CypA was no longer detectable in the high-density nsp9-containing fraction of CsA-treated lysates. This suggests that CsA can prevent the cosedimentation of CypA with the membrane-associated EAV RTCs.

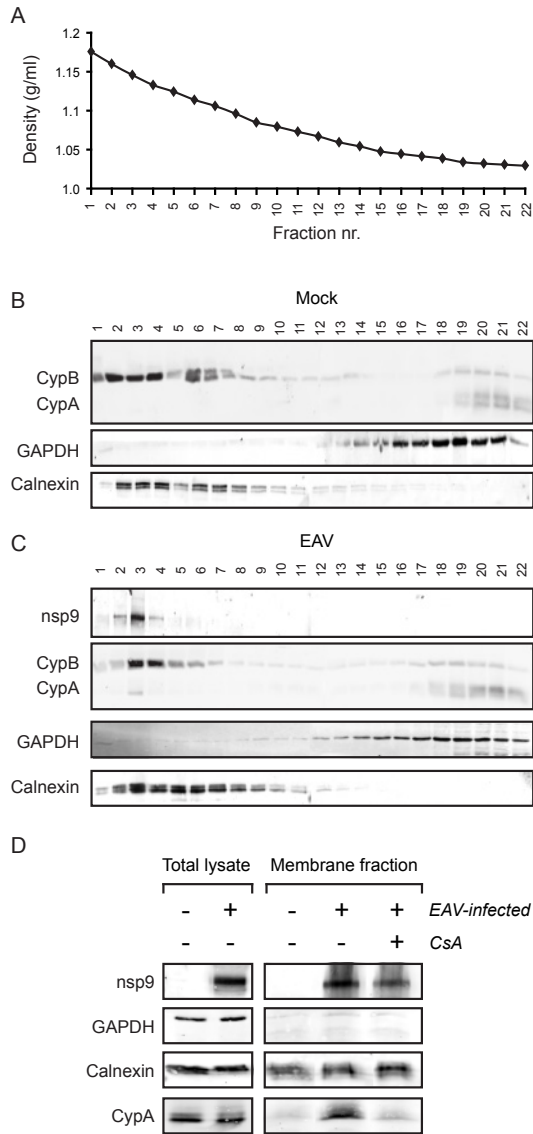


Fig. 7. Co-sedimentation of CypA with EAV RTCs in density gradients. The post-nuclear supernatant of EAV- and mock-infected Vero E6 cells was fractionated using a continuous 0-30% OptiPrep density gradient. (A) Densities of the fractions were determined with a refractometer. (B) Distribution of CypA, CypB, the cytosolic marker protein GAPDH, and ER marker protein calnexin in density gradient fractions of mock-infected cell lysates as analyzed by Western blotting. (C) Distribution of CypA, CypB, the cytosolic marker protein GAPDH, ER marker protein calnexin and EAV RdRp nsp9 in density gradient fractions of EAV-infected cells as analyzed by Western blotting. (D) Before loading on a 0-30% OptiPrep gradient, PNS was pretreated with 12 μ M CsA for 30 minutes on ice. Western blot analysis of the sedimentation of CypA, the ER marker protein Calnexin, and the cytosolic marker protein GAPDH in nsp9-containing membrane fractions of CsA-treated and untreated PNS, and a fraction with the same density prepared from mock-infected cells.

DISCUSSION

Our study shows that arterivirus replication can be inhibited by the cyclophilin inhibitor CsA and the non-immunosuppressive CsA-analog Debio-064, which inhibit EAV RNA synthesis, likely through their effect on the host protein CypA that appears to be recruited to EAV RTCs. CsA inhibits the PPlase function of CsA-sensitive Cyp family members, like CypA, by binding to their active site [279]. We here show that low-micromolar concentrations of CsA can block the replication of both EAV and PRRSV, two prominent representatives of the arterivirus family. PRRSV-GFP replication was inhibited with an IC_{50} of 5.22 μ M and an almost complete block was observed upon treatment with 16 μ M CsA (Fig. 1C). These values are comparable to those previously observed for the inhibition of coronavirus replication by CsA [276, 277]. Compared to PRRSV and coronaviruses, the inhibitory effect of CsA was even stronger for EAV, for which we calculated IC_{50} values of 0.95 μ M (Fig. 1A). The IC_{50} values obtained for arteriviruses are in the range of those observed for other viruses, like HCV [274, 299], several flaviviruses [275], vaccinia virus [300], and HIV-1 [272]. A remarkable and yet not understood phenomenon is that a small fraction (1-5%) of PRRSV-infected MARC-145 cells and, previously, coronavirus-infected Vero E6, 17Cl1, or Huh7 cells [276] appeared to be refractive to CsA treatment, even at high concentrations. This effect was not observed for EAV-infected BHK-21 cells (Fig. 3C), which might be explained by the higher sensitivity of EAV to the compound. In any case, the fact that the distantly related coronaviruses [276, 277] and arteriviruses can both be inhibited by CsA suggests the nidovirus-wide conservation of a cyclophilin-dependent function in viral replication.

Previously, CsA was found to inhibit the replication of a variety of RNA viruses, including important human pathogens like HCV, HIV-1, and Dengue virus (reviewed in [281]). For example, both CypA and CypB were found to specifically interact with the flaviviral nonstructural proteins NS5A and NS5B and these interactions are sensitive to CsA treatment [273, 301-303]. In the case of the interaction of CypA with HCV NS5A, the PPlase activity of the former was proposed to induce a conformational change in the latter [304] that promotes RNA binding to NS5A and enhances RNA replication [305]. Chatterji *et al.* reported that, in addition to the CypA-NS5A interaction, HCV replication also depends on the binding of CypA to the enzymatic pocket of NS5B, the viral RdRp, thus enhancing its affinity for RNA. On the other hand, PPlase-defective CypA failed to interact with HCV NS5B [306], suggesting that the isomerase activity of CypA is an essential factor in the interaction with NS5B that promotes HCV replication. Liu *et al.* showed that the binding of CypA to NS5B mediates the proper folding of enzymatically active NS5B and facilitates the incorporation of the latter into replication complexes. The interaction between CypA and NS5B can be inhibited by CsA [307]. In addition, Kaul *et al.* showed that the development of resistance against the Cyp inhibitor Debio-025

involved mutations (V2440A and V2440L) in HCV NS5B that are close to the NS5A/NS5B cleavage site. These are thought to delay processing of the NS5A/NS5B junction, thus extending the time during which the CypA binding site in NS5B is accessible [308]. As a result, lower amounts of CypA would suffice to mediate the proper folding of NS5B and its incorporation into replication complexes. Similar functions were attributed to CypB, since also the interaction between CypB and NS5B was found to be essential for RNA binding by NS5B and for HCV replication as a whole [309]. Furthermore, Japanese encephalitis virus replication depends on the binding of CypB to NS4A and on CypB isomerase activity [273]. For a number of RNA viruses, CypA was found to be incorporated into newly formed virions, although the functional relevance of this finding remains to be addressed in more detail [271, 310, 311]. CypA also interacts with the SARS-CoV N protein [312] suggesting that the protein could be incorporated into virions [312], although coronavirus N proteins have also been implicated in viral RNA synthesis [313, 314] and are associated with intracellular replication structures [32].

We here show that expression of CypA is required for efficient EAV replication, as siRNA-mediated knockdown of CypA drastically reduced EAV-GFP replication (Fig. 6), while targeting CypB or Cyp40 (Fig. 6 and data not shown) had no effect. The importance of - the normally cytosolic - CypA was further substantiated by its co-sedimentation with RTC-containing membrane structures in the high-density gradient fractions of EAV-infected cell lysates. In such gradients, the sedimentation of the ER marker protein calnexin was essentially similar when comparing infected and mock-infected PNS (Fig. 7B-C). Furthermore, CsA treatment was able to prevent the sedimentation of CypA to the part of the gradient that also contained the EAV RTCs, following their biochemical isolation from infected cells (Fig. 7D), and the *in vitro* RNA synthesizing activity of such replication structures was found to be inhibited by CsA and Debio-064 (Fig. 5B-C). The distribution of CypB appeared to be less dispersed in gradients containing infected cell lysates compared to mock-infected lysates, even though EAV-GFP replication was not affected by the siRNA-mediated knockdown of CypB levels (Fig. 6). This suggests that although the subcellular localization of CypB might be affected by the extensive EAV-driven modification of intracellular membranes [29], this does not have a measurable effect on virus replication. By using fluorescence microscopy, colocalization of CypA and viral RTCs could not be observed, presumably because the fraction of CypA that localizes to replication structures is too small (data not shown). Interestingly, we could previously not measure an effect on SARS-CoV replication when CypA or CypB expression was (largely) silenced [276] in the same 293/ACE2 used here for our EAV studies. The ~20% residual Cyp expression that remained after siRNA-mediated knockdown may have been sufficient to support normal SARS-CoV replication, whereas it appears insufficient to support the efficient replication of the apparently more sensitive EAV, in line with the higher sensitivity of this arterivirus to CsA treatment.

As reported for HCV [305-307], the association of CypA with the EAV replication structures suggests the existence of a functional – presumably PPlase activity-dependent – interaction that is essential for virus replication. This member of the cyclophilin protein family appears to directly promote the RNA-synthesizing activity of the EAV RTC (Fig. 5). Based on studies that analyzed binding sites for CypA using a set of 40 potential CypA-inhibiting peptides [315], we identified several potential CypA binding sites in EAV nsp10, the viral helicase protein. A functionally important interaction with such a key enzyme in arterivirus RNA synthesis could certainly explain that efficient EAV replication depends on the availability of sufficient CypA. Clearly, at this moment, we cannot exclude (direct or indirect) interactions with any of the other viral proteins, including – in analogy to HCV [306] – the viral RdRp subunit (nsp9). In line with the ideas regarding the influence of CypA on the RNA-binding capacity of HCV NS5A and NS5B, EAV RTC-associated CypA may be involved in the proper folding or activation of viral enzymes and/or their binding to viral RNA, which might directly affect their function in RNA synthesis.

CsA analogs like Debio-025, NIM811, and SCY635, which have an increased affinity for CyPs and lack the undesired immunosuppressive effect of CsA [284, 285, 297], can be considered promising antiviral compounds, as they could block HCV replication almost completely and resistance to these compounds does not easily develop, compared to inhibitors directly targeting viral enzymes [316]. In our study we compared the inhibition of EAV and PRRSV replication by CsA with that caused by the non-immunosuppressive CsA-analog Debio-064. For Debio-064 we obtained an IC_{50} value of 0.32 μ M, 3-fold lower than that of CsA (Fig. 2), which is in line with Debio-064's higher affinity for CyPs. We also observed an inhibitory effect of Debio-064 on PRRSV-GFP replication, although in contrast to EAV, its IC_{50} was similar to that of CsA. Therefore, more potent (non-immunosuppressive) CsA analogs not only constitute a promising class of molecules for the treatment of viral infections, but these compounds are also valuable research tools for mechanistic studies into the role of cyclophilins in the replication of nidoviruses and other +RNA viruses.

ACKNOWLEDGMENTS

We thank Prof. Johan Neyts for helpful discussions and Corrine Beugeling for excellent technical assistance. This research was supported in part by TOP grant 700.57.301 from the Council for Chemical Sciences of the Netherlands Organization for Scientific Research (NWO-CW) and by the European Union Seventh Framework Programme (FP7/2007-2013) under SILVER grant agreement n° 260644.

Chapter 4

Cyclosporin A inhibits the replication of diverse coronaviruses

Adriaan H. de Wilde, Jessika C. Zevenhoven-Dobbe, Yvonne van der Meer, Volker Thiel, Krishna Narayanan, Shinji Makino, Eric J. Snijder, and Martijn J. van Hemert

J. Gen. Virol. (2011), Vol. 92, pp 2542-2548

Reprinted with permission

ABSTRACT

Low micromolar, non-cytotoxic concentrations of cyclosporin A (CsA) strongly affected the replication of SARS-coronavirus (SARS-CoV), human coronavirus 229E, and mouse hepatitis virus in cell culture, as was evident from the strong inhibition of green fluorescent protein reporter gene expression and up to 4 log reduced progeny titres. Upon high-multiplicity infection, CsA treatment rendered SARS-CoV RNA and protein synthesis almost undetectable, suggesting an early block in replication. siRNA-mediated knock-down of the expression of the prominent CsA targets cyclophilin A and B did not affect SARS-CoV replication, suggesting that either these specific cyclophilin family members are dispensable or that the reduced expression levels suffice to support replication.

MAIN TEXT

The 2003 outbreak of Severe Acute Respiratory Syndrome (SARS) sparked a renewed interest in coronaviruses, a group of positive-strand RNA viruses that can cause respiratory or gastrointestinal disease in humans and livestock (reviewed in [317]). Several inhibitors of coronavirus enzymes (reviewed in [318]) and compounds that inhibit replication in cell culture have been described [143, 159, 319], but effective treatment of coronavirus infections is currently unavailable [187]. An inherent risk of the use of inhibitors directed against viral functions is the development of antiviral resistance due to the rapid adaptive evolution of RNA viruses. Coronavirus replication relies on a variety of host factors [320-322], which also constitute potentially interesting targets for antiviral therapy, as resistance is less likely to develop when host factors are targeted instead of viral proteins.

While aiming to identify host factors involved in SARS-coronavirus (SARS-CoV) replication, we established that the drug cyclosporin A (CsA) inhibited coronavirus replication. CsA affects the function of many members of the cyclophilin family, which consists of peptidyl-prolyl isomerases that act as chaperones and facilitate protein folding (reviewed in [279]). CsA was previously reported to inhibit the replication of human immunodeficiency virus [272], vesicular stomatitis virus [271], hepatitis C virus (HCV) [274, 299, 323] and other flaviviruses [273, 275].

Initially, using GFP-expressing recombinant coronaviruses, we investigated the effect of CsA on the replication of representatives of different coronavirus genera, i.e. human coronavirus 229E (HCoV-229E), mouse hepatitis virus (MHV) and SARS-CoV. In order to rigorously evaluate the inhibitory potential of the drug, each of these viruses was tested in single-cycle, high-multiplicity of infection (MOI) experiments, in which the drug was added upon removal of the inoculum at 1 h post infection (p.i.). Experiments were performed in 96-well plate format and GFP expression was quantified using a Berthold Mithras plate reader. When using SARS-CoV-GFP [324] and Vero E6 cells (MOI 10), a CsA dose range of 0 to 64 μM was used and cells were fixed at 18 h p.i. CsA inhibited SARS-CoV-GFP replication in a dose-dependent manner, with GFP expression becoming undetectable upon treatment with 16 μM CsA (Fig. 1a, upper panel). Cell viability was not affected at any of the CsA concentrations tested (Fig. 1a, lower panel). To confirm that CsA also inhibits SARS-CoV replication in human cells, the experiment was repeated using 293/ACE2 cells, which stably express the SARS-CoV receptor ACE2 [74]. Indeed, in these cells, CsA inhibited SARS-CoV-GFP replication to the same extent as in Vero E6 cells (Fig. 1b).

To investigate whether CsA also inhibits the replication of other coronaviruses, Huh7 cells infected with HCoV-229E-GFP [325] and 17CL1 cells infected with MHV-GFP [326] were given CsA at 1 h p.i. and GFP expression was quantified at 24 and 18 h p.i., respectively (Fig. 1c and d, upper panels). As in the case of SARS-CoV-GFP, MHV-GFP replication

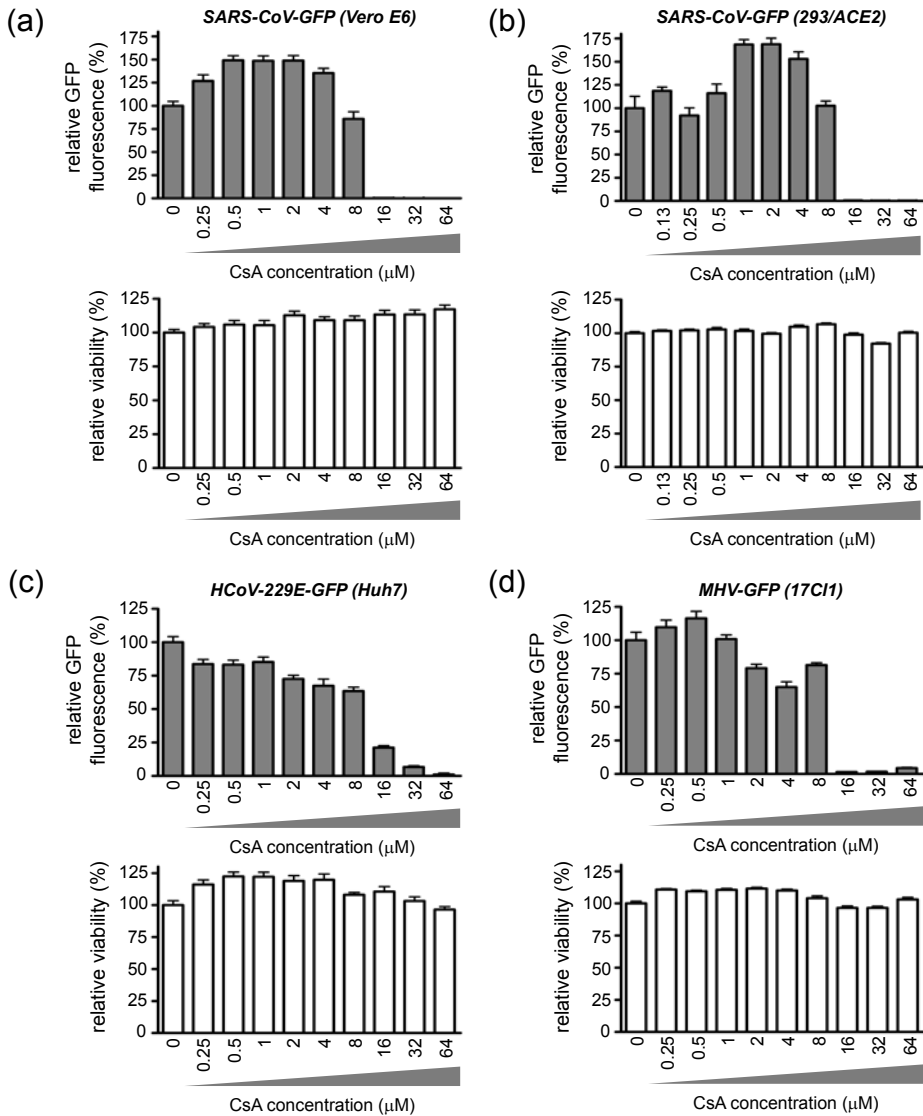


Fig. 1. CsA inhibits the replication of GFP-expressing recombinant coronaviruses. Vero E6 cells (a) or 293/ACE2 cells (b) were infected with SARS-CoV-GFP at a MOI of 10 and at 1 h p.i. the inoculum was replaced by medium containing different CsA concentrations. Cells were fixed at 18 h p.i. and GFP reporter expression was measured and normalized to the signal in control cells (100%) that were treated with DMSO, the solvent used for CsA (upper panels, grey bars). Huh7 cells infected with HCoV-229E-GFP were treated with CsA from 1 h p.i. on and were fixed for GFP measurements at 24 h p.i. (c, upper panel). 17CL1 cells were infected with MHV-GFP, treated with CsA from 1 to 18 h p.i., and GFP fluorescence was quantified (d, upper panel). The effect of CsA treatment on the viability of the various cell lines used, compared to untreated control cells (a-d, lower panels) was determined using the Cell Titer 96 AQ MTS assay (Promega). Graphs show the results (average and SD) of a representative quadruplicate experiment. All experiments were repeated at least twice.

was strongly inhibited by 16 μM CsA. HCoV-229E-GFP appeared to be somewhat less sensitive, as complete inhibition of GFP expression required 32 μM CsA (Fig. 1c). The viability of 17CL1 and Huh7 cells was not affected by the CsA concentrations used (Fig. 1c and d, lower panels). It should be noted that SARS-CoV replication appeared to be somewhat enhanced by low CsA doses (up to 4 μM).

Western blot analysis of SARS-CoV-GFP-infected Vero E6 cells that were treated with 0 to 32 μM CsA from 1 to 10 h p.i. showed that the expression of SARS-CoV non-structural protein (nsp) 8, nucleocapsid (N) protein and GFP was strongly reduced in cells treated with 16 μM CsA (Fig. 2a). This suggested that CsA treatment strongly inhibited an early step in the SARS-CoV replicative cycle. To verify the inhibitory effect of CsA with wild-type (wt) SARS-CoV, we repeated the experiments using the Frankfurt-1 isolate (Fig. 2b) and found that the expression of nsp8 and N protein was barely detectable upon treatment with 16 μM CsA. At lower CsA concentrations, little effect on viral protein synthesis was observed, indicating that the replication of recombinant and wt SARS-CoV is equally sensitive to CsA treatment. The steep dose-response curve, showing a strong reduction in SARS-CoV replication between 8 and 16 μM CsA, is in line with the observations made for several other +RNA viruses, like HCV [274, 299, 327].

The conclusions from Western blot studies were further substantiated by immunofluorescence labelling of nsp4 and dsRNA in SARS-CoV-infected cells, as markers for viral protein and RNA synthesis, respectively (Fig. 2c). Hardly any nsp4 or dsRNA was detectable upon treatment with 16 μM CsA and the immunolabelling for these markers was visibly reduced when 8 or 4 μM CsA was given. Remarkably, about 1-5% of the infected cells remained SARS-CoV positive in immunofluorescence analysis, even at CsA concentrations up to 64 μM , suggesting they were somehow insensitive to CsA treatment and remained capable of supporting a certain level of SARS-CoV replication. Compared to untreated cells the signals for nsp4 and dsRNA were clearly reduced in these cells, although - probably due to the relatively high avidity of the antibodies used - the N protein remained readily detectable (data not shown), suggesting that SARS-CoV replication was indeed impaired although not fully blocked.

To assess whether CsA treatment also affected the production of infectious progeny, virus titres were determined for supernatants harvested at 16 h p.i. from CsA-treated Vero E6 cultures infected with wt SARS-CoV or SARS-CoV-GFP (Fig. 2d). CsA indeed dramatically reduced progeny titres, with a 16 μM CsA dose resulting in approximately 4- and 3-log reductions for SARS-CoV-GFP and wt SARS-CoV, respectively. These data correlate well with the barely detectable expression of GFP, nsp4, nsp8 and N protein after treatment with 16 μM CsA (Fig. 1a and 2a-c). The 3-4 log progeny titre reduction also suggested that the low percentage of cells that remained SARS-CoV positive in immunofluorescence assays upon treatment with 16 μM CsA produced reduced levels of infectious progeny. CsA also affected HCoV-229E-GFP titres (Fig. 2e), although a 32- μM

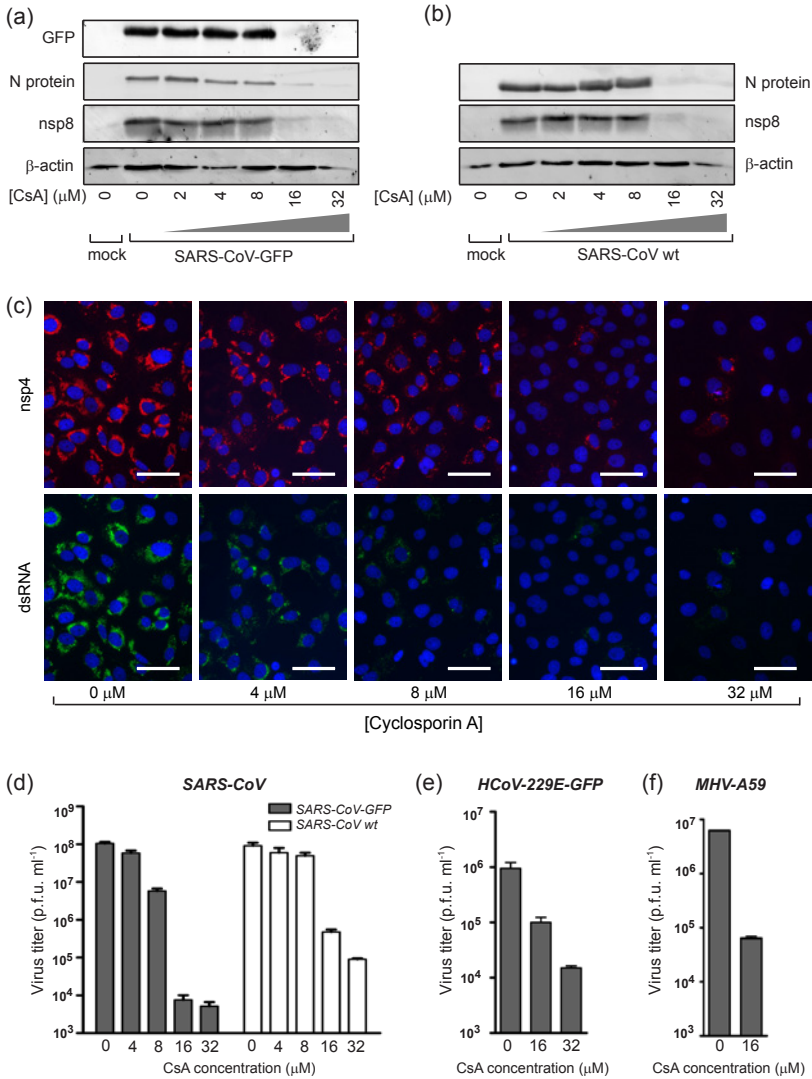


Fig. 2. CsA treatment inhibits coronavirus protein and RNA synthesis, and the production of infectious progeny. Vero E6 cells were infected with SARS-CoV-GFP (a) or wt SARS-CoV (b) and treated with CsA from 1 to 10 h p.i. Viral protein expression was analysed by Western blotting using polyclonal rabbit antisera against nsp8 [53], the N protein [295], and GFP as indicated next to the panels. β-actin, detected with a rabbit antiserum (Sigma), was used as loading control. (c) Immunofluorescence analysis of Vero E6 cells infected with SARS-CoV (MOI 10) and treated from 1 to 10 h p.i. with the CsA concentration indicated below each panel. Cells were stained with an anti-SARS-CoV nsp4 rabbit antiserum (upper panel; [53]) or an anti-dsRNA monoclonal antibody (lower panel; [30]). Scale bar: 50 μm. (d) Vero E6 cells infected with SARS-CoV-GFP (grey bars) or wt SARS-CoV (white bars) were treated with various concentrations of CsA from 1 h p.i. on, and virus titres in the culture supernatant were determined at 16 h p.i. by plaque assay on Vero E6 cells. Huh7 cells infected with HCoV-229E-GFP (e) or 17CL1 cells infected with MHV-A59 (f) were treated with CsA from 1 h p.i. on, and infectious progeny titres were determined at 30 h p.i. and 8 h p.i., respectively. The graphs show the mean of two independent duplicate experiments.

CsA concentration was required to achieve a 2-log reduction. Progeny titres of MHV, the fastest replicating of the three coronaviruses tested, were also 2-log reduced upon treatment with 16 μ M CsA (Fig. 2f). Also, as observed for SARS-CoV-infected cells, a sub-population of the HCoV-229E-infected Huh7 and MHV-infected 17CL1 cells appeared to be resistant to CsA treatment.

CsA inhibits the peptidyl-prolyl isomerase activity of several members of the cyclophilin family [279]. Specifically cyclophilin A (CypA) [271, 307, 308, 328] and B (CypB) [273, 309] have been reported to enhance the replication of several viruses. Furthermore, CypA was identified as interaction partner of the SARS-CoV N protein [312]. CsA might exert its inhibitory effect on coronavirus replication by inhibiting cyclophilin function or - alternatively - by direct inhibition of a virus-specific function. A direct inhibitory effect on the activity of the SARS-CoV nsp12 RNA-dependent RNA polymerase, was excluded using an *in vitro* assay and recombinant nsp12 (data not shown; [329]). We next analysed the effect of siRNA-mediated knock-down of cellular CypA and CypB expression (for 48 h) on the replication of SARS-CoV-GFP in 293/ACE2 cells. Western blot analysis of cells transfected with siRNAs targeting CypA and CypB confirmed that protein levels

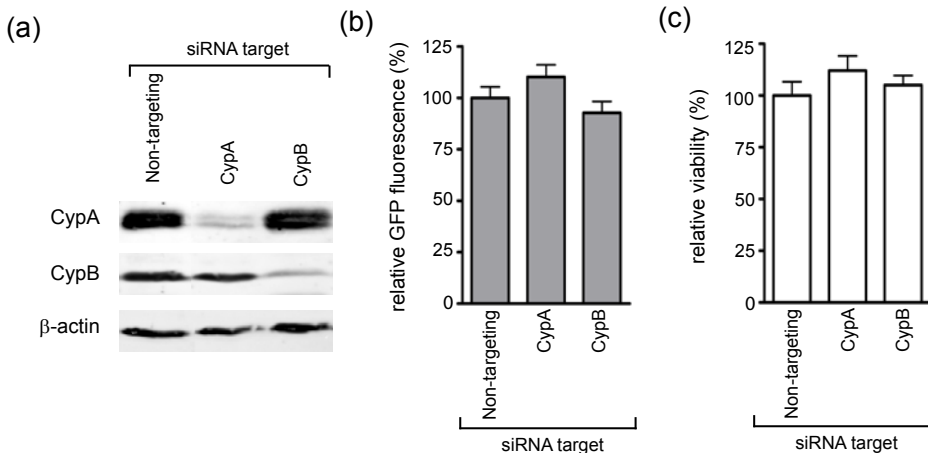


Fig. 3. SARS-CoV-GFP replication in Cyclophilin A- or B-depleted cells. Using DharmaFECT1 (Dharmacon), 293/ACE2 cells were transfected with siRNAs (Dharmacon ON-Target PLUS pools) targeting CypA and CypB mRNAs. Non-targeting siRNA, and siRNA targeting GAPDH expression were used as negative and positive control for transfection and depletion efficiency, respectively. Expression levels of CypA (a, upper panel) and CypB (a, middle panel) in cells transfected with the siRNA pools indicated below the lanes, were analysed by Western blotting using specific antisera (Abcam). β -actin, detected with a rabbit antiserum (Sigma), was used as loading control. The viability of cells transfected with the various siRNAs was monitored using the Cell Titer 96 AQ MTS assay (b). Data were normalized to the average MTS assay value of cells transfected with non-targeting control siRNAs (100%). Forty eight hours after siRNA transfection, cells were infected with SARS-CoV-GFP and 24 h later cells were fixed and GFP fluorescence was quantified (c). The level of GFP expression was normalized to that in infected cells transfected with non-targeting siRNA.

were significantly reduced, to approximately 25 % of the original level (Fig. 3a). Depletion of CypA or CypB did not affect cell viability (Fig. 3b), but did also not significantly inhibit the replication of SARS-CoV-GFP in 293/ACE2 cells, compared to infected cells transfected with a non-targeting control siRNA (Fig. 3c). These data suggest that these specific cyclophilins, which have been implicated in the replication of other viruses, are not required for SARS-CoV replication. Alternatively, the remaining cyclophilin levels in siRNA-treated cells may suffice to support normal virus replication.

In conclusion, CsA inhibits the replication of diverse coronaviruses at non-cytotoxic, low-micromolar concentrations. Treatment of infected cells with 16 μM CsA strongly reduced viral and reporter gene expression of SARS-CoV-GFP, the amount of dsRNA in infected cells and the virus titre in culture supernatants (by more than 3 logs). In cells infected with HCoV-229E-GFP and MHV-GFP reporter gene expression and the production of infectious progeny were also significantly decreased upon CsA treatment. Compared to other RNA viruses [272-274, 299, 330], somewhat higher CsA concentrations were required to block coronavirus replication (16 versus 0.5-3 μM), suggesting coronaviruses to be less sensitive to CsA treatment. However, we cannot exclude that this may in part be due to differences in experimental set-up, including the cells and high MOI used and whether or not cells were pretreated with CsA [275, 307, 327].

The inhibitory effect of CsA and its analogues and the role of cyclophilins in virus replication have been studied in considerable detail for HCV and several other RNA viruses. In the case of HCV, cyclophilin inhibitors lacking the undesirable immunosuppressive properties of CsA – NIM811, Debio-025 and SCY-635 - are currently being tested in clinical trials [283-285]. Several mechanism of action studies on the inhibitory effect of CsA identified mainly CypA and CypB to be involved in virus replication. CypA was found to interact with HCV NS2 [331], NS5A [302, 304, 332] and NS5B [306] and was shown to be required for HCV replication. Furthermore, CypA was found to functionally interact with West Nile Virus NS5 [275] and vesicular stomatitis virus N protein [271]. In addition, an interaction between CypB and Japanese encephalitis virus NS4A [273] was documented and CypB also appears to be a functional regulator of the HCV polymerase [309]. Also Cyp40 was found to play a role in HCV replication [303, 333].

Although the exact mechanism by which CsA inhibits coronavirus replication remains to be established, it is likely that the drug also interferes with functional interactions between viral proteins and one or multiple members of the large cyclophilin family. If this indeed proves to be true, it will be interesting to explore the potential of these host proteins for the development of a coronavirus-wide antiviral strategy.

ACKNOWLEDGMENTS

We are grateful to Corrine Beugeling, Marjolein Kikkert, Aartjan te Velthuis and Kazimier Wannee for technical assistance. We kindly thank Dr. Albrecht von Brunn (University of Munich, Germany) and Dr. Pierre Talbot and Dr. Dominique Favreau (University of Quebec, Canada) for sharing and discussing their unpublished data on CsA and coronaviruses. This research was supported by the Netherlands Organisation for Scientific Research (NWO-CW TOP grant #700-57-301), the EU-FP7-Health project SILVER (Grant #260644), the Swiss National Science Foundation (V.T.) and by NIH Public Health Service grant AI72493 (S.M.).

Chapter 5

A kinome-wide siRNA screen identifies proviral and antiviral host factors in SARS-coronavirus replication, including PKR and early secretory pathway proteins

Adriaan H. de Wilde[†], Kazimier F. Wannee[†], Florine E.M. Scholte, Jelle J. Goeman, Peter ten Dijke, Eric J. Snijder, Marjolein Kikkert[‡], and Martijn J. van Hemert[‡]

^{†,‡} These authors contributed equally

Manuscript submitted

ABSTRACT

To identify host factors that influence SARS-coronavirus (SARS-CoV) replication, we performed an siRNA library screen targeting the human kinome. Protein kinases are key regulators of many cellular functions and the systematic knockdown of their expression should provide a broad perspective on factors and pathways promoting or antagonizing coronavirus replication. In addition to 40 proviral proteins that promote SARS-CoV replication, our study identified 90 factors with an antiviral effect. Pathway analysis grouped subsets of these factors in specific cellular pathways, like the innate immune response and the metabolism of complex lipids, which thus appear to play an important role in SARS-CoV-infected cells. Two factors were selected for more extensive validation and follow-up experiments. In cells depleted for the beta 2 subunit of the coatamer protein complex (COPB2), the strongest proviral hit, we observed reduced SARS-CoV protein expression and a 2-log reduction in virus yield. The effect of knockdown of the COPB2-related factors COPB1 and Golgi-specific brefeldin A-resistance guanine nucleotide exchange factor 1 (GBF1) also suggested that COPI-coated vesicles and/or the early secretory pathway are important for SARS-CoV replication. Depletion of the antiviral double-stranded RNA-activated protein kinase (PKR) enhanced virus replication, and validation experiments using PKR-directed siRNAs confirmed increased SARS-CoV protein expression and virus production upon PKR depletion. The inventory of pro- and antiviral host factors and pathways described in this study expands our understanding of the replication of SARS-CoV, and may contribute to the identification of novel targets for antiviral therapy.

INTRODUCTION

Positive-stranded RNA (+RNA) viruses interact with the infected host cell at many levels during their replicative cycle, and thus far numerous host cell proteins with a role in virus replication have been identified [60-65]. These include on the one hand host factors that are used by the virus during the various stages of its life cycle, and on the other hand factors that are part of the host defense against virus infection. Such proteins may constitute interesting targets in the development of novel antiviral strategies, as drug resistance is less likely to develop when cellular rather than viral functions are targeted. Antiviral drug resistance is a serious problem, in particular when combating RNA viruses, due to their high mutation rate and potential for rapid adaptation.

Systems biology approaches have been instrumental in advancing our knowledge of individual proteins and cellular pathways that influence +RNA virus infection. For example, systematic functional genomics screens using small interfering RNA (siRNA) libraries have identified numerous host genes with a role in the replication of important human pathogens like West Nile virus [334], Dengue virus [335], human immunodeficiency virus 1 [336], hepatitis C virus [337-342], and influenza virus [338, 343, 344]. For coronaviruses a number of relevant host proteins were previously described ([321], and reviewed in [65, 320]), but the use of larger-scale siRNA screens to systematically identify such factors was not documented thus far.

Coronaviruses, and other members of the order Nidovirales [286], have the largest RNA genomes known to date (27-31 kb [37]) and the complexity of their molecular biology clearly distinguishes them from other +RNA virus groups. Although infection with most human coronaviruses is associated with relatively mild respiratory disease [19, 345], the 2003 outbreak of severe acute respiratory syndrome (SARS) highlighted the potential of coronaviruses to cause lethal disease in humans. The zoonotic transfer of SARS-coronavirus (SARS-CoV), which likely originated from bats, initiated an outbreak that affected about 8,000 humans, with a mortality of about 10% [317]. Strikingly, a similar outbreak of coronavirus-induced severe respiratory disease has been developing in a number of Arab countries since April 2012, with 9 of the 15 confirmed cases thus far (March 2013) having a fatal outcome (http://www.who.int/csr/don/archive/disease/coronavirus_infections/en/). The causative agent, human coronavirus EMC/2012, was recently identified as a previously unknown member of betacoronavirus subgroup 2c [15, 16]. Although the source of this emerging human pathogen remains to be identified, it is striking that – as in the case of SARS-CoV – its closest known relatives are coronaviruses circulating in bats [16]. These recent developments highlight once again the relevance of the systematic dissection of coronavirus-host interactions and the development of antiviral approaches to combat coronavirus infection.

Many aspects of coronavirus molecular biology remain poorly understood. SARS-CoV RNA synthesis, like that of many +RNA viruses [56], takes place at modified cytoplasmic membranes [30, 53]. The viral replication and transcription complexes (RTCs) are associated with a reticulovesicular network (RVN) of modified endoplasmic reticulum [30], which is thought to form a suitable microenvironment for RNA synthesis and possibly protects against cellular antiviral activities. Multiple host factors and cellular processes are likely involved in RVN formation and also the RTCs themselves may include various host factors in addition to the SARS-CoV nonstructural proteins (nsps) that drive viral RNA synthesis.

Previous studies identified a number of interactions between coronavirus factors and the antiviral immune response [65, 277, 320, 321]. Several evasion mechanisms were attributed to protein functions that can be either conserved across CoVs or specific for certain CoV lineages. Proteins such as nsp1 [346], the nsp3 papain-like proteinase [347], the nsp16 2'-O-methyltransferase [348], the nucleocapsid (N) protein [349], and the products of SARS-CoV ORFs 3b, 6, and 7a [105, 109, 350, 351] have all been reported to prevent interferon (IFN) induction and/or signalling.

To gain more insight into the role of host factors in the replicative cycle of SARS-CoV, we set out to systematically identify kinase-regulated cellular processes that influence virus replication. Protein kinases are key regulators in signal transduction and control a wide variety of cellular processes. Thus, assessing their relevance for virus replication can provide a broad perspective on cellular factors and pathways that influence SARS-CoV replication, as previously illustrated by studies identifying cellular kinases as host factors in various stages of the replicative cycle of other +RNA viruses [340, 341, 352, 353].

In this study, we screened an siRNA library that targets the cellular kinome (779 genes) and identified 40 proviral and 90 antiviral factors, whose depletion significantly reduced or enhanced SARS-CoV replication, respectively. Pathway analysis grouped several subsets of hits in specific cellular pathways, suggesting that these play an important role in the SARS-CoV-infected cell. Two prominent hits from the siRNA screen, the proviral beta 2 subunit of the coatamer complex (COPB2) and the antiviral double-stranded RNA-activated protein kinase (PKR), were selected for independent validation and follow-up analysis, which confirmed their importance for SARS-CoV replication. Our data offer a glimpse into the complex interplay between SARS-CoV and the host cell, and provide a basis for more focused studies to enhance our understanding of coronavirus replication and coronavirus-host interactions.

MATERIALS AND METHODS

Cell culture, viruses, and virus titration

293/ACE2 [74] and Vero E6 cells were cultured as described previously [354]. SARS-CoV strain Frankfurt-1 [208] and GFP-expressing recombinant SARS-CoV (Urbani strain) [324] were used to infect cell monolayers as described previously [354]. Virus titrations were performed essentially as described before [355]. All work with live wild-type (wt) SARS-CoV and SARS-CoV-GFP was performed inside biosafety cabinets in a biosafety level 3 facility at Leiden University Medical Center.

siRNA library and transfection reagents

The ON-TARGETplus SMARTpool Protein Kinases siRNA Library that targets the mRNAs of 779 genes, comprising the complete human kinome and some additional targets, was obtained from Dharmacon. Each individual siRNA SMARTpool consisted of four siRNAs targeting the same gene. A non-targeting (scrambled) siRNA (cat. nr. D-001810-10; Dharmacon) served as a negative control and a GAPDH-targeting siRNA (cat. nr. D-001830-10; Dharmacon) was used to routinely monitor transfection and knockdown efficiency. Stock solutions (2 μM) of siRNA SMARTpools were prepared by dissolving 0.5 nmol of siRNA SMARTpools in 250 μl of 1x siRNA buffer (60 mM KCl, 6 mM HEPES (pH 7.5), 0.2 mM MgCl_2 ; Dharmacon), according to the manufacturer's instructions. Using a 96-well pipettor (Rainin Liquidator 96), the contents of the siRNA library master plates were aliquoted into volumes appropriate for individual screening experiments. The resulting ten deep-well 96-well library plates (Greiner Bio-One) were stored at -80°C until further use.

siRNA library screening

In each siRNA screen, 293/ACE2 cells in 96-well plates containing $\sim 10^4$ cells per well were transfected with a 100- μl mixture containing 100 nM siRNA, 0.2 μg DharmaFECT1 (Dharmacon), OptiMEM (Invitrogen), and antibiotic-free cell culture medium, supplemented with 8% FCS and 2.5mM L-Glutamine, according to the manufacturer's instructions. Transfection mixes were prepared in the ten deep-well 96-well plates that together contained the complete library of 779 siRNA SMARTpools (see above). Using the contents of these library plates, we transfected black and transparent 96-well plates with 293/ACE2 cells, each in triplicate. For a schematic representation of the experimental set-up and plate lay-out, see Figs. 2A and 3A. Transfection of individual siRNA duplexes targeting PKR (cat. nr. LU-003527-00; Dharmacon), or siRNA SMARTpools targeting COPB1 (cat. nr. L-017940-01) and GBF1 (cat. nr. L-019783-00) was performed as described previously [354]. Twenty-four hours post transfection (p.t.), the medium was replaced, and cells were incubated for another 24 h at 37°C . At 48 h p.t., cells were infected with SARS-CoV-

GFP at an MOI of 10, and 24 h later they were fixed with 3% paraformaldehyde (PFA) in PBS. GFP expression was quantified by measuring fluorescence in a 96-well plate reader (Berthold Mithras LB 940), using excitation and emission wavelengths of 485 and 535 nm, respectively. The fluorescence in wells containing mock-infected cells was used to correct for background signal.

GAPDH and cell viability assays

At 48 h p.t., GAPDH enzyme activity in lysates of siRNA-transfected cells was measured using the KDaAlert™ GAPDH Assay Kit (Ambion) according to the manufacturer's instructions. Possible cytotoxic effects of siRNA transfection were analyzed (in triplicate) at 48 h p.t., using the CellTiter 96® AQueous Non-Radioactive Cell Proliferation Assay (Promega). After 90 min, the reaction was terminated by the addition of 25 µl of 10% SDS and absorbance at 490 nm (A_{490}) was measured using a 96-well plate reader (Berthold).

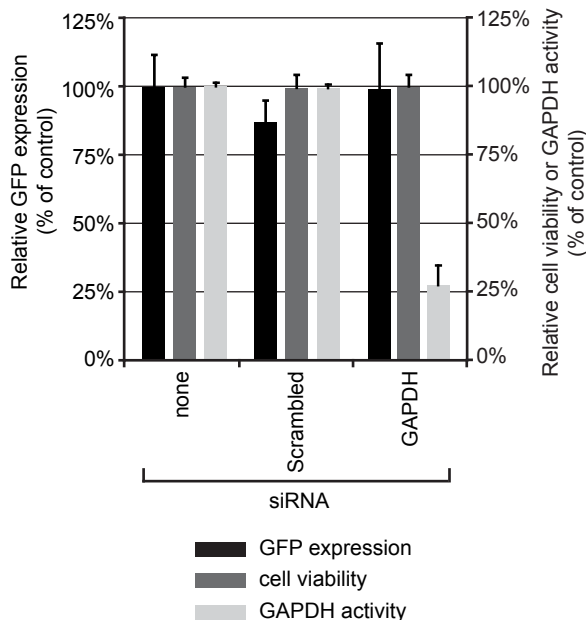


Fig. 1. siRNA-transfected 293/ACE2 cells are susceptible to SARS-CoV infection. 293/ACE2 cells were transfected with siRNAs targeting GAPDH mRNA and a scrambled control siRNA. At 48 h p.t., the cells were infected with SARS-CoV-GFP (MOI 10) and 24 h later cells were fixed and GFP fluorescence was measured (black bars). Cell viability (dark grey bars) was analyzed at 48 h after siRNA transfection and knockdown of GAPDH expression was monitored by measuring enzymatic activity (light grey bars). All values were normalized to those obtained with non-transfected control cells (100%).

Data analysis

Raw data from GFP fluorescence and cell viability measurements were analyzed per individual screen with the Bioductor/R package CellHTS2 [356] with minor modifications (see results section and Fig. 2B for details). The average GFP expression ($n=3$) and cell viability were calculated and normalized to the signals of scrambled siRNA-transfected (control) cells. A two-sided one-sample Student's t test was used on the \log_2 -transformed normalized values to determine the significance ($p < 0.05$) of the changes in GFP expression caused by siRNA transfection. The siRNA transfection was considered non-cytotoxic when the normalized cell viability assay readings (A_{490}) were above 0.85 ($p < 0.05$). Significance was determined using a one-sided one-sample Student's t test on the \log_2 -transformed normalized values using $\mu \leq 0.85$ as the null hypothesis.

Gene silencing using lentivirus-expressed shRNAs

Vectors for expression of short hairpin RNAs (shRNAs) targeting human COPB2 (cat. nr. TRCN-065114; accession nr. NM_004766) or human PKR (cat. nr. TRCN-001382; accession nr. NM_002759) were picked from the MISSION TRC-1 library of shRNA-expressing lentiviruses (Sigma) and lentivirus stocks were prepared according to the manufacturer's instructions. A lentivirus expressing a non-targeting (scrambled) shRNA (cat. nr. SHC-002) was used as negative control. Lentivirus particle titers were determined using a p24 ELISA (Zeptometrix) according to the manufacturer's instructions. Wells (4 cm^2) containing 8×10^4 293/ACE2 cells were transduced with shRNA-expressing lentiviruses at an MOI of 3 in culture medium containing $8 \mu\text{g/ml}$ polybrene, and after 24 h fresh medium was given. At 72 h p.t., cells were infected with wt SARS-CoV or SARS-CoV-GFP (MOI 0.01), or depletion of COPB2 or PKR was validated by Western blot analysis of cell lysates using target-specific antibodies.

Protein analysis and antibodies

Total cell lysates were prepared in 4x Laemmli sample buffer (100 mM Tris-HCl, pH 6.8, 40% glycerol, 8% sodium dodecyl sulfate (SDS), 40 mM DTT, 0.04 mg/ml bromophenol blue), after which samples were heated at 95°C for 15 min. Following SDS-PAGE, proteins were transferred to Hybond-LFP membranes (GE Healthcare) by semi-dry blotting, and membranes were blocked with 1% casein in PBS containing 0.1% Tween-20 (PBST). The following antisera against cellular proteins were used: rabbit anti-PKR (cat. nr. 610764; BD Biosciences), goat anti-COPB2 (sc-13332; Santa-Cruz), and mouse monoclonal antibodies against β -actin (A5316; Sigma) and the transferrin receptor (TfR; cat. nr. 13-6890; Invitrogen). Rabbit antisera against SARS-CoV nsp8 and N protein [30, 52] were used to analyze viral protein expression. After overnight incubation with the primary antibody, membranes were probed with biotinylated secondary antibodies (biotinylated rabbit anti-goat, swine anti-rabbit, or goat anti-mouse) for 1 h at RT, after which a tertiary

mouse anti-biotin-Cy3 antibody was used to visualize protein bands using a Typhoon 9410 scanner (GE Healthcare).

Canonical pathway analysis

The Ingenuity Pathway Analysis (IPA™) package was used to place hits in canonical cellular pathways. The significance of the association between the data set and the respective pathways was determined in two ways: (i) the number of molecules from the

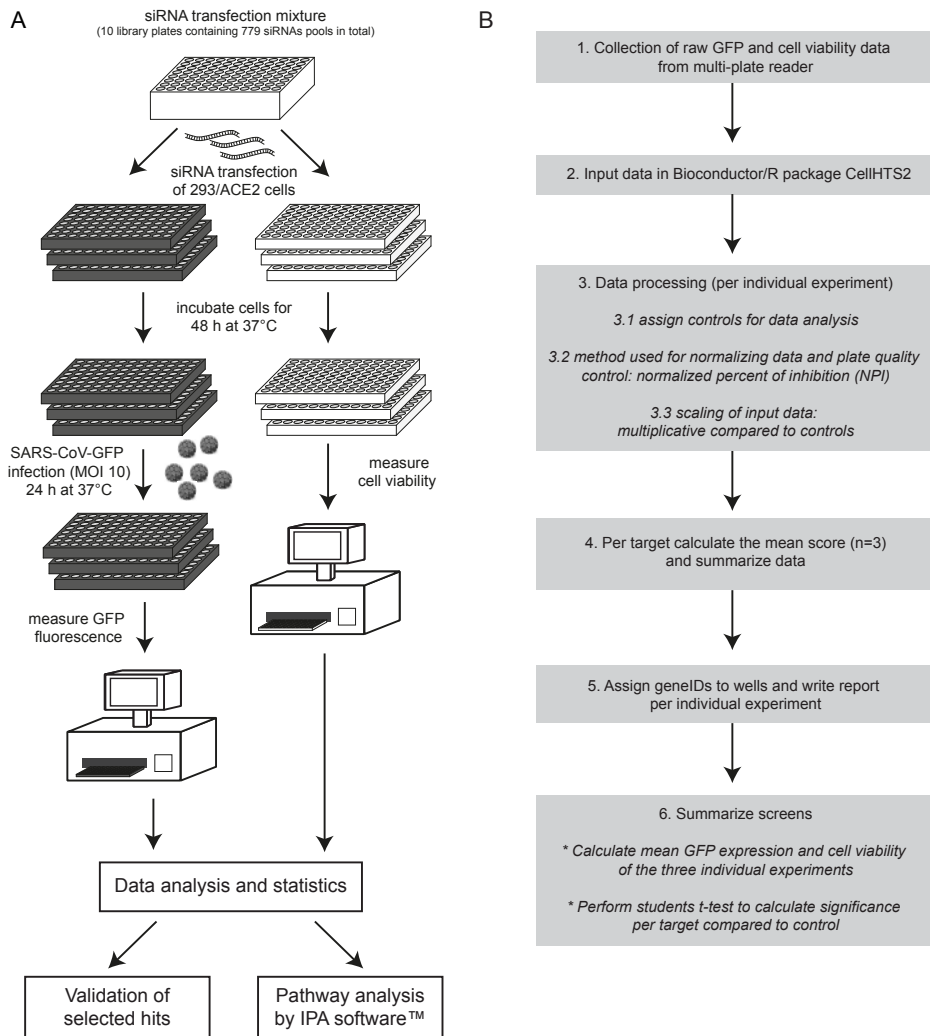


Fig 2. siRNA library screening procedure and data analysis. (A) Schematic overview of the experimental design of the siRNA library screen. See text for details. (B) Flow chart outlining the data analysis procedure that was performed with the Bioconductor/R package CellHTS2. See text for details.

data set that map to a specific pathway divided by the total number of molecules in that canonical pathway (the higher the percentage of hits identified in a specific pathway, the higher the likelihood it plays a role in the viral replicative cycle); (ii) Fisher's exact test was used to determine the probability that the association between the genes in the dataset and the canonical pathway is explained by chance alone.

RESULTS

Developing siRNA library screening for host factors involved in nidovirus replication.

A commercial human kinome-directed siRNA library (779 targets) was used to assess the effect of systematic knockdown of individual host kinases on the replicative cycle of the coronavirus SARS-CoV (this study) and the distantly related arterivirus EAV (K. F. Wansee, A. H. de Wilde *et al.*, unpublished data). We performed our siRNA screens in 293/ACE2 cells [74], which express the SARS-CoV receptor angiotensin-converting enzyme 2 and, in contrast to other cell lines tested, were found to be permissive to infection with both SARS-CoV and EAV. This property facilitates direct comparative studies between these two distantly related nidoviruses [354]. Furthermore, 293/ACE2 cells could be efficiently transfected with siRNAs, as illustrated by a consistent ~75% reduction of GAPDH activity at 48 h p.t. with an siRNA SMARTpool targeting the GAPDH mRNA (Fig. 1; light grey bars). No change in cell viability was detected by 48 h p.t. following transfection with either a scrambled siRNA or the GAPDH-specific siRNA (Fig. 1; dark grey bars). When these siRNA-transfected 293/ACE2 cells were subsequently infected with SARS-CoV-GFP (MOI 10), no significant differences in GFP expression were observed at 24 h p.i. compared to control cells that had not been transfected with siRNAs. This demonstrated that the siRNA transfection procedure per se did not adversely affect SARS-CoV-GFP replication (Fig. 1; black bars).

siRNA screening for host kinases involved in SARS-CoV replication.

A human kinome-directed siRNA screen was performed to identify host cell kinases that affect SARS-CoV-GFP replication, according to the experimental set-up outlined in Fig. 2A. For each independent siRNA screening experiment, we used a set of ten 96-well library plates, each containing approximately 80 specific siRNA SMARTpools and several controls (see plate layout in Fig. 3A). Transfection mixes (final concentration of 100 nM siRNA) were prepared in these library plates and their contents was used to transfect - per library plate - 293/ACE2 cells in three black and three transparent 96-well plates. Forty-eight hours after siRNA transfection, the black plates were infected with the SARS-CoV-GFP reporter virus (MOI 10), and at 24 h p.i. GFP expression was analyzed by

fluorimetric quantitation. At the moment of infection, the transparent plates were used to monitor (potential) cytotoxic effects of siRNA transfection using a colorimetric cell viability assay. The complete siRNA screen, i.e. the viability controls and the quantitation of SARS-CoV-driven GFP expression (in triplicate for each siRNA), was repeated three times, after which data sets were processed as outlined in Fig. 2B. The data, obtained from a 96-well plate reader (step 1) were processed with the Bioconductor/R package CellHTS2 as described [356] (step 2). Experimental controls were assigned (step 3.1 and Fig. 3A), and the NPI method (normalized percent of inhibition; step 3.2) was used to normalize GFP fluorescence values to those of scrambled siRNA-transfected cells, and to correct for plate-to-plate variation. Subsequently, the GFP data were transformed to a multiplicative scale (the value obtained using scrambled siRNA-transfected cells was set to 1; step 3.3). Next, the results for each replicate library screen were summarized and used for further data analysis (step 4), including the assignment of GeneIDs to each well (step 5). Finally, the data of the three independent library screens were combined and summarized (step 6).

The processed data output of a representative library screen, showing the distribution of the hits for each plate, is depicted in Fig. 3A. Column 1 of each plate contained the infected control cells described above, whereas column 12 contained mock-infected cells. Host cell kinases were considered to have a proviral effect when their siRNA-mediated knockdown reduced the GFP signal (negative score values) and kinases were considered antiviral when the GFP signal increased upon their knockdown (positive score values). Graphical representations of the hit distribution per plate were visually inspected in order to minimize the chance of false positive or false negative hits due to major (technical) artifacts (Fig. 3A).

Using scrambled siRNA-transfected control cells as a reference, the knockdown of most cellular kinases was found to be non-cytotoxic within the time frame of this experiment (Fig. 3B and Data set S1). The cut-off value below which siRNA treatment was considered to be toxic was set at 85% cell viability relative to scrambled siRNA-transfected control cells ($p < 0.05$) (Fig. 3B). Using this criterion, 222 out of 779 (28.5%) transfections with the specific siRNA pools appeared to be toxic to the cells. A minor fraction (50 targets; 6.4%) appeared to be highly detrimental (normalized viability value below 75%). To prevent false-positive proviral hits due to a general negative effect on cell viability or cell division, we excluded all targets whose knockdown was associated with viability measurements below 85%. Such data filtering was not applied for antiviral hits (i.e. knockdown enhancing GFP expression) since siRNA-induced cytotoxicity is expected to inhibit virus replication and should therefore not give rise to false-positive antiviral hits.

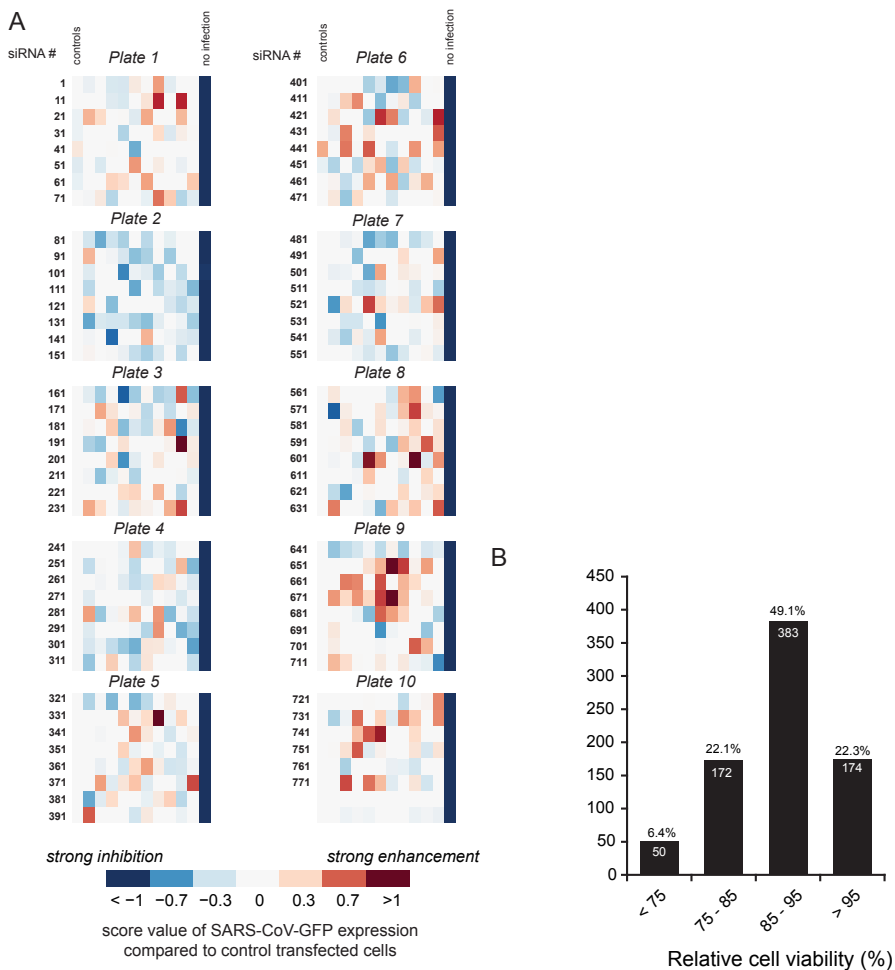


Fig. 3. Quality plots of the siRNA screen for host factors involved in SARS-CoV replication. (A) Plate-wise quality-plots of the score values for one replicate of a representative siRNA library screen. In total, three screens, each consisting of three replicates, were performed. Score values of -1, 0, and 1 represent 0%, 100%, and 200% SARS-CoV-driven GFP expression compared to infected control wells, respectively. Cells transfected with control siRNAs were present in the first column (“controls”) of each plate, while the cells in column 12 were mock-infected to allow correction for background GFP signal. The remaining wells of each plate (columns 2-11) contained cells transfected with the siRNA SMARTpools. The GFP expression level in each well compared to that of control siRNA-transfected cells (score value) is represented by the color-coded squares according to the legend below panel A. (B) Relative cell viability of cells transfected with the 779 siRNA pools in the kinome-wide siRNA library. Viability assays were done at 48 h p.t. and the data were normalized to the measurements for control cells transfected with scrambled siRNA (100%). Data were binned into 4 viability categories and the number in each bar is the absolute number of targets within that category, which represents the percentage of the 779 siRNA targets in the screen that is indicated above each bar. The viability data are the average of three independent library screens, each including triplicate measurements for each siRNA pool in the library.

Identification of proviral and antiviral hits and pathways influencing SARS-CoV-GFP infection.

After exclusion of toxic siRNA SMARTpools that decreased GFP expression (see above), the remaining 684 targets were ranked on the basis of the GFP signal measured in SARS-CoV-GFP-infected cells (\log_2 -fold GFP expression compared to control cells; Fig. 4). Targets were qualified as antiviral or proviral hits if GFP expression differed significantly from that in control cells transfected with the scrambled siRNA pool ($p < 0.05$). Knockdown of the majority of the targets (552 proteins) did not significantly alter GFP reporter gene expression ($p > 0.05$). However, as common in this kind of screening experiments, we cannot formally exclude that our results may have been influenced by insufficient knockdown of certain target genes by the library's siRNA pools.

Using the criteria outlined above, a total of 90 cellular proteins (19.4% of all targets) were identified as antiviral factors, since their depletion significantly increased GFP expression. For 36 of these antiviral hits, knockdown resulted in an increase of at least 1.5-fold (Fig. 5A). Forty proviral factors were identified and the knockdown of nine of those reduced GFP expression by more than 2-fold (Fig. 5B; for the complete data set, see Dataset S2).

Although, according to the criteria formulated above ($p < 0.05$), ANGPT4 (214%; $p = 0.0555$) and PKR (210%; $p = 0.0884$) formally did not qualify as antiviral hits, we have included these proteins in view of the exceptionally strong stimulation of GFP expression triggered by their knockdown (Fig. 5A). Furthermore, since its knockdown resulted in an almost 3-fold decrease of GFP signal (35%; $p = 0.0004$), DGKE was included as a proviral hit, despite the fact that the viability assay did not rigorously exclude cytotoxic effects for this siRNA pool (viability 88%, $p = 0.0540$).

The pro- and antiviral hits identified in the siRNA screen were mapped to cellular pathways using the IPA software package. Fig. 6 shows the canonical pathways and more general functional categories (highlighted in color) in which the proviral (red) and antiviral (green) hits were strongly represented ($p < 0.05$). The pathways included apoptosis, cellular immune response, growth factor signaling, cellular homeostasis, metabolism of complex lipids, and intracellular and second messenger signaling.

Validation of COPB2 as a proviral factor in SARS-CoV replication.

COPB2 (or β' -COP) was identified as the strongest proviral hit in our screen, as its knockdown resulted in an 82% decrease of GFP expression ($p = 0.0143$; Fig. 5B). The coatamer protein complex, of which COPB2 is a subunit, contains a total of seven protein subunits (α -, β -, β' -, γ -, δ -, ϵ -, and ζ -COP), and drives the formation of COPI-coated vesicles, which function in retrograde transport in the early secretory pathway [357]. To validate its role as a proviral host factor in SARS-CoV replication, COPB2 was depleted by transducing 293/ACE2 cells with lentiviruses expressing COPB2 mRNA-specific shRNAs. This reduced

COPB2 levels by ~70%, compared to control cells transduced with a lentivirus expressing a scrambled shRNA (Fig. 7A), and this reduction in COPB2 levels did not affect cell viability (Fig. 7B). Subsequent infection of COPB2-depleted cells with SARS-CoV-GFP (MOI 0.01) resulted in a decrease of N protein and GFP expression at 32 h p.i. (Fig. 7C; left panel). To verify that knockdown experiments with recombinant SARS-CoV-GFP properly reflected the characteristics of the wt virus, we analyzed viral protein expression and

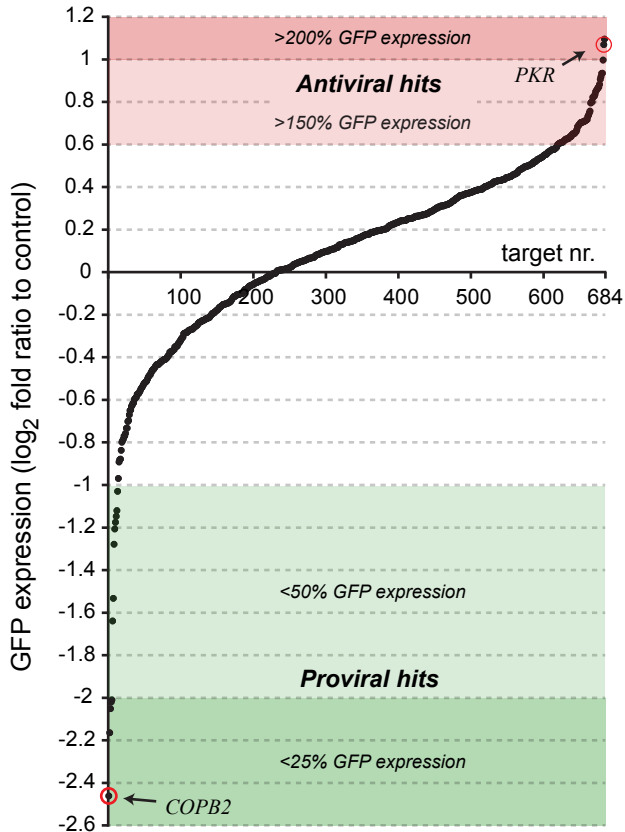


Fig. 4. Results of the siRNA screens for host factors influencing SARS-CoV replication. The plot shows the distribution of the \log_2 -transformed values of reporter gene expression by SARS-CoV-GFP in siRNA-transfected cells, normalized to the GFP signal of infected control cells that were transfected with scrambled siRNA. Targets were ranked based on the magnitude of the effect of their knockdown on SARS-CoV replication. Targets were considered to have an important antiviral effect when their knockdown increased reporter gene expression to at least 150% (red area above x-axis). Proviral hits, whose knockdown induced an at least 2-fold reduction in GFP expression, are depicted in the green area below the x-axis. Proviral targets whose knockdown reduced cell viability to below 85% were excluded (see main text), leaving a total of 684 targets included in the final analysis. The positions of the targets used for follow-up validation experiments (COPB2 and PKR) are indicated. The plot represents the average of three library screens (each done in triplicate).

virus yield in COPB2-depleted cells at 24 h after infection with wt SARS-CoV (MOI 0.01). As for SARS-CoV-GFP, a clear reduction in N protein expression was observed compared to cells transduced with a lentivirus expressing a scrambled shRNA (Fig. 7C; right panel). Titration of culture supernatants from SARS-CoV-GFP-infected cells (32 h p.i.) and wt SARS-CoV-infected cells (24 h p.i.) revealed a 2- to 3-log reduction for both viruses (Fig. 7D).

Proteins of the early secretory pathway are important for SARS-CoV replication.

To further substantiate the importance of COPI-coated vesicles for SARS-CoV replication, the expression of another component of the coatamer protein complex, subunit beta 1 (COPB1) was depleted by transfection of 293/ACE2 cells with a COPB1 mRNA-specific siRNA SMARTpool. After 48 h, transfected cells were infected with SARS-CoV-GFP (MOI 10) and 24 h later GFP expression was quantified. Depletion of COPB1 resulted in a reduction of SARS-CoV-driven GFP expression with 83% (Fig. 7E). The formation of COPI-coated vesicles is mediated through activation of ADP-ribosylation factor 1 (Arf1) by Golgi-specific brefeldin A-resistance guanine nucleotide exchange factor 1 (GBF1) [358]. Therefore, we also analyzed the importance of GBF1. GFP reporter gene expression by SARS-CoV-GFP was reduced by 89% in 293/ACE2 cells that had been depleted for GBF1 by siRNA transfection and were subsequently infected at 48 h p.t. (Fig. 7E). Taken together, these data suggest that COPB2 and COPI-coated vesicles play an essential role in SARS-CoV replication.

Validation of PKR as antiviral hit affecting SARS-CoV replication.

PKR was one of the strongest of the 90 antiviral hits that were identified in the siRNA library screen. In two independent follow-up experiments with PKR-specific siRNA SMARTpools, a more than 2-fold increase in GFP expression by SARS-CoV-GFP was observed (data not shown), suggesting that PKR is a bona fide antiviral hit. PKR is a serine/threonine protein kinase that is activated by double-stranded (ds)RNA, a hallmark of RNA virus infection, and the activated form of PKR blocks translation initiation through eIF-2 α phosphorylation (reviewed in [68]).

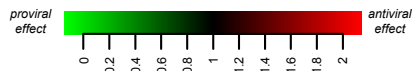
To further validate the antiviral role of PKR in SARS-CoV replication, a deconvoluted set of four individual PKR-directed siRNAs was used. Transfection of 293/ACE2 cells with three of these siRNAs (numbers 2, 3, and 4) significantly increased SARS-CoV-driven GFP expression (Fig. 8A; black bars). Cell viability was slightly reduced after transfection with these PKR-directed siRNAs, in particular using siRNA 2 which caused a 14% reduction in cell viability (Fig 8A; grey bars). Nevertheless, despite the fact that this siRNA adversely affected cell viability, an increase rather than a decrease of SARS-CoV-driven GFP expression was observed.

A

<i>GeneID</i>	GFP expression (fold increase)			average	<i>p</i> -value	<i>Accession</i>	<i>Gene name</i>
	1	2	3				
ANGPT4	1.8	3.1	1.8	2.1	0.0555*	NM_015985	Angiotensinogen 4
PKR	3.0	1.4	2.3	2.1	0.0884*	NM_002759	Double-stranded RNA-activated protein kinase
CLK1	2.1	2.1	1.8	2.0	0.0077	NM_004071	CDC-like kinase 1
MAP2K6	2.0	2.0	1.8	1.9	0.0014	NM_002758	Mitogen-activated protein kinase kinase 6
CSNK1G1	1.7	2.1	1.8	1.9	0.0067	NM_022048	Casein kinase 1, gamma 1
EPHA3	1.7	1.6	2.1	1.8	0.0176	NM_005233	EPH receptor A3
CDK6	1.7	2.1	1.7	1.8	0.0140	NM_001259	Cyclin-dependent kinase 6
AURKB	1.9	1.8	1.8	1.8	0.0016	NM_004217	Aurora kinase B
GCK	1.8	2.0	1.6	1.8	0.0119	NM_000162	Glucokinase (hexokinase 4, maturity onset diabetes of the young 2)
DGKD	1.8	1.6	2.0	1.8	0.0135	NM_003648	Diacylglycerol kinase, delta 130kDa
STK24	2.0	1.5	1.9	1.8	0.0241	NM_003576	Serine/threonine kinase 24 (STE20 homolog, yeast)
CKS1B	2.1	1.6	1.6	1.7	0.0298	NM_001826	CDC28 protein kinase regulatory subunit 1B
CLK4	1.6	2.1	1.6	1.7	0.0282	NM_020666	CDC-like kinase 4
HK1	1.6	2.1	1.5	1.7	0.0318	NM_000188	Hexokinase 1
ACVR1	1.7	1.7	1.6	1.7	0.0018	NM_001105	Activin A receptor, type I
AKAP6	1.8	1.7	1.5	1.7	0.0068	NM_004274	A kinase (PRKA) anchor protein 6
FLJ12476	1.7	1.6	1.6	1.6	0.0004	NM_022784	IQ motif containing H
LATS1	1.8	1.6	1.5	1.6	0.0074	NM_004690	LATS, large tumor suppressor, homolog 1 (Drosophila)
CDKL2	1.4	1.8	1.7	1.6	0.0265	NM_003948	Cyclin-dependent kinase-like 2 (CDC2-related kinase)
MAPK9	1.9	1.6	1.5	1.6	0.0207	NM_002752	Mitogen-activated protein kinase 9
PTPRG	1.9	1.4	1.6	1.6	0.0259	NM_002841	Protein tyrosine phosphatase, receptor type, G
BMPR2	1.7	1.4	1.8	1.6	0.0261	NM_001204	Bone morphogenetic protein receptor, type II (serine/threonine kinase)
DCK	1.6	1.5	1.7	1.6	0.0051	NM_000788	Deoxycytidine kinase
MAP2K3	1.6	1.9	1.4	1.6	0.0369	NM_002756	Mitogen-activated protein kinase kinase 3
MYO3B	1.7	1.5	1.5	1.6	0.0087	NM_138995	Myosin IIIb
EIF2AK3	1.6	1.6	1.5	1.6	0.0014	NM_004836	Eukaryotic translation initiation factor 2-alpha kinase 3
CLK3	1.7	1.6	1.4	1.6	0.0138	NM_001292	CDC-like kinase 3
FYB	1.8	1.5	1.4	1.6	0.0217	NM_001465	FYN binding protein (FYB-120/130)
ALS2CR7	1.5	1.8	1.4	1.5	0.0327	NM_139158	Cyclin-dependent kinase 15
STK25	1.7	1.4	1.6	1.5	0.0224	NM_006374	Serine/threonine kinase 25 (STE20 homolog, yeast)
HAK	1.5	1.7	1.5	1.5	0.0130	NM_052947	Alpha-kinase 2
ITK	1.6	1.5	1.5	1.5	0.0004	NM_005546	IL2-inducible T-cell kinase
MAPK1	1.6	1.5	1.5	1.5	0.0042	NM_002745	Mitogen-activated protein kinase 1
DGUOK	1.5	1.6	1.5	1.5	0.0007	NM_001929	Deoxyguanosine kinase
MVD	1.7	1.4	1.5	1.5	0.0211	NM_002461	Mevalonate (diphospho) decarboxylase
EK1	1.7	1.4	1.4	1.5	0.0172	NM_018638	Ethanolamine kinase 1
EPHA5	1.4	1.4	1.8	1.5	0.0385	NM_004439	EPH receptor A5
DAPK3	1.4	1.7	1.5	1.5	0.0141	NM_001348	Death-associated protein kinase 3

B

<i>GeneID</i>	GFP expression (fold increase)			average	<i>p</i> -value	<i>Accession</i>	<i>Gene name</i>
	1	2	3				
COPB2	0.2	0.3	0.1	0.2	0.0143	NM_004766	Coatomer protein complex, subunit beta 2 (beta prime)
CDK5R2	0.2	0.4	0.2	0.2	0.0251	NM_003936	Cyclin-dependent kinase 5, regulatory subunit 2 (p39)
PFTK1	0.4	0.3	0.3	0.3	0.0087	NM_012395	PFTAIRE protein kinase 1
ABI1	0.4	0.3	0.3	0.3	0.0055	NM_005470	Abl-interactor 1
DGKE	0.3	0.4	0.4	0.4	0.0004 [†]	NM_003647	Diacylglycerol kinase, epsilon 64kDa
NME2	0.5	0.4	0.4	0.4	0.0027	NM_002512	Non-metastatic cells 2
AZU1	0.5	0.4	0.5	0.4	0.0075	NM_001700	Azurocidin 1 (cationic antimicrobial protein 37)
IHPK1	0.5	0.3	0.5	0.5	0.0405	NM_153273	Inositol hexaphosphate kinase 1
PSKH1	0.5	0.5	0.4	0.5	0.0094	NM_006742	Protein serine kinase H1
PRKCI	0.6	0.4	0.6	0.5	0.0157	NM_002740	Protein kinase C, iota



* Note: not a significant hit ($p > 0.05$), but PKR and ANGPT4 were also included as antiviral hits

[†] Note: siRNAs are slightly toxic to cells (88% viability, but $p = 0.0540$)

Fig. 5. Heat-maps of the identified pro- and antiviral hits. (A) List of the antiviral hits causing an at least 1.5-fold increase in GFP expression ($p < 0.05$). (B) Proviral hits yielding a more than 2-fold decrease in GFP expression ($p < 0.05$). For each target, the *p*-value, accession number, and gene name are shown. Each data point represents the result of a single library screen and is the average of the 3 replicates that were done in each screen.

Transfection with PKR-specific siRNAs reduced PKR levels in 293/ACE2 cells up to 87% compared to control cells, depending on the siRNA used (Fig. 8B). To verify that PKR knockdown increased wt SARS-CoV replication, siRNA-transfected 293/ACE2 cells were infected with wt SARS-CoV (MOI 0.01) and viral protein expression was analyzed at 24 h p.i. by Western blot analysis. In line with the effect of PKR siRNA 2 on 293/ACE2 cell viability (Fig. 8A), cells transfected with this siRNA contained reduced levels of β -actin, which was used as loading control (Fig. 8C; lower panel). Transfection with two of the

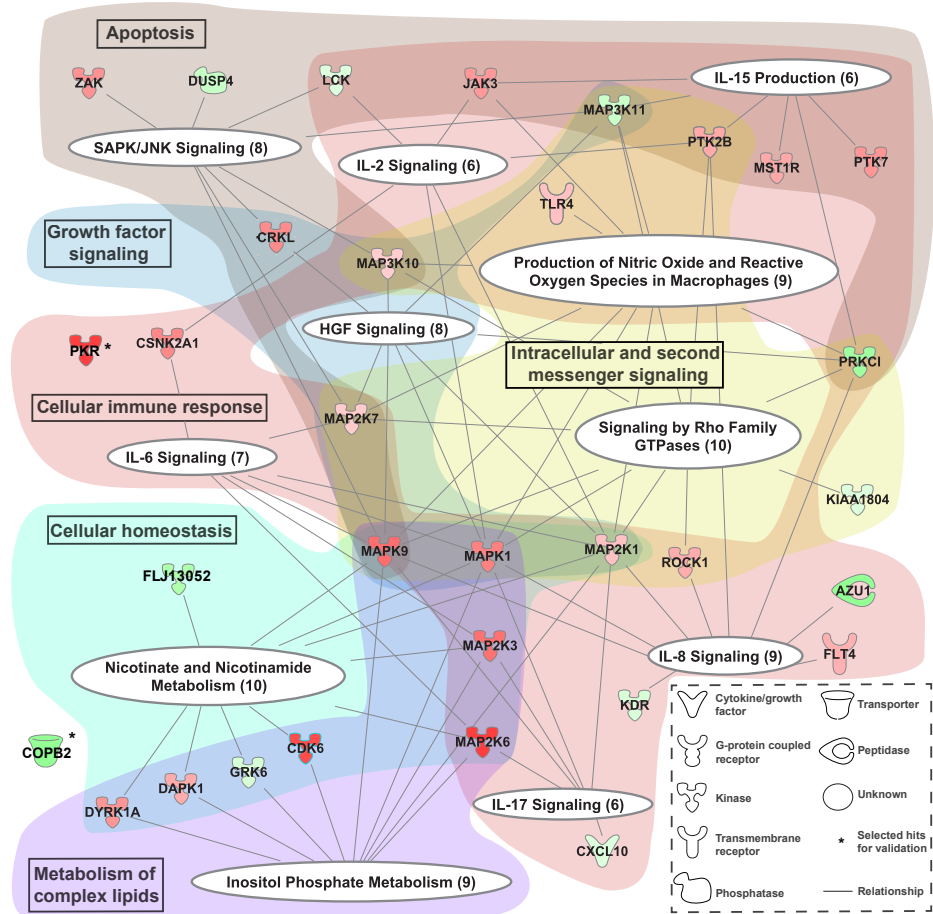


Fig. 6. Cellular pathways influencing SARS-CoV-GFP replication. Graphical representation of the canonical pathways (white ellipses) identified in the siRNA library screen for cellular factors affecting SARS-CoV replication. The proviral (red) and antiviral hits (green) are represented by nodes with lines linking them to one or more canonical pathways. The color intensity of the nodes indicates the strength of the pro- or antiviral effect (\log_2 ratio of GFP expression normalized to infected control cells), e.g. factors with a stronger antiviral effect have a more intense red color. The identified canonical pathways were clustered into more general categories that are indicated by text boxes in the colored background shading.

four individual PKR-directed siRNAs (siRNA 2 and 3) clearly increased the expression of SARS-CoV N protein (Fig. 8C, upper panel), and also led to an ~1-log increase in infectious progeny titers (Fig. 8D). Taken together, the increases in GFP signal, N expression

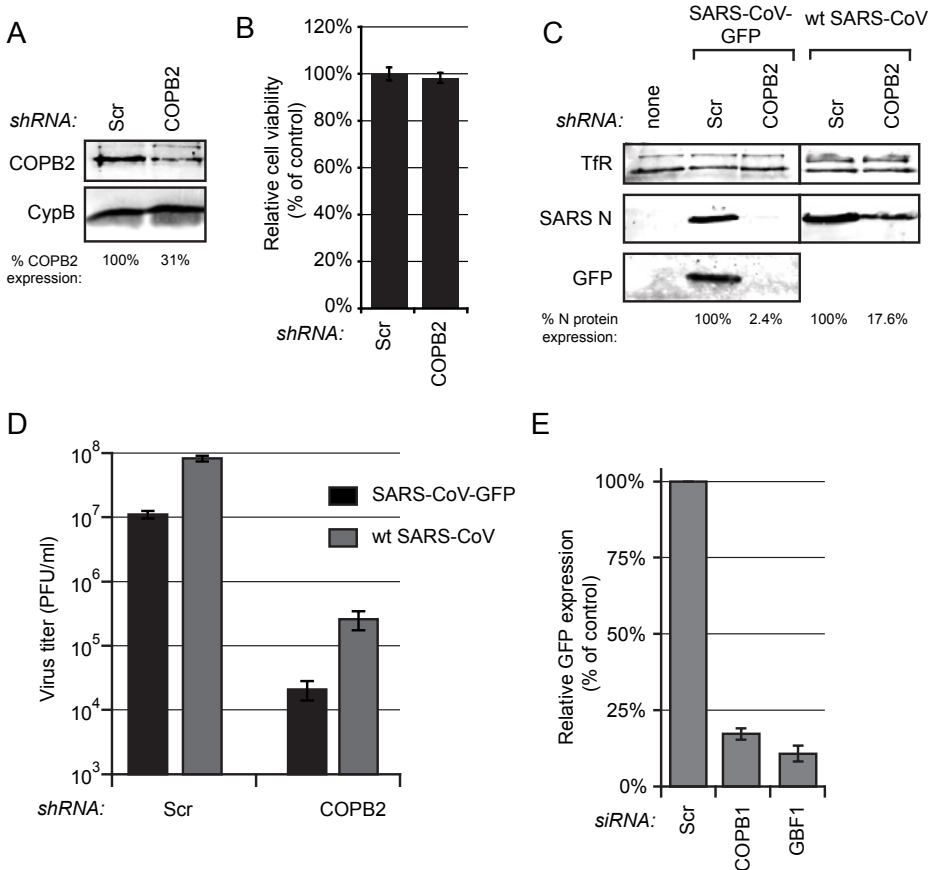


Fig. 7. Proteins of the early secretory pathway are important for SARS-CoV replication. (A) 293/ACE2 cells were transduced with lentiviruses expressing a COP2 mRNA-specific or a scrambled shRNA. Knockdown of COP2 expression at 48 h p.t. was monitored by Western blotting with a COP2-specific antiserum and cyclophilin B (CypB) was used as loading control. (B) Cell viability in COP2-depleted 293/ACE2 cells was analyzed at 48 h after transduction (% of value for cells transduced with lentiviruses expressing a scrambled shRNA). (C) COP2-depleted and control cells were infected with either SARS-CoV-GFP or wt SARS-CoV and protein expression was analyzed by Western blotting with N-specific and GFP-specific antisera, using the Tfr as a loading control. SARS-CoV N protein expression was quantified and its level normalized to the value for scrambled siRNA-transfected cells (100%) is indicated under each lane. (D) SARS-CoV-GFP (black bars) and wt SARS-CoV (grey bars) progeny titers in the culture supernatant of infected, COP2-depleted and control cells. (E) Normalized GFP expression by SARS-CoV-GFP in 293/ACE2 cells transfected with siRNA SMARTpools targeting COP1 or GBF1 and a scrambled control siRNA. Cells were infected 48 h p.t. at an MOI of 10 and 24 h later GFP fluorescence was quantified and normalized to that in infected cells transfected with a scrambled siRNA.

and infectious progeny titer correlate well with the magnitude of PKR knockdown, which makes an off-target effect in the initial siRNA library screen unlikely and suggests a true antiviral role for PKR in SARS-CoV infected cells.

DISCUSSION

In the past decade functional genomics studies have - in a systematic way - identified host factors that can influence the replication of diverse +RNA viruses [334, 335, 338-340, 352, 359]. We here describe a human kinome-wide siRNA screen for factors influencing the entry and replication of SARS-CoV, to our knowledge the first systematic functional genomics study of this kind for any coronavirus. As kinases are key regulators of many cellular processes, the pro- and antiviral factors identified by this strategy should pinpoint cellular pathways that are important for SARS-CoV replication.

For SARS-CoV, screening of the kinome-directed library of 779 siRNA SMARTpools resulted in the identification of 90 antiviral and 40 proviral proteins. Canonical cellular processes and pathways in which these factors were strongly represented included inositol phosphate metabolism, signaling by Rho family GTPases, and SAPK/JNK signaling (Fig. 6). Many hits could also be mapped to the interleukin (IL)-2, -6, -8, and IL-17 signaling pathways, which have previously been implicated in controlling coronavirus infection and coronavirus-induced inflammation (reviewed in [65]). For example, the SARS-CoV spike (S) protein was shown to induce the expression of the pro-inflammatory cytokine IL-8 [360], and IL-6 and IL-8 levels were elevated in the serum of SARS-CoV-infected patients [360, 361]. Furthermore, mouse hepatitis virus (MHV) and infectious bronchitis virus (IBV) infections were reported to upregulate the synthesis of these same cytokines [362, 363]. Although our siRNA library screen did not target interleukins directly, the identification of (kinase-regulated) interleukin signaling pathways is in line with these earlier studies, and emphasizes their importance in SARS-CoV infection.

Coronavirus replication is associated with a cytoplasmic RVN of modified ER, including double-membrane vesicles and convoluted membranes [30]. Despite the in-depth characterization of their ultrastructure, the biogenesis of these membrane structures and the cellular factors involved have remained largely uncharacterized. For example, the membrane source of these virus-induced structures is still controversial, with advanced EM analyses showing the RVN to be derived from and continuous with the ER [30, 208, 295] and other studies implicating the autophagy pathway [54] or EDEMosomes [55] as the primary membrane source. Our earlier work already suggested that the integrity of the early secretory pathway is important for efficient SARS-CoV replication, as brefeldin A (BFA) treatment of SARS-CoV-infected cells significantly reduced replication as well as the accumulation of virus-induced membrane structures [295]. In line with these find-

ings, COPI-coated vesicles were also implicated in the biogenesis of MHV replication structures [364, 365]. In addition, SARS-CoV nsp3 was shown to interact with three COPI subunits [366]. In none of these previous SARS-CoV and MHV studies a complete block of virus replication could be achieved, neither by reducing COPI vesicle formation by depletion of one of the coatomer subunits, nor by treatment with BFA. These results might partially be explained by incomplete knockdown or the presence of residual COPI vesicles (complete knockdown is probably not possible due to its detrimental effect on intracellular trafficking and cell viability). Although our study clearly demonstrates the importance of COPI-vesicles in SARS-CoV replication, the role of COPI vesicles in the formation of the SARS-CoV-induced RVN remains elusive and requires a more in-depth

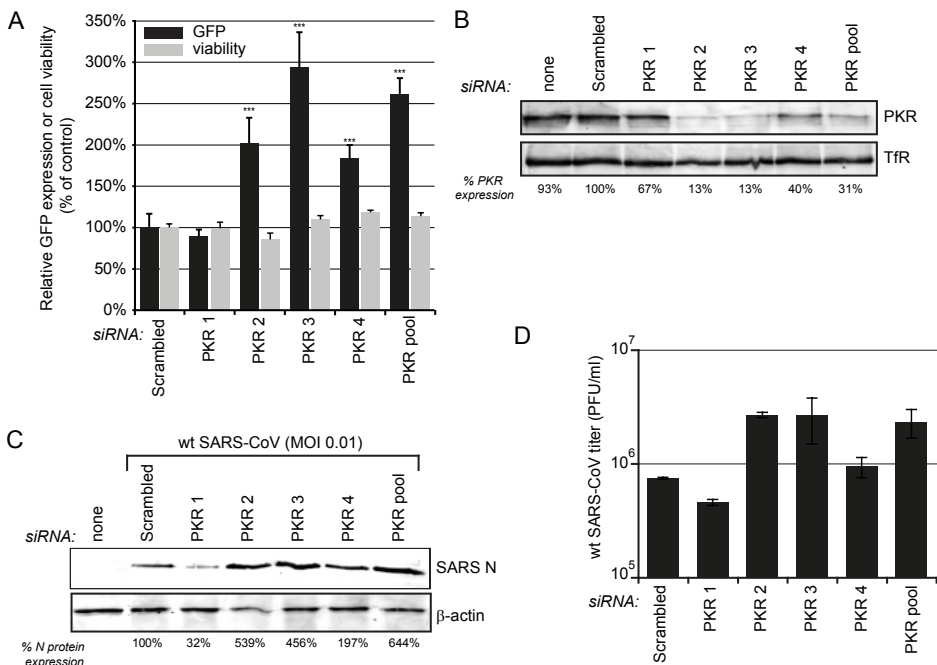


Fig. 8. Validation of PKR as an antagonist of SARS-CoV replication. 293/ACE2 cells were transfected with four individual siRNAs targeting PKR or a scrambled control siRNA. (A) At 48 h p.t. cells were infected with SARS-CoV-GFP (MOI 10), fixed 24 later, and GFP fluorescence (black bars) was quantified and normalized to the value measured in infected, scrambled siRNA-transfected cells (100%). The effect of siRNA transfection on cell viability was analyzed in parallel (grey bars) and values were normalized to those of scrambled siRNA-transfected control cells (100%). Average \pm SD is given (***) p -value < 0.001). (B) Knockdown of PKR expression at 48 h p.t. was monitored by Western blotting with a PKR-specific antiserum and Tfr was used as loading control. The percentage of remaining PKR expression compared to scrambled siRNA-transfected cells is shown below each lane. (C) Cells transfected with PKR specific siRNAs and control cells were infected with SARS-CoV (MOI 0.01) and 24 h later these cells were lysed to assess SARS-CoV N levels by Western blotting (shown below the panels as percentage of control), using β -actin as loading control. (D) Virus titers in the 24-h p.i. culture supernatants of wt SARS-CoV-infected cells (MOI 0.01) transfected with PKR-specific or scrambled siRNA.

analysis. The importance of COPI-coated vesicles is further supported by their essential role in the replication of many other RNA viruses, such as poliovirus [367, 368], other enterovirus family members [353, 369-371], vesicular stomatitis virus [372], *Drosophila C* virus [373], and influenza A virus [344, 374].

Interestingly, our screen yielded a relatively high proportion of antiviral hits, with PKR knockdown having one of the strongest effects (~2-fold increase of GFP expression in SARS-CoV-GFP-infected cells). During hit validation, three out of four individual PKR-directed siRNAs caused a clear increase in SARS-CoV protein expression and virus yield (Fig. 8C-D). PKR is one of four mammalian kinases that can phosphorylate eIF-2 α in response to stress signals (the others being the PKR-like endoplasmic reticulum kinase (PERK), GCN2, and HRI). Many virus families have evolved gene products and strategies to counteract or evade the antiviral action of PKR, illustrating the importance of this kinase in the antiviral defense. Previously, it was found that PKR inhibits the replication of the coronavirus IBV, as overexpression of a kinase-defective PKR mutant enhanced IBV replication by almost 2-fold. Furthermore IBV appeared to (weakly) antagonize the antiviral activity of PKR through two independent mechanisms, including the partial blockage of PKR activation [69]. For the distantly related arterivirus porcine reproductive and respiratory syndrome virus (PRRSV), it was shown that IFN- β - [375] and IFN- γ -treated [376] MARC-145 cells were no longer permissive to infection, while treatment with the PKR inhibitor 2-aminopurine restored PRRSV replication. This suggests an important antiviral role for PKR in controlling PRRSV infection. Krähling *et al.* show that PKR was activated in SARS-CoV-infected 293/ACE2 cells, but conclude that knockdown of PKR did not significantly affect virus replication, despite the fact that a ~1-log increase in SARS-CoV titer was observed in their experiments [377]. This is in contrast to our PKR knockdown experiments that point to an antiviral role for PKR (Fig. 8). Our data clearly shows that depletion of PKR significantly increased SARS-CoV-driven GFP expression (Fig. 8A), and also enhanced N protein expression (Fig. 8C) and virus progeny release (Fig. 8D). This discrepancy cannot be due to host cell differences, as the same 293/ACE2 cells were used in both studies [377], and might be due to differences in the experimental set-up, choice of controls, or normalization and interpretation of data.

In line with the findings for PKR, reducing the expression of PERK (or EIF2AK3), one of the other kinases known to phosphorylate eIF-2 α , resulted in an increase of SARS-CoV-GFP reporter gene expression by 57% ($p < 0.01$; Fig. 5A). The unfolded protein response - i.e. the detection of misfolded proteins within the ER lumen - activates PERK, which in turn phosphorylates eIF2 α , and ultimately triggers apoptosis. The relatively strong antiviral effect of PERK observed in this study is in line with previous studies suggesting that the phosphorylation of eIF-2 α in SARS-CoV-infected cells is mediated by the activation of PERK [377]. Our findings support the hypothesis that upon SARS-CoV infection the unfolded protein response is activated as an antiviral strategy. Multiple cellular re-

sponses that induce apoptosis, including the activation of PKR and PERK, might actually be involved in controlling SARS-CoV infection, which could also explain several other hits involved in apoptosis, like those from the SAPK/JNK pathway.

In conclusion, our kinome-wide siRNA screen has identified several cellular proteins and processes that influence SARS-CoV replication. These include novel factors that may play a role in coronavirus infections in general. Our data thus provide a starting point for further validation and in-depth mechanistic studies, preferably involving multiple factors from the identified pathways, which should enhance our understanding of the complex interplay between coronaviruses and their host.

ACKNOWLEDGMENTS

We thank Ali Tas, Emmely Treffers, and Maarten van Dinther for helpful discussions and excellent technical assistance and Shinji Makino for providing 293/ACE2 cells. We are grateful to Martijn Rabelink and Rob Hoeben (Department of Molecular Cell Biology) for sharing their lentivirus expertise and for providing plasmids and reagents for generating shRNA-expressing lentiviruses. This research was supported by TOP grant 700.57.301 from the Council for Chemical Sciences of the Netherlands Organization for Scientific Research (NWO-CW).

Chapter 6

MERS-coronavirus replication induces severe *in vitro* cytopathology and is strongly inhibited by cyclosporin A or interferon-alpha treatment

Adriaan H. de Wilde, V. Stalin Raj, Diede Oudshoorn, Theo M. Bestebroer, Stefan van Nieuwkoop, Ronald W. A. L. Limpens, Clara C. Posthuma, Yvonne van der Meer, Montserrat Bárcena, Bart L. Haagmans, Eric J. Snijder and Bernadette G. van den Hoogen

J. Gen. Virol. (2013) Vol. 94, pp 1749-1760

Reprinted with permission

ABSTRACT

Coronavirus (CoV) infections are commonly associated with respiratory and enteric disease in humans and animals. The 2003 outbreak of severe acute respiratory syndrome (SARS) highlighted the potentially lethal consequences of CoV-induced disease in humans. In 2012, a novel CoV (Middle East Respiratory Syndrome coronavirus; MERS-CoV) emerged, causing 49 human cases thus far, of which 23 had a fatal outcome. In this study, we characterized MERS-CoV replication and cytotoxicity in human and monkey cell lines. Electron microscopy of infected Vero cells revealed extensive membrane rearrangements, including the formation of double membrane vesicles and convoluted membranes, which were previously implicated in the RNA synthesis of SARS-CoV and other CoVs. Following infection, we observed rapidly increasing viral RNA synthesis and release of high titres of infectious progeny, followed by pronounced cytopathology. These characteristics were used to develop an assay for antiviral compound screening in 96-well format, which was used to identify cyclosporin A as an inhibitor of MERS-CoV replication in cell culture. Furthermore, MERS-CoV was found to be 50-100 times more sensitive to interferon-alpha (IFN- α) treatment than SARS-CoV, an observation that may have important implications for the treatment of MERS-CoV-infected patients. MERS-CoV infection did not prevent the IFN-induced nuclear translocation of phosphorylated STAT1, in contrast to infection with SARS-CoV where this block inhibits the expression of antiviral genes. These findings highlight relevant differences between these distantly related zoonotic CoVs in terms of their interaction with and evasion of the cellular innate immune response.

INTRODUCTION

In June 2012, a previously unknown coronavirus was isolated from a 60 year-old Saudi-Arabian patient who died from acute respiratory distress syndrome and multiple organ failure [15]. Subsequently, the novel virus was isolated from several additional residents and visitors of the Arabian Peninsula suffering from similar respiratory symptoms. In retrospect, also a cluster of respiratory infections in Jordan (April 2012) was linked to the same agent, although no convincing evidence for human-to-human transmission was obtained. This was clearly different for a cluster of three U.K. cases in early 2013, consisting of a patient who had travelled to Saudi Arabia and two family members without recent travel history outside the U.K. In the past year, various names have been used to refer to this newly identified CoV, including novel (beta)coronavirus (nCoV) and human coronavirus EMC (HCoV-EMC), but following a recent recommendation by the coronavirus study group of ICTV and other experts [14] we will use Middle East Respiratory Syndrome coronavirus (MERS-CoV) throughout this paper. Up to May 2013, 49 confirmed MERS cases, including 23 fatalities, have been recorded (http://www.who.int/csr/don/archive/disease/coronavirus_infections/en/).

Coronavirus (CoV) infections are associated with respiratory and enteric disease in humans and animals. Since the 1960s, two human CoVs (HCoVs OC43 and 229E) were known to cause mild respiratory disease [20, 21], but it was the 2003 outbreak of severe acute respiratory syndrome (SARS; fatality rate ~10%) that revealed the potentially lethal consequences of CoV-induced disease in humans [6, 7]. Two years later, bats were identified as the most likely animal reservoir for this zoonotic CoV [11, 12]. Subsequently, a wide variety of bat-associated CoVs was discovered [378, 379] and also two additional human CoVs (NL63 and HKU1; [22, 23, 380]) were identified. Although the general capacity of bat CoVs to switch hosts appears to be rather restricted [18], the possibility of SARS-CoV re-emergence or zoonotic transfer of other animal CoVs has remained a public health concern over the past 10 years.

Coronaviruses are classified in four genera (alpha-, beta-, gamma- and deltacoronaviruses; [286]) and our previous analysis of the MERS-CoV genome [16] identified the newly emerging agent as a member of lineage C of the genus Betacoronavirus. Strikingly, as in the case of SARS-CoV, the closest known relatives of MERS-CoV are bat coronaviruses, like HKU-4 and HKU-5 [16, 378]. The evolutionary distance to SARS-CoV (lineage B) is considerable, a notion further supported by recent comparative studies revealing important differences in receptor usage [18, 381].

Mammalian viruses have to cope with the host cell's innate responses, including those triggered by activation of the type I interferon (IFN) pathway (reviewed in [382]). Coronaviruses, including SARS-CoV, appear to have evolved a variety of mechanisms to block or evade such antiviral responses (reviewed in [65, 317]). For example, it was

postulated that the sensing of double-stranded (ds) RNA replication intermediates by the innate immune system is inhibited by the elaborate virus-induced membrane structures with which CoV RNA synthesis is associated [30, 383]. Other evasion mechanisms were attributed to protein functions that can be either conserved across CoVs or specific for certain CoV lineages. Proteins such as the nsp3 proteinase [347], the nsp16 2'-O-methyltransferase [348], and the products of SARS-CoV ORFs 3b, 6 and 7a [105, 109, 350, 351] have all been described to prevent IFN induction/signalling. In particular, the SARS-CoV ORF6 protein is known to inhibit IFN-induced JAK-STAT signalling by blocking the nuclear translocation of phosphorylated STAT1 (p-STAT1), which contributes to the pathogenic potential of the virus in a mouse model [384]. In spite of these immune evasion strategies, treatment with type I IFNs can inhibit CoV replication *in vitro* [188-192] and, for example, protected type I pneumocytes against SARS-CoV infection in macaques [190].

Clearly, well-characterized systems for MERS-CoV replication in cell culture will be invaluable for future studies into basic virus properties and interactions with the host, including innate immune responses. Therefore, we set out to characterize the replication of MERS-CoV in different cell lines. Using this information, an assay to screen for antiviral compounds was developed, which identified cyclosporin A (CsA) as an inhibitor of MERS-CoV replication. Our first screening experiments also established that, compared to SARS-CoV, MERS-CoV replication is more sensitive to type I interferon treatment.

MATERIALS AND METHODS

Cells culture and virus infection

Vero cells (ATCC: CCL-81) were cultured in Eagle's minimal essential medium (EMEM; Lonza) with 8% fetal calf serum (FCS; PAA) and antibiotics. Huh7 cells were grown in Dulbecco's Modified Eagle Medium (DMEM; Lonza) containing 8% FCS, 2 mM L-Glutamine (PAA), non-essential amino acids (PAA), and antibiotics. Vero E6 and Calu3/2B4 cells were cultured as previously described [208, 385]. Infection of Vero, Vero E6, Huh7, and Calu3/2B4 cells with MERS-CoV (strain EMC/2012; [15, 16]) at high multiplicity of infection (MOI 5) was done in PBS containing 50 µg/ml DEAE-dextran and 2% FCS. Inoculations with a low dose (MOI ≤ 0.05) of MERS-CoV or SARS-CoV (strain HKU-39849; [386]) were done directly in EMEM containing 2% FCS. Virus titrations by plaque assay were performed as described before [355]. All work with live MERS-CoV and SARS-CoV was performed inside biosafety cabinets in biosafety level 3 facilities at Leiden University Medical Center or Erasmus Medical Center.

Antibodies and drugs

Rabbit antisera recognizing the SARS-CoV replicase subunits nsp3, nsp4, nsp5 and nsp8 have been described previously [53, 208]. Rabbit antisera recognizing the SARS-CoV nucleocapsid (N) protein and MHV nsp4 were raised as described [222]. Antigens were a full-length recombinant SARS-CoV N protein (purified from *E. coli*) and a synthetic peptide representing the 23 C-terminal residues of MHV nsp4, respectively. p-STAT1 was detected with Alexa Fluor 488-labelled mouse-anti-STAT1 (pY701) (BD Biosciences) and FITC-labelled anti-mouse-IgG was used to enhance the green fluorescence. Virus infection was detected using the above-mentioned anti-nsp3 sera and Alexa Fluor 594-labeled anti-rabbit IgG.

Cyclosporin A (CsA; Sigma) was dissolved in DMSO and a 10-mM stock was stored in aliquots for single use at -20°C. Peg-interferon alfa-2b (PEG-IFN; Pegintron, Merck, USA) was prepared according to the manufacturer's instruction as a 100 μ g/ml stock stored at 4°C.

Immunofluorescence microscopy

Cells were grown on coverslips and fixed with 3% paraformaldehyde in PBS or with 4% formaldehyde and 70% ethanol (p-STAT1 experiments), permeabilized with 0.1% Triton X-100, and processed for immunofluorescence microscopy as described previously [33]. Specimens were examined with a Zeiss Axioskop 2 fluorescence microscope with an Axiocam HRc camera and Zeiss Axiovision 4.4 software or with a confocal microscope (Zeiss, LSM 700) (p-STAT1 experiments).

Electron microscopy

Vero cells were grown on sapphire discs and fixed at 8 h p.i. for 30 min at room temperature with 3% paraformaldehyde and 0.25% glutaraldehyde in 0.1 M PHEM buffer pH 6.9 [60 mM piperazine-1,4-bis (2-ethanesulfonic acid), 25 mM HEPES, 2mM MgCl₂, 10mM EGTA] containing 50% diluted Eagle's minimal essential medium and 1% FCS. Cells were stored in fixative at 4°C for 72 h and then high-pressure frozen using a Leica EM PACT2. Freeze-substitution was performed in an automated system (Leica AFS2) using as freeze-substitution medium acetone containing 1% OsO₄, 0.5% uranyl acetate and 10% H₂O. First, the samples were maintained at -90°C for 6 h in this medium and then slowly warmed to -20°C within 14 h, kept at -20°C for 1 h, warmed to 0°C at a 5°C/h rate and left at 0°C for 1 h before letting the samples reach room temperature. After washing with acetone, the samples were gradually infiltrated with epoxy resin LX-112 and polymerized at 60°C. The samples were cut into thin sections (100 nm) and counterstained with uranyl acetate and lead citrate. Imaging was performed in an FEI Tecnai12 TWIN electron microscope operating at 120 kV and equipped with an Eagle 4k cooled slow-

scan charge-coupled device (CCD) camera (FEI company). The images were acquired using binning mode 2.

Intracellular viral RNA analysis

Isolation of intracellular viral RNA was described previously [102]. After drying of the gel, viral mRNAs were detected by hybridization with a ^{32}P -labeled oligonucleotide probe (5'-GCAAATCATCTAATTAGCCTAATC-3') complementary to the 3'-end of all MERS-CoV mRNAs. Equal loading was verified in a second hybridization using a ^{32}P -labeled oligonucleotide probe (5'-GTAACCCGTTGAACCCATT-3') recognizing 18S ribosomal RNA [52]. ImageQuant TL (GE Healthcare) software was used for quantification.

Real-time reverse transcription-polymerase chain reaction (RT-PCR)

RNA from 200 μl culture medium of CoV-infected cells was isolated with the MagnaPure LC total nucleic acid isolation kit (Roche) and eluted in 100 μl . RT-PCR conditions for quantifying MERS-CoV and SARS-CoV RNA and amplification parameters were described previously [8, 381]. Dilutions of viral RNA isolated from MERS-CoV or SARS-CoV virus stocks with a known virus titre were used to produce a standard curve.

Development of a screening assay for antiviral compounds

Huh7 or Vero cells were seeded in 96-well plates at a density of 10^4 or 2×10^4 cells per well, respectively. After overnight growth, cells were infected with an MOI of 0.005 or 0.05. One to three days after incubation, differences in cell viability caused by virus-induced CPE or by compound-specific side effects were analysed using the CellTiter 96[®] AQ_{ueous} Non-Radioactive Cell Proliferation Assay (Promega), according to the manufacturer's instructions. Absorbance (A_{490}) was measured using a Berthold Mithras LB 940 96-well plate reader. Infected cells were given CsA or DMSO (solvent control) prior to infection (MOI 0.005). Cytotoxic effects caused by CsA treatment alone were monitored in parallel plates containing mock-infected cells.

IFN sensitivity and p-STAT1 translocation experiments

One day prior to infection, Vero cells were plated at a density of 104 cells per well in a 96-well plate format. At -4, 0 and 4 h p.i., cells were incubated with 0 to 1000 ng/ml PEG-IFN in 250 μl . At $t=0$ h, all wells were washed with PBS and infected with MERS-CoV or SARS-CoV (100 TCID_{50} per 100 μl medium). Those cultures receiving treatment from $t=-4$ or $t=0$ were infected in the presence of the indicated concentration PEG-IFN. After 1 h, 150 μl medium was added to the cultures of $t=-4$ or $t=0$ cultures, and 100 μl medium was added to the untreated cultures, which at 4 h p.i. received 50 μl medium supplemented with PEG-IFN to reach a final concentration of 0 to 1000 ng/ml PEG-IFN. At 48 h p.i., RNA was isolated from 50 μl cell culture supernatant and quantified using virus-specific real

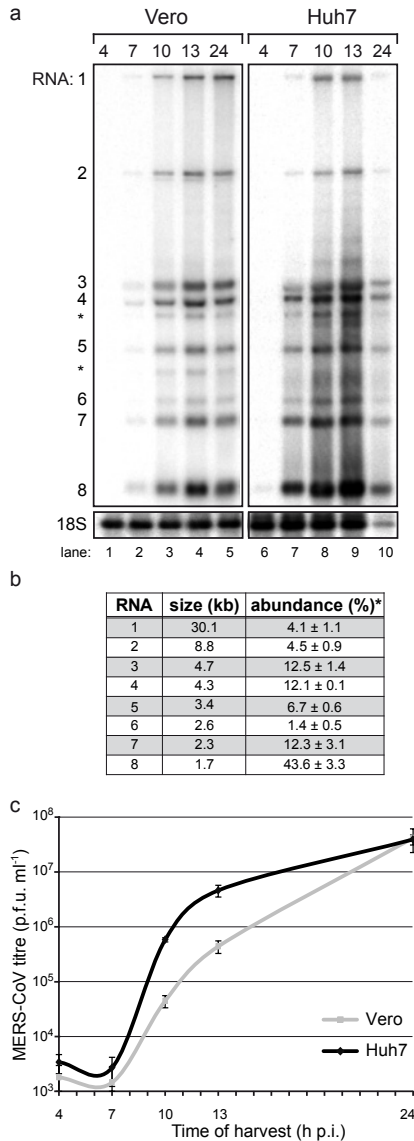


Fig. 1. Kinetics of MERS-CoV replication in Vero and Huh7 cells. Vero and Huh7 cells were infected with MERS-CoV (MOI 5). (a) Hybridization analysis of viral mRNAs isolated from MERS-CoV-infected cells using an oligonucleotide recognizing the viral genome and all sg mRNAs. Additional minor bands of ~3 and ~4 kb were observed (*) and may represent additional viral mRNA species that remain to be studied in more detail. However, the corresponding positions in the ORF4a/b and ORF5 coding regions do not contain a canonical core TRS sequence (AACGAA; [16] that might provide a direct explanation for their synthesis. (b) Analysis of the relative molarities of viral genome and each of the sg mRNAs (% of total viral mRNA). mRNA sizes were calculated on the basis of the TRS positions in the viral genome sequence [16]. Phosphorimager quantification was performed on the gel lanes with the RNA samples isolated from Vero cells at 10, 13 and 24 h p.i. (Fig. 1a; lanes 3, 4, and 5; avg ± SD). (c) Release of infectious MERS-CoV progeny into the medium of infected Vero or Huh7 cells at the indicated time points, as determined by plaque assay (avg ± SD; n=4).

time RT-PCR assays (see above). Furthermore at 48 h p.i., CPE was scored microscopically as either (0) none, (1) mild, (2) moderate, (3) severe or (4) complete.

For p-STAT1 nuclear translocation experiments, Vero cells were infected with MERS-CoV or SARS-CoV (MOI 1). At 8 h p.i., cells were treated with 1000 ng/ml PEG-IFN for 30 min and fixed with 4% formaldehyde and 70% ethanol and subsequently stained for presence of viral antigen and p-STAT1 translocation.

RESULTS

Kinetics of MERS-CoV replication in Vero and Huh7 cells

Only a few laboratory studies on MERS-CoV replication have been reported thus far. Cells from a variety of mammalian hosts were found to be susceptible and infection can induce pronounced cytopathology and cell death [15, 18]. Following entry, the CoV replicative cycle starts with the translation of the positive-stranded RNA genome into replicase polyproteins that are cleaved into 16 nsps [16, 37]. These direct both genome replication and the synthesis of the subgenomic (sg) mRNAs required to express the structural and accessory proteins. To investigate MERS-CoV replication in more detail, we used Vero and Huh7 cells to analyse viral RNA synthesis and progeny release in single-cycle infection experiments.

Hybridisation analysis of the accumulation of viral RNA revealed the presence of genome RNA and seven sg transcripts, with sizes closely matching those previously predicted from the positions of conserved transcription regulatory sequences (TRS) in the viral genome [16] (Fig. 1a). The relative abundance of the various sg mRNAs is similar to what has been observed for other CoVs, with the smallest species (encoding the N protein) being by far the most abundant transcript (Fig. 1b). In both cell lines, viral mRNAs could be readily detected at 7 h p.i. and reached maximum levels around 13 h p.i. (Fig. 1a). Viral RNA levels remained more or less constant until 24 h p.i. in Vero cells, whereas the amount isolated from Huh7 cells declined due to the more rapid development of cytopathology in this cell line between 13 and 24 h p.i. (see below). After the peak of viral RNA accumulation had been reached, the titre of virus released from MERS-CoV-infected Vero cells steadily increased from $\sim 5 \times 10^5$ to $\sim 5 \times 10^7$ PFU per ml (Fig. 1c). Interestingly, the bulk of the viral progeny was released significantly earlier from Huh7 cells, although the final titre at 24 h p.i. was comparable to that obtained from Vero cells.

Antisera raised against non-structural proteins of other betacoronaviruses cross-react with MERS-CoV proteins

Despite the relatively large evolutionary distance to better-characterized CoVs, we tested a panel of antisera from our laboratory for cross-reactivity with MERS-CoV-

infected cells. In contrast to a polyclonal serum recognizing the SARS-CoV nucleocapsid (N) protein (data not shown), antisera against various SARS-CoV nsps (nsp3, nsp5, nsp8; [208]) raised using purified recombinant proteins as antigen, were found to strongly cross-react (Fig. 2a). In addition, rabbit antisera raised against synthetic peptides (23-mers) representing a small but conserved C-terminal part of SARS-CoV and MHV nsp4 strongly cross-reacted with MERS-CoV. Only small but apparently immunogenic parts of these peptides (e.g., LYQPP) are absolutely conserved between MHV and MERS-CoV nsp4 (Fig. 2b). Conservation in other betacoronaviruses (data not shown) suggests that antisera recognizing this nsp4 region may be used for immunodetection of additional (newly emerging) CoVs.

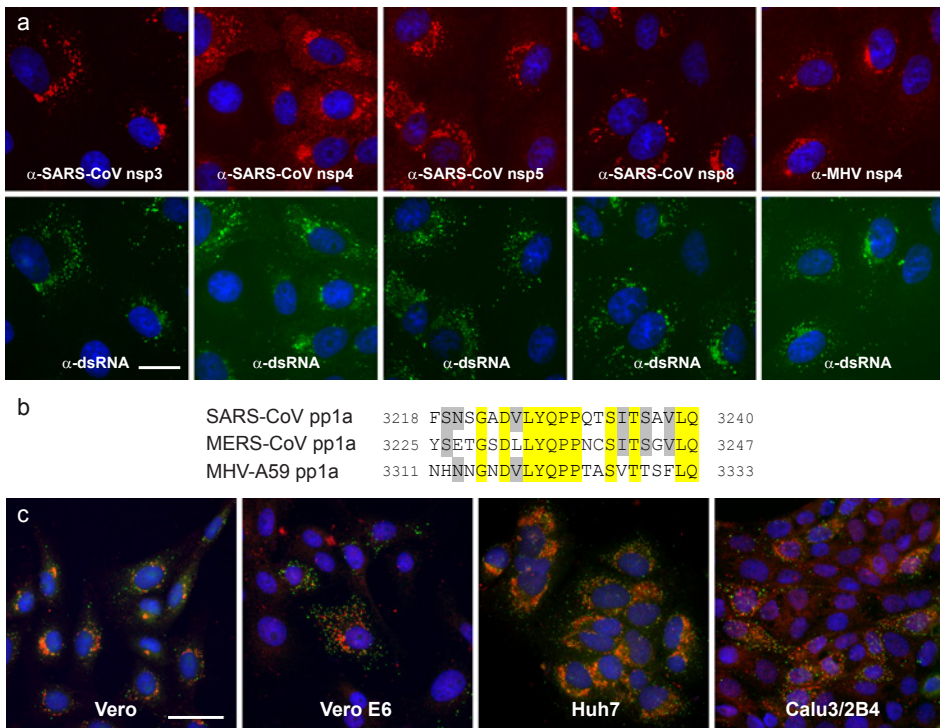


Fig. 2. Selected rabbit antisera raised against SARS-CoV and MHV nsps cross-react with MERS-CoV proteins. (a) MERS-CoV-infected Vero cells (MOI 5) were fixed at 8 h p.i. For immunofluorescence microscopy, cells were double-labelled with a mouse monoclonal antibody recognizing dsRNA (bottom row) and rabbit antisera raised against SARS-CoV nsp3, nsp4, nsp5 or nsp8, or MHV nsp4 (top row). Bar, 20 μ m. (b) Sequence comparison of the C-terminal domain of nsp4 of SARS-CoV (isolate Frankfurt 1), MERS-CoV (strain EMC/2012) and MHV (strain A59). The SARS-CoV and MHV sequences corresponds to the synthetic peptides used to raise rabbit anti-nsp4 sera. Residues conserved in all three viruses are highlighted in yellow, whereas residues conserved in two out of three are highlighted in grey. Amino acid numbers refer to the full-length pp1a sequence. (c) Monolayers of Vero, Vero E6, Huh7 and Calu3/2B4 cells were infected with MERS-CoV (MOI 5) and double-labelled for dsRNA (green) and nsp3 (red). Bar, 40 μ m.

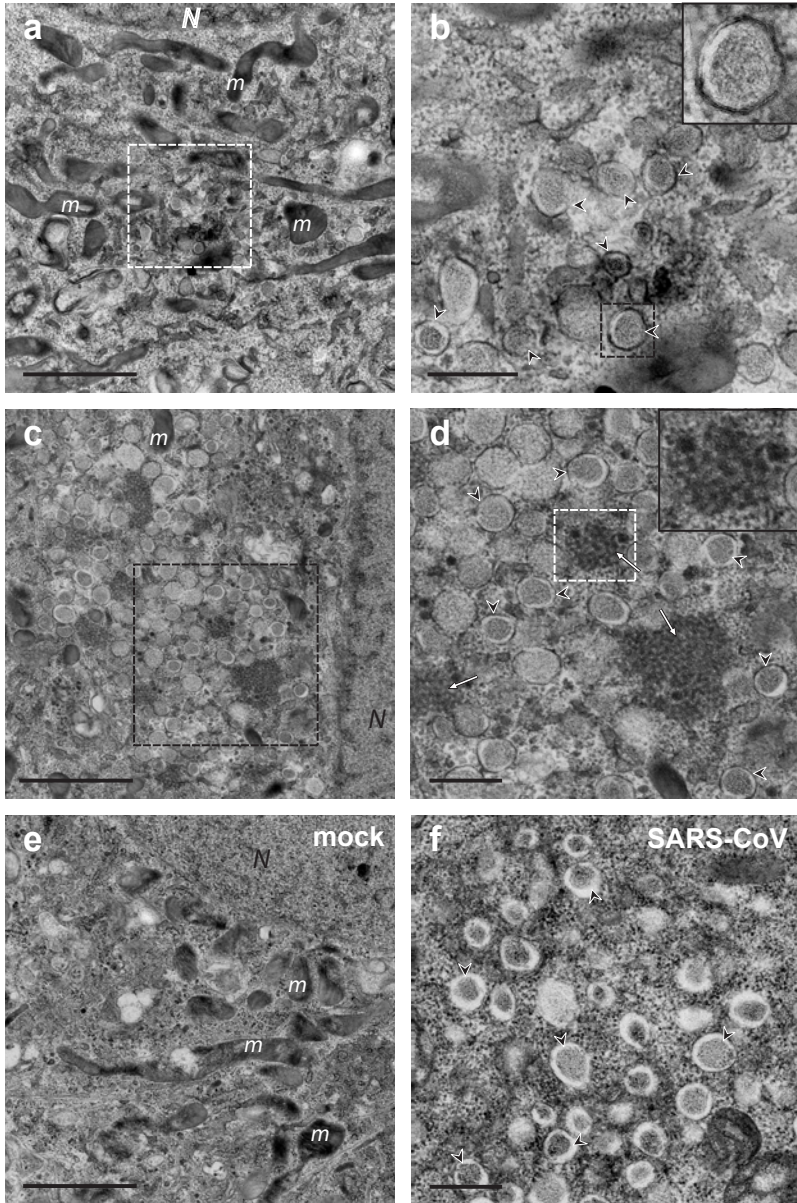


Fig. 3. Membrane structures induced by MERS-CoV infection. Electron micrographs of thin sections (100 nm) of (a-d) MERS-CoV-infected Vero cells at 8 h p.i. (a) Low magnification images of a cell containing a small cluster of double-membrane vesicles, enlarged in (b). Some DMVs are indicated by black arrowheads and the inset displays a close-up of the boxed DMV in (b). (c) Extensive membrane alterations in the perinuclear region. The boxed area in (c) is displayed at higher magnification in (d), where CMs (white arrows, inset) embedded in clusters of DMVs (black arrowheads) can be observed. For comparison, (e) shows the unaltered cytoplasm of a mock-infected cell and (f) contains SARS-CoV-induced DMV (black arrowheads) as observed after HPF and freeze substitution. N, nucleus; m, mitochondria. Scale bars, 2 μm (a,c,e), 500 nm (b,d,f).

MERS-CoV replication structures

Subsequently, we employed a monoclonal antibody recognizing dsRNA to localize intermediates in viral RNA synthesis [30, 387]. In various cell types, the immunolabelling signals for both replicase and dsRNA localized to the perinuclear region (Fig. 2c), where the replication structures induced by other CoVs are known to accumulate [30, 31, 34-36, 208].

We next used electron microscopy (EM) to investigate the ultra-structural and potentially cytopathic changes that MERS-CoV induces in infected cells, and focused on the membranous replication structures that support MERS-CoV RNA synthesis. The preservation of such structures, typically double-membrane vesicles (DMVs) and convoluted membranes (CMs), was previously found to be significantly improved by using protocols that include cryo-fixation and freeze-substitution [30, 208]. We now applied these advanced preservation techniques, including newly developed protocols for high-pressure freezing (HPF), to MERS-CoV-infected Vero cells. Images of similarly prepared SARS-CoV-infected Vero E6 cells are included for comparison (Fig. 3f).

Compared to mock-infected control cells (Fig. 3e), different degrees of distinct alterations were observed at 8 h p.i. Some cells contained relatively small DMV clusters (Fig. 3a,b; black arrowheads, inset), whereas in others large numbers of DMVs occupied extensive areas of the perinuclear region (Fig. 3c,d), differences that likely reflect different stages in infection progression. The diameter of MERS-CoV-induced DMVs ranged from 150 to 320 nm, comparable to what was previously measured for SARS-CoV-induced structures [30]. An interesting morphological difference with our previous studies of SARS-CoV-infected cells was the presence of a dense inner DMV core, which can be attributed to technical differences in sample preparation. In terms of ultrastructural preservation, HPF is widely considered superior to the previously used plunge-freezing protocols. Also in the case of SARS-CoV (Fig. 3f) and the distantly related equine arteritis virus [29], a similar dense DMV core became apparent when HPF was employed. Although DMV cores are known to contain dsRNA, the implications of these ultrastructural observations remain unclear. Interestingly, CMs were always surrounded by DMV clusters and were only observed in cells that appeared to be more advanced in infection (Fig. 3c,d; white arrows, inset). This observation strengthens the notion that DMV formation precedes the development of CMs, as previously postulated for SARS-CoV [30].

MERS-CoV-induced cytopathology and cell death.

In cell culture, many CoVs induce severe cytopathic effect (CPE) and cell death. Infection with a number of CoVs can also induce extensive syncytium formation, due to fusion activity of the viral spike protein at neutral pH (reviewed in [388]). MERS-CoV-induced cytopathology was monitored by light microscopy following low-MOI inoculation of monkey and human cells (Fig. 4). In line with previous observations [15], Vero cells de-

veloped clear CPE at 2 days post infection (d p.i.) and detached at 3 d p.i. (Fig. 4a). Similar observations were made for Calu3/2B4 cells (Fig. 4b). In contrast, MERS-CoV-infected Vero E6 cells displayed only mild CPE starting at 3 d p.i and cell death was not complete after six days (Fig. 4c). The development of CPE in Huh7 cells was strikingly faster compared to the three other cell lines and, following extensive syncytium formation, cells detached already around 17 h (Fig. 4d). Given the low MOI used and the viral replication kinetics (Fig. 1), the syncytium formation in these only partially infected Huh7 cultures

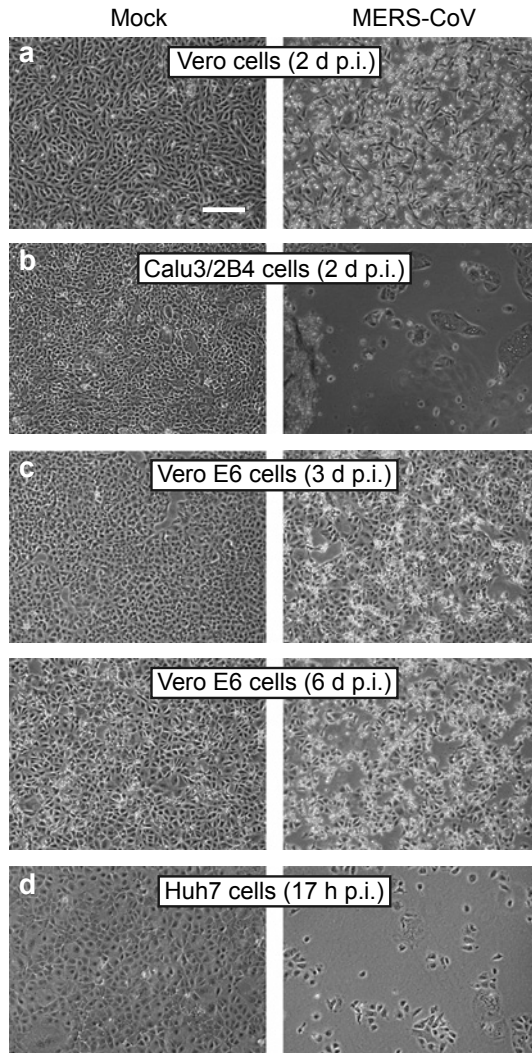


Fig. 4. MERS-CoV infection induces severe cytopathology in monkey and human cell lines. Monolayers of Vero (a), Calu3/2B4 (b), Vero E6 (c) and Huh7 (d) cells infected with MERS-CoV (MOI 0.05) and analysed by light microscope at the indicated time points. Bar, 100 μ m.

appeared to be a major factor in CPE development. DPP4 expression on Vero and Huh7 cells [381] and expression levels of DPP4 on Calu3/2B4 and Vero E6 cells correlated with susceptibility to MERS-CoV (data not shown).

Development of an assay to screen for compounds inhibiting MERS-CoV replication.

The virus-induced CPE in Vero and Huh7 cells was used to develop a first assay to screen for compounds that inhibit MERS-CoV replication in cell culture. Vero cells were seeded in 96-well plates and infected at an MOI of 0.005 or 0.05 (Fig. 5a). After two and three days, CPE formation was monitored microscopically and cytotoxicity was measured using a commercial cell viability assay. Moderate CPE was observed on day 2, and by day 3 cell viability had dropped below 10% with both virus doses used (Fig. 5a), indicating near-complete cell death. In MERS-CoV-infected Huh7 cells (Fig. 5b), already after day 1, cell viability had dropped to 79% or 24% (after MOI 0.005 or 0.05 infection, respectively), which was in line with our observations on rapid syncytium formation and CPE in this particular cell line (Fig. 4d). One day later, CPE was complete for both virus doses used and cells had detached (Fig. 5b). Based on this comparison, further experiments were done using an MOI of 0.005 and Huh7 and Vero cells were incubated for two or three days, respectively, before measuring cell viability.

Previously, it was shown that replication of various CoVs, including SARS-CoV, can be inhibited by the immunosuppressive drug CsA [276, 277]. Therefore, while testing whether the CPE-based assay described above could be used as an antiviral screening method, we used CsA treatment to obtain a first proof of principle. Infected Vero cells were given 3 or 9 μM of CsA and were analysed at 3 d p.i. At the concentrations used, CsA did not adversely affect the viability of mock-infected cells (Fig. 5c). Treatment with 9 μM completely inhibited CPE and left cell viability unchanged compared to mock-infected control cells. The inhibitory effect of CsA was confirmed in Huh7 cells (Fig. 5d), which displayed reduced and lack of CPE upon treatment with 7.5 μM and 15 μM CsA, respectively. These results were corroborated by immunofluorescence microscopy analysis of CsA-treated and high MOI-infected Vero and Huh7 cells and by determining virus titres released into the medium. Both assays confirmed an almost complete block of MERS-CoV-infection (data not shown). However, as previously reported for other CoVs [276], a small fraction of MERS-CoV-infected cells appeared to be refractive to CsA treatment and supported a low level of MERS-CoV replication, even at high CsA concentrations (data not shown).

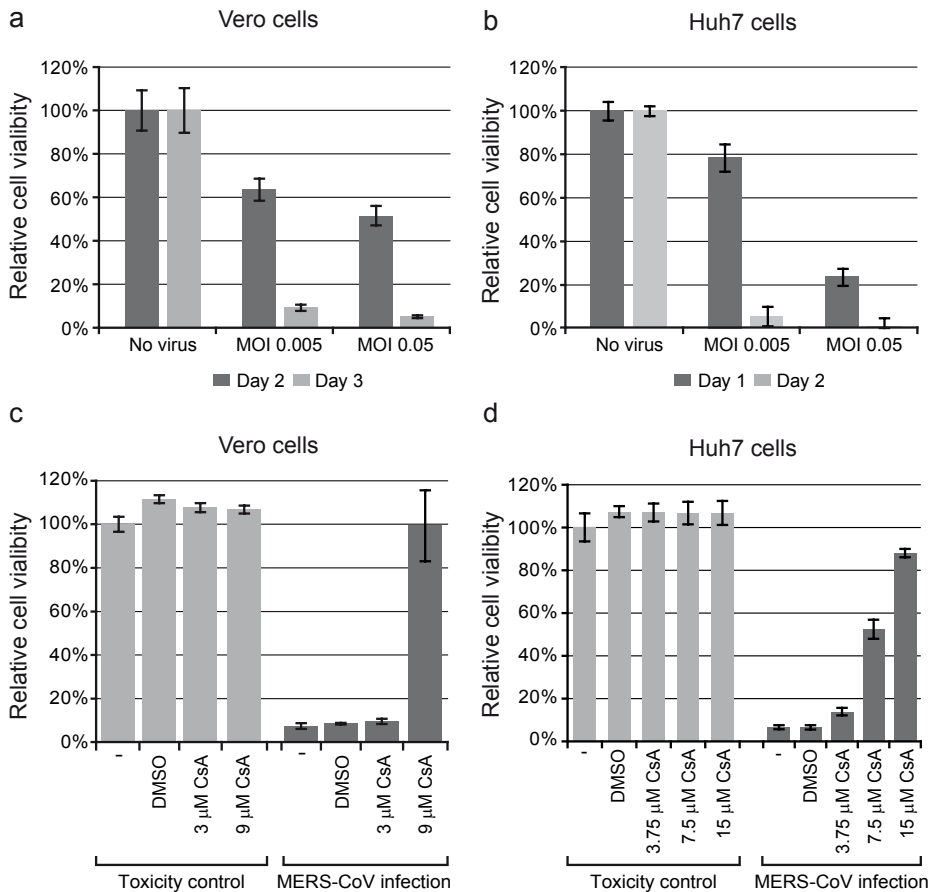


Fig. 5. Development of an assay to screen for compounds inhibiting MERS-CoV replication. (a,c) Vero and (b,d) Huh7 cells in a 96-well plate format were infected at an MOI of 0.005 or 0.05. Mock-infected cells were used as reference for unchanged cell viability (their relative viability was set at 100%). (a) Infected Vero cells were incubated for 2 or 3 days and (b) Huh7 cells were incubated for 1 or 2 days. (c) Vero cells were infected with MERS-CoV (MOI 0.005) in the presence of 3 μM or 9 μM Csa, or 0.09% DMSO as solvent control. (d) Huh7 cells were infected with MERS-CoV (MOI 0.005) in the presence of 3.75 to 15 μM Csa, or 0.15% DMSO. (c,d) Graphs show the results of a representative experiment (avg ± SD; n=4). All experiments were repeated at least twice.

Enhanced sensitivity of MERS-CoV to pegylated IFN-α treatment in comparison to SARS-CoV.

Type I IFNs inhibit CoV replication and can protect against infection in animal models [189, 190]. We therefore compared the effect of pegylated interferon-α (PEG-IFN) treatment on MERS-CoV and SARS-CoV replication *in vitro*. Vero cells were given PEG-IFN 4 h before low-MOI infection, together with the inoculum or 4 h after infection. At 2 d p.i. CPE was scored microscopically.

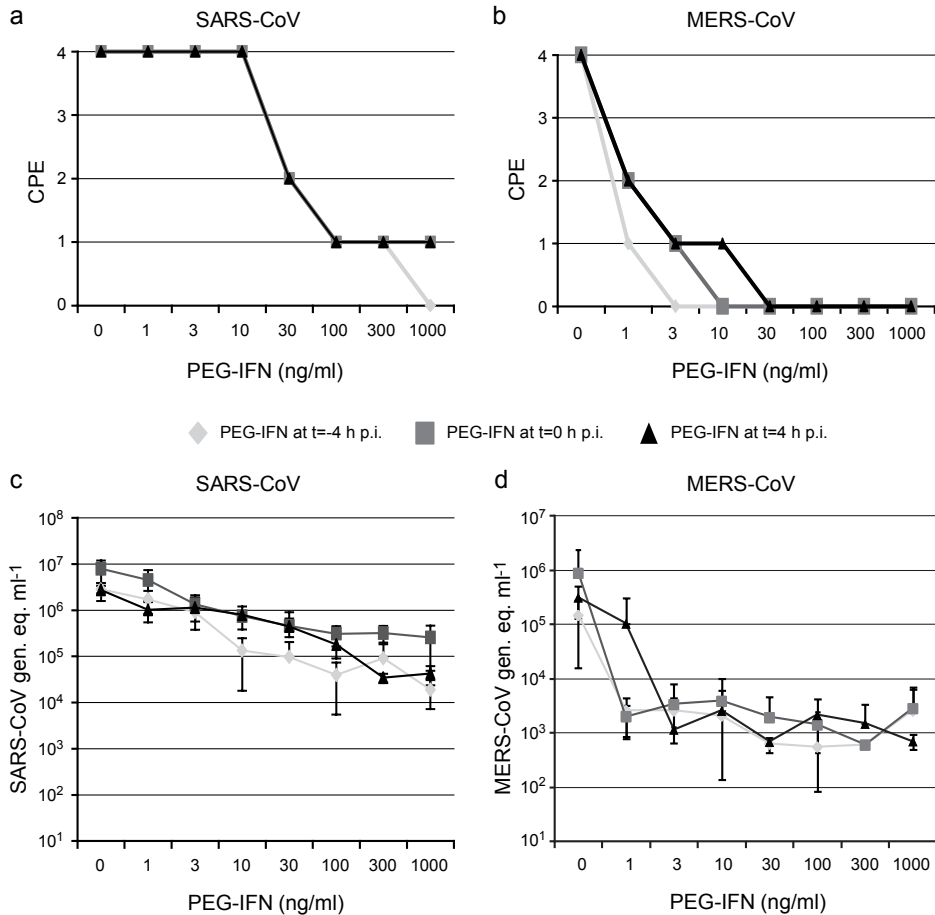


Fig. 6. Sensitivity of MERS-CoV and SARS-CoV to PEG-IFN. Vero cells were incubated with 0 to 1000 ng/ml PEG-IFN at $t=-4$, $t=0$, at $t=4$ h p.i. Cells were infected with 100 TCID₅₀ virus per well. (a,b) At 2 d p.i. cells were examined for CPE. Effect of PEG-IFN treatment on CPE induced by (a) SARS-CoV or (b) MERS-CoV. CPE was scored as either (0) none, (1) mild, (2) moderate, (3) severe or (4) complete. (c,d) Viral genomes in the culture medium of virus-infected cells were determined by RT-PCR. Influence of PEG-IFN treatment on the viral RNA load (genome equivalents (gen. eq.) per ml) in the supernatants of cells infected with (c) SARS-CoV or (d) MERS-CoV.

Treatment with PEG-IFN profoundly inhibited both MERS-CoV- and SARS-CoV-induced CPE and RNA levels in a dose-dependent manner (Fig. 6). At 2 d p.i., SARS-CoV-induced CPE was reduced for all time points of PEG-IFN addition when using a dose of at least 30 ng/ml PEG-IFN (Fig. 6a), whereas MERS-CoV-induced CPE already decreased using a dose of 1 ng/ml (Fig. 6b). For SARS-CoV, only pre-treatment with 1000 ng/ml PEG-IFN completely prevented CPE. For MERS-CoV, complete inhibition of CPE was observed at much lower concentrations, specifically 3, 10 or 30 ng/ml when the drug was added to the cells before, during or after infection, respectively. Although decreased CPE was also

observed in SARS-CoV-infected cultures treated with 30 ng/ml PEG-IFN, only a 30-fold reduction of viral RNA was detected in their medium at 2 d p.i. (Fig. 6c). For comparison, treatment of MERS-CoV-infected cells with the same PEG-IFN dose completely blocked CPE and reduced viral RNA levels in the medium 600- to 2,000-fold, depending on the timing of PEG-IFN addition (Fig. 6d).

Our data revealed that in the same cell line MERS-CoV infection is 50-100 times more sensitive to PEG-IFN treatment than SARS-CoV infection. This difference may be explained by important lineage-specific genetic differences between these two zoonotic betacoronaviruses in terms of accessory protein genes encoded in the 3' part of the genome [16, 389]. In particular, MERS-CoV does not encode a homolog of the SARS-CoV ORF6 protein, which was reported to block the IFN-induced nuclear translocation of phosphorylated transcription factor STAT1. As nuclear translocation of p-STAT1 is essential for transcriptional activation of downstream antiviral genes, the ORF6 protein makes SARS-CoV less sensitive to treatment with type I IFN [105, 384]. IFN-induced translocation of p-STAT1 was readily observed in IFN-treated mock-infected Vero cells (Fig. 7a-d), but not in IFN-treated SARS-CoV-infected cells (Fig. 7e,f). In contrast, in MERS-CoV-infected and IFN-treated cultures the translocation of p-STAT1 was detected (Fig. 7g,h). Together with the data on IFN sensitivity (Fig. 5), these observations highlight important differences between SARS-CoV and MERS-CoV in terms of their interaction with the IFN signalling pathways.

DISCUSSION

Following the 2003 SARS epidemic, global CoV hunting efforts identified a wealth of previously unknown family members, in particular in bat species from several continents [286]. Moreover, at least three of the four current 'established' human CoVs (NL63, 229E, and OC43) were postulated to have originated from zoonotic reservoirs [24, 390, 391]. Recently, about a decade after the SARS outbreak, MERS-CoV was identified as the next zoonotic CoV [15] and appears to be highly pathogenic to humans: of the 49 cases confirmed thus far, 23 had a fatal outcome (http://www.who.int/csr/don/archive/disease/coronavirus_infections/en/). Whether zoonotic CoVs cause transient epidemics or establish a long-lasting relationship with the human host, an in-depth understanding of virus-host interactions will be required to develop effective countermeasures. In this study, we defined several basic but important parameters of MERS-CoV replication in cell culture (Figs. 1-4). Among the tools for MERS-CoV research developed are immunoassays based on cross-reacting antisera raised against other betacoronaviruses (Fig. 2) and a CPE-based assay that can be used to screen for antiviral effects (Figs. 5-6).

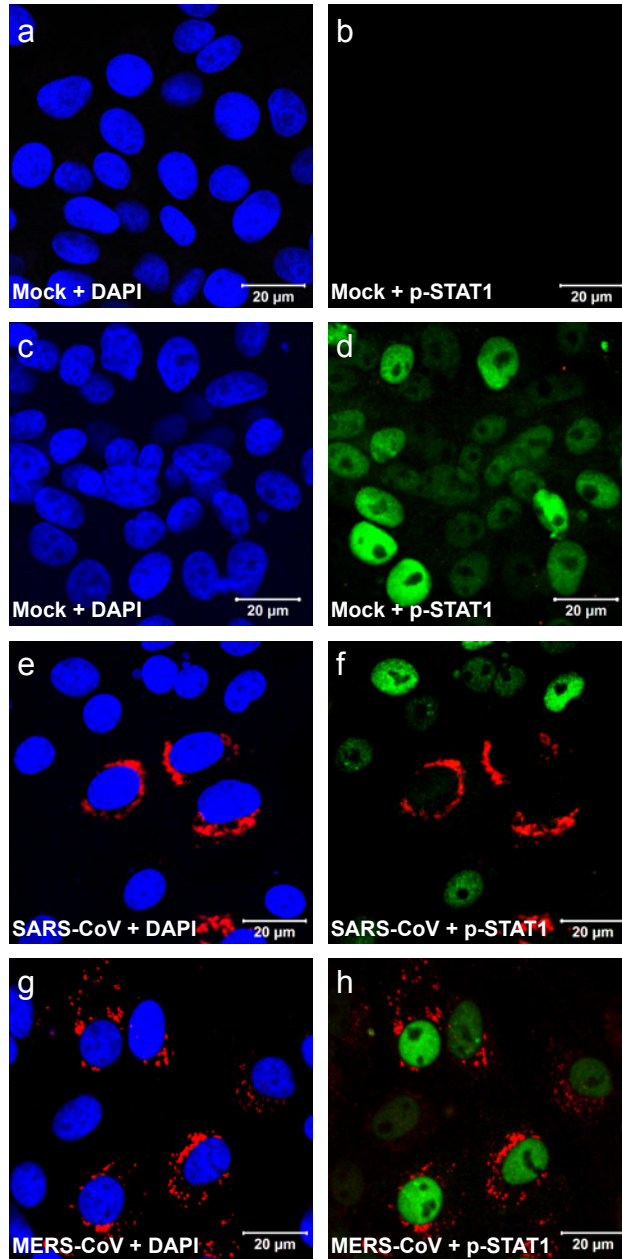


Fig. 7. IFN- α induced nuclear translocation of p-STAT1 in MERS-CoV-infected Vero cells. Confocal immunofluorescence microscopy of uninfected Vero cells (a-d) and Vero cells infected (MOI 1) with SARS-CoV (e,f) or MERS-CoV (g,h). At 8 h p.i. cells were (a, b) left untreated or (c-h) treated with 1000 ng/ml PEG-IFN for 30 minutes, fixed and double-labelled with antisera against SARS-CoV nsp3 (red; a-h), or p-STAT1 (green; b,d,f,h), and nuclear DNA was stained with DAPI (blue; a,c,e,g).

Following the development of a high-throughput screening method for antiviral effects, proof of principle was obtained using CsA, a recently discovered inhibitor of CoV replication [276, 277]. This drug affects the function of several members of the cellular cyclophilin (Cyp) family and appears to block functional interactions between viral proteins and one or multiple cyclophilin family members [281]. Low-micromolar CsA concentrations blocked MERS-CoV-induced CPE in Vero and Huh7 cells (9 μM and 15 μM , respectively) as previously observed for other CoVs [276, 277]. As in those previous studies [276], a small fraction of the cells somehow remained susceptible to MERS-CoV infection, even at high CsA concentrations. Thus, virus replication could not be completely eliminated, which may ultimately lead to the development of CsA resistance in cell culture. In conclusion, these experiments established that monitoring MERS-CoV-induced CPE can be a valuable and rapid tool in screening for the potential antiviral activity of e.g. small-molecule compounds or FDA-approved drugs like PEG-IFN.

Type I IFN induction, a hallmark of the early innate immune response, is counteracted by different CoV-encoded proteins. Despite these evasion strategies, IFN can be detected in sera of CoV-infected mice and humans [188, 189, 392], and CoV-infected plasmacytoid DCs have been identified as a source of high IFN- α levels [393, 394]. The SARS-CoV ORF6 protein, however, (partially) disrupts the downstream IFN-induced signalling in infected cells by inhibiting the nuclear translocation of p-STAT1, a critical component of both the IFN- α and IFN- γ signalling pathways [105]. Although contributions from additional immune evasion mechanisms are likely, the lack of a SARS-CoV ORF6 homolog [16] may be a major factor in the higher sensitivity of MERS-CoV to PEG-IFN treatment, as observed in this study and other recent work [395]. This was further substantiated by the finding that nuclear translocation of p-STAT1 is not blocked in MERS-CoV-infected cells (Fig. 7), which indicates that MERS-CoV has not evolved an alternative strategy to achieve the same goal. MHV has been shown to be relatively insensitive to IFN pre-treatment, however also this virus does not block activation and translocation of p-STAT1 but instead inhibits the induction of a subset of ISGs by IFN- α/β [396]. Future studies may elucidate whether MERS-CoV has evolved alternative strategies to cope with the host's IFN response. In addition, it will be important to test whether MERS-CoV is attenuated *in vivo* as a result of the relative high IFN sensitivity.

PEG-IFN is a registered drug used for the treatment of chronic hepatitis B and C infections in humans [397]. Several CoVs, including SARS-CoV, were shown to be sensitive to both type I IFN treatment *in vitro* and PEG-IFN treatment *in vivo* [190-192], and in this study we established a relatively high sensitivity for MERS-CoV. For example, in cynomolgus macaques plasma levels of 1-5 ng/ml were reached [190], a dose which in this study significantly reduced MERS-CoV replication *in vitro*. The sensitivity of MERS-CoV to exogenous IFN suggests that administration of recombinant IFN merits further

evaluation as a therapeutic intervention strategy if new infections with the novel virus would occur.

ACKNOWLEDGMENTS

We are grateful to Ron Fouchier, Chris Lauber and Alexander Gorbalenya for helpful discussions, and we thank Dennis Ninaber and Corrine Beugeling for technical assistance. This research was supported in part by TOP grant 700.57.301 from the Council for Chemical Sciences (CW) and MEERVOUD grant 836.10.003 from the Council for Earth and Life Sciences (ALW) of the Netherlands Organization for Scientific Research (NWO) and the EU-FP7-Health project SILVER (Grant #260644).

Chapter 7

General discussion

THE NEED FOR ANTIVIRAL THERAPIES AGAINST PATHOGENIC CORONAVIRUS INFECTIONS

The 2003 SARS-CoV outbreak, which had an immense global impact and almost led to a pandemic, and the ongoing MERS-CoV outbreak illustrate it is important to be prepared for emerging pathogenic coronaviruses. The re-emergence of SARS-CoV or the zoonotic transfer of other animal coronaviruses like MERS-CoV to humans remains a serious public health concern. The preparedness for these outbreaks should obviously include the availability of antiviral intervention strategies. The number of confirmed MERS cases that have been reported is relatively low (94 cases and 46 deaths till August 2013), but the mortality rate in this group of patients is alarmingly high (~50%). Moreover, in view of the distribution of these cases in time and over distant geographical locations, it is now widely assumed that the actual number of human infections could be much higher. A major factor that may contribute to an underestimation of that number obviously is the possibility of mild or asymptomatic infections, but also inadequate surveillance, lack of proper diagnostic procedures and/or the political and social climate in the Middle East may play a role. Therefore, the true number of cases and the risk of the virus spreading to other regions might be underestimated. Nevertheless, in-depth analysis of the small MERS clusters described so far suggests that the currently circulating MERS-CoV strains do not have pandemic potential [398].

The SARS outbreak triggered the rapid development of vaccine candidates (reviewed in [399]) and one of these even entered a phase I clinical trial [400] within a relatively short period of time, but still 1.5 years after the start of the outbreak. Since the 2002/2003 global SARS outbreak was controlled within about 4 months and only a few additional cases have been reported since then, no further clinical trials were conducted. Considering the time required to test and register a vaccine, it is important to develop alternative intervention strategies (e.g. pan-coronavirus inhibitors) as a first line of defence, to combat any new pathogenic coronavirus that might emerge in the future.

A better understanding of coronavirus replication and the complex interplay between the abovementioned viruses and their host should provide starting points for the development of such antiviral strategies. They may also offer possibilities to limit or circumvent the problem of antiviral drug resistance, a common problem when using compounds that directly target RNA viruses, due to their high mutation rate and rapid adaptation. Therefore, there is a growing interest in druggable host targets to block virus replication [401], as drug resistance is less likely to develop when cellular rather than viral functions are targeted (reviewed in [130, 131]). **Chapters 2, 3 and 5** of this thesis shed some light on the interplay between nidoviruses and the host cell. The different approaches used in these studies, each with their own benefits and limitations, identified a variety of host factors that can influence nidovirus replication. Studies using isolated,

functional replication and transcription complexes (RTCs) from arterivirus-infected cells contributed to the identification of antiviral compounds and proviral host factors. An siRNA screen identified kinases and various other host factors that affect SARS-CoV replication. Finally, the cyclophilins (CyPs), a promising class of host targets for antiviral therapy, were shown to play a role in the replication of both arteri- and coronaviruses (**Chapters 3, 4 and 6**). Below, a selection of these host factors, their functions in the host cell and their role in nidovirus replication will be discussed in more detail.

Characterisation of replication complexes isolated from infected cells

The isolation of viral replication complexes (RCs) from infected cells and the development of *in vitro* assays (IVRAs) to analyse their RNA synthesising activity have provided mechanistic insights into the replication of several +RNA viruses, including human pathogens like poliovirus [259, 264, 268, 402], West Nile virus [227, 244], Japanese encephalitis virus [403], and HCV [254, 404]. The development of such assays for model viruses like Sindbis virus [228], brome mosaic virus [261] and Flock house virus [405] has contributed to our understanding of +RNA virus replication in general. Besides providing information on viral RNA synthesis mechanisms and the role of membrane structures in replication, also the involvement of host proteins in RNA synthesis [264, 406] was established and the mode of action of certain inhibitors was resolved, for example in the case of Gliotoxin, which was shown to be an inhibitor of the poliovirus polymerase 3D^{pol} [407].

For nidoviruses, several previous attempts to study RNA synthesis using RTCs isolated from infected cells [236, 239, 240] resulted in barely detectable activities *in vitro*. **Chapter 2** describes a robust assay to study nidovirus RNA synthesis *in vitro*. A crude cytoplasmic fraction from cells infected with the prototype arterivirus EAV, contained RTCs that were able to synthesise EAV genomic RNA and all sg mRNAs *in vitro*. Further subcellular fractionation yielded a membrane fraction that contained these functional RTCs. Strikingly, their RNA synthesising activity was strongly dependent on a cytosolic host factor that was not physically associated with the RTCs after their isolation. In parallel to this study of the arterivirus RTCs, the same phenomenon was observed for RTCs isolated from SARS-CoV-infected cells [53]. This host factor could be partially purified from the cytosol of (uninfected) HeLa cells by size-exclusion chromatography and was found to have a native mass of 59-70 kDa. Several other chromatographic methods were applied in attempts to further purify and identify the host factor necessary for EAV RNA synthesis, and it still remains to be seen whether it is the same factor that is crucial for SARS-CoV replication. Its identification was hampered by the fact that all protein fractions purified need to be assayed for their ability to reconstitute the activity of pelleted (inactive) EAV RTCs, and that the preparation of these complexes is laborious and complicated, in particular since they lose their RNA-synthesising activity relatively quickly. Comparative quantitative mass spectrometry (in collaboration with the LUMC

Biomolecular Mass Spectrometry Facility) has now narrowed down the list of candidates to six proteins (de Wilde *et al.*, unpublished data), but unfortunately the exact identity of this host protein remains to be established. Only a small amount of this factor is needed for EAV RTC activity, since a 50-fold diluted HeLa cell lysate or chromatography fractions containing almost undetectable amounts of protein can still reconstitute viral RNA synthesis (de Wilde *et al.*, unpublished data). The need for a host factor that apparently has no permanent physical interaction with the viral RTC was also observed for poliovirus RNA synthesis in a study by Barton *et al.* [264], and the identity of this factor is currently still unknown. I hypothesise that this factor modifies (by e.g. phosphorylation) and activates a host or viral protein within the RTC that is required for efficient RNA synthesis. Its unequivocal identification and functional characterisation, using siRNAs, chemical inhibitors and heterologous expression and purification is currently ongoing.

Viral RNA synthesis is a logical target for developing antiviral strategies and inhibitors of this step of the replicative cycle have been successfully developed for several +RNA viruses (reviewed in [318, 408, 409]). *In vitro* assays have been used to analyse nidovirus RNA synthesis but also for screening for compounds that inhibit RNA synthesis, as exemplified by the identification of CsA (**Chapter 3**) and Zn²⁺ [159]. An advantage of screening for inhibitors in an *in vitro* system is that cellular uptake does not pose any limitations, which allows the identification of (cell-impermeable) lead compounds that would have been missed in cell-based screens. A disadvantage of this approach is that it would probably not identify inhibitors that need to be metabolised first, like Ribavirin. Another drawback is that potential cytotoxic effects caused by the compound are not detected at an early stage. It obviously remains important to test inhibitors that are identified *in vitro*, in cell-based assays to evaluate their toxicity and efficacy (see also **Chapter 3**).

In conclusion, the biochemical studies and *in vitro* activity assays provided more insight into the composition and characteristics of the nidovirus RTC and form a good basis for more in-depth studies, for example on their composition and the function and origin of the associated membranes. This would require more sophisticated – thus far unsuccessful – RTC purification strategies in combination with for example mass-spectrometry.

SYSTEMS VIROLOGY AND ITS POTENTIAL TO IDENTIFY HOST FACTORS INVOLVED IN CORONAVIRUS REPLICATION

The application of systems biology approaches in virology (systems virology) has provided a wealth of information on the role of individual proteins and cellular pathways in the replication of RNA viruses (for a recent review, see [410]). This relatively new, interdisciplinary field focuses on the complex virus-host interactions that occur within

the cell or even in the whole organism and aims to provide an unbiased perspective. The applied techniques include transcriptomics (the analysis of gene expression profiles in infected cells), metabolomics (metabolic changes induced during infection), proteomics (to analyse changes in the cellular proteome caused by infection) and phenomics, which includes RNA interference (RNAi) screening. RNAi is a method that enables the specific degradation of cellular or viral mRNAs by transfecting small interfering RNA (siRNA) molecules that are complementary to the target RNA. This method is widely used to study virus-host interactions and it has identified numerous host genes involved in the replication of important human pathogens like WNV [334], DENV [335], HIV-1 [336], HCV [337-342] and influenza virus [338, 343, 344].

For coronaviruses a number of host proteins that affect the replicative cycle have been described previously ([321] and reviewed in [65, 320]), but large(r)-scale siRNA screens to systematically identify such factors have not been reported thus far. **Chapter 5** describes an siRNA screen to identify host cell kinases that influence SARS-CoV replication. Protein kinases are key regulators in signal transduction and control a wide variety of cellular processes [411]. Consequently they have been the subject of many studies aiming to develop therapeutic strategies for the treatment of a variety of diseases, and indeed many registered drugs have cellular kinases as their target [412, 413]. In addition, kinases have been shown to play important roles in the replicative cycle of many +RNA viruses.

The siRNA screen that is described in **Chapter 5** yielded a relatively high proportion of antiviral hits (90 of 778 factors; ~12% of all factors) for SARS-CoV, compared to human kinome-directed screens that have been performed with other viruses [341, 414, 415]. This might indicate that compared to other viruses, SARS-CoV replication is more restricted by cellular factors. However, differences in experimental set-up exist and should also be taken into account.

Pathway analysis mapped multiple hits to cellular immune responses, like interleukin (IL) signalling. Within the IL signalling pathways, IL-6 and IL-8 signalling have previously been implicated in controlling coronavirus infection and coronavirus-induced inflammation (reviewed in [65]), and the results described in **Chapter 5** (once again) emphasise their importance in SARS-CoV infection.

Several hits of our siRNA screen are part of the p38 MAPK pathway, which has also been implicated in nidovirus replication previously, as it regulates IL-6-, IL-8- and IL-10-mediated pro-inflammatory cytokine signalling [360, 361, 416]. This, for example, explains why MEK3, a key player in the p38 MAPK signalling pathway, was identified as antiviral hit for SARS-CoV. These results imply that activation of the p38 MAPK pathway limits SARS-CoV replication in cell culture and *in vivo*. Liao *et al.* showed that the avian coronavirus IBV induces IL-6 and IL-8 expression. Meanwhile, the same study showed that IBV has evolved a strategy to counteract IL-6 and IL-8 expression by inducing the

expression of dual-specificity phosphatase 1 (DUSP1), a negative regulator of p38 MAPK [362]. Although viral protein expression seemed not directly affected by IL-6 and IL-8, IBV apparently interferes with p38 MAPK signalling to limit expression of these pro-inflammatory cytokines. In contrast to IBV, MHV infection activates p38 MAPK signalling and the increased IL-6 production actually promotes MHV-specific protein synthesis and virus production [363]. Follow-up studies on the role of MAPKs in SARS-CoV infection and their link with the immune response and other pathways should provide more insight into the exact role of these pathways in coronavirus replication and pathogenesis, and in the apparently virus-specific (opposite) effects observed among coronaviruses.

The IL-17 signalling pathway that was identified as antiviral in the SARS-CoV siRNA screen, was recently found to be activated in epithelial cells during SARS-CoV and MERS-CoV infection [417]. Since this pathway plays a pivotal role in host defence responses against microbial invaders, the authors suggested that this pathway might be an interesting therapeutic target to limit coronavirus-induced cytopathicity and lung injury.

In parallel to the SARS-CoV siRNA screen described in **Chapter 5**, a similar screen using the same cell line was performed to identify cellular kinases that affect EAV replication [418]. For EAV, 38 proviral (40 for SARS-CoV) and 116 antiviral hits (90 for SARS-CoV) were identified. There was a remarkably small overlap between the hits identified for SARS-CoV and EAV, as only 5 common proviral (~12% of all hits) and 18 common antiviral (20% of all hits) hits were found. Apparently, these distantly related nidoviruses differ significantly in their interactions with the host. Nonetheless, the few common factors that have been identified (diacylglycerol kinase epsilon, suppressor of cytokine signalling 5, protein serine kinase H1, AarF domain containing kinase 4, and coatomer protein complex subunit beta-2) should be further evaluated as they could represent interesting targets for the development of broad-spectrum antiviral strategies against nidoviruses.

The application of RNAi screens was considered a revolution in genetics [419]. However, one should keep in mind that it also has drawbacks and that data must be interpreted with caution. This is illustrated, for example, by the fact that only three common hits were identified when data sets of three independent large-scale RNAi screens for host factors involved in HIV-1 replication were compared (reviewed in [420]). One of the major drawbacks of RNAi screening is that this method is relatively error prone and major concerns include the identification of false positive hits due to off-target effects, e.g. siRNAs might down-regulate multiple transcripts, siRNAs might stimulate the immune response, or exogenous siRNAs could saturate the RNAi machinery to block processing of essential cellular (mi)RNAs (reviewed in [421]). False negative hits could be observed due to insufficient knockdown of the factor that is being analysed [422]. Bearing this in mind, one should consider hits from siRNA screens only as a starting point for further analysis rather than a definitive list of host factors involved in virus replication. It also demonstrates the importance of validation experiments after the primary screen,

for example using a deconvoluted set of siRNAs targeting the same gene, lentivirus-expressed shRNAs and/or chemical inhibitors, if available for the target. A drawback of the use of chemical inhibitors is their potential lack of specificity. Overexpression studies of the identified proteins are generally expected to show an effect opposite of that found in the siRNA screen, although - depending on the endogenous level of the host factor - these effects might be limited or absent. However, the combined results of such follow-up/validation studies should increase the reliability of hit identification.

The sets of pro- and antiviral host factors that were identified for SARS-CoV provides a good starting point for in-depth analysis of nidovirus-host interactions and the cellular pathways that influence replication, which might ultimately lead to the development of host factor-directed antiviral strategies.

COP-I COATED VESICLES AND MEMBRANES IN CORONAVIRUS REPLICATION

COPB2 (or β' -COP), a subunit of the coatamer protein complex, was identified in our siRNA screen as a proviral factor for SARS-CoV, as its depletion strongly inhibited SARS-CoV protein expression and progeny titres (**Chapter 5**). Other proteins involved in the formation of COP-I coated vesicles also play a role, as depletion of COPB1 and GBF1 severely affected SARS-CoV replication. A schematic overview of (factors involved in) the formation of COP-I coated vesicles is shown in Fig. 1.

There is some controversy on the role of COP-I coated vesicles and other membrane structures in coronavirus replication. Using advanced EM analyses, our group has shown that the SARS-CoV-induced reticulovesicular network (RVN) is derived from and continuous with the ER [30, 208, 295]. In contrast, other studies implicated either the autophagic pathway [32, 54] or EDEMosomes [55] as the primary membrane source. Earlier work by our laboratory [295] and others [364-366] already suggested that (the integrity of) the early secretory pathway is important for efficient SARS-CoV replication, but its exact role remained unclear since conflicting results have been reported. Knoops *et al.* have previously shown that Brefeldin A (BFA) treatment inhibits SARS-CoV replication, but does not completely block viral RNA synthesis, as ~20% of the activity remains in BFA-treated cells, compared to untreated infected cells. Furthermore, the lack of colocalisation of SARS-CoV replicase subunits with COP-I vesicles argues against a direct association of coronavirus RTCs with these COP-I-coated vesicles [295]. Using MHV-infected cells, Verheije *et al.* showed that depletion of Arf1 and GBF1, thus blocking COP-I coated vesicle formation, and BFA treatment almost completely abolishes replication of this distantly related coronavirus. In line with the work of Knoops *et al.*, co-localisation of MHV RTCs with COP-I vesicles was not observed [365]. Our data from the siRNA screen further corroborate the importance of COP-I coated vesicles and the secretory pathway

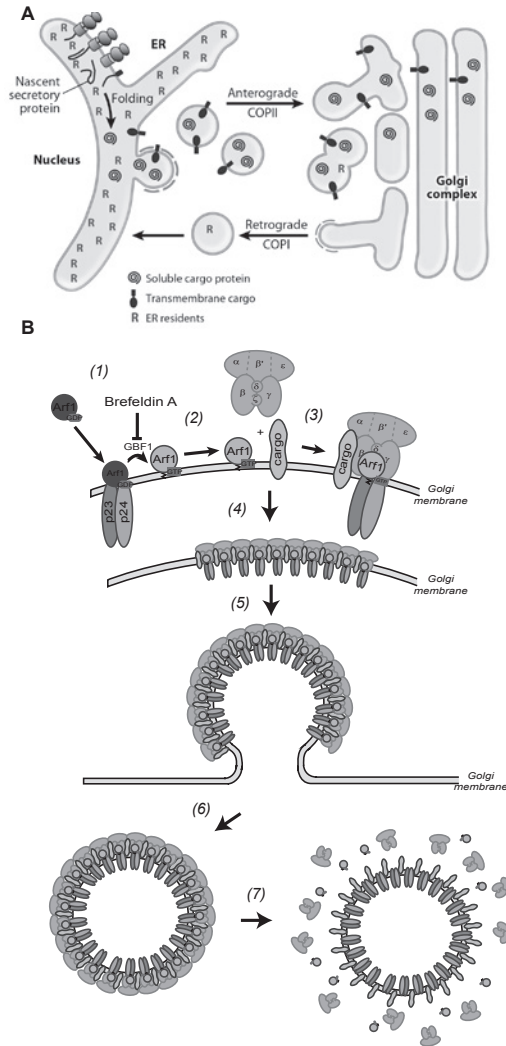


Fig. 1. (A) Model depicting bidirectional transport between the ER and Golgi compartments. After translation and folding of nascent secretory proteins, membrane cargo and soluble secretory cargo are exported from the ER in COPII-formed transport vesicles. ER-derived vesicles traffic in an anterograde direction to fuse with or to form pre-Golgi compartments. COP-I coats bud retrograde-directed vesicles from pre-Golgi and Golgi compartments to recycle vesicle components and retrieve resident proteins (R) that have escaped the ER. This rapid cycling process allows anterograde transport of secretory cargo, whereas resident proteins remain dynamically localised to early secretory compartments. Reprinted with permission from [423]. (B) Schematic overview of COP-I coated vesicle formation. Arf1-GDP binds to the cytoplasmic tails of p23/p24 hetero-oligomers (1), and is subsequently activated by the GDP/GTP exchange that is mediated by GBF1. This activation step can be blocked by BFA (2). Coatomer subsequently binds both the p24 oligomer and Arf1-GTP. Cargo can be captured by the α/β' -COP subunits (3) and after coat polymerisation (4), a COP-I vesicle can pinch off the donor membrane (5,6). These vesicles uncoat due to hydrolysis of Arf1-GTP to Arf1-GDP (7). Based on models described in [357, 424].

for SARS-CoV replication, since we observed an almost complete inhibition of SARS-CoV replication upon depletion of COP-I coatomer components (**Chapter 5**).

COP-I-coated vesicles have also been implicated in the replication of many other RNA viruses, such as poliovirus [367, 368], other enteroviruses [353, 369-371], VSV [372], Drosophila C virus [373], and influenza A virus [344, 374] and components of the early secretory pathway have also been identified in siRNA screens for many RNA viruses [338, 344, 373, 374, 425]. These data suggest that the secretory pathway or its components are commonly used by RNA viruses. A variety of mechanisms regarding the role of the early secretory pathway have been suggested. For example, replication of the enterovirus EV11 appeared to depend on the association of COP-I with membranes [369]. On the contrary, Belov *et al.* showed that GBF1, BIG1/2 and Arf proteins, but not COP-I coatomer components, are recruited to Golgi membranes to enable RC formation [367, 368]. Hsu *et al.* reported similar observations since Arf1 and GBF1 recruit PI4KB to membranes on which RCs associate to cause a change in lipid composition. This change is favourable for the binding of other components of the RC complex [353].

To date, there is no data that suggests a direct link between COP-I vesicles and coronavirus RNA synthesis, which supports the idea that these vesicles do not contain the viral RTC but have an indirect – still to be determined – effect on coronavirus replication. COP-I vesicles might transport cargo needed for the formation or activity of viral RTCs, or the observed effects might merely be due to a general disruption of cellular endocytic transport or cellular homeostasis.

TARGETING CYCLOPHILINS TO BLOCK +RNA VIRUS REPLICATION

Cyclosporin A is a well-known immunosuppressive drug that binds to cellular cyclophilins (Cyps), yielding a Cyp-CsA complex that can inhibit calcineurin. Inhibition of calcineurin prevents the dephosphorylation and translocation of nuclear factor of activated T cells (NF-AT) from the cytosol into the nucleus (Fig. 2), which prevents the transcription of immune genes, such as IL-2 (reviewed in [279, 280, 426]). A total of 17 Cyps have been identified thus far, of which nine are targeted by CsA. Cyps are also known as peptidyl-prolyl isomerases (PPIases) and many of them have chaperone and foldase activities [279, 427] that facilitate protein folding. Cyps are involved in various signalling pathways (reviewed in [280]), and processes such as apoptosis [428] and RNA splicing [429, 430].

CsA has been reported to block the replication of a variety of RNA viruses, like hepatitis C virus [274, 299], HIV-1 [272, 432] and several others [271, 273, 275, 433]. In line with the inhibitory effect of CsA treatment, Cyps and in particular the cytosolic CypA and the ER-associated CypB have been concluded to be essential host components in the replicative cycle of many RNA viruses [271, 273, 303, 306, 307, 309, 311, 434, 435].

The work presented in this thesis shows that CsA also is a potent inhibitor of arterivirus (**Chapter 3**) and coronavirus replication (**Chapters 4 and 6**). MERS-CoV-induced cytopathology was severely reduced upon treatment with 9 μM of CsA (**Chapter 6** and unpublished observations), and SARS-CoV replication was completely blocked upon treatment with 16 μM of CsA (**Chapter 4**). Similar results were obtained for the arterivirus PRRSV (IC_{50} of 5.5 μM ; complete block at 16 μM), and EAV replication appeared even five-fold more sensitive to CsA treatment (IC_{50} of 0.95 μM). Similar results were reported for feline coronavirus (FCoV)-induced cytopathology, which was blocked at 25 μM CsA. Pfefferle *et al.* have demonstrated that low micromolar concentrations of CsA block the replication of multiple coronaviruses, including SARS-CoV and HCoV-229E [277]. Noteworthy, Cyp levels may differ between test systems and therefore it is difficult to compare the sensitivities of different nidoviruses to CsA. Despite the apparently nidovirus-wide inhibitory effect of CsA, the exact mechanism by which the drug blocks nidovirus replication remains unclear. For SARS-CoV, we could not identify which specific (if any) Cyp was involved in CsA-mediated inhibition of virus replication (**Chapter 4**). This might be due to the fact that Cyp expression could not be sufficiently depleted with specific siRNAs (~25% remaining expression). The replication of SARS-CoV was not blocked by a non-immunosuppressive CsA analogue (De Wilde *et al.*, unpublished data) suggesting that PPlase activity and/or direct interaction with replicase subunits might not be involved in the proviral effect of Cyps. Pfefferle *et al.* suggested that SARS-CoV nsp1 is an activator of the NF-AT signalling pathway that induces a broad and systemic dysregulation of cytokine expression [277]. Combined with our data, this would argue against a direct role for Cyps in SARS-CoV replication, but suggests that the NF-AT pathway is somehow (indirectly) involved. This model is not supported by the data obtained for FCoV replication in the feline cell line fcwf-4. The authors suggested that FCoV does not depend on a functional NF-AT signalling pathway since FCoV replication was blocked at CsA or FK506 concentrations that did not affect signalling in these cells [278]. However, these results should be interpreted with caution. At first, concentrations that were shown to block FCoV-induced cytopathicity were not tested, and secondly, the authors do not show whether or not FCoV infection activates NF-AT signalling. Therefore, it would be interesting to investigate whether FCoV induces NF-AT nuclear translocation and whether FCoV replication is sensitive to treatment with non-immunosuppressive CsA analogues. More importantly, the role of the NF-AT pathway in SARS-CoV replication should be further investigated.

In contrast to coronaviruses, replication of the arteriviruses EAV and PRRSV is inhibited by the non-immunosuppressive CsA analogue Debio-064 (**Chapter 3**). Like Debio-025, NIM811, and SCY635, this compound has a higher affinity for Cyps than CsA and lacks its undesired immunosuppressive side-effect, since NF-AT signalling is not affected by this drug. For the treatment of HCV infection, non-immunosuppressive Cyp inhibitors are

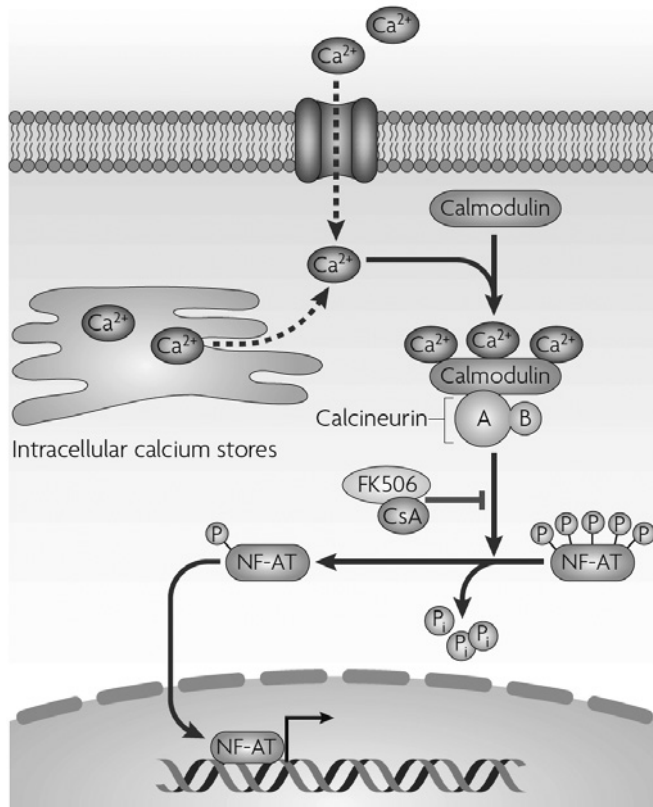


Fig. 2. The NF-AT signalling pathway. The calcineurin catalytic subunit (A), when bound to the regulatory subunit (B) and calmodulin–Ca²⁺ complex, dephosphorylates NF-AT in the cytoplasm, leading to nuclear translocation of this transcription factor and the subsequent activation of gene transcription. CsA binds to Cyps, and FK506 to FK506-binding proteins (FKBPs) and these Cyp–CsA or FK506–FKBP complexes inhibit Calcineurin activity, to reduce NF-AT dephosphorylation. Reprinted with permission from [431].

considered a promising class of antiviral compounds, and their potency was explored in phase III clinical trials, in combination with pegylated IFN and Ribavirin [436]. The non-immunosuppressive CsA analogues are not only interesting because of their therapeutic potential, they are also valuable research tools for studying the proviral mode of action of Cyps. These compounds allow us to discriminate between the direct involvement of Cyps in viral replication and indirect effects involving e.g. (dysregulation) of the NF-AT signalling pathway.

Mainly based on data obtained for HCV, different mechanisms have been proposed to explain the role(s) of Cyps in the viral replicative cycle [437]. First of all, Cyps are components of the HCV replication complex and are important for the proper folding of the HCV polymerase (NS5B) [308]. Kaul *et al.* have shown that the development of resistance against the Cyp inhibitor Debio-025 involves mutations in HCV NS5B that are close to the NS5A/NS5B cleavage site. These are thought to delay processing of the NS5A/NS5B junction.

tion, thus extending the time during which the CypA binding site in NS5B is accessible [308]. As a result, lower amounts of CypA would suffice to mediate the proper folding of NS5B and its incorporation into replication complexes. Others have postulated that the CsA treatment of infected cells leads to the depletion of CypA from the RC and that this interferes with the formation of these complexes [307, 332]. Finally, it was hypothesised that binding of the viral polymerase to the enzymatic pocket of CypA is essential for RNA synthesis [306]. Although the exact mechanism remains to be elucidated, Chatterji *et al.* suggested that the isomerase activity of CypA might be essential for NS5B function and thus for HCV replication [306], since CypA mutants that lack the PPIase activity showed a reduced binding to NS5B and PPIase-defective CypA reduced HCV replication. This hypothesis is supported by recent studies demonstrating that CsA resistance is linked to mutations in NS5B that increase its affinity for viral RNA, thus rendering the enzyme less dependent on CypA [438].

Chapter 4 describes that depletion of CypA affects EAV replication and that CypA cosediments with the membrane-associated viral RTCs. Furthermore, CsA treatment was able to prevent the cosedimentation of CypA and EAV RTCs. Although we were unable to show a direct interaction between CypA and any of the EAV nsps (unpublished observations), this suggests that the mechanism by which CypA associates with the viral RTC is sensitive to CsA. In addition, CsA completely blocked EAV RNA synthesis *in vitro*, presumably by targeting the functional association of CypA with preformed RTCs. Therefore, in the most likely model CypA is somehow directly involved in arterivirus RNA synthesis, by interacting with one of the key components of the EAV RTC. In this context, viral the helicase (nsp10) is of particular interest since it plays a role in RNA synthesis and contains several predicted CypA binding domains (**Chapter 3**). Previously, for SARS-CoV it has been shown that CypA interacts with the RNA-binding N protein [312]. In the case of EAV, it is unlikely that an interaction between CypA and N is crucial for viral RNA synthesis, since the N protein was found to be completely dispensable for both genome replication and sg mRNA synthesis [270].

The different sensitivities to the non-immunosuppressive CsA analogue Debio-064 suggest that mechanistic differences exist between corona- and arteriviruses with respect to the role of Cyps in their replication. EAV and PRRSV replication was inhibited by Debio-064, while SARS-CoV replication was not affected by this compound. This notion is further supported by the fact that CypA or CypB knockdown did not affect SARS-CoV replication, whereas EAV replication was reduced upon CypA depletion. In line with the results of Pfeifferle *et al.* [277] and a recent study by Carbajo-Lozoya *et al.* [439], this suggests that the NF-AT pathway is relevant for SARS-CoV replication. In contrast, the Cyps themselves probably directly affect EAV replication. Analysis of mutations acquired by CsA-resistant (escape) mutants of EAV and other nidoviruses might shed light on

the viral proteins involved in functional interactions with CypA and on the mechanistic details of their role in nidovirus replication.

ANTIVIRAL RESEARCH ON CURRENT AND FUTURE EMERGING CORONAVIRUSES

Vaccination was the basis for some of the greatest successes in the history of medicine, including the eradication of smallpox, the near-eradication of polio, and the prevention of considerable morbidity and mortality caused by viral infections. Vaccine development currently is a slow process that is not equipped to combat outbreaks of rapidly emerging viruses (see above), although this may improve in the longer run, for example due better production platforms and vaccine engineering on the basis of viral reverse genetics. An alternative way to combat, or at least slow down, emerging infections is the use of antiviral compounds. Thus far, global research efforts to develop antiviral drugs have resulted in treatments for only a handful of human pathogens, i.e. herpesviruses (herpes simplex virus, varicella zoster virus, Epstein-Barr virus, cytomegalovirus), HIV-1, influenza virus and HCV, the only +RNA virus for which approved antiviral therapy is available.

Antiviral drugs can be divided in two main classes: direct-acting antivirals (DAA) and host-directed antivirals (HDA). DAAs directly target (the function of) viral proteins, during entry, replication or assembly of the virus. In general, due to their specificity, these compounds are very potent viral inhibitors, however the quick rise of viral resistance remains a major issue. Successful antiviral therapies are therefore commonly based on the use of a combination of antiviral drugs, in order to increase the barrier of resistance. To reduce this problem of resistance, the development of HDAs is current receiving more attention, especially for the treatment of HCV. Registered antiviral therapies for HCV are based on targeting the viral protease with Telaprevir or Boceprevir, in combination with stimulation of the antiviral response by treatment with IFNs and using the nucleoside analogue Ribavirin [440-442]. This treatment accomplishes a sustained viral response, which means no detectable virus in the blood for six months after the end of treatment, in up to 75%-85% of the cases [443]. This example illustrates the high potential of combined treatment with DAAs (nucleosides and/or protease inhibitors) and HDAs (IFN). However, adverse effects are common during the current anti-HCV therapy, with half of the patients exhibiting flu-like symptoms and a third experiencing emotional problems. These adverse effects are mainly attributed to the use of IFN. For HCV treatment, the effect of Cyp inhibitors, in combination with Ribavirin and pegylated IFN, is currently being explored in phase III clinical trials [436, 444], although these have been (temporarily) put on hold by the FDA due to safety concerns since a patient died from pancreas failure.

As discussed at the start of this chapter, vaccines that need to be developed at the start are not very suitable against outbreaks that only last for a few months, and a more promising approach is to develop treatments with (broad-spectrum) antiviral drugs. In the case of SARS-CoV infection, the gap of ~10 days between the onset of early symptoms and the peak of viral load provides a good window of opportunity for antiviral treatment [445]. A variety of coronavirus inhibitors has been identified in *in vitro* systems and in cell culture (for an overview, see **Chapter 1**). To evaluate the efficacy of these compounds *in vivo* and to study SARS-CoV pathogenesis, multiple animal models have been developed. Mouse-adapted SARS-CoV strain MA15 [446], transgenic mice expressing the human ACE2 receptor [447], and a SARS-CoV ferret model [190] have all been used to study SARS-CoV infection [399]. However, a well-tolerated and effective treatment of SARS-CoV infection is still not available [187]. It therefore remains very important to continue identifying and optimizing SARS-CoV inhibitors or preferentially pan-coronavirus inhibitors and to keep evaluating those in the available animal models.

Since the start of the MERS outbreak in June 2012, the search for antivirals and the development of convenient animal models have been ongoing in many institutes. So far, virus replication was only observed in rhesus macaques [448] and the lack of (cost-effective) small animal models hampers antiviral studies and is one of the reasons to evaluate already registered drugs for their potential to inhibit MERS-CoV [449]. These drugs have already been evaluated in clinical trials and have well-documented safety and pharmacokinetic profiles in patients. Therefore, using these drugs would greatly accelerate the development of antiviral therapy for MERS infections. We (**Chapter 6**) and others [395, 450-452] have reported that MERS-CoV replication was very sensitive to several FDA approved drugs. Especially IFN treatment strongly inhibited MERS infection, and MERS-CoV was up to 100 times more sensitive to type-I IFNs than SARS-CoV. In cell culture, MERS-CoV replication was inhibited by CsA (**Chapter 6**) and the registered drugs lopinavir and chloroquine (de Wilde *et al*, unpublished observations), which provides a promising starting point for the development of intervention strategies for MERS infections. These antivirals would be desperately needed if the MERS outbreak increases in magnitude and severity and could be a treatment option for other zoonotic coronaviruses that might emerge in the future.

References

REFERENCES

1. **Morens, D. M., and A. S. Fauci.** 2013. Emerging Infectious Diseases: Threats to Human Health and Global Stability. *PLoS Pathog.* **9**:e1003467.
2. http://www.who.int/topics/emerging_diseases/en/
3. <http://www.who.int/topics/influenza/en/>
4. <http://www.who.int/hiv/>
5. <http://www.who.int/mediacentre/factsheets/fs164/en/>
6. **Drosten, C., S. Gunther, W. Preiser, S. van der Werf, H. R. Brodt, S. Becker, H. Rabenau, M. Panning, et al.** 2003. Identification of a novel coronavirus in patients with severe acute respiratory syndrome. *N. Engl. J. Med.* **348**:1967-1976.
7. **Ksiazek, T. G., D. Erdman, C. S. Goldsmith, S. R. Zaki, T. Peret, S. Emery, S. Tong, C. Urbani, et al.** 2003. A novel coronavirus associated with severe acute respiratory syndrome. *N. Engl. J. Med.* **348**:1953-1966.
8. **Kuiken, T., R. A. Fouchier, M. Schutten, G. F. Rimmelzwaan, G. van Amerongen, D. van Riel, J. D. Laman, T. de Jong, et al.** 2003. Newly discovered coronavirus as the primary cause of severe acute respiratory syndrome. *Lancet* **362**:263-270.
9. http://www.who.int/csr/sars/country/table2004_04_21/
10. **Keogh-Brown, M. R., and R. D. Smith.** 2008. The economic impact of SARS: how does the reality match the predictions? *Health policy* **88**:110-120.
11. **Lau, S. K., P. C. Woo, K. S. Li, Y. Huang, H. W. Tsoi, B. H. Wong, S. S. Wong, S. Y. Leung, et al.** 2005. Severe acute respiratory syndrome coronavirus-like virus in Chinese horseshoe bats. *Proc. Natl. Acad. Sci. USA* **102**:14040-14045.
12. **Li, W., Z. Shi, M. Yu, W. Ren, C. Smith, J. H. Epstein, H. Wang, G. Crameri, et al.** 2005. Bats are natural reservoirs of SARS-like coronaviruses. *Science* **310**:676-679.
13. **Li, W., C. Zhang, J. Sui, J. H. Kuhn, M. J. Moore, S. Luo, S. K. Wong, I. C. Huang, et al.** 2005. Receptor and viral determinants of SARS-coronavirus adaptation to human ACE2. *EMBO J.* **24**:1634-1643.
14. **de Groot, R. J., S. C. Baker, R. S. Baric, C. S. Brown, C. Drosten, L. Enjuanes, R. A. Fouchier, M. Galiano, et al.** 2013. Middle East Respiratory Syndrome Coronavirus (MERS-CoV); Announcement of the Coronavirus Study Group. *J. Virol.*
15. **Zaki, A. M., S. van Boheemen, T. M. Bestebroer, A. D. Osterhaus, and R. A. Fouchier.** 2012. Isolation of a novel coronavirus from a man with pneumonia in Saudi Arabia. *N. Engl. J. Med.* **367**:1814-1820.
16. **van Boheemen, S., M. de Graaf, C. Lauber, T. M. Bestebroer, V. S. Raj, A. M. Zaki, A. D. Osterhaus, B. L. Haagmans, et al.** 2012. Genomic characterization of a newly discovered coronavirus associated with acute respiratory distress syndrome in humans. *MBio* **3**:e00473-00412.
17. http://www.who.int/csr/don/archive/disease/coronavirus_infections/en/
18. **Muller, M. A., V. S. Raj, D. Muth, B. Meyer, S. Kallies, S. L. Smits, R. Wollny, T. M. Bestebroer, et al.** 2012. Human Coronavirus EMC Does Not Require the SARS-Coronavirus Receptor and Maintains Broad Replicative Capability in Mammalian Cell Lines. *MBio* **3**:e00515-00512.
19. **van der Hoek, L.** 2007. Human coronaviruses: what do they cause? *Antivir. Ther.* **12**:651-658.
20. **McIntosh, K., J. H. Dees, W. B. Becker, A. Z. Kapikian, and R. M. Chanock.** 1967. Recovery in tracheal organ cultures of novel viruses from patients with respiratory disease. *Proc. Natl. Acad. Sci. USA* **57**:933-940.

21. **Hamre, D., and J. J. Procknow.** 1966. A new virus isolated from the human respiratory tract. *Proc. Soc. Exp. Biol. Med.* **121**:190-193.
22. **van der Hoek, L., K. Pyrc, M. F. Jebbink, W. Vermeulen-Oost, R. J. Berkhout, K. C. Wolthers, P. M. Wertheim-van Dillen, J. Kaandorp, et al.** 2004. Identification of a new human coronavirus. *Nat. Med.* **10**:368-373.
23. **Woo, P. C., S. K. Lau, C. M. Chu, K. H. Chan, H. W. Tsoi, Y. Huang, B. H. Wong, R. W. Poon, et al.** 2005. Characterization and complete genome sequence of a novel coronavirus, coronavirus HKU1, from patients with pneumonia. *J. Virol.* **79**:884-895.
24. **Huynh, J., S. Li, B. Yount, A. Smith, L. Sturges, J. C. Olsen, J. Nagel, J. B. Johnson, et al.** 2012. Evidence supporting a zoonotic origin of human coronavirus strain NL63. *J. Virol.* **86**:12816-12825.
25. **www.promedmail.org**
26. **Snijder, E. J., and M. Kikkert.** 2013. Arteriviruses, p. 859-879. In D. M. Knipe and P. M. Howley (ed.), *Fields Virology*, 6 ed. Lippincott Williams & Wilkins, Philadelphia, PA.
27. **Holtkamp, D. J., J. B. Kliebenstein, E. J. Neumann, J. J. Zimmerman, H. Rotto, T. K. Yoder, C. Wang, P. Yeske, et al.** 2011. Presented at the 2011 International PRRS Symposium, Chicago, Illinois, USA.
28. **Belov, G. A., and F. J. van Kuppeveld.** 2012. (+)RNA viruses rewire cellular pathways to build replication organelles. *Current opinion in virology*.
29. **Knoops, K., M. Barcena, R. W. Limpens, A. J. Koster, A. M. Mommaas, and E. J. Snijder.** 2012. Ultrastructural characterization of arterivirus replication structures: reshaping the endoplasmic reticulum to accommodate viral RNA synthesis. *J. Virol.* **86**:2474-2487.
30. **Knoops, K., M. Kikkert, S. H. Worm, J. C. Zevenhoven-Dobbe, Y. van der Meer, A. J. Koster, A. M. Mommaas, and E. J. Snijder.** 2008. SARS-coronavirus replication is supported by a reticulo-vesicular network of modified endoplasmic reticulum. *PLoS Biol.* **6**:e226.
31. **Gosert, R., A. Kanjanahaluethai, D. Egger, K. Bienz, and S. C. Baker.** 2002. RNA replication of mouse hepatitis virus takes place at double-membrane vesicles. *J. Virol.* **76**:3697-3708.
32. **van der Meer, Y., E. J. Snijder, J. C. Dobbe, S. Schleich, M. R. Denison, W. J. Spaan, and J. Krijnse Locker.** 1999. Localization of mouse hepatitis virus nonstructural proteins and RNA synthesis indicates a role for late endosomes in viral replication. *J. Virol.* **73**:7641-7657.
33. **van der Meer, Y., H. van Tol, J. Krijnse Locker, and E. J. Snijder.** 1998. ORF1a-encoded replicase subunits are involved in the membrane association of the arterivirus replication complex. *J. Virol.* **72**:6689-6698.
34. **Brockway, S. M., C. T. Clay, X. T. Lu, and M. R. Denison.** 2003. Characterization of the expression, intracellular localization, and replication complex association of the putative mouse hepatitis virus RNA-dependent RNA polymerase. *J. Virol.* **77**:10515-10527.
35. **Stertz, S., M. Reichelt, M. Spiegel, T. Kuri, L. Martinez-Sobrido, A. Garcia-Sastre, F. Weber, and G. Kochs.** 2007. The intracellular sites of early replication and budding of SARS-coronavirus. *Virology* **361**:304-315.
36. **Ulasli, M., M. H. Verheije, C. A. de Haan, and F. Reggiori.** 2010. Qualitative and quantitative ultrastructural analysis of the membrane rearrangements induced by coronavirus. *Cell. Microbiol.* **12**:844-861.
37. **Gorbalenya, A. E., L. Enjuanes, J. Ziebuhr, and E. J. Snijder.** 2006. Nidovirales: evolving the largest RNA virus genome. *Virus Res.* **117**:17-37.

38. **Nga, P. T., C. Parquet Mdel, C. Lauber, M. Parida, T. Nabeshima, F. Yu, N. T. Thuy, S. Inoue, et al.** 2011. Discovery of the first insect nidovirus, a missing evolutionary link in the emergence of the largest RNA virus genomes. *PLoS Pathog.* **7**:e1002215.
39. **Sawicki, S. G., and D. L. Sawicki.** 1995. Coronaviruses use discontinuous extension for synthesis of subgenome-length negative strands. *Adv. Exp. Med. Biol.* **380**:499-506.
40. **Pasternak, A. O., W. J. Spaan, and E. J. Snijder.** 2006. Nidovirus transcription: how to make sense...? *J. Gen. Virol.* **87**:1403-1421.
41. **Snijder, E. J., S. Siddell, and A. E. Gorbalenya.** 2005. The order Nidovirales, p. 390–404. In B. W. Mahy and V. ter Meulen (ed.), *Topley and Wilson's Microbiology and Microbial Infections: Virology Volume*. Hodder Arnold, London.
42. **den Boon, J. A., E. J. Snijder, E. D. Chirside, A. A. de Vries, M. C. Horzinek, and W. J. Spaan.** 1991. Equine arteritis virus is not a togavirus but belongs to the coronaviruslike superfamily. *J. Virol.* **65**:2910-2920.
43. **Brierley, I., and F. J. Dos Ramos.** 2006. Programmed ribosomal frameshifting in HIV-1 and the SARS-CoV. *Virus Res.* **119**:29-42.
44. **Brierley, I., P. Digard, and S. C. Inglis.** 1989. Characterization of an efficient coronavirus ribosomal frameshifting signal: requirement for an RNA pseudoknot. *Cell* **57**:537-547.
45. **Van Hemert, M. J., and E. J. Snijder.** 2008. The Arterivirus Replicase. In S. Perlman, T. Gallagher, and E. J. Snijder (ed.), *Nidoviruses*. ASM Press.
46. **Ziebuhr, J.** 2006. The coronavirus replicase: insights into a sophisticated enzyme machinery. *Adv. Exp. Med. Biol.* **581**:3-11.
47. **Fang, Y., and E. J. Snijder.** 2010. The PRRSV replicase: exploring the multifunctionality of an intriguing set of nonstructural proteins. *Virus Res.* **154**:61-76.
48. **Lauber, C., J. Ziebuhr, S. Junglen, C. Drosten, F. Zirkel, P. T. Nga, K. Morita, E. J. Snijder, and A. E. Gorbalenya.** 2012. Mesoniviridae: a proposed new family in the order Nidovirales formed by a single species of mosquito-borne viruses. *Arch. Virol.* **157**:1623-1628.
49. **Ulferts, R., and J. Ziebuhr.** 2011. Nidovirus ribonucleases: Structures and functions in viral replication. *RNA Biol.* **8**:295-304.
50. **Denison, M. R., R. L. Graham, E. F. Donaldson, L. D. Eckerle, and R. S. Baric.** 2011. Coronaviruses: an RNA proofreading machine regulates replication fidelity and diversity. *RNA Biol.* **8**:270-279.
51. **Bouvet, M., I. Imbert, L. Subissi, L. Gluais, B. Canard, and E. Decroly.** 2012. RNA 3'-end mismatch excision by the severe acute respiratory syndrome coronavirus nonstructural protein nsp10/nsp14 exoribonuclease complex. *Proc. Natl. Acad. Sci. USA* **109**:9372-9377.
52. **van Hemert, M. J., A. H. de Wilde, A. E. Gorbalenya, and E. J. Snijder.** 2008. The *in vitro* RNA synthesizing activity of the isolated arterivirus replication/transcription complex is dependent on a host factor. *J. Biol. Chem.* **283**:16525-16536.
53. **van Hemert, M. J., S. H. van den Worm, K. Knoops, A. M. Mommaas, A. E. Gorbalenya, and E. J. Snijder.** 2008. SARS-coronavirus replication/transcription complexes are membrane-protected and need a host factor for activity *in vitro*. *PLoS Pathog.* **4**:e1000054.
54. **Prentice, E., W. G. Jerome, T. Yoshimori, N. Mizushima, and M. R. Denison.** 2004. Coronavirus replication complex formation utilizes components of cellular autophagy. *J. Biol. Chem.* **279**:10136-10141.
55. **Reggiori, F., I. Monastyrska, M. H. Verheije, T. Cali, M. Ulasli, S. Bianchi, R. Bernasconi, C. A. de Haan, and M. Molinari.** 2010. Coronaviruses Hijack the LC3-I-positive EDEMosomes, ER-derived vesicles exporting short-lived ERAD regulators, for replication. *Cell Host Microbe* **7**:500-508.

56. **Miller, S., and J. Krijnse-Locker.** 2008. Modification of intracellular membrane structures for virus replication. *Nat. Rev. Microbiol.* **6**:363-374.
57. **Krijnse-Locker, J., M. Ericsson, P. J. Rottier, and G. Griffiths.** 1994. Characterization of the budding compartment of mouse hepatitis virus: evidence that transport from the RER to the Golgi complex requires only one vesicular transport step. *J. Cell. Biol.* **124**:55-70.
58. **Wieringa, R., A. A. de Vries, J. van der Meulen, G. J. Godeke, J. J. Onderwater, H. van Tol, H. K. Koerten, A. M. Mommaas, et al.** 2004. Structural protein requirements in equine arteritis virus assembly. *J. Virol.* **78**:13019-13027.
59. **Griffiths, G., and P. Rottier.** 1992. Cell biology of viruses that assemble along the biosynthetic pathway. *Semin. Cell. Biol.* **3**:367-381.
60. **Nagy, P. D., and J. Pogany.** 2012. The dependence of viral RNA replication on co-opted host factors. *Nat. Rev. Microbiol.* **10**:137-149.
61. **Li, Z., and P. D. Nagy.** 2011. Diverse roles of host RNA binding proteins in RNA virus replication. *RNA Biol.* **8**:305-315.
62. **Ahlquist, P., A. O. Noueiry, W. M. Lee, D. B. Kushner, and B. T. Dye.** 2003. Host factors in positive-strand RNA virus genome replication. *J. Virol.* **77**:8181-8186.
63. **Moriishi, K., and Y. Matsuura.** 2007. Host factors involved in the replication of hepatitis C virus. *Rev. Med. Virol.* **17**:343-354.
64. **Watanabe, T., S. Watanabe, and Y. Kawaoka.** 2010. Cellular networks involved in the influenza virus life cycle. *Cell Host Microbe* **7**:427-439.
65. **Zhong, Y., Y. W. Tan, and D. X. Liu.** 2012. Recent progress in studies of arterivirus- and coronavirus-host interactions. *Viruses* **4**:980-1010.
66. **Walsh, D., and I. Mohr.** 2011. Viral subversion of the host protein synthesis machinery. *Nat. Rev. Microbiol.* **9**:860-875.
67. **Jackson, R. J., C. U. Hellen, and T. V. Pestova.** 2010. The mechanism of eukaryotic translation initiation and principles of its regulation. *Nat. Rev. Mol. Cell Biol.* **11**:113-127.
68. **Dauber, B., and T. Wolff.** 2009. Activation of the Antiviral Kinase PKR and Viral Countermeasures. *Viruses* **1**:523-544.
69. **Wang, X., Y. Liao, P. L. Yap, K. J. Png, J. P. Tam, and D. X. Liu.** 2009. Inhibition of protein kinase R activation and upregulation of GADD34 expression play a synergistic role in facilitating coronavirus replication by maintaining de novo protein synthesis in virus-infected cells. *J. Virol.* **83**:12462-12472.
70. **Cruz, J. L., I. Sola, M. Becares, B. Alberca, J. Plana, L. Enjuanes, and S. Zuniga.** 2011. Coronavirus gene 7 counteracts host defenses and modulates virus virulence. *PLoS Pathog.* **7**:e1002090.
71. **Xiao, H., L. H. Xu, Y. Yamada, and D. X. Liu.** 2008. Coronavirus spike protein inhibits host cell translation by interaction with eIF3f. *PLoS One* **3**:e1494.
72. **Lokugamage, K. G., K. Narayanan, C. Huang, and S. Makino.** 2012. SARS coronavirus nsp1 protein is a novel eukaryotic translation inhibitor that represses multiple steps of translation initiation. *J. Virol.*
73. **Kamitani, W., C. Huang, K. Narayanan, K. G. Lokugamage, and S. Makino.** 2009. A two-pronged strategy to suppress host protein synthesis by SARS coronavirus Nsp1 protein. *Nat. Struct. Mol. Biol.* **16**:1134-1140.
74. **Kamitani, W., K. Narayanan, C. Huang, K. Lokugamage, T. Ikegami, N. Ito, H. Kubo, and S. Makino.** 2006. Severe acute respiratory syndrome coronavirus nsp1 protein suppresses host gene expression by promoting host mRNA degradation. *Proc. Natl. Acad. Sci. USA* **103**:12885-12890.

75. **Mackenzie, J.** 2005. Wrapping things up about virus RNA replication. *Traffic* **6**:967-977.
76. **Welsch, S., S. Miller, I. Romero-Brey, A. Merz, C. K. Bleck, P. Walther, S. D. Fuller, C. Antony, et al.** 2009. Composition and three-dimensional architecture of the dengue virus replication and assembly sites. *Cell Host Microbe* **5**:365-375.
77. **Gillespie, L. K., A. Hoenen, G. Morgan, and J. M. Mackenzie.** 2010. The endoplasmic reticulum provides the membrane platform for biogenesis of the flavivirus replication complex. *J. Virol.* **84**:10438-10447.
78. **Kopeck, B. G., G. Perkins, D. J. Miller, M. H. Ellisman, and P. Ahlquist.** 2007. Three-dimensional analysis of a viral RNA replication complex reveals a virus-induced mini-organelle. *PLoS Biol.* **5**:e220.
79. **Spuul, P., G. Balistreri, L. Kaariainen, and T. Ahola.** 2010. Phosphatidylinositol 3-kinase-, actin-, and microtubule-dependent transport of Semliki Forest Virus replication complexes from the plasma membrane to modified lysosomes. *J. Virol.* **84**:7543-7557.
80. **Belov, G. A., V. Nair, B. T. Hansen, F. H. Hoyt, E. R. Fischer, and E. Ehrenfeld.** 2012. Complex dynamic development of poliovirus membranous replication complexes. *J. Virol.* **86**:302-312.
81. **Romero-Brey, I., A. Merz, A. Chiramel, J. Y. Lee, P. Chlanda, U. Haselman, R. Santarella-Mellig, A. Habermann, et al.** 2012. Three-dimensional architecture and biogenesis of membrane structures associated with hepatitis C virus replication. *PLoS Pathog.* **8**:e1003056.
82. **Norbury, C., and P. Nurse.** 1992. Animal cell cycles and their control. *Annu. Rev. Biochem.* **61**:441-470.
83. **Nigg, E. A.** 1995. Cyclin-dependent protein kinases: key regulators of the eukaryotic cell cycle. *BioEssays : news and reviews in molecular, cellular and developmental biology* **17**:471-480.
84. **Davy, C., and J. Doorbar.** 2007. G2/M cell cycle arrest in the life cycle of viruses. *Virology* **368**:219-226.
85. **Xu, L. H., M. Huang, S. G. Fang, and D. X. Liu.** 2011. Coronavirus infection induces DNA replication stress partly through interaction of its nonstructural protein 13 with the p125 subunit of DNA polymerase delta. *J. Biol. Chem.* **286**:39546-39559.
86. **Xu, L., S. Khadijah, S. Fang, L. Wang, F. P. Tay, and D. X. Liu.** 2010. The cellular RNA helicase DDX1 interacts with coronavirus nonstructural protein 14 and enhances viral replication. *J. Virol.* **84**:8571-8583.
87. **Bhardwaj, K., P. Liu, J. L. Leibowitz, and C. C. Kao.** 2012. The coronavirus endoribonuclease Nsp15 interacts with retinoblastoma tumor suppressor protein. *J. Virol.* **86**:4294-4304.
88. **Chen, C. J., and S. Makino.** 2004. Murine coronavirus replication induces cell cycle arrest in G0/G1 phase. *J. Virol.* **78**:5658-5669.
89. **Chen, C. J., K. Sugiyama, H. Kubo, C. Huang, and S. Makino.** 2004. Murine coronavirus non-structural protein p28 arrests cell cycle in G0/G1 phase. *J. Virol.* **78**:10410-10419.
90. **Jensen, S., and A. R. Thomsen.** 2012. Sensing of RNA viruses: a review of innate immune receptors involved in recognizing RNA virus invasion. *J. Virol.* **86**:2900-2910.
91. **Schoggins, J. W., and C. M. Rice.** 2011. Interferon-stimulated genes and their antiviral effector functions. *Current opinion in virology* **1**:519-525.
92. **Jiang, X., and Z. J. Chen.** 2012. The role of ubiquitylation in immune defence and pathogen evasion. *Nat. Rev. Immunol.* **12**:35-48.
93. **Versteeg, G. A., and A. Garcia-Sastre.** 2010. Viral tricks to grid-lock the type I interferon system. *Curr. Opin. Microbiol.* **13**:508-516.

94. **Barretto, N., D. Jukneliene, K. Ratia, Z. Chen, A. D. Mesecar, and S. C. Baker.** 2005. The papain-like protease of severe acute respiratory syndrome coronavirus has deubiquitinating activity. *J. Virol.* **79**:15189-15198.
95. **Zheng, D., G. Chen, B. Guo, G. Cheng, and H. Tang.** 2008. PLP2, a potent deubiquitinase from murine hepatitis virus, strongly inhibits cellular type I interferon production. *Cell Res.* **18**:1105-1113.
96. **Chen, Z., Y. Wang, K. Ratia, A. D. Mesecar, K. D. Wilkinson, and S. C. Baker.** 2007. Proteolytic processing and deubiquitinating activity of papain-like proteases of human coronavirus NL63. *J. Virol.* **81**:6007-6018.
97. **Lindner, H. A., N. Fotouhi-Ardakani, V. Lytvyn, P. Lachance, T. Sulea, and R. Menard.** 2005. The papain-like protease from the severe acute respiratory syndrome coronavirus is a deubiquitinating enzyme. *J. Virol.* **79**:15199-15208.
98. **Wojdyła, J. A., I. Manolaridis, P. B. van Kasteren, M. Kikkert, E. J. Snijder, A. E. Gorbalenya, and P. A. Tucker.** 2010. Papain-like protease 1 from transmissible gastroenteritis virus: crystal structure and enzymatic activity toward viral and cellular substrates. *J. Virol.* **84**:10063-10073.
99. **Clementz, M. A., Z. Chen, B. S. Banach, Y. Wang, L. Sun, K. Ratia, Y. M. Baez-Santos, J. Wang, et al.** 2010. Deubiquitinating and interferon antagonism activities of coronavirus papain-like proteases. *J. Virol.* **84**:4619-4629.
100. **Sun, Z., Z. Chen, S. R. Lawson, and Y. Fang.** 2010. The cysteine protease domain of porcine reproductive and respiratory syndrome virus nonstructural protein 2 possesses deubiquitinating and interferon antagonism functions. *J. Virol.* **84**:7832-7846.
101. **van Kasteren, P. B., C. Beugeling, D. K. Ninaber, N. Frias-Staheli, S. van Boheemen, A. Garcia-Sastre, E. J. Snijder, and M. Kikkert.** 2012. Arterivirus and nairovirus ovarian tumor domain-containing Deubiquitinases target activated RIG-I to control innate immune signaling. *J. Virol.* **86**:773-785.
102. **van Kasteren, P. B., B. A. Bailey-Elkin, T. W. James, D. K. Ninaber, C. Beugeling, M. Khajehpour, E. J. Snijder, B. L. Mark, and M. Kikkert.** 2013. Deubiquitinase function of arterivirus papain-like protease 2 suppresses the innate immune response in infected host cells. *Proc. Natl. Acad. Sci. USA* **110**:E838-847.
103. **Totura, A. L., and R. S. Baric.** 2012. SARS coronavirus pathogenesis: host innate immune responses and viral antagonism of interferon. *Current opinion in virology* **2**:264-275.
104. **Wathelet, M. G., M. Orr, M. B. Frieman, and R. S. Baric.** 2007. Severe acute respiratory syndrome coronavirus evades antiviral signaling: role of nsp1 and rational design of an attenuated strain. *J. Virol.* **81**:11620-11633.
105. **Frieman, M., B. Yount, M. Heise, S. A. Kopecky-Bromberg, P. Palese, and R. S. Baric.** 2007. Severe acute respiratory syndrome coronavirus ORF6 antagonizes STAT1 function by sequestering nuclear import factors on the rough endoplasmic reticulum/Golgi membrane. *J. Virol.* **81**:9812-9824.
106. **Kopecky-Bromberg, S. A., L. Martinez-Sobrido, M. Frieman, R. A. Baric, and P. Palese.** 2007. Severe acute respiratory syndrome coronavirus open reading frame (ORF) 3b, ORF 6, and nucleocapsid proteins function as interferon antagonists. *J. Virol.* **81**:548-557.
107. **Patel, D., Y. Nan, M. Shen, K. Ritthipichai, X. Zhu, and Y. J. Zhang.** 2010. Porcine reproductive and respiratory syndrome virus inhibits type I interferon signaling by blocking STAT1/STAT2 nuclear translocation. *J. Virol.* **84**:11045-11055.

108. **Wang, R., Y. Nan, Y. Yu, and Y. J. Zhang.** 2013. Porcine reproductive and respiratory syndrome virus Nsp1beta inhibits interferon-activated JAK/STAT signal transduction by inducing karyopherin-alpha1 degradation. *J. Virol.* **87**:5219-5228.
109. **Zhou, P., H. Li, H. Wang, L. F. Wang, and Z. Shi.** 2012. Bat severe acute respiratory syndrome-like coronavirus ORF3b homologues display different interferon antagonist activities. *J. Gen. Virol.* **93**:275-281.
110. **Frieman, M., K. Ratia, R. E. Johnston, A. D. Mesecar, and R. S. Baric.** 2009. Severe acute respiratory syndrome coronavirus papain-like protease ubiquitin-like domain and catalytic domain regulate antagonism of IRF3 and NF-kappaB signaling. *J. Virol.* **83**:6689-6705.
111. **Wang, G., G. Chen, D. Zheng, G. Cheng, and H. Tang.** 2011. PLP2 of mouse hepatitis virus A59 (MHV-A59) targets TBK1 to negatively regulate cellular type I interferon signaling pathway. *PLoS One* **6**:e17192.
112. **Siu, K. L., K. H. Kok, M. H. Ng, V. K. Poon, K. Y. Yuen, B. J. Zheng, and D. Y. Jin.** 2009. Severe acute respiratory syndrome coronavirus M protein inhibits type I interferon production by impeding the formation of TRAF3.TANK.TBK1/IKKepsilon complex. *J. Biol. Chem.* **284**:16202-16209.
113. **Devaraj, S. G., N. Wang, Z. Chen, M. Tseng, N. Barretto, R. Lin, C. J. Peters, C. T. Tseng, et al.** 2007. Regulation of IRF-3-dependent innate immunity by the papain-like protease domain of the severe acute respiratory syndrome coronavirus. *J. Biol. Chem.* **282**:32208-32221.
114. **Enjuanes, L., F. Almazan, I. Sola, S. Zuniga, E. Alvarez, J. Reguera, and C. Capiscol.** 2006. Biochemical aspects of coronavirus replication. *Adv. Exp. Med. Biol.* **581**:13-24.
115. **Spagnolo, J. F., and B. G. Hogue.** 2000. Host protein interactions with the 3' end of bovine coronavirus RNA and the requirement of the poly(A) tail for coronavirus defective genome replication. *J. Virol.* **74**:5053-5065.
116. **Galan, C., I. Sola, A. Nogales, B. Thomas, A. Akoulitchev, L. Enjuanes, and F. Almazan.** 2009. Host cell proteins interacting with the 3' end of TGEV coronavirus genome influence virus replication. *Virology* **391**:304-314.
117. **Wang, X., J. Bai, L. Zhang, X. Wang, Y. Li, and P. Jiang.** 2012. Poly(A)-binding protein interacts with the nucleocapsid protein of porcine reproductive and respiratory syndrome virus and participates in viral replication. *Antiviral Res.* **96**:315-323.
118. **Beura, L. K., P. X. Dinh, F. A. Osorio, and A. K. Pattnaik.** 2011. Cellular poly(c) binding proteins 1 and 2 interact with porcine reproductive and respiratory syndrome virus nonstructural protein 1beta and support viral replication. *J. Virol.* **85**:12939-12949.
119. **Wang, Y., and X. Zhang.** 1999. The nucleocapsid protein of coronavirus mouse hepatitis virus interacts with the cellular heterogeneous nuclear ribonucleoprotein A1 *in vitro* and *in vivo*. *Virology* **265**:96-109.
120. **Luo, H., Q. Chen, J. Chen, K. Chen, X. Shen, and H. Jiang.** 2005. The nucleocapsid protein of SARS coronavirus has a high binding affinity to the human cellular heterogeneous nuclear ribonucleoprotein A1. *FEBS Lett.* **579**:2623-2628.
121. **Li, H. P., X. Zhang, R. Duncan, L. Comai, and M. M. Lai.** 1997. Heterogeneous nuclear ribonucleoprotein A1 binds to the transcription-regulatory region of mouse hepatitis virus RNA. *Proc. Natl. Acad. Sci. USA* **94**:9544-9549.
122. **Huang, P., and M. M. Lai.** 2001. Heterogeneous nuclear ribonucleoprotein a1 binds to the 3'-untranslated region and mediates potential 5'-3'-end cross talks of mouse hepatitis virus RNA. *J. Virol.* **75**:5009-5017.

123. **Jourdan, S. S., F. Osorio, and J. A. Hiscox.** 2012. An interactome map of the nucleocapsid protein from a highly pathogenic North American porcine reproductive and respiratory syndrome virus strain generated using SILAC-based quantitative proteomics. *Proteomics* **12**:1015-1023.
124. **Tijms, M. A., and E. J. Snijder.** 2003. Equine arteritis virus non-structural protein 1, an essential factor for viral subgenomic mRNA synthesis, interacts with the cellular transcription co-factor p100. *J. Gen. Virol.* **84**:2317-2322.
125. **Kwak, H., M. W. Park, and S. Jeong.** 2011. Annexin A2 binds RNA and reduces the frameshifting efficiency of infectious bronchitis virus. *PLoS One* **6**:e24067.
126. **Nanda, S. K., and J. L. Leibowitz.** 2001. Mitochondrial aconitase binds to the 3' untranslated region of the mouse hepatitis virus genome. *J. Virol.* **75**:3352-3362.
127. **Tan, Y. W., W. Hong, and D. X. Liu.** 2012. Binding of the 5'-untranslated region of coronavirus RNA to zinc finger CCHC-type and RNA-binding motif 1 enhances viral replication and transcription. *Nucleic Acids Res.* **40**:5065-5077.
128. **Maines, T. R., M. Young, N. N. Dinh, and M. A. Brinton.** 2005. Two cellular proteins that interact with a stem loop in the simian hemorrhagic fever virus 3'(+)NCR RNA. *Virus Res.* **109**:109-124.
129. **Li, H. P., P. Huang, S. Park, and M. M. Lai.** 1999. Polypyrimidine tract-binding protein binds to the leader RNA of mouse hepatitis virus and serves as a regulator of viral transcription. *J. Virol.* **73**:772-777.
130. **Kellam, P.** 2006. Attacking pathogens through their hosts. *Genome Biol.* **7**:201.
131. **Schwegmann, A., and F. Brombacher.** 2008. Host-directed drug targeting of factors hijacked by pathogens. *Sci. Signal* **1**:re8.
132. **Yeh, K. M., T. S. Chiueh, L. K. Siu, J. C. Lin, P. K. Chan, M. Y. Peng, H. L. Wan, J. H. Chen, et al.** 2005. Experience of using convalescent plasma for severe acute respiratory syndrome among healthcare workers in a Taiwan hospital. *J. Antimicrob. Chemother.* **56**:919-922.
133. **Cheng, Y., R. Wong, Y. O. Soo, W. S. Wong, C. K. Lee, M. H. Ng, P. Chan, K. C. Wong, et al.** 2005. Use of convalescent plasma therapy in SARS patients in Hong Kong. *Eur. J. Clin. Microbiol. Infect. Dis.* **24**:44-46.
134. **Tong, T. R.** 2009. Therapies for coronaviruses. Part I of II – viral entry inhibitors. *Expert Opin. Ther. Pat.* **19**:357-367.
135. **van den Brink, E. N., J. Ter Meulen, F. Cox, M. A. Jongeneelen, A. Thijsse, M. Throsby, W. E. Marissen, P. M. Rood, et al.** 2005. Molecular and biological characterization of human monoclonal antibodies binding to the spike and nucleocapsid proteins of severe acute respiratory syndrome coronavirus. *J. Virol.* **79**:1635-1644.
136. **ter Meulen, J., A. B. Bakker, E. N. van den Brink, G. J. Weverling, B. E. Martina, B. L. Haagmans, T. Kuiken, J. de Kruif, et al.** 2004. Human monoclonal antibody as prophylaxis for SARS coronavirus infection in ferrets. *Lancet* **363**:2139-2141.
137. **ter Meulen, J., E. N. van den Brink, L. L. Poon, W. E. Marissen, C. S. Leung, F. Cox, C. Y. Cheung, A. Q. Bakker, et al.** 2006. Human monoclonal antibody combination against SARS coronavirus: synergy and coverage of escape mutants. *PLoS Med.* **3**:e237.
138. **Takano, T., Y. Katoh, T. Doki, and T. Hohdatsu.** 2013. Effect of chloroquine on feline infectious peritonitis virus infection *in vitro* and *in vivo*. *Antiviral Res.* **99**:100-107.
139. **Keyaerts, E., S. Li, L. Vijgen, E. Rysman, J. Verbeeck, M. Van Ranst, and P. Maes.** 2009. Antiviral activity of chloroquine against human coronavirus OC43 infection in newborn mice. *Antimicrob. Agents Chemother.* **53**:3416-3421.
140. **Krzystyniak, K., and J. M. Dupuy.** 1984. Entry of mouse hepatitis virus 3 into cells. *J. Gen. Virol.* **65 (Pt 1)**:227-231.

141. **Payne, H. R., J. Storz, and W. G. Henk.** 1990. Initial events in bovine coronavirus infection: analysis through immunogold probes and lysosomotropic inhibitors. *Arch. Virol.* **114**:175-189.
142. **Kreutz, L. C., and M. R. Ackermann.** 1996. Porcine reproductive and respiratory syndrome virus enters cells through a low pH-dependent endocytic pathway. *Virus Res.* **42**:137-147.
143. **Kono, M., K. Tatsumi, A. M. Imai, K. Saito, T. Kuriyama, and H. Shirasawa.** 2008. Inhibition of human coronavirus 229E infection in human epithelial lung cells (L132) by chloroquine: involvement of p38 MAPK and ERK. *Antiviral Res.* **77**:150-152.
144. **Keyaerts, E., L. Vijgen, P. Maes, J. Neyts, and M. Van Ranst.** 2004. In vitro inhibition of severe acute respiratory syndrome coronavirus by chloroquine. *Biochem. Biophys. Res. Commun.* **323**:264-268.
145. **Du, L., Y. He, Y. Zhou, S. Liu, B. J. Zheng, and S. Jiang.** 2009. The spike protein of SARS-CoV--a target for vaccine and therapeutic development. *Nat. Rev. Microbiol.* **7**:226-236.
146. **Fernandez-Montero, J. V., P. Barreiro, and V. Soriano.** 2009. HIV protease inhibitors: recent clinical trials and recommendations on use. *Expert Opin. Pharmacother.* **10**:1615-1629.
147. **Clark, V. C., J. A. Peter, and D. R. Nelson.** 2013. New therapeutic strategies in HCV: second-generation protease inhibitors. *Liver Int.* **33 Suppl 1**:80-84.
148. **Yang, H., W. Xie, X. Xue, K. Yang, J. Ma, W. Liang, Q. Zhao, Z. Zhou, et al.** 2005. Design of wide-spectrum inhibitors targeting coronavirus main proteases. *PLoS Biol.* **3**:e324.
149. **Ghosh, A. K., J. Takayama, K. V. Rao, K. Ratia, R. Chaudhuri, D. C. Mulhearn, H. Lee, D. B. Nichols, et al.** 2010. Severe acute respiratory syndrome coronavirus papain-like novel protease inhibitors: design, synthesis, protein-ligand X-ray structure and biological evaluation. *J. Med. Chem.* **53**:4968-4979.
150. **Hsu, J. T., C. J. Kuo, H. P. Hsieh, Y. C. Wang, K. K. Huang, C. P. Lin, P. F. Huang, X. Chen, and P. H. Liang.** 2004. Evaluation of metal-conjugated compounds as inhibitors of 3CL protease of SARS-CoV. *FEBS Lett.* **574**:116-120.
151. **Kuo, C. J., H. G. Liu, Y. K. Lo, C. M. Seong, K. I. Lee, Y. S. Jung, and P. H. Liang.** 2009. Individual and common inhibitors of coronavirus and picornavirus main proteases. *FEBS Lett.* **583**:549-555.
152. **Wu, C. Y., J. T. Jan, S. H. Ma, C. J. Kuo, H. F. Juan, Y. S. Cheng, H. H. Hsu, H. C. Huang, et al.** 2004. Small molecules targeting severe acute respiratory syndrome human coronavirus. *Proc. Natl. Acad. Sci. USA* **101**:10012-10017.
153. **Ratia, K., S. Pegan, J. Takayama, K. Sleeman, M. Coughlin, S. Baliji, R. Chaudhuri, W. Fu, et al.** 2008. A noncovalent class of papain-like protease/deubiquitinase inhibitors blocks SARS virus replication. *Proc. Natl. Acad. Sci. USA* **105**:16119-16124.
154. **Crotty, S., D. Maag, J. J. Arnold, W. Zhong, J. Y. Lau, Z. Hong, R. Andino, and C. E. Cameron.** 2000. The broad-spectrum antiviral ribonucleoside ribavirin is an RNA virus mutagen. *Nat. Med.* **6**:1375-1379.
155. **Morgenstern, B., M. Michaelis, P. C. Baer, H. W. Doerr, and J. Cinatl, Jr.** 2005. Ribavirin and interferon-beta synergistically inhibit SARS-associated coronavirus replication in animal and human cell lines. *Biochem. Biophys. Res. Commun.* **326**:905-908.
156. **Stroher, U., A. DiCaro, Y. Li, J. E. Strong, F. Aoki, F. Plummer, S. M. Jones, and H. Feldmann.** 2004. Severe acute respiratory syndrome-related coronavirus is inhibited by interferon- alpha. *J. Infect. Dis.* **189**:1164-1167.
157. **Saijo, M., S. Morikawa, S. Fukushi, T. Mizutani, H. Hasegawa, N. Nagata, N. Iwata, and I. Kurane.** 2005. Inhibitory effect of mizoribine and ribavirin on the replication of severe acute respiratory syndrome (SARS)-associated coronavirus. *Antiviral Res.* **66**:159-163.

158. **Knowles, S. R., E. J. Phillips, L. Dresser, and L. Matukas.** 2003. Common adverse events associated with the use of ribavirin for severe acute respiratory syndrome in Canada. *Clin. Infect. Dis.* **37**:1139-1142.
159. **te Velthuis, A. J., S. H. van den Worm, A. C. Sims, R. S. Baric, E. J. Snijder, and M. J. van Hemert.** 2010. Zn(2+) inhibits coronavirus and arterivirus RNA polymerase activity *in vitro* and zinc ionophores block the replication of these viruses in cell culture. *PLoS Pathog.* **6**:e1001176.
160. **Liu, K., X. Feng, Z. Ma, C. Luo, B. Zhou, R. Cao, L. Huang, D. Miao, et al.** 2012. Antiviral activity of phage display selected peptides against Porcine reproductive and respiratory syndrome virus *in vitro*. *Virology* **432**:73-80.
161. **Tanner, J. A., B. J. Zheng, J. Zhou, R. M. Watt, J. Q. Jiang, K. L. Wong, Y. P. Lin, L. Y. Lu, et al.** 2005. The adamantane-derived bananins are potent inhibitors of the helicase activities and replication of SARS coronavirus. *Chem. Biol.* **12**:303-311.
162. **Yang, N., J. A. Tanner, Z. Wang, J. D. Huang, B. J. Zheng, N. Zhu, and H. Sun.** 2007. Inhibition of SARS coronavirus helicase by bismuth complexes. *Chem. Commun. (Camb)*:4413-4415.
163. **Yang, N., J. A. Tanner, B. J. Zheng, R. M. Watt, M. L. He, L. Y. Lu, J. Q. Jiang, K. T. Shum, et al.** 2007. Bismuth complexes inhibit the SARS coronavirus. *Angew. Chem. Int. Ed. Engl.* **46**:6464-6468.
164. **Yu, M. S., J. Lee, J. M. Lee, Y. Kim, Y. W. Chin, J. G. Jee, Y. S. Keum, and Y. J. Jeong.** 2012. Identification of myricetin and scutellarein as novel chemical inhibitors of the SARS coronavirus helicase, nsP13. *Bioorg. Med. Chem. Lett.* **22**:4049-4054.
165. **Kim, M. K., M. S. Yu, H. R. Park, K. B. Kim, C. Lee, S. Y. Cho, J. Kang, H. Yoon, et al.** 2011. 2,6-Bis-arylmethoxy-5-hydroxychromones with antiviral activity against both hepatitis C virus (HCV) and SARS-associated coronavirus (SCV). *Eur. J. Med. Chem.* **46**:5698-5704.
166. **Bouvet, M., C. Debarnot, I. Imbert, B. Selisko, E. J. Snijder, B. Canard, and E. Decroly.** 2010. In vitro reconstitution of SARS-coronavirus mRNA cap methylation. *PLoS Pathog.* **6**:e1000863.
167. **He, R., A. Adonov, M. Traykova-Adonova, J. Cao, T. Cutts, E. Grudesky, Y. Deschambaul, J. Berry, et al.** 2004. Potent and selective inhibition of SARS coronavirus replication by aurintricarboxylic acid. *Biochem. Biophys. Res. Commun.* **320**:1199-1203.
168. **Ke, M., Y. Chen, A. Wu, Y. Sun, C. Su, H. Wu, X. Jin, J. Tao, et al.** 2012. Short peptides derived from the interaction domain of SARS coronavirus nonstructural protein nsp10 can suppress the 2'-O-methyltransferase activity of nsp10/nsp16 complex. *Virus Res.* **167**:322-328.
169. **Wilson, L., P. Gage, and G. Ewart.** 2006. Hexamethylene amiloride blocks E protein ion channels and inhibits coronavirus replication. *Virology* **353**:294-306.
170. **Neuman, B. W., D. A. Stein, A. D. Kroeker, M. J. Churchill, A. M. Kim, P. Kuhn, P. Dawson, H. M. Moulton, et al.** 2005. Inhibition, escape, and attenuated growth of severe acute respiratory syndrome coronavirus treated with antisense morpholino oligomers. *J. Virol.* **79**:9665-9676.
171. **Burrer, R., B. W. Neuman, J. P. Ting, D. A. Stein, H. M. Moulton, P. L. Iversen, P. Kuhn, and M. J. Buchmeier.** 2007. Antiviral effects of antisense morpholino oligomers in murine coronavirus infection models. *J. Virol.* **81**:5637-5648.
172. **Ahn, D. G., W. Lee, J. K. Choi, S. J. Kim, E. P. Plant, F. Almazan, D. R. Taylor, L. Enjuanes, and J. W. Oh.** 2011. Interference of ribosomal frameshifting by antisense peptide nucleic acids suppresses SARS coronavirus replication. *Antiviral Res.* **91**:1-10.
173. **van den Born, E., D. A. Stein, P. L. Iversen, and E. J. Snijder.** 2005. Antiviral activity of morpholino oligomers designed to block various aspects of Equine arteritis virus amplification in cell culture. *J. Gen. Virol.* **86**:3081-3090.

174. **Zhang, Y. J., D. A. Stein, S. M. Fan, K. Y. Wang, A. D. Kroeker, X. J. Meng, P. L. Iversen, and D. O. Matson.** 2006. Suppression of porcine reproductive and respiratory syndrome virus replication by morpholino antisense oligomers. *Vet. Microbiol.* **117**:117-129.
175. **Patel, D., T. Opriessnig, D. A. Stein, P. G. Halbur, X. J. Meng, P. L. Iversen, and Y. J. Zhang.** 2008. Peptide-conjugated morpholino oligomers inhibit porcine reproductive and respiratory syndrome virus replication. *Antiviral Res.* **77**:95-107.
176. **Han, X., S. Fan, D. Patel, and Y. J. Zhang.** 2009. Enhanced inhibition of porcine reproductive and respiratory syndrome virus replication by combination of morpholino oligomers. *Antiviral Res.* **82**:59-66.
177. **Opriessnig, T., D. Patel, R. Wang, P. G. Halbur, X. J. Meng, D. A. Stein, and Y. J. Zhang.** 2011. Inhibition of porcine reproductive and respiratory syndrome virus infection in piglets by a peptide-conjugated morpholino oligomer. *Antiviral Res.* **91**:36-42.
178. **He, Y. X., R. H. Hua, Y. J. Zhou, H. J. Qiu, and G. Z. Tong.** 2007. Interference of porcine reproductive and respiratory syndrome virus replication on MARC-145 cells using DNA-based short interfering RNAs. *Antiviral Res.* **74**:83-91.
179. **Li, G., P. Jiang, Y. Li, X. Wang, J. Huang, J. Bai, J. Cao, B. Wu, et al.** 2009. Inhibition of porcine reproductive and respiratory syndrome virus replication by adenovirus-mediated RNA interference both in porcine alveolar macrophages and swine. *Antiviral Res.* **82**:157-165.
180. **Heinrich, A., D. Riethmuller, M. Gloger, G. F. Schusser, M. Giese, and S. Ulbert.** 2009. RNA interference protects horse cells *in vitro* from infection with Equine Arteritis Virus. *Antiviral Res.* **81**:209-216.
181. **Zhang, Y., T. Li, L. Fu, C. Yu, Y. Li, X. Xu, Y. Wang, H. Ning, et al.** 2004. Silencing SARS-CoV Spike protein expression in cultured cells by RNA interference. *FEBS Lett.* **560**:141-146.
182. **Wu, C. J., H. W. Huang, C. Y. Liu, C. F. Hong, and Y. L. Chan.** 2005. Inhibition of SARS-CoV replication by siRNA. *Antiviral Res.* **65**:45-48.
183. **DeVincenzo, J. P.** 2012. The promise, pitfalls and progress of RNA-interference-based antiviral therapy for respiratory viruses. *Antivir. Ther.* **17**:213-225.
184. **Burnett, J. C., J. J. Rossi, and K. Tiemann.** 2011. Current progress of siRNA/shRNA therapeutics in clinical trials. *Biotechnol. J.* **6**:1130-1146.
185. **Shi, Y., D. H. Yang, J. Xiong, J. Jia, B. Huang, and Y. X. Jin.** 2005. Inhibition of genes expression of SARS coronavirus by synthetic small interfering RNAs. *Cell Res.* **15**:193-200.
186. **Li, B. J., Q. Tang, D. Cheng, C. Qin, F. Y. Xie, Q. Wei, J. Xu, Y. Liu, et al.** 2005. Using siRNA in prophylactic and therapeutic regimens against SARS coronavirus in Rhesus macaque. *Nat. Med.* **11**:944-951.
187. **Stockman, L. J., R. Bellamy, and P. Garner.** 2006. SARS: systematic review of treatment effects. *PLoS Med.* **3**:e343.
188. **Garlinghouse, L. E., Jr., A. L. Smith, and T. Holford.** 1984. The biological relationship of mouse hepatitis virus (MHV) strains and interferon: *in vitro* induction and sensitivities. *Arch. Virol.* **82**:19-29.
189. **Taguchi, F., and S. G. Siddell.** 1985. Difference in sensitivity to interferon among mouse hepatitis viruses with high and low virulence for mice. *Virology* **147**:41-48.
190. **Haagmans, B. L., T. Kuiken, B. E. Martina, R. A. Fouchier, G. F. Rimmelzwaan, G. van Amerongen, D. van Riel, T. de Jong, et al.** 2004. Pegylated interferon-alpha protects type 1 pneumocytes against SARS coronavirus infection in macaques. *Nat. Med.* **10**:290-293.
191. **Paragas, J., L. M. Blatt, C. Hartmann, J. W. Huggins, and T. P. Endy.** 2005. Interferon alfacon1 is an inhibitor of SARS-corona virus in cell-based models. *Antiviral Res.* **66**:99-102.

192. **Zheng, B., M. L. He, K. L. Wong, C. T. Lum, L. L. Poon, Y. Peng, Y. Guan, M. C. Lin, and H. F. Kung.** 2004. Potent inhibition of SARS-associated coronavirus (SCOV) infection and replication by type I interferons (IFN-alpha/beta) but not by type II interferon (IFN-gamma). *J. Interferon Cytokine Res.* **24**:388-390.
193. **Dusheiko, G.** 1997. Side effects of alpha interferon in chronic hepatitis C. *Hepatology* **26**:1125-1215.
194. **Mitsuki, Y. Y., K. Ohnishi, H. Takagi, M. Oshima, T. Yamamoto, F. Mizukoshi, K. Terahara, K. Kobayashi, et al.** 2008. A single amino acid substitution in the S1 and S2 Spike protein domains determines the neutralization escape phenotype of SARS-CoV. *Microbes Infect.* **10**:908-915.
195. **Salonen, A., T. Ahola, and L. Kaariainen.** 2005. Viral RNA replication in association with cellular membranes. *Curr. Top. Microbiol. Immunol.* **285**:139-173.
196. **Sawicki, S. G., D. L. Sawicki, and S. G. Siddell.** 2007. A contemporary view of coronavirus transcription. *J. Virol.* **81**:20-29.
197. **Ng, L. F., and D. X. Liu.** 2002. Membrane association and dimerization of a cysteine-rich, 16-kilodalton polypeptide released from the C-terminal region of the coronavirus infectious bronchitis virus 1a polyprotein. *J. Virol.* **76**:6257-6267.
198. **Harcourt, B. H., D. Jukneliene, A. Kanjanahaluethai, J. Bechill, K. M. Severson, C. M. Smith, P. A. Rota, and S. C. Baker.** 2004. Identification of severe acute respiratory syndrome coronavirus replicase products and characterization of papain-like protease activity. *J. Virol.* **78**:13600-13612.
199. **Shi, S. T., J. J. Schiller, A. Kanjanahaluethai, S. C. Baker, J. W. Oh, and M. M. Lai.** 1999. Colocalization and membrane association of murine hepatitis virus gene 1 products and De novo-synthesized viral RNA in infected cells. *J. Virol.* **73**:5957-5969.
200. **Denison, M. R., W. J. Spaan, Y. van der Meer, C. A. Gibson, A. C. Sims, E. Prentice, and X. T. Lu.** 1999. The putative helicase of the coronavirus mouse hepatitis virus is processed from the replicase gene polyprotein and localizes in complexes that are active in viral RNA synthesis. *J. Virol.* **73**:6862-6871.
201. **Pedersen, K. W., M. Y. van der, N. Roos, and E. J. Snijder.** 1999. Open reading frame 1a-encoded subunits of the arterivirus replicase induce endoplasmic reticulum-derived double-membrane vesicles which carry the viral replication complex. *J. Virol.* **73**:2016-2026.
202. **van Dinten, L. C., A. L. Wassenaar, A. E. Gorbalenya, W. J. Spaan, and E. J. Snijder.** 1996. Processing of the equine arteritis virus replicase ORF1b protein: identification of cleavage products containing the putative viral polymerase and helicase domains. *J. Virol.* **70**:6625-6633.
203. **Bi, W., J. D. Pinon, S. Hughes, P. J. Bonilla, K. V. Holmes, S. R. Weiss, and J. L. Leibowitz.** 1998. Localization of mouse hepatitis virus open reading frame 1A derived proteins. *J. Neurovirol.* **4**:594-605.
204. **Bost, A. G., R. H. Carnahan, X. T. Lu, and M. R. Denison.** 2000. Four proteins processed from the replicase gene polyprotein of mouse hepatitis virus colocalize in the cell periphery and adjacent to sites of virion assembly. *J. Virol.* **74**:3379-3387.
205. **Bost, A. G., E. Prentice, and M. R. Denison.** 2001. Mouse hepatitis virus replicase protein complexes are translocated to sites of M protein accumulation in the ERGIC at late times of infection. *Virology* **285**:21-29.
206. **Ivanov, K. A., V. Thiel, J. C. Dobbe, Y. van der Meer, E. J. Snijder, and J. Ziebuhr.** 2004. Multiple enzymatic activities associated with severe acute respiratory syndrome coronavirus helicase. *J. Virol.* **78**:5619-5632.

207. **Prentice, E., J. McAuliffe, X. Lu, K. Subbarao, and M. R. Denison.** 2004. Identification and characterization of severe acute respiratory syndrome coronavirus replicase proteins. *J. Virol.* **78**:9977-9986.
208. **Snijder, E. J., M. Y. van der, J. Zevenhoven-Dobbe, J. J. Onderwater, M. J. van der, H. K. Koerten, and A. M. Mommaas.** 2006. Ultrastructure and origin of membrane vesicles associated with the severe acute respiratory syndrome coronavirus replication complex. *J. Virol.* **80**:5927-5940.
209. **Pol, J. M., F. Wagenaar, and J. E. Reus.** 1997. Comparative morphogenesis of three PRRS virus strains. *Vet. Microbiol.* **55**:203-208.
210. **Wood, O., N. Tauraso, and H. Liebhaber.** 1970. Electron microscopic study of tissue cultures infected with simian haemorrhagic fever virus. *J. Gen. Virol.* **7**:129-136.
211. **Goldsmith, C. S., K. M. Tatti, T. G. Ksiazek, P. E. Rollin, J. A. Comer, W. W. Lee, P. A. Rota, B. Bankamp, et al.** 2004. Ultrastructural characterization of SARS coronavirus. *Emerg. Infect. Dis.* **10**:320-326.
212. **Ng, M. L., S. H. Tan, E. E. See, E. E. Ooi, and A. E. Ling.** 2003. Proliferative growth of SARS coronavirus in Vero E6 cells. *J. Gen. Virol.* **84**:3291-3303.
213. **Snijder, E. J., and J. J. Meulenberg.** 1998. The molecular biology of arteriviruses. *J. Gen. Virol.* **79** (Pt 5):961-979.
214. **Van Aken, D., J. Zevenhoven-Dobbe, A. E. Gorbalenya, and E. J. Snijder.** 2006. Proteolytic maturation of replicase polyprotein pp1a by the nsp4 main proteinase is essential for equine arteritis virus replication and includes internal cleavage of nsp7. *J. Gen. Virol.* **87**:3473-3482.
215. **Beerens, N., B. Selisko, S. Ricagno, I. Imbert, L. van der Zanden, E. J. Snijder, and B. Canard.** 2007. De novo initiation of RNA synthesis by the arterivirus RNA-dependent RNA polymerase. *J. Virol.*
216. **Seybert, A., L. C. van Dinten, E. J. Snijder, and J. Ziebuhr.** 2000. Biochemical characterization of the equine arteritis virus helicase suggests a close functional relationship between arterivirus and coronavirus helicases. *J. Virol.* **74**:9586-9593.
217. **Snijder, E. J., H. van Tol, N. Roos, and K. W. Pedersen.** 2001. Non-structural proteins 2 and 3 interact to modify host cell membranes during the formation of the arterivirus replication complex. *J. Gen. Virol.* **82**:985-994.
218. **Franklin, R. M.** 1967. Replication of bacteriophage ribonucleic acid: some physical properties of single-stranded, double-stranded, and branched viral ribonucleic acid. *J. Virol.* **1**:64-75.
219. **Sawicki, S. G., and D. L. Sawicki.** 1990. Coronavirus transcription: subgenomic mouse hepatitis virus replicative intermediates function in RNA synthesis. *J. Virol.* **64**:1050-1056.
220. **de Vries, A. A., E. D. Chirnside, M. C. Horzinek, and P. J. Rottier.** 1992. Structural proteins of equine arteritis virus. *J. Virol.* **66**:6294-6303.
221. **Igarashi, A.** 1978. Isolation of a Singh's *Aedes albopictus* cell clone sensitive to Dengue and Chikungunya viruses. *J. Gen. Virol.* **40**:531-544.
222. **Snijder, E. J., A. L. Wassenaar, and W. J. Spaan.** 1994. Proteolytic processing of the replicase ORF1a protein of equine arteritis virus. *J. Virol.* **68**:5755-5764.
223. **van Dinten, L. C., S. Rensen, A. E. Gorbalenya, and E. J. Snijder.** 1999. Proteolytic processing of the open reading frame 1b-encoded part of arterivirus replicase is mediated by nsp4 serine protease and is essential for virus replication. *J. Virol.* **73**:2027-2037.
224. **van Marle, G., L. C. van Dinten, W. J. Spaan, W. Luytjes, and E. J. Snijder.** 1999. Characterization of an equine arteritis virus replicase mutant defective in subgenomic mRNA synthesis. *J. Virol.* **73**:5274-5281.

225. **van Marle, G., J. C. Dobbe, A. P. Gultyaev, W. Luytjes, W. J. Spaan, and E. J. Snijder.** 1999. Arterivirus discontinuous mRNA transcription is guided by base pairing between sense and antisense transcription-regulating sequences. *Proc. Natl. Acad. Sci. USA* **96**:12056-12061.
226. **Chu, P. W., and E. G. Westaway.** 1985. Replication strategy of Kunjin virus: evidence for recycling role of replicative form RNA as template in semiconservative and asymmetric replication. *Virology* **140**:68-79.
227. **Grun, J. B., and M. A. Brinton.** 1986. Characterization of West Nile virus RNA-dependent RNA polymerase and cellular terminal adenylyl and uridylyl transferases in cell-free extracts. *J. Virol.* **60**:1113-1124.
228. **Barton, D. J., S. G. Sawicki, and D. L. Sawicki.** 1991. Solubilization and immunoprecipitation of alphavirus replication complexes. *J. Virol.* **65**:1496-1506.
229. **Uchil, P. D., and V. Satchidanandam.** 2003. Characterization of RNA synthesis, replication mechanism, and *in vitro* RNA-dependent RNA polymerase activity of Japanese encephalitis virus. *Virology* **307**:358-371.
230. **Hardy, S. F., T. L. German, L. S. Loesch-Fries, and T. C. Hall.** 1979. Highly active template-specific RNA-dependent RNA polymerase from barley leaves infected with brome mosaic virus. *Proc. Natl. Acad. Sci. USA* **76**:4956-4960.
231. **Snijder, E. J., A. L. Wassenaar, L. C. van Dinten, W. J. Spaan, and A. E. Gorbalenya.** 1996. The arterivirus nsp4 protease is the prototype of a novel group of chymotrypsin-like enzymes, the 3C-like serine proteases. *J. Biol. Chem.* **271**:4864-4871.
232. **Wassenaar, A. L., W. J. Spaan, A. E. Gorbalenya, and E. J. Snijder.** 1997. Alternative proteolytic processing of the arterivirus replicase ORF1a polyprotein: evidence that NSP2 acts as a cofactor for the NSP4 serine protease. *J. Virol.* **71**:9313-9322.
233. **Snijder, E. J., A. L. Wassenaar, and W. J. Spaan.** 1992. The 5' end of the equine arteritis virus replicase gene encodes a papainlike cysteine protease. *J. Virol.* **66**:7040-7048.
234. **Tijms, M. A., D. D. Nedialkova, J. C. Zevenhoven-Dobbe, A. E. Gorbalenya, and E. J. Snijder.** 2007. Arterivirus subgenomic mRNA synthesis and virion biogenesis depend on the multifunctional nsp1 autoprotease. *J. Virol.*
235. **Tijms, M. A., L. C. van Dinten, A. E. Gorbalenya, and E. J. Snijder.** 2001. A zinc finger-containing papain-like protease couples subgenomic mRNA synthesis to genome translation in a positive-stranded RNA virus. *Proc. Natl. Acad. Sci. USA* **98**:1889-1894.
236. **Brayton, P. R., M. M. Lai, C. D. Patton, and S. A. Stohlman.** 1982. Characterization of two RNA polymerase activities induced by mouse hepatitis virus. *J. Virol.* **42**:847-853.
237. **Brayton, P. R., S. A. Stohlman, and M. M. Lai.** 1984. Further characterization of mouse hepatitis virus RNA-dependent RNA polymerases. *Virology* **133**:197-201.
238. **Mahy, B. W., S. Siddell, H. Wege, and V. ter Meulen.** 1983. RNA-dependent RNA polymerase activity in murine coronavirus-infected cells. *J. Gen. Virol.* **64** (Pt 1):103-111.
239. **Compton, S. R., D. B. Rogers, K. V. Holmes, D. Fertsch, J. Remenick, and J. J. McGowan.** 1987. *In vitro* replication of mouse hepatitis virus strain A59. *J. Virol.* **61**:1814-1820.
240. **Dennis, D. E., and D. A. Brian.** 1982. RNA-dependent RNA polymerase activity in coronavirus-infected cells. *J. Virol.* **42**:153-164.
241. **Sawicki, S. G., and D. L. Sawicki.** 1986. Coronavirus minus-strand RNA synthesis and effect of cycloheximide on coronavirus RNA synthesis. *J. Virol.* **57**:328-334.
242. **Barton, D. J., and J. B. Flanagan.** 1993. Coupled translation and replication of poliovirus RNA *in vitro*: synthesis of functional 3D polymerase and infectious virus. *J. Virol.* **67**:822-831.

243. **Ehrenfeld, E., and D. Brown.** 1981. Stability of poliovirus RNA in cell-free translation systems utilizing two initiation sites. *J. Biol. Chem.* **256**:2656-2661.
244. **Chu, P. W., and E. G. Westaway.** 1987. Characterization of Kunjin virus RNA-dependent RNA polymerase: reinitiation of synthesis *in vitro*. *Virology* **157**:330-337.
245. **Tomassini, J. E., E. Boots, L. Gan, P. Graham, V. Munshi, B. Wolanski, J. F. Fay, K. Getty, and R. LaFemina.** 2003. An *in vitro* Flaviviridae replicase system capable of authentic RNA replication. *Virology* **313**:274-285.
246. **Sreevalsan, T., and F. H. Yin.** 1969. Sindbis virus-induced viral ribonucleic acid polymerase. *J. Virol.* **3**:599-604.
247. **Polatnick, J., and R. B. Arlinghaus.** 1967. Foot-and-mouth disease virus-induced ribonucleic acid polymerase in baby hamster kidney cells. *Virology* **31**:601-608.
248. **Rosenberg, H., B. Diskin, L. Oron, and A. Traub.** 1972. Isolation and subunit structure of polycytidylate-dependent RNA polymerase of encephalomyocarditis virus. *Proc. Natl. Acad. Sci. USA* **69**:3815-3819.
249. **Quadt, R., and E. M. Jaspars.** 1990. Purification and characterization of brome mosaic virus RNA-dependent RNA polymerase. *Virology* **178**:189-194.
250. **Baltimore, D., and R. M. Franklin.** 1963. A New Ribonucleic Acid Polymerase Appearing after Mengovirus Infection of L-Cells. *J. Biol. Chem.* **238**:3395-3400.
251. **Svitkin, Y. V., and N. Sonenberg.** 2003. Cell-free synthesis of encephalomyocarditis virus. *J. Virol.* **77**:6551-6555.
252. **Yin, F. H., and E. Knight, Jr.** 1972. *In vivo* and *in vitro* synthesis of human rhinovirus type 2 ribonucleic acid. *J. Virol.* **10**:93-98.
253. **Warrilow, D., W. B. Lott, S. Greive, and E. J. Gowans.** 2000. Properties of the bovine viral diarrhoea virus replicase in extracts of infected MDBK cells. *Arch. Virol.* **145**:2163-2171.
254. **Lai, V. C., S. Dempsey, J. Y. Lau, Z. Hong, and W. Zhong.** 2003. *In vitro* RNA replication directed by replicase complexes isolated from the subgenomic replicon cells of hepatitis C virus. *J. Virol.* **77**:2295-2300.
255. **Hardy, R. W., J. Marcotrigiano, K. J. Blight, J. E. Majors, and C. M. Rice.** 2003. Hepatitis C virus RNA synthesis in a cell-free system isolated from replicon-containing hepatoma cells. *J. Virol.* **77**:2029-2037.
256. **Takegami, T., and S. Hotta.** 1989. *In vitro* synthesis of Japanese encephalitis virus (JEV) RNA: membrane and nuclear fractions of JEV-infected cells possess high levels of virus-specific RNA polymerase activity. *Virus Res.* **13**:337-350.
257. **Qureshi, A. A., and D. W. Trent.** 1972. Saint Louis encephalitis viral ribonucleic acid replication complex. *J. Virol.* **9**:565-573.
258. **Li, M. L., Y. H. Lin, and V. Stollar.** 2005. A cell-free system for the synthesis of Sindbis virus subgenomic RNA: importance of the concentration of the initiating NTP. *Virology* **341**:24-33.
259. **Baltimore, D., H. J. Eggers, R. M. Franklin, and I. Tamm.** 1963. Poliovirus-induced RNA polymerase and the effects of virus-specific inhibitors on its production. *Proc. Natl. Acad. Sci. USA* **49**:843-849.
260. **Ali, N., K. D. Tardif, and A. Siddiqui.** 2002. Cell-free replication of the hepatitis C virus subgenomic replicon. *J. Virol.* **76**:12001-12007.
261. **Sun, J. H., S. Adkins, G. Faurote, and C. C. Kao.** 1996. Initiation of (-)-strand RNA synthesis catalyzed by the BMV RNA-dependent RNA polymerase: synthesis of oligonucleotides. *Virology* **226**:1-12.

262. **Molenkamp, R., B. C. Rozier, S. Greve, W. J. Spaan, and E. J. Snijder.** 2000. Isolation and characterization of an arterivirus defective interfering RNA genome. *J. Virol.* **74**:3156-3165.
263. **Egger, D., N. Teterina, E. Ehrenfeld, and K. Bienz.** 2000. Formation of the poliovirus replication complex requires coupled viral translation, vesicle production, and viral RNA synthesis. *J. Virol.* **74**:6570-6580.
264. **Barton, D. J., E. P. Black, and J. B. Flanagan.** 1995. Complete replication of poliovirus *in vitro*: preinitiation RNA replication complexes require soluble cellular factors for the synthesis of VPg-linked RNA. *J. Virol.* **69**:5516-5527.
265. **Shi, S. T., K. J. Lee, H. Aizaki, S. B. Hwang, and M. M. Lai.** 2003. Hepatitis C virus RNA replication occurs on a detergent-resistant membrane that cofractionates with caveolin-2. *J. Virol.* **77**:4160-4168.
266. **Westaway, E. G., A. A. Khromykh, and J. M. Mackenzie.** 1999. Nascent flavivirus RNA colocalized in situ with double-stranded RNA in stable replication complexes. *Virology* **258**:108-117.
267. **Arlinghaus, R. B., and J. Polatnick.** 1969. In vitro products of a membrane-free foot-and-mouth disease virus ribonucleic acid polymerase. *Virology* **37**:252-261.
268. **Etchison, D., and E. Ehrenfeld.** 1981. Comparison of replication complexes synthesizing poliovirus RNA. *Virology* **111**:33-46.
269. **Ehrenfeld, E., J. V. Maizel, and D. F. Summers.** 1970. Soluble RNA polymerase complex from poliovirus-infected HeLa cells. *Virology* **40**:840-846.
270. **Molenkamp, R., H. van Tol, B. C. Rozier, M. Y. van der, W. J. Spaan, and E. J. Snijder.** 2000. The arterivirus replicase is the only viral protein required for genome replication and subgenomic mRNA transcription. *J. Gen. Virol.* **81**:2491-2496.
271. **Bose, S., M. Mathur, P. Bates, N. Joshi, and A. K. Banerjee.** 2003. Requirement for cyclophilin A for the replication of vesicular stomatitis virus New Jersey serotype. *J. Gen. Virol.* **84**:1687-1699.
272. **Briggs, C. J., D. E. Ott, L. V. Coren, S. Oroszlan, and J. Tozser.** 1999. Comparison of the effect of FK506 and cyclosporin A on virus production in H9 cells chronically and newly infected by HIV-1. *Arch. Virol.* **144**:2151-2160.
273. **Kambara, H., H. Tani, Y. Mori, T. Abe, H. Katoh, T. Fukuhara, S. Taguwa, K. Moriishi, and Y. Matsuura.** 2011. Involvement of cyclophilin B in the replication of Japanese encephalitis virus. *Virology* **412**:211-219.
274. **Nakagawa, M., N. Sakamoto, N. Enomoto, Y. Tanabe, N. Kanazawa, T. Koyama, M. Kurosaki, S. Maekawa, et al.** 2004. Specific inhibition of hepatitis C virus replication by cyclosporin A. *Biochem. Biophys. Res. Commun.* **313**:42-47.
275. **Qing, M., F. Yang, B. Zhang, G. Zou, J. M. Robida, Z. Yuan, H. Tang, and P. Y. Shi.** 2009. Cyclosporine inhibits flavivirus replication through blocking the interaction between host cyclophilins and viral NS5 protein. *Antimicrob. Agents Chemother.* **53**:3226-3235.
276. **de Wilde, A. H., J. C. Zevenhoven-Dobbe, Y. van der Meer, V. Thiel, K. Narayanan, S. Makino, E. J. Snijder, and M. J. van Hemert.** 2011. Cyclosporin A inhibits the replication of diverse coronaviruses. *J. Gen. Virol.* **92**:2542-2548.
277. **Pfefferle, S., J. Schopf, M. Kogl, C. C. Friedel, M. A. Muller, J. Carbajo-Lozoya, T. Stellberger, E. von Dall'armi, et al.** 2011. The SARS-Coronavirus-Host Interactome: Identification of Cyclophilins as Target for Pan-Coronavirus Inhibitors. *PLoS Pathog.* **7**:e1002331.
278. **Tanaka, Y., Y. Sato, S. Osawa, M. Inoue, S. Tanaka, and T. Sasaki.** 2012. Suppression of feline coronavirus replication *in vitro* by cyclosporin A. *Vet. Res.* **43**:41.

279. **Davis, T. L., J. R. Walker, V. Campagna-Slater, P. J. Finerty, R. Paramanathan, G. Bernstein, F. MacKenzie, W. Tempel, et al.** 2010. Structural and biochemical characterization of the human cyclophilin family of peptidyl-prolyl isomerases. *PLoS Biol.* **8**:e1000439.
280. **Barik, S.** 2006. Immunophilins: for the love of proteins. *Cell. Mol. Life Sci.* **63**:2889-2900.
281. **Nagy, P. D., R. Y. Wang, J. Pogany, A. Hafren, and K. Makinen.** 2011. Emerging picture of host chaperone and cyclophilin roles in RNA virus replication. *Virology* **411**:374-382.
282. **Tedesco, D., and L. Haragsim.** 2012. Cyclosporine: a review. *J. Transplant.* **2012**:230386.
283. **Flisiak, R., S. V. Feinman, M. Jablkowski, A. Horban, W. Kryczka, M. Pawlowska, J. E. Heathcote, G. Mazzella, et al.** 2009. The cyclophilin inhibitor Debio 025 combined with PEG IFNalpha2a significantly reduces viral load in treatment-naive hepatitis C patients. *Hepatology* **49**:1460-1468.
284. **Flisiak, R., A. Horban, P. Gallay, M. Bobardt, S. Selvarajah, A. Wiercinska-Drapalo, E. Siwak, I. Cielniak, et al.** 2008. The cyclophilin inhibitor Debio-025 shows potent anti-hepatitis C effect in patients coinfecting with hepatitis C and human immunodeficiency virus. *Hepatology* **47**:817-826.
285. **Lawitz, E., E. Godofsky, R. Rouzier, T. Marbury, T. Nguyen, J. Ke, M. Huang, J. Praetgaard, et al.** 2011. Safety, pharmacokinetics, and antiviral activity of the cyclophilin inhibitor NIM811 alone or in combination with pegylated interferon in HCV-infected patients receiving 14 days of therapy. *Antiviral Res.* **89**:238-245.
286. **de Groot, R. J., J. A. Cowley, L. Enjuanes, K. S. Faaberg, S. Perlman, P. J. Rottier, E. J. Snijder, J. Ziebuhr, and A. E. Gorbalenya.** 2012. Order of Nidovirales, p. 785-795. In A. King, M. Adams, E. Carstens, and E. J. Lefkowitz (ed.), *Virus Taxonomy, the 9th Report of the International Committee on Taxonomy of Viruses*. Academic Press.
287. **Snijder, E. J., and W. J. M. Spaan.** 2007. Arteriviruses, p. 1337-1355. In D. M. Knipe and P. M. Howley (ed.), *Fields Virology*, 5 ed. Lippincott, Williams & Wilkins, Philadelphia, Pa.
288. **Nedialkova, D. D., A. E. Gorbalenya, and E. J. Snijder.** 2010. Arterivirus Nsp1 modulates the accumulation of minus-strand templates to control the relative abundance of viral mRNAs. *PLoS Pathog.* **6**:e1000772.
289. **Kim, H. S., J. Kwang, I. J. Yoon, H. S. Joo, and M. L. Frey.** 1993. Enhanced replication of porcine reproductive and respiratory syndrome (PRRS) virus in a homogeneous subpopulation of MA-104 cell line. *Arch. Virol.* **133**:477-483.
290. **Bryans, J. T., M. E. Crowe, E. R. Doll, and W. H. McCollum.** 1957. Isolation of a filterable agent causing arteritis of horses and abortion by mares; its differentiation from the equine abortion (influenza) virus. *Cornell Vet.* **47**:3-41.
291. **van den Born, E., C. C. Posthuma, K. Knoops, and E. J. Snijder.** 2007. An infectious recombinant equine arteritis virus expressing green fluorescent protein from its replicase gene. *J. Gen. Virol.* **88**:1196-1205.
292. **Fang, Y., R. R. Rowland, M. Roof, J. K. Lunney, J. Christopher-Hennings, and E. A. Nelson.** 2006. A full-length cDNA infectious clone of North American type 1 porcine reproductive and respiratory syndrome virus: expression of green fluorescent protein in the Nsp2 region. *J. Virol.* **80**:11447-11455.
293. **Sun, Z., Y. Li, R. Ransburgh, E. J. Snijder, and Y. Fang.** 2012. Nonstructural protein 2 of porcine reproductive and respiratory syndrome virus inhibits the antiviral function of interferon-stimulated gene 15. *J. Virol.* **86**:3839-3850.
294. **MacLachlan, N. J., U. B. Balasuriya, J. F. Hedges, T. M. Schweidler, W. H. McCollum, P. J. Timoney, P. J. Hullinger, and J. F. Patton.** 1998. Serologic response of horses to the structural proteins of equine arteritis virus. *J. Vet. Diagn. Invest.* **10**:229-236.

295. **Knoops, K., C. Swett-Tapia, S. H. van den Worm, A. J. Te Velthuis, A. J. Koster, A. M. Mommaas, E. J. Snijder, and M. Kikkert.** 2010. Integrity of the early secretory pathway promotes, but is not required for, severe acute respiratory syndrome coronavirus RNA synthesis and virus-induced remodeling of endoplasmic reticulum membranes. *J. Virol.* **84**:833-846.
296. **Schreiber, S. L., and G. R. Crabtree.** 1992. The mechanism of action of cyclosporin A and FK506. *Immunol. Today* **13**:136-142.
297. **Hopkins, S., B. Dimassimo, P. Rusnak, D. Heuman, J. Lalezari, A. Sluder, B. Scorenaux, S. Mosier, et al.** 2012. The cyclophilin inhibitor SCY-635 suppresses viral replication and induces endogenous interferons in patients with chronic HCV genotype 1 infection. *J. Hepatol.* **57**:47-54.
298. **Wenger, R., M. Mutter, P. Garrouste, R. Lysek, O. Turpin, G. Vuagniaux, V. Nicolas, L. Novaroli Zanolari, and R. Crabbé.** November 2009. Cycloundecadepsipeptide compounds and use of said compounds as a medicament. patent WO 2010/052559.
299. **Watashi, K., M. Hijikata, M. Hosaka, M. Yamaji, and K. Shimotohno.** 2003. Cyclosporin A suppresses replication of hepatitis C virus genome in cultured hepatocytes. *Hepatology* **38**:1282-1288.
300. **Damaso, C. R., and S. J. Keller.** 1994. Cyclosporin A inhibits vaccinia virus replication *in vitro*. *Arch. Virol.* **134**:303-319.
301. **Chatterji, U., P. Lim, M. D. Bobardt, S. Wieland, D. G. Cordek, G. Vuagniaux, F. Chisari, C. E. Cameron, et al.** 2010. HCV resistance to cyclosporin A does not correlate with a resistance of the NS5A-cyclophilin A interaction to cyclophilin inhibitors. *J. Hepatol.* **53**:50-56.
302. **Fernandes, F., I. U. Ansari, and R. Striker.** 2010. Cyclosporine inhibits a direct interaction between cyclophilins and hepatitis C NS5A. *PLoS One* **5**:e9815.
303. **Gaither, L. A., J. Borawski, L. J. Anderson, K. A. Balabanis, P. Devay, G. Joberty, C. Rau, M. Schirle, et al.** 2010. Multiple cyclophilins involved in different cellular pathways mediate HCV replication. *Virology* **397**:43-55.
304. **Coelmont, L., X. Hanouille, U. Chatterji, C. Berger, J. Snoeck, M. Bobardt, P. Lim, I. Vliegen, et al.** 2010. DEB025 (Alisporivir) inhibits hepatitis C virus replication by preventing a cyclophilin A induced cis-trans isomerisation in domain II of NS5A. *PLoS One* **5**:e13687.
305. **Foster, T. L., P. Gallay, N. J. Stonehouse, and M. Harris.** 2011. Cyclophilin A interacts with domain II of hepatitis C virus NS5A and stimulates RNA binding in an isomerase-dependent manner. *J. Virol.* **85**:7460-7464.
306. **Chatterji, U., M. Bobardt, S. Selvarajah, F. Yang, H. Tang, N. Sakamoto, G. Vuagniaux, T. Parkinson, and P. Gallay.** 2009. The isomerase active site of cyclophilin A is critical for hepatitis C virus replication. *J. Biol. Chem.* **284**:16998-17005.
307. **Liu, Z., F. Yang, J. M. Robotham, and H. Tang.** 2009. Critical role of cyclophilin A and its prolyl-peptidyl isomerase activity in the structure and function of the hepatitis C virus replication complex. *J. Virol.* **83**:6554-6565.
308. **Kaul, A., S. Stauffer, C. Berger, T. Pertel, J. Schmitt, S. Kallis, M. Zayas, V. Lohmann, et al.** 2009. Essential role of cyclophilin A for hepatitis C virus replication and virus production and possible link to polyprotein cleavage kinetics. *PLoS Pathog.* **5**:e1000546.
309. **Watashi, K., N. Ishii, M. Hijikata, D. Inoue, T. Murata, Y. Miyanari, and K. Shimotohno.** 2005. Cyclophilin B is a functional regulator of hepatitis C virus RNA polymerase. *Mol. Cell* **19**:111-122.
310. **Castro, A. P., T. M. Carvalho, N. Moussatche, and C. R. Damaso.** 2003. Redistribution of cyclophilin A to viral factories during vaccinia virus infection and its incorporation into mature particles. *J. Virol.* **77**:9052-9068.

311. **Liu, X., L. Sun, M. Yu, Z. Wang, C. Xu, Q. Xue, K. Zhang, X. Ye, et al.** 2009. Cyclophilin A interacts with influenza A virus M1 protein and impairs the early stage of the viral replication. *Cell. Microbiol.*
312. **Luo, C., H. Luo, S. Zheng, C. Gui, L. Yue, C. Yu, T. Sun, P. He, et al.** 2004. Nucleocapsid protein of SARS coronavirus tightly binds to human cyclophilin A. *Biochem. Biophys. Res. Commun.* **321**:557-565.
313. **Almazan, F., C. Galan, and L. Enjuanes.** 2004. The nucleoprotein is required for efficient coronavirus genome replication. *J. Virol.* **78**:12683-12688.
314. **Schelle, B., N. Karl, B. Ludewig, S. G. Siddell, and V. Thiel.** 2006. Nucleocapsid protein expression facilitates coronavirus replication. *Adv. Exp. Med. Biol.* **581**:43-48.
315. **Pang, X., M. Zhang, L. Zhou, F. Xie, H. Lu, W. He, S. Jiang, L. Yu, and X. Zhang.** 2011. Discovery of a potent peptidic cyclophilin A inhibitor Trp-Gly-Pro. *Eur. J. Med. Chem.* **46**:1701-1705.
316. **Puyang, X., D. L. Poulin, J. E. Mathy, L. J. Anderson, S. Ma, Z. Fang, S. Zhu, K. Lin, et al.** 2010. Mechanism of resistance of hepatitis C virus replicons to structurally distinct cyclophilin inhibitors. *Antimicrob. Agents Chemother.* **54**:1981-1987.
317. **Perlman, S., and J. Netland.** 2009. Coronaviruses post-SARS: update on replication and pathogenesis. *Nat. Rev. Microbiol.* **7**:439-450.
318. **Tong, T. R.** 2009. Drug targets in severe acute respiratory syndrome (SARS) virus and other coronavirus infections. *Infect. Disord. Drug Targets* **9**:223-245.
319. **Vincent, M. J., E. Bergeron, S. Benjannet, B. R. Erickson, P. E. Rollin, T. G. Ksiazek, N. G. Seidah, and S. T. Nichol.** 2005. Chloroquine is a potent inhibitor of SARS coronavirus infection and spread. *Virol. J.* **2**:69.
320. **de Haan, C. A., and P. J. Rottier.** 2006. Hosting the severe acute respiratory syndrome coronavirus: specific cell factors required for infection. *Cell. Microbiol.* **8**:1211-1218.
321. **Vogels, M. W., B. W. van Balkom, D. V. Kaloyanova, J. J. Batenburg, A. J. Heck, J. B. Helms, P. J. Rottier, and C. A. de Haan.** 2011. Identification of host factors involved in coronavirus replication by quantitative proteomics analysis. *Proteomics* **11**:64-80.
322. **Zhang, L., Z. P. Zhang, X. E. Zhang, F. S. Lin, and F. Ge.** 2010. Quantitative proteomics analysis reveals BAG3 as a potential target to suppress severe acute respiratory syndrome coronavirus replication. *J. Virol.* **84**:6050-6059.
323. **Nakagawa, M., N. Sakamoto, Y. Tanabe, T. Koyama, Y. Itsui, Y. Takeda, C. H. Chen, S. Kakimoto, et al.** 2005. Suppression of hepatitis C virus replication by cyclosporin A is mediated by blockade of cyclophilins. *Gastroenterology* **129**:1031-1041.
324. **Sims, A. C., S. E. Burkett, B. Yount, and R. J. Pickles.** 2008. SARS-CoV replication and pathogenesis in an *in vitro* model of the human conducting airway epithelium. *Virus Res.* **133**:33-44.
325. **Cervantes-Barragan, L., R. Züst, R. Maier, S. Sierro, J. Janda, F. Levy, D. Speiser, P. Romero, et al.** 2010. Dendritic cell-specific antigen delivery by coronavirus vaccine vectors induces long-lasting protective antiviral and antitumor immunity. *MBio* **1**:e00171-00110.
326. **Das Sarma, J., E. Scheen, S. H. Seo, M. Koval, and S. R. Weiss.** 2002. Enhanced green fluorescent protein expression may be used to monitor murine coronavirus spread *in vitro* and in the mouse central nervous system. *J. Neurovirol.* **8**:381-391.
327. **Ishii, N., K. Watashi, T. Hishiki, K. Goto, D. Inoue, M. Hijikata, T. Wakita, N. Kato, and K. Shimotohno.** 2006. Diverse effects of cyclosporine on hepatitis C virus strain replication. *J. Virol.* **80**:4510-4520.
328. **Manel, N., B. Hogstad, Y. Wang, D. E. Levy, D. Unutmaz, and D. R. Littman.** 2010. A cryptic sensor for HIV-1 activates antiviral innate immunity in dendritic cells. *Nature* **467**:214-217.

329. **te Velthuis, A. J., J. J. Arnold, C. E. Cameron, S. H. van den Worm, and E. J. Snijder.** 2010. The RNA polymerase activity of SARS-coronavirus nsp12 is primer dependent. *Nucleic Acids Res.* **38**:203-214.
330. **Paeshuysse, J., A. Kaul, E. De Clercq, B. Rosenwirth, J. M. Dumont, P. Scalfaro, R. Bartenschlager, and J. Neyts.** 2006. The non-immunosuppressive cyclosporin DEBIO-025 is a potent inhibitor of hepatitis C virus replication *in vitro*. *Hepatology* **43**:761-770.
331. **Ciesek, S., E. Steinmann, H. Wedemeyer, M. P. Manns, J. Neyts, N. Tautz, V. Madan, R. Bartenschlager, et al.** 2009. Cyclosporine A inhibits hepatitis C virus nonstructural protein 2 through cyclophilin A. *Hepatology* **50**:1638-1645.
332. **Chatterji, U., M. D. Bobardt, P. Lim, and P. A. Gallay.** 2010. Cyclophilin A-independent recruitment of NS5A and NS5B into hepatitis C virus replication complexes. *J. Gen. Virol.* **91**:1189-1193.
333. **Goto, K., K. Watashi, D. Inoue, M. Hijikata, and K. Shimotohno.** 2009. Identification of cellular and viral factors related to anti-hepatitis C virus activity of cyclophilin inhibitor. *Cancer Sci.* **100**:1943-1950.
334. **Krishnan, M. N., A. Ng, B. Sukumaran, F. D. Gilfoy, P. D. Uchil, H. Sultana, A. L. Brass, R. Adametz, et al.** 2008. RNA interference screen for human genes associated with West Nile virus infection. *Nature* **455**:242-245.
335. **Sessions, O. M., N. J. Barrows, J. A. Souza-Neto, T. J. Robinson, C. L. Hershey, M. A. Rodgers, J. L. Ramirez, G. Dimopoulos, et al.** 2009. Discovery of insect and human dengue virus host factors. *Nature* **458**:1047-1050.
336. **Zhou, H., M. Xu, Q. Huang, A. T. Gates, X. D. Zhang, J. C. Castle, E. Stec, M. Ferrer, et al.** 2008. Genome-scale RNAi screen for host factors required for HIV replication. *Cell Host Microbe* **4**:495-504.
337. **Ng, T. I., H. Mo, T. Pilot-Matias, Y. He, G. Koev, P. Krishnan, R. Mondal, R. Pithawalla, et al.** 2007. Identification of host genes involved in hepatitis C virus replication by small interfering RNA technology. *Hepatology* **45**:1413-1421.
338. **Tai, A. W., Y. Benita, L. F. Peng, S. S. Kim, N. Sakamoto, R. J. Xavier, and R. T. Chung.** 2009. A functional genomic screen identifies cellular cofactors of hepatitis C virus replication. *Cell Host Microbe* **5**:298-307.
339. **Li, Q., A. L. Brass, A. Ng, Z. Hu, R. J. Xavier, T. J. Liang, and S. J. Elledge.** 2009. A genome-wide genetic screen for host factors required for hepatitis C virus propagation. *Proc. Natl. Acad. Sci. USA* **106**:16410-16415.
340. **Reiss, S., I. Rebhan, P. Backes, I. Romero-Brey, H. Erfle, P. Matula, L. Kaderali, M. Poenisch, et al.** 2011. Recruitment and activation of a lipid kinase by hepatitis C virus NS5A is essential for integrity of the membranous replication compartment. *Cell Host Microbe* **9**:32-45.
341. **Supekova, L., F. Supek, J. Lee, S. Chen, N. Gray, J. P. Pezacki, A. Schlapbach, and P. G. Schultz.** 2008. Identification of human kinases involved in hepatitis C virus replication by small interference RNA library screening. *J. Biol. Chem.* **283**:29-36.
342. **Randall, G., M. Panis, J. D. Cooper, T. L. Tellinghuisen, K. E. Sukhodolets, S. Pfeffer, M. Landthaler, P. Landgraf, et al.** 2007. Cellular cofactors affecting hepatitis C virus infection and replication. *Proc. Natl. Acad. Sci. USA* **104**:12884-12889.
343. **Hao, L., A. Sakurai, T. Watanabe, E. Sorensen, C. A. Nidom, M. A. Newton, P. Ahlquist, and Y. Kawaoka.** 2008. *Drosophila* RNAi screen identifies host genes important for influenza virus replication. *Nature* **454**:890-893.

344. **Karlas, A., N. Machuy, Y. Shin, K. P. Pleissner, A. Artarini, D. Heuer, D. Becker, H. Khalil, et al.** 2010. Genome-wide RNAi screen identifies human host factors crucial for influenza virus replication. *Nature* **463**:818-822.
345. **Pyrk, K., B. Berkhout, and L. van der Hoek.** 2007. The novel human coronaviruses NL63 and HKU1. *J. Virol.* **81**:3051-3057.
346. **Narayanan, K., C. Huang, and S. Makino.** 2008. SARS coronavirus accessory proteins. *Virus Res.* **133**:113-121.
347. **Ratia, K., K. S. Saikatendu, B. D. Santarsiero, N. Barretto, S. C. Baker, R. C. Stevens, and A. D. Mesecar.** 2006. Severe acute respiratory syndrome coronavirus papain-like protease: structure of a viral deubiquitinating enzyme. *Proc. Natl. Acad. Sci. USA* **103**:5717-5722.
348. **Zust, R., L. Cervantes-Barragan, M. Habjan, R. Maier, B. W. Neuman, J. Ziebuhr, K. J. Szretter, S. C. Baker, et al.** 2011. Ribose 2'-O-methylation provides a molecular signature for the distinction of self and non-self mRNA dependent on the RNA sensor Mda5. *Nat. Immunol.* **12**:137-143.
349. **Ye, Y., K. Hauns, J. O. Langland, B. L. Jacobs, and B. G. Hogue.** 2007. Mouse hepatitis coronavirus A59 nucleocapsid protein is a type I interferon antagonist. *J. Virol.* **81**:2554-2563.
350. **Kopecky-Bromberg, S. A., L. Martinez-Sobrido, and P. Palese.** 2006. 7a protein of severe acute respiratory syndrome coronavirus inhibits cellular protein synthesis and activates p38 mitogen-activated protein kinase. *J. Virol.* **80**:785-793.
351. **Hussain, S., S. Perlman, and T. M. Gallagher.** 2008. Severe acute respiratory syndrome coronavirus protein 6 accelerates murine hepatitis virus infections by more than one mechanism. *J. Virol.* **82**:7212-7222.
352. **Coyne, C. B., R. Bozym, S. A. Morosky, S. L. Hanna, A. Mukherjee, M. Tudor, K. S. Kim, and S. Cherry.** 2011. Comparative RNAi screening reveals host factors involved in enterovirus infection of polarized endothelial monolayers. *Cell Host Microbe* **9**:70-82.
353. **Hsu, N. Y., O. Ilnytska, G. Belov, M. Santiana, Y. H. Chen, P. M. Takvorian, C. Pau, H. van der Schaar, et al.** 2010. Viral reorganization of the secretory pathway generates distinct organelles for RNA replication. *Cell* **141**:799-811.
354. **de Wilde, A. H., Y. Li, Y. van der Meer, G. Vuagniaux, R. Lysek, Y. Fang, E. J. Snijder, and M. J. van Hemert.** 2013. Cyclophilin inhibitors block arterivirus replication by interfering with viral RNA synthesis. *J. Virol.* **87**:1454-1464.
355. **van den Worm, S. H., K. K. Eriksson, J. C. Zevenhoven, F. Weber, R. Zust, T. Kuri, R. Dijkman, G. Chang, et al.** 2012. Reverse genetics of SARS-related coronavirus using vaccinia virus-based recombination. *PLoS One* **7**:e32857.
356. **Boutros, M., L. P. Bras, and W. Huber.** 2006. Analysis of cell-based RNAi screens. *Genome Biol.* **7**:R66.
357. **Beck, R., M. Rawet, F. T. Wieland, and D. Cassel.** 2009. The COPI system: molecular mechanisms and function. *FEBS Lett.* **583**:2701-2709.
358. **Niu, T. K., A. C. Pfeifer, J. Lippincott-Schwartz, and C. L. Jackson.** 2005. Dynamics of GBF1, a Brefeldin A-sensitive Arf1 exchange factor at the Golgi. *Mol. Biol. Cell.* **16**:1213-1222.
359. **Cherry, S., T. Doukas, S. Armknecht, S. Whelan, H. Wang, P. Sarnow, and N. Perrimon.** 2005. Genome-wide RNAi screen reveals a specific sensitivity of IRES-containing RNA viruses to host translation inhibition. *Genes Dev.* **19**:445-452.
360. **Chang, Y. J., C. Y. Liu, B. L. Chiang, Y. C. Chao, and C. C. Chen.** 2004. Induction of IL-8 release in lung cells via activator protein-1 by recombinant baculovirus displaying severe acute respiratory syndrome-coronavirus spike proteins: identification of two functional regions. *J. Immunol.* **173**:7602-7614.

361. **Zhang, X., K. Wu, D. Wang, X. Yue, D. Song, Y. Zhu, and J. Wu.** 2007. Nucleocapsid protein of SARS-CoV activates interleukin-6 expression through cellular transcription factor NF-kappaB. *Virology* **365**:324-335.
362. **Liao, Y., X. Wang, M. Huang, J. P. Tam, and D. X. Liu.** 2011. Regulation of the p38 mitogen-activated protein kinase and dual-specificity phosphatase 1 feedback loop modulates the induction of interleukin 6 and 8 in cells infected with coronavirus infectious bronchitis virus. *Virology* **420**:106-116.
363. **Banerjee, S., K. Narayanan, T. Mizutani, and S. Makino.** 2002. Murine coronavirus replication-induced p38 mitogen-activated protein kinase activation promotes interleukin-6 production and virus replication in cultured cells. *J. Virol.* **76**:5937-5948.
364. **Oostro, M., E. G. te Lintelo, M. Deijs, M. H. Verheije, P. J. Rottier, and C. A. de Haan.** 2007. Localization and membrane topology of coronavirus nonstructural protein 4: involvement of the early secretory pathway in replication. *J. Virol.* **81**:12323-12336.
365. **Verheije, M. H., M. Raaben, M. Mari, E. G. Te Lintelo, F. Reggiori, F. J. van Kuppeveld, P. J. Rottier, and C. A. de Haan.** 2008. Mouse hepatitis coronavirus RNA replication depends on GBF1-mediated ARF1 activation. *PLoS Pathog.* **4**:e1000088.
366. **Neuman, B. W., J. S. Joseph, K. S. Saikatendu, P. Serrano, A. Chatterjee, M. A. Johnson, L. Liao, J. P. Klaus, et al.** 2008. Proteomics analysis unravels the functional repertoire of coronavirus nonstructural protein 3. *J. Virol.* **82**:5279-5294.
367. **Belov, G. A., N. Altan-Bonnet, G. Kovtunovych, C. L. Jackson, J. Lippincott-Schwartz, and E. Ehrenfeld.** 2007. Hijacking components of the cellular secretory pathway for replication of poliovirus RNA. *J. Virol.* **81**:558-567.
368. **Belov, G. A., M. H. Fogg, and E. Ehrenfeld.** 2005. Poliovirus proteins induce membrane association of GTPase ADP-ribosylation factor. *J. Virol.* **79**:7207-7216.
369. **Gazina, E. V., J. M. Mackenzie, R. J. Gorrell, and D. A. Anderson.** 2002. Differential requirements for COPI coats in formation of replication complexes among three genera of Picornaviridae. *J. Virol.* **76**:11113-11122.
370. **Wang, J., Z. Wu, and Q. Jin.** 2012. COPI Is Required for Enterovirus 71 Replication. *PLoS One* **7**:e38035.
371. **van der Linden, L., H. M. van der Schaar, K. H. Lanke, J. Neyts, and F. J. van Kuppeveld.** 2010. Differential effects of the putative GBF1 inhibitors Golgicide A and AG1478 on enterovirus replication. *J. Virol.* **84**:7535-7542.
372. **Cureton, D. K., R. Burdeinick-Kerr, and S. P. Whelan.** 2012. Genetic inactivation of COPI coat-omer separately inhibits vesicular stomatitis virus entry and gene expression. *J. Virol.* **86**:655-666.
373. **Cherry, S., A. Kunte, H. Wang, C. Coyne, R. B. Rawson, and N. Perrimon.** 2006. COPI activity coupled with fatty acid biosynthesis is required for viral replication. *PLoS Pathog.* **2**:e102.
374. **Konig, R., S. Stertz, Y. Zhou, A. Inoue, H. H. Hoffmann, S. Bhattacharyya, J. G. Alamares, D. M. Tscherne, et al.** 2010. Human host factors required for influenza virus replication. *Nature* **463**:813-817.
375. **He, D., C. Overend, J. Ambrogio, R. J. Maganti, M. J. Grubman, and A. E. Garmendia.** 2011. Marked differences between MARC-145 cells and swine alveolar macrophages in IFNbeta-induced activation of antiviral state against PRRSV. *Vet. Immunol. Immunopathol.* **139**:57-60.
376. **Rowland, R. R., B. Robinson, J. Stefanick, T. S. Kim, L. Guanghua, S. R. Lawson, and D. A. Benfield.** 2001. Inhibition of porcine reproductive and respiratory syndrome virus by interferon-gamma and recovery of virus replication with 2-aminopurine. *Arch. Virol.* **146**:539-555.

377. **Krahling, V., D. A. Stein, M. Spiegel, F. Weber, and E. Muhlberger.** 2009. Severe acute respiratory syndrome coronavirus triggers apoptosis via protein kinase R but is resistant to its antiviral activity. *J. Virol.* **83**:2298-2309.
378. **Woo, P. C., M. Wang, S. K. Lau, H. Xu, R. W. Poon, R. Guo, B. H. Wong, K. Gao, et al.** 2007. Comparative analysis of twelve genomes of three novel group 2c and group 2d coronaviruses reveals unique group and subgroup features. *J. Virol.* **81**:1574-1585.
379. **Vijaykrishna, D., G. J. Smith, J. X. Zhang, J. S. Peiris, H. Chen, and Y. Guan.** 2007. Evolutionary insights into the ecology of coronaviruses. *J. Virol.* **81**:4012-4020.
380. **Fouchier, R. A., N. G. Hartwig, T. M. Bestebroer, B. Niemeyer, J. C. de Jong, J. H. Simon, and A. D. Osterhaus.** 2004. A previously undescribed coronavirus associated with respiratory disease in humans. *Proc. Natl. Acad. Sci. USA* **101**:6212-6216.
381. **Raj, V. S., H. Mou, S. L. Smits, D. H. Dekkers, M. A. Muller, R. Dijkman, D. Muth, J. A. Demmers, et al.** 2013. Dipeptidyl peptidase 4 is a functional receptor for the emerging human coronavirus-EMC. *Nature* **495**:251-254.
382. **Randall, R. E., and S. Goodbourn.** 2008. Interferons and viruses: an interplay between induction, signalling, antiviral responses and virus countermeasures. *J. Gen. Virol.* **89**:1-47.
383. **Versteeg, G. A., P. J. Bredenbeek, S. H. van den Worm, and W. J. Spaan.** 2007. Group 2 coronaviruses prevent immediate early interferon induction by protection of viral RNA from host cell recognition. *Virology* **361**:18-26.
384. **Sims, A. C., S. C. Tilton, V. D. Menachery, L. E. Gralinski, A. Schafer, M. M. Matzke, B. J. Webb-Robertson, J. Chang, et al.** 2013. Release of severe acute respiratory syndrome coronavirus nuclear import block enhances host transcription in human lung cells. *J Virol* **87**:3885-3902.
385. **Yoshikawa, T., T. E. Hill, N. Yoshikawa, V. L. Popov, C. L. Galindo, H. R. Garner, C. J. Peters, and C. T. Tseng.** 2010. Dynamic innate immune responses of human bronchial epithelial cells to severe acute respiratory syndrome-associated coronavirus infection. *PLoS One* **5**:e8729.
386. **Zeng, F. Y., C. W. Chan, M. N. Chan, J. D. Chen, K. Y. Chow, C. C. Hon, K. H. Hui, J. Li, et al.** 2003. The complete genome sequence of severe acute respiratory syndrome coronavirus strain HKU-39849 (HK-39). *Exp. Biol. Med.* **228**:866-873.
387. **Weber, F., V. Wagner, S. B. Rasmussen, R. Hartmann, and S. R. Paludan.** 2006. Double-stranded RNA is produced by positive-strand RNA viruses and DNA viruses but not in detectable amounts by negative-strand RNA viruses. *J. Virol.* **80**:5059-5064.
388. **Belouzard, S., J. K. Millet, B. N. Licitra, and G. R. Whittaker.** 2012. Mechanisms of coronavirus cell entry mediated by the viral spike protein. *Viruses* **4**:1011-1033.
389. **Snijder, E. J., P. J. Bredenbeek, J. C. Dobbe, V. Thiel, J. Ziebuhr, L. L. Poon, Y. Guan, M. Roza-nov, et al.** 2003. Unique and conserved features of genome and proteome of SARS-coronavirus, an early split-off from the coronavirus group 2 lineage. *J. Mol. Biol.* **331**:991-1004.
390. **Vijgen, L., E. Keyaerts, E. Moes, I. Thoelen, E. Wollants, P. Lemey, A. M. Vandamme, and M. Van Ranst.** 2005. Complete genomic sequence of human coronavirus OC43: molecular clock analysis suggests a relatively recent zoonotic coronavirus transmission event. *J. Virol.* **79**:1595-1604.
391. **Pfefferle, S., S. Oppong, J. F. Drexler, F. Gloza-Rausch, A. Ipsen, A. Seebens, M. A. Muller, A. Annan, et al.** 2009. Distant relatives of severe acute respiratory syndrome coronavirus and close relatives of human coronavirus 229E in bats, Ghana. *Emerg. Infect. Dis.* **15**:1377-1384.
392. **Cameron, M. J., A. A. Kelvin, A. J. Leon, C. M. Cameron, L. Ran, L. Xu, Y. K. Chu, A. Danesh, et al.** 2012. Lack of innate interferon responses during SARS coronavirus infection in a vaccination and reinfection ferret model. *PLoS One* **7**:e45842.

393. **Roth-Cross, J. K., L. Martinez-Sobrido, E. P. Scott, A. Garcia-Sastre, and S. R. Weiss.** 2007. Inhibition of the alpha/beta interferon response by mouse hepatitis virus at multiple levels. *J. Virol.* **81**:7189-7199.
394. **Cervantes-Barragan, L., R. Zust, F. Weber, M. Spiegel, K. S. Lang, S. Akira, V. Thiel, and B. Ludewig.** 2007. Control of coronavirus infection through plasmacytoid dendritic-cell-derived type I interferon. *Blood* **109**:1131-1137.
395. **Kindler, E., H. R. Jonsdottir, D. Muth, O. J. Hamming, R. Hartmann, R. Rodriguez, R. Geffers, R. A. Fouchier, et al.** 2013. Efficient Replication of the Novel Human Betacoronavirus EMC on Primary Human Epithelium Highlights Its Zoonotic Potential. *MBio* **4**:e00611-00612.
396. **Rose, K. M., R. Elliott, L. Martinez-Sobrido, A. Garcia-Sastre, and S. R. Weiss.** 2010. Murine coronavirus delays expression of a subset of interferon-stimulated genes. *J. Virol.* **84**:5656-5669.
397. **Bergman, S. J., M. C. Ferguson, and C. Santanello.** 2011. Interferons as therapeutic agents for infectious diseases. *Infect. Dis. Clin. North. Am.* **25**:819-834.
398. **Breban, R., J. Riou, and A. Fontanet.** 2013. Interhuman transmissibility of Middle East respiratory syndrome coronavirus: estimation of pandemic risk. *Lancet.*
399. **Roberts, A., E. W. Lamirande, L. Vogel, J. P. Jackson, C. D. Paddock, J. Guarner, S. R. Zaki, T. Sheahan, et al.** 2008. Animal models and vaccines for SARS-CoV infection. *Virus Res.* **133**:20-32.
400. **Martin, J. E., M. K. Louder, L. A. Holman, I. J. Gordon, M. E. Enama, B. D. Larkin, C. A. Andrews, L. Vogel, et al.** 2008. A SARS DNA vaccine induces neutralizing antibody and cellular immune responses in healthy adults in a Phase I clinical trial. *Vaccine* **26**:6338-6343.
401. **Hopkins, A. L., and C. R. Groom.** 2002. The druggable genome. *Nat. Rev. Drug Discov.* **1**:727-730.
402. **Bienz, K., D. Egger, T. Pfister, and M. Troxler.** 1992. Structural and functional characterization of the poliovirus replication complex. *J. Virol.* **66**:2740-2747.
403. **Zebovitz, E., J. K. Leong, and S. C. Doughty.** 1974. Involvement of the host cell nuclear envelope membranes in the replication of Japanese encephalitis virus. *Infect. Immun.* **10**:204-211.
404. **Quinkert, D., R. Bartenschlager, and V. Lohmann.** 2005. Quantitative analysis of the hepatitis C virus replication complex. *J. Virol.* **79**:13594-13605.
405. **Ahlquist, P., S. X. Wu, P. Kaesberg, C. C. Kao, R. Quadt, W. DeJong, and R. Hershberger.** 1994. Protein-protein interactions and glycerophospholipids in bromovirus and nodavirus RNA replication. *Arch. Virol. Suppl.* **9**:135-145.
406. **Kovalev, N., J. Pogany, and P. D. Nagy.** 2012. A Co-Opted DEAD-Box RNA helicase enhances tobusvirus plus-strand synthesis. *PLoS Pathog.* **8**:e1002537.
407. **Rodriguez, P. L., and L. Carrasco.** 1992. Gliotoxin: inhibitor of poliovirus RNA synthesis that blocks the viral RNA polymerase 3Dpol. *J. Virol.* **66**:1971-1976.
408. **Gerber, L., T. M. Welzel, and S. Zeuzem.** 2013. New therapeutic strategies in HCV: polymerase inhibitors. *Liver Int.* **33 Suppl 1**:85-92.
409. **Tsai, C. H., P. Y. Lee, V. Stollar, and M. L. Li.** 2006. Antiviral therapy targeting viral polymerase. *Curr. Pharm. Des.* **12**:1339-1355.
410. **Law, G. L., M. J. Korth, A. G. Benecke, and M. G. Katze.** 2013. Systems virology: host-directed approaches to viral pathogenesis and drug targeting. *Nat. Rev. Microbiol.* **11**:455-466.
411. **Johnson, S. A., and T. Hunter.** 2005. Kinomics: methods for deciphering the kinome. *Nat. Methods* **2**:17-25.
412. **Dar, A. C., and K. M. Shokat.** 2011. The evolution of protein kinase inhibitors from antagonists to agonists of cellular signaling. *Annu. Rev. Biochem.* **80**:769-795.
413. **Schang, L. M.** 2011. Cellular Protein Kinases as Antiviral Targets, p. 305-347. In B. Klebl, G. Müller, and M. Hamacher (ed.), *Protein Kinases as Drug Targets*. Wiley-VCH Verlag GmbH & Co. KGaA.

414. **Lupberger, J., M. B. Zeisel, F. Xiao, C. Thumann, I. Fofana, L. Zona, C. Davis, C. J. Mee, et al.** 2011. EGFR and EphA2 are host factors for hepatitis C virus entry and possible targets for antiviral therapy. *Nat. Med.* **17**:589-595.
415. **Moser, T. S., R. G. Jones, C. B. Thompson, C. B. Coyne, and S. Cherry.** 2010. A kinome RNAi screen identified AMPK as promoting poxvirus entry through the control of actin dynamics. *PLoS Pathog.* **6**:e1000954.
416. **Song, S., J. Bi, D. Wang, L. Fang, L. Zhang, F. Li, H. Chen, and S. Xiao.** 2013. Porcine reproductive and respiratory syndrome virus infection activates IL-10 production through NF-kappaB and p38 MAPK pathways in porcine alveolar macrophages. *Dev. Comp. Immunol.* **39**:265-272.
417. **Josset, L., V. D. Menachery, L. E. Gralinski, S. Agnihothram, P. Sova, V. S. Carter, B. L. Yount, R. L. Graham, et al.** 2013. Cell Host Response to Infection with Novel Human Coronavirus EMC Predicts Potential Antivirals and Important Differences with SARS Coronavirus. *MBio* **4**.
418. **Wannee, K. F., A. H. De Wilde, M. Rabelink, R. Hoeben, J. J. Goeman, P. ten Dijke, E. J. Snijder, M. Kikkert, and M. J. van Hemert.** 2013. Kinome-targeted siRNA library screening identifies common cellular factors and signaling pathways influencing the replication of distantly related nidoviruses. Manuscript in Preparation.
419. **Novina, C. D., and P. A. Sharp.** 2004. The RNAi revolution. *Nature* **430**:161-164.
420. **Bushman, F. D., N. Malani, J. Fernandes, I. D'Orso, G. Cagney, T. L. Diamond, H. Zhou, D. J. Hazuda, et al.** 2009. Host cell factors in HIV replication: meta-analysis of genome-wide studies. *PLoS Pathog.* **5**:e1000437.
421. **Jackson, A. L., and P. S. Linsley.** 2010. Recognizing and avoiding siRNA off-target effects for target identification and therapeutic application. *Nat. Rev. Drug Discov.* **9**:57-67.
422. **Echeverri, C. J., P. A. Beachy, B. Baum, M. Boutros, F. Buchholz, S. K. Chanda, J. Downward, J. Ellenberg, et al.** 2006. Minimizing the risk of reporting false positives in large-scale RNAi screens. *Nat. Methods* **3**:777-779.
423. **Dancourt, J., and C. Barlowe.** 2010. Protein sorting receptors in the early secretory pathway. *Annu. Rev. Biochem.* **79**:777-802.
424. **Bethune, J., F. Wieland, and J. Moelleken.** 2006. COPI-mediated transport. *J. Membr. Biol.* **211**:65-79.
425. **Brass, A. L., D. M. Dykxhoorn, Y. Benita, N. Yan, A. Engelman, R. J. Xavier, J. Lieberman, and S. J. Elledge.** 2008. Identification of host proteins required for HIV infection through a functional genomic screen. *Science* **319**:921-926.
426. **Tanaka, Y., Y. Sato, and T. Sasaki.** 2013. Suppression of coronavirus replication by cyclophilin inhibitors. *Viruses* **5**:1250-1260.
427. **Gething, M. J., and J. Sambrook.** 1992. Protein folding in the cell. *Nature* **355**:33-45.
428. **Schinzel, A. C., O. Takeuchi, Z. Huang, J. K. Fisher, Z. Zhou, J. Rubens, C. Hetz, N. N. Danial, et al.** 2005. Cyclophilin D is a component of mitochondrial permeability transition and mediates neuronal cell death after focal cerebral ischemia. *Proc. Natl. Acad. Sci. USA* **102**:12005-12010.
429. **Teigelkamp, S., T. Achsel, C. Mundt, S. F. Gothel, U. Cronshagen, W. S. Lane, M. Marahiel, and R. Luhrmann.** 1998. The 20kD protein of human [U4/U6.U5] tri-snRNPs is a novel cyclophilin that forms a complex with the U4/U6-specific 60kD and 90kD proteins. *RNA* **4**:127-141.
430. **Horowitz, D. S., E. J. Lee, S. A. Mabon, and T. Misteli.** 2002. A cyclophilin functions in pre-mRNA splicing. *EMBO J.* **21**:470-480.
431. **Steinbach, W. J., J. L. Reedy, R. A. Cramer, Jr., J. R. Perfect, and J. Heitman.** 2007. Harnessing calcineurin as a novel anti-infective agent against invasive fungal infections. *Nature reviews. Microbiology* **5**:418-430.

432. **Wainberg, M. A., A. Dascal, N. Blain, L. Fitz-Gibbon, F. Boulterice, K. Numazaki, and M. Tremblay.** 1988. The effect of cyclosporine A on infection of susceptible cells by human immunodeficiency virus type 1. *Blood* **72**:1904-1910.
433. **Montano-Loza, A. J., S. Wasilenko, J. Bintner, and A. L. Mason.** 2010. Cyclosporine A inhibits *in vitro* replication of betaretrovirus associated with primary biliary cirrhosis. *Liver Int.* **30**:871-877.
434. **Luban, J., K. L. Bossolt, E. K. Franke, G. V. Kalpana, and S. P. Goff.** 1993. Human immunodeficiency virus type 1 Gag protein binds to cyclophilins A and B. *Cell* **73**:1067-1078.
435. **Yang, F., J. M. Robotham, H. B. Nelson, A. Irsigler, R. Kenworthy, and H. Tang.** 2008. Cyclophilin A is an essential cofactor for hepatitis C virus infection and the principal mediator of cyclosporine resistance *in vitro*. *J. Virol.* **82**:5269-5278.
436. <http://www.clinicaltrials.gov/>
437. **Fischer, G., P. Gallay, and S. Hopkins.** 2010. Cyclophilin inhibitors for the treatment of HCV infection. *Curr. Opin. Investig. Drugs* **11**:911-918.
438. **Liu, Z., J. M. Robida, S. Chinnaswamy, G. Yi, J. M. Robotham, H. B. Nelson, A. Irsigler, C. C. Kao, and H. Tang.** 2009. Mutations in the hepatitis C virus polymerase that increase RNA binding can confer resistance to cyclosporine A. *Hepatology* **50**:25-33.
439. **Carbajo-Lozoya, J., M. A. Muller, S. Kallies, V. Thiel, C. Drosten, and A. von Brunn.** 2012. Replication of human coronaviruses SARS-CoV, HCoV-NL63 and HCoV-229E is inhibited by the drug FK506. *Virus Res.* **165**:112-117.
440. **McHutchison, J. G., E. J. Lawitz, M. L. Shiffman, A. J. Muir, G. W. Galler, J. McCone, L. M. Nyberg, W. M. Lee, et al.** 2009. Peginterferon alfa-2b or alfa-2a with ribavirin for treatment of hepatitis C infection. *N. Engl. J. Med.* **361**:580-593.
441. **Manns, M. P., J. G. McHutchison, S. C. Gordon, V. K. Rustgi, M. Shiffman, R. Reindollar, Z. D. Goodman, K. Koury, et al.** 2001. Peginterferon alfa-2b plus ribavirin compared with interferon alfa-2b plus ribavirin for initial treatment of chronic hepatitis C: a randomised trial. *Lancet* **358**:958-965.
442. **Fried, M. W., M. L. Shiffman, K. R. Reddy, C. Smith, G. Marinos, F. L. Goncales, Jr., D. Haussinger, M. Diago, et al.** 2002. Peginterferon alfa-2a plus ribavirin for chronic hepatitis C virus infection. *N. Engl. J. Med.* **347**:975-982.
443. **McHutchison, J. G., M. P. Manns, A. J. Muir, N. A. Terrault, I. M. Jacobson, N. H. Afdhal, E. J. Heathcote, S. Zeuzem, et al.** 2010. Telaprevir for previously treated chronic HCV infection. *N. Engl. J. Med.* **362**:1292-1303.
444. **Flisiak, R., J. Jaroszewicz, I. Flisiak, and T. Lapinski.** 2012. Update on alisporivir in treatment of viral hepatitis C. *Expert Opin Investig Drugs* **21**:375-382.
445. **Chan-Yeung, M., and R. H. Xu.** 2003. SARS: epidemiology. *Respirology* **8 Suppl**:S9-14.
446. **Roberts, A., D. Deming, C. D. Paddock, A. Cheng, B. Yount, L. Vogel, B. D. Herman, T. Sheahan, et al.** 2007. A mouse-adapted SARS-coronavirus causes disease and mortality in BALB/c mice. *PLoS Pathog.* **3**:e5.
447. **McCray, P. B., Jr., L. Pewe, C. Wohlford-Lenane, M. Hickey, L. Manzel, L. Shi, J. Netland, H. P. Jia, et al.** 2007. Lethal infection of K18-hACE2 mice infected with severe acute respiratory syndrome coronavirus. *J. Virol.* **81**:813-821.
448. **Munster, V. J., E. de Wit, and H. Feldmann.** 2013. Pneumonia from human coronavirus in a macaque model. *N. Engl. J. Med.* **368**:1560-1562.
449. **Madrid, P. B., S. Chopra, I. D. Manger, L. Gilfillan, T. R. Keepers, A. C. Shurtleff, C. E. Green, L. V. Iyer, et al.** 2013. A systematic screen of FDA-approved drugs for inhibitors of biological threat agents. *PLoS One* **8**:e60579.

450. **Falzarano, D., E. de Wit, C. Martellaro, J. Callison, V. J. Munster, and H. Feldmann.** 2013. Inhibition of novel beta coronavirus replication by a combination of interferon-alpha2b and ribavirin. *Sci. Rep.* **3**:1686.
451. **Chan, R. W., M. C. Chan, S. Agnihothram, L. L. Chan, D. I. Kuok, J. H. Fong, Y. Guan, L. L. Poon, et al.** 2013. Tropism and innate immune responses of the novel human betacoronavirus lineage C virus in human ex vivo respiratory organ cultures. *J. Virol.*
452. **Zielecki, F., M. Weber, M. Eickmann, L. Spiegelberg, A. M. Zaki, M. Matrosovich, S. Becker, and F. Weber.** 2013. Human cell tropism and innate immune system interactions of human respiratory coronavirus EMC compared to those of severe acute respiratory syndrome coronavirus. *J. Virol.* **87**:5300-5304.

Nederlandse samenvatting

NEDERLANDSE SAMENVATTING

Ten gevolge van de Severe Acute Respiratory Syndrome-coronavirus (SARS-CoV) uitbraak in 2003 zijn wereldwijd ruim 8000 besmettingen en ongeveer 800 sterfgevallen geregistreerd. Er waren geen antivirale middelen of vaccins tegen SARS-CoV voorhanden en de uitbraak werd na 4 maanden uiteindelijk onder controle gebracht met behulp van traditionele maatregelen, zoals opsporing en quarantaine van patiënten, en controle van hun contacten. Tien jaar na de SARS-epidemie, in de zomer van 2012, dook in Saoedi-Arabië een onbekend coronavirus op: Middle East Respiratory Syndrome-coronavirus (MERS-CoV). Tot september 2013 werden meer dan 100 besmettingen formeel vastgesteld en ongeveer de helft van deze patiënten is overleden. Hoewel er officieel relatief weinig gevallen geregistreerd zijn, wordt aangenomen dat mogelijk (tien)duizenden mensen (ongemerkt) besmet zijn met dit virus. De recente MERS-uitbraak maakt duidelijk dat er 10 jaar na de SARS-epidemie nog steeds geen specifieke behandelmethoden zijn voor patiënten die besmet zijn met dit soort coronavirussen. Voor de ontwikkeling van antivirale strategieën is het noodzakelijk om de virale levenscyclus beter te begrijpen om zo aangrijpingspunten te vinden voor gerichte antivirale therapie.

Dit proefschrift verschaft meer inzicht in de vermenigvuldiging (replicatie) van nidovirussen, de groep waartoe ook de coronavirussen MERS-CoV en SARS-CoV behoren. Het genetisch materiaal van nidovirussen bestaat *net als* voor veel andere belangrijke humane ziekteverwekkers (pathogenen) uit een zogenaamd positiefstrengig RNA (+RNA) genoom. Dit genoom kan na infectie direct door de gastheercel vertaald worden in virale eiwitten. Deze virale eiwitten (niet-structurele eiwitten; nsps) vormen de replicatie- en transcriptiecomplexen (RTCs) die vervolgens het virale genetisch materiaal kopiëren en zorgen dat de structurele eiwitten tot expressie komen. Samen met het virale RNA genoom vormen deze eiwitten nieuwe virusdeeltjes die omhuld zijn met een membraan. Nidovirus RTCs zijn, *net als* de replicatiecomplexen van andere +RNA virussen, geassocieerd met speciale, viraal geïnduceerde intracellulaire membraanstructuren. Het onderzoek beschreven in dit proefschrift is gedaan om meer inzicht te verkrijgen in nidovirus RTCs en het samenspel tussen nidovirussen en de gastheercel. In het bijzonder is gekeken naar de rol van gastheerfactoren betrokken bij nidovirusreplicatie.

Voor dit onderzoek is in eerste instantie gebruik gemaakt van het paardenvirus Equine arteritis virus (EAV), een voor de mens ongevaarlijk maar goed gekarakteriseerd modelvirus. In **hoofdstuk 2** wordt een methode beschreven voor het isoleren van actieve RTCs uit EAV-geïnfecteerde cellen. Met deze methode kan de RNA-synthetiserende activiteit van deze RTCs *in vitro* in detail bestudeerd worden. Het bleek dat diverse nsps geassocieerd zijn met cellulaire membranen. Een van deze nsps is het RNA-afhankelijke RNA polymerase (RdRp) dat het virale RNA kopieert. Deze membranen leken het complex te beschermen en waren cruciaal voor virale RNA synthese. Bovendien bleek de

RNA synthese activiteit absoluut afhankelijk te zijn van een gastheereiwit met een massa van 60-70 kDa, dat opmerkelijk genoeg niet permanent geassocieerd is met de membraangebonden complexen. De identificatie van dit eiwit is gaande.

Hoofdstuk 3 beschrijft het remmende effect van Cyclosporine A (CsA) op de replicatie van de arterivirussen EAV en het varkensvirus Porcine Reproductive and Respiratory Syndrome Virus. Behandeling van geïnfecteerde cellen met CsA blokkeert de aanmaak van virale eiwitten en ook de productie van nieuwe virusdeeltjes. De in hoofdstuk 2 beschreven *in vitro* methode werd gebruikt om aan te tonen dat CsA een direct effect heeft op de synthese van het EAV RNA. Van CsA is bekend dat het de activiteit remt van een specifieke groep van cellulaire eiwitten: de cyclophilins (Cyps). Het belang van enkele van deze Cyps, voornamelijk cyclophilin A (CypA) en CypB, is al eerder beschreven voor o.a. hepatitis C virus (HCV). Door gebruik te maken van een techniek (RNA interferentie) om het expressieniveau van specifieke eiwitten in de cel te verlagen, kon worden aangetoond dat CypA belangrijk is voor EAV replicatie. Verder zijn er aanwijzingen gevonden dat dit eiwit aanwezig is in EAV replicatiecomplexen en daar mogelijk een essentiële rol speelt. CsA is een onderdrukker van het immuunsysteem en is daardoor niet direct geschikt als antiviraal middel. Er bestaan echter varianten van CsA die wel de activiteit van Cyps blokkeren maar het immuunsysteem niet onderdrukken. Verscheidene van deze moleculen zijn al in klinische studies geëvalueerd voor de behandeling van HCV infecties. Eén van deze niet-immuunsuppressieve CsA-varianten, Debio-064, remt de EAV infectie. Dit bevestigt de betrokkenheid van Cyps bij arterivirus replicatie en suggereert dat deze klasse van middelen in de toekomst mogelijk ook ingezet kan worden als antivirale therapie tegen arterivirussen.

In **hoofdstuk 4** wordt aangetoond dat ook de replicatie van SARS-CoV, humaan coronavirus 229E (HCoV-229E), en het modelcoronavirus muizenhepatitis virus (MHV) wordt geremd door CsA. Echter kon geen duidelijke betrokkenheid van één of meer specifieke Cyps bij de SARS-CoV replicatie worden vastgesteld, wat erop zou kunnen wijzen dat de remming van de replicatie van SARS-CoV en EAV door CsA op verschillende mechanismen gebaseerd is. Dit verklaart ook mogelijk het verschil in gevoeligheid van deze virussen voor deze gastheercelgerichte remmer.

Om inzicht te krijgen in de rol van gastheerfactoren in de virale levenscyclus zijn voor een aantal virussen zogenaamde siRNA screens uitgevoerd, waarbij op systematische wijze de hoeveelheid van een bepaald gastheereiwit in de cel wordt verminderd, waarna het effect daarvan op virusreplicatie wordt gemeten. Op deze manier kunnen zowel provirale factoren (nodig voor virusreplicatie) als antivirale factoren (die virusreplicatie remmen) worden geïdentificeerd. **Hoofdstuk 5** beschrijft een dergelijke RNAi screen naar de rol van kinasen - eiwitten die vele cellulaire processen reguleren - in de SARS-CoV levenscyclus. Van de ~800 onderzochte eiwitten bleken er 90 een antiviraal effect te hebben, waarvan een groot deel een rol bleek te spelen in de signaaloverdracht binnen

het immuunsysteem. Verder werden 40 provirale factoren geïdentificeerd, waaronder enkele die betrokken (kunnen) zijn bij de virus-geïnduceerde membraanveranderingen. De rol van twee van de gevonden factoren – de antivirale factor PKR en de provirale factor COPB2 – is vervolgens in meer detail bestudeerd. PKR is eerder beschreven als antivirale factor voor andere virussen, en depletie van dit eiwit bleek inderdaad een stimulerend effect op SARS-CoV replicatie te hebben. COPB2 is een component van COPI-gecoate blaasjes die het transport vanuit het Golgi-complex regelen. Vermindering van COPB2 expressie resulteerde in een vermindering van SARS-CoV eiwit- en virusproductie. Niet alleen COPB2, maar ook andere componenten die betrokken zijn bij de vorming van de COPI-gecoate blaasjes, zoals COPB1 en GBF1, bleken een proviraal effect te hebben. Deze resultaten wijzen erop dat de vorming en/of aanwezigheid van deze blaasjes essentieel is voor efficiënte SARS-CoV replicatie. De resultaten van de RNAi experimenten vormen een goede basis voor het onderzoeken van de rol van gastheerfactoren in de SARS-CoV replicatie.

In **hoofdstuk 6** wordt inzicht verschaft in MERS-CoV replicatie. Verschillende cellen, waaronder Vero, VeroE6, Huh7 en Calu3 cellen, bleken met dit virus geïnficeerd te kunnen worden. Met behulp van elektronenmicroscopie konden in MERS-CoV-geïnficeerde Vero cellen blaasjes met een dubbel membraan (double-membrane vesicles; DMVs) en “in elkaar gedraaide” membranen (convoluted membranes; CM) worden waargenomen. Deze structuren zijn typerend voor coronavirusgeïnficeerde cellen. In dezelfde studie wordt aangetoond dat MERS-CoV snelle celdood induceert in Vero en Huh7 cellen. Dit fenomeen is gebruikt om een methode te ontwikkelen voor de identificatie van antivirale middelen, waarin het remmen van MERS-CoV-geïnduceerde celdood door deze middelen kwantitatief kan worden bepaald. CsA is gebruikt als “proof-of-principle” antiviraal middel en bleek inderdaad MERS-CoV te remmen bij vergelijkbare concentraties als gevonden voor SARS-CoV. Verder bleek interferon- α een potente remmer van MERS-CoV-geïnduceerde celdood en virus productie. Interessant is dat MERS-CoV ongeveer 50-100 keer gevoeliger is voor interferon- α behandeling dan SARS-CoV. Een mogelijke (deel)verklaring voor dit verschil is dat MERS-CoV geen homoloog van het SARS-CoV ORF6 eiwit heeft, zodat dit virus de immunrespons van de gastheer mogelijk minder efficiënt onderdrukt. Deze bevindingen bieden mogelijk een aangrijpingspunt voor de ontwikkeling van antivirale therapieën tegen MERS-CoV infecties.

Curriculum Vitae

CURRICULUM VITAE

Adriaan Hugo de Wilde werd geboren op 6 augustus 1984 te Hazerswoude-Dorp. In 2002 behaalde hij zijn Atheneum diploma aan de Christelijke scholengemeenschap Driestar College te Gouda. Daarna begon hij aan de opleiding Life, Science & Technology aan de Universiteit Leiden en de Technische Universiteit Delft. Na het behalen van zijn bachelordiploma in 2005 startte hij met de onderzoeksmaster studie Biomedische Wetenschappen aan het Leids Universitair Medisch Centrum (LUMC). Tijdens deze studie voerde hij zijn eerste stage uit bij de Tumorummunologie groep van de afdeling Immunohematologie en Bloedtransfusie (LUMC) onder begeleiding van dr. Muriël van den Hende en prof. dr. Sjoerd van der Burg. Een tweede masterstage werd gedaan in het laboratorium voor Moleculaire Virologie van de afdeling Medische Microbiologie (LUMC) onder begeleiding van dr. Martijn van Hemert en prof. dr. Eric Snijder. Na het behalen van zijn Master graad in 2008 is hij op de afdeling Medische Microbiologie van het LUMC begonnen aan een promotieonderzoek naar de immuunevasiestrategieën van het Epstein-Barr virus, onder begeleiding van dr. Maaïke Rensing en prof. dr. Emmanuel Wiertz. In verband met het vertrek van de betreffende onderzoeksgroep uit Leiden is in februari 2009 de overstap gemaakt naar de groep van prof. dr. Eric Snijder, alwaar onder directe begeleiding van co-promotor dr. Martijn van Hemert het in dit proefschrift beschreven onderzoek is uitgevoerd. In het laatste stadium van zijn promotietraject heeft zijn onderzoek zich voornamelijk toegespitst op de analyse van het recent ontdekte MERS-coronavirus en de identificatie van antivirale middelen tegen dit virus en andere coronavirussen. Deze onderzoekslijn zal Adriaan na zijn promotie nog enige tijd voortzetten binnen dezelfde groep.

List of publications

LIST OF PUBLICATIONS

Martijn J. van Hemert, **Adriaan H. de Wilde**, Alexander E. Gorbalenya, and Eric J. Snijder. The in Vitro RNA Synthesizing Activity of the Isolated Arterivirus Replication/Transcription Complex Is Dependent on a Host Factor. *The Journal of Biological Chemistry* (2008)

Adriaan H. de Wilde, Jessika C. Zevenhoven-Dobbe, Yvonne van der Meer, Volker Thiel, Krishna Narayanan, Shinji Makino, Eric J. Snijder, and Martijn J. van Hemert. Cyclosporin A inhibits the replication of diverse coronaviruses. *Journal of General Virology* (2011)

Adriaan H. de Wilde, Yanhua Li, Yvonne van der Meer, Grégoire Vuagniaux, Robert Lysek, Ying Fang, Eric J. Snijder, and Martijn J. van Hemert. Arterivirus replication is inhibited by cyclophilin inhibitors and depends on cyclophilin A. *Journal of Virology* (2013)

Adriaan H. de Wilde*, Kazimier F. Wannee*, Jelle Goeman, Peter ten Dijke, Eric J. Snijder, Marjolein Kikkert, and Martijn J. van Hemert. A kinome-wide siRNA screen identifies pro- and antiviral host factors for SARS-coronavirus replication, including PKR and proteins of the early secretory pathway. *Journal of Virology*. Submitted.

Sytse J. Piersma*, **Adriaan H. de Wilde***, Anita N. Kremer, Daniëlle Horst, Mateusz Makuch, Daphne van Leeuwen, Marieke S. van Ham, Lindsey Hutt-Fletcher, Marieke Griffioen, Emmanuel J. Wiertz, and Maaïke E. Rensing. Epstein-Barr virus glycoproteins gH, gL, and gp42 co-operate to impose potent HLA class II-restricted T cell evasion. Manuscript in preparation.

Adriaan H. de Wilde, V. Stalin Raj, Diede Oudshoorn, Theo M. Bestebroer, Stefan van Nieuwkoop, Ronald W. A. L. Limpens, Clara C. Posthuma, Yvonne van der Meer, Montserrat Bárcena, Bart L. Haagmans, Eric J. Snijder and Bernadette G. van den Hoogen. MERS-coronavirus replication induces severe *in vitro* cytopathology and is strongly inhibited by cyclosporin A or interferon-alpha treatment. *Journal of General Virology* (2013)

